2017

Multi-Model Structural Analysis

Wesley Holt
University of South Carolina

Multi-Model Structural Analysis

by

Wesley Holt

Bachelor of Science
Tennessee Technological University 2007

Submitted in Partial Fulfillment of the Requirements

for the Degree of Master of Science in

Civil Engineering

College of Engineering and Computing

University of South Carolina

2017

Accepted by:

Juan Caicedo, Director of Thesis

Dimitris Rizos, Reader

Paul Ziehl, Reader

Cheryl L. Addy, Vice Provost and Dean of the Graduate School

Acknowledgments

I would like to sincerely thank my advisor, Dr Juan Caicedo, for his guidance, expertise, and extremely valuable time. I would also like to thank my thesis committee members, Dr. Dimitris Rizos and Dr. Paul Ziehl for their time and insights.

Abstract

The uncertainty in modeling earthquake loading is investigated through the comparison of various openSEES models. A series of models is created and the responses compared with each other as well as with a full scale shake table experiment. The openSEES models selected for comparison include two linear models, a nonlinear model using the Steel01 material for the entire cross section, and eight fiber models using reinforcing steel material and various concrete materials.

The models are subjected to a series of nine simulated earthquakes, matching the excitations applied to the shake table test. It is found that all of the models under-predict the maximum base reactions. However, the nonlinear model using the Steel01 material generates the most accurate response of the models tested. It is seen that accumulated damage from each excitation affects the response of the column during the subsequent excitations and that the effect of this accumulated damage contributes to the total amount of uncertainty in the models.

A method of combining the responses of the different models to create a single probabilistic output is presented and some potential real world challenges to implementing probabilistic models are discussed.

Table of Contents

List of Tables

List of Figures

Chapter 1

Background

1.1 Variability in Structural Models

In the world of structural engineering, there are a number of different analytical tools that an engineer could use to analyze a particular problem. These tools include: simple hand calculations combined with engineering judgment, vigorous hand calculations, open source software, and commercial software. Ideally, each method of analyzing the same problem would generate the same results - or at least similar results. However, often the case is that different analysis techniques present different results. Further complicating the matter is the fact that even the same analysis software can return different results based on how the particular problem is modeled. This inherent variability of structural models can be described as uncertainty in the models. The hypothesis behind this work is that a structural engineer can perform an estimate of this uncertainty by combining the results of several models of the same problem. The scope focuses in studying the inherent variability of different structural models and providing information for the uncertainty quantification.

A selection of models were created and analyzed with a program called openSEES (http://opensees.berkeley.edu/). The structure modeled was a single reinforced concrete column, representing a bridge pier. The details of the models are described in Chapter 2. The column was loaded with gravity loads and a dynamic time history loading taken from a series of recorded seismic events. The results from these models were compared with each other along with the results from a full scale shake table

test of the same column using the same dynamic time history loading. The results are presented in Chapter 3. Finally, in Chapter 4, some thoughts are presented regarding the resulting uncertainty from the point of view of a professional engineer.

1.2 Modeling Software

Most engineers today choose to use some sort of analysis software to model their structure. A few of the commercial software packages that are available include: RISA, RAM, STAAD, SAP2000, Etabs, and GTStrudl. Most commercial software is similar in the fact that is has a graphical user interface and allows the engineer to see their structure in 3-dimensions, apply loads, and analyze load combinations. These software packages typically give results in the form of member stresses, deflections, base reactions, and have a variety of different code checks that can be chosen from, such as AISC and ACI. These programs are directly suited for structural engineers to use for professional design purposes.

Other commercial analysis packages include finite element analysis software such as ANSYS, Abaqus, and Solidworks simulation. The results generated from these types of packages are typically limited to internal stresses and deformations/deflections of the members. They may not be able to directly compare the member stresses to the applicable building code (such as AISC or ACI).

In addition to commercial software packages, there are also many different types of open-source software that can be used. These options typically have a much less refined user interface than the commercial software options. Open source software also typically has more limited functionality and may only be capable of a particular type of analysis.

OpenSEES is a structural analysis program used by many engineers and researchers worldwide to model the dynamic effects of earthquakes on structures. It is an open source program that was developed by the University of California, Berkeley,

in the 1990's (http://opensees.berkeley.edu/). Over the years, many engineers have developed different modeling techniques to attempt to create the most accurate prediction of the real-world structural response of their particular problem. The result is that there are now several ways to model the same problem that result in different responses. A selection of these models was chosen for comparison.

With currently available design tools, it is not realistic to expect the time history analysis to accurately predict the results from the shake table test. The behavior of reinforced concrete subjected to these loads is simply too complex to predict with a high level of certainty. Therefore, the objective of creating and analyzing models is to get as close as possible and a "good" model is defined as a model that predicts a response that is more accurate than other available models.

1.3 Blind Test

In addition to comparing the analysis results with each other, they were also compared with a full scale test that was performed at the University of California, San Diego in 2010 and published by the Pacific Earthquake Engineering Research Center (PEER) [2, 3]. In this experiment, a full scale reinforced concrete column was built on a shake table and subjected to earthquake motions recorded during historic seismic events. The data from this experiment is publicly available (NEES-2010-0987 from https://www.designsafe-ci.org/data/browser/public/nees.public/).

The experiment was part of a blind contest performed by PEER [1]. In this contest, engineers and researches from around the world were asked to predict the response of the column. Figure 1.1 below shows the range of predictions that were received for the maximum deflection at the top of the column. All contestants were given the same information to model the column, yet the range of predicted maximum deflections was very large. The range of predictions of the maximum moment at the column base is also shown below in figure 1.2. Similarly, this range was very large.

It is easy to see how the uncertainty in these models could pose a problem when the engineer has to determine whether or not the column is adequate.

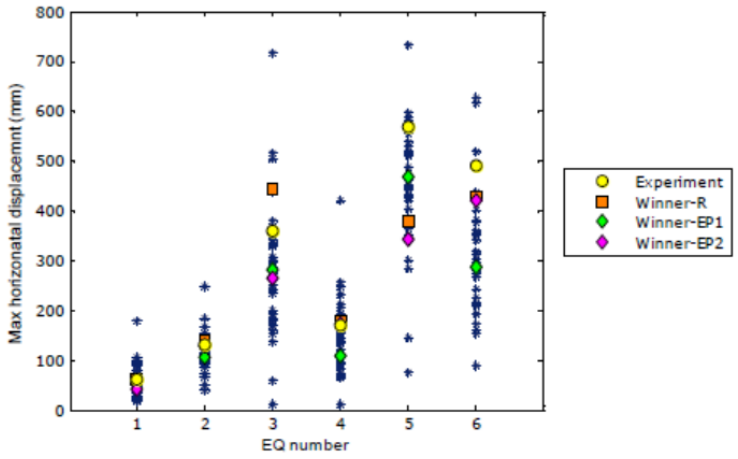

Figure 1.1: PEER contest predictions of maximum displacement at the top of column verses measured response [1]

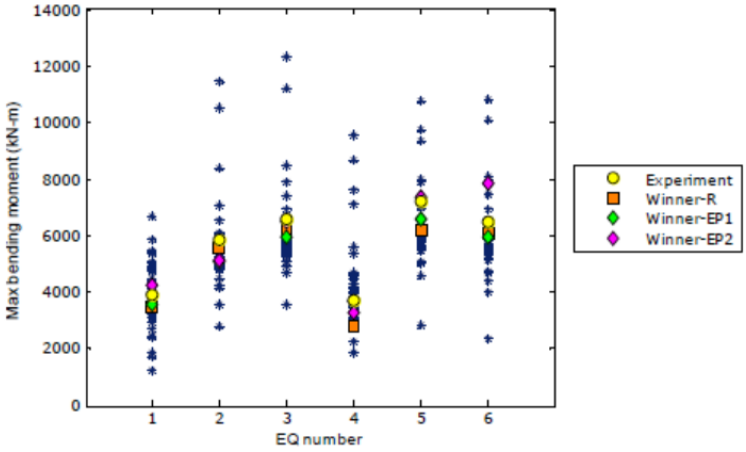

Figure 1.2: PEER contest predictions of maximum moment at the base of the column verses measured response [1]

1.4 Related Work

Periera et al performed similar research using openSEES for numerical modeling and compared the results with experimental data [4]. A fiber model was chosen and the

uncertainty stemming solely from applying different material profiles was studied. A total of 56 material combinations were analyzed in this work. It was found that the accuracy of the models depended on the stress level in the column and that no single model accurately predicted the response for the entire range of loading.

Similar work was also performed by Pan et al [5], [6], who investigated the effects of bond slip on their fiber model of the same PEER column [2]. It was concluded that including bond slip parameters made a substantial contribution toward the accuracy of the predicted column deflection.

Chapter 2

Models

2.1 General

The full scale test that the models were based on was performed at the Network for Earthquake Engineering Simulation (NEES) shake table at the University of California, San Diego [2, 3]. In that experiment, a full scale bridge pier was built on the shake table with a 522 kip concrete block on top of the pier to simulate the weight of a bridge. The 522 kip block at the top of the pier was required to get realistic inertial forces acting on the concrete pier. The pier itself had a round cross-section with a diameter of 48". It was reinforced with eighteen #11 longitudinal bars and #5 hoops spaced every 6 inches. See Figure 2.1 below. The pier was 24 feet tall, excluding the foundation, which was 4 feet thick. The rebar was tied into the foundation to create a moment connection and allow the pier to function as a simple cantilever column. The mass of concrete at the top of the column was connected so that the center of gravity of the mass was in line with the top of the column (24 feet above the top of concrete of the footing). The connection between the pier and the superstructure mass was designed so that there was no contact between the mass and the column below 24 feet above TOC of the footing.

The researchers placed 250 gages and instruments onto the column prior to testing [2]. The instrumentation included accelerometers on the foundation. This accelerometer data was used as the input acceleration for the openSEES models. The PEER report [2] provided the maximum base shear, maximum base moment, and

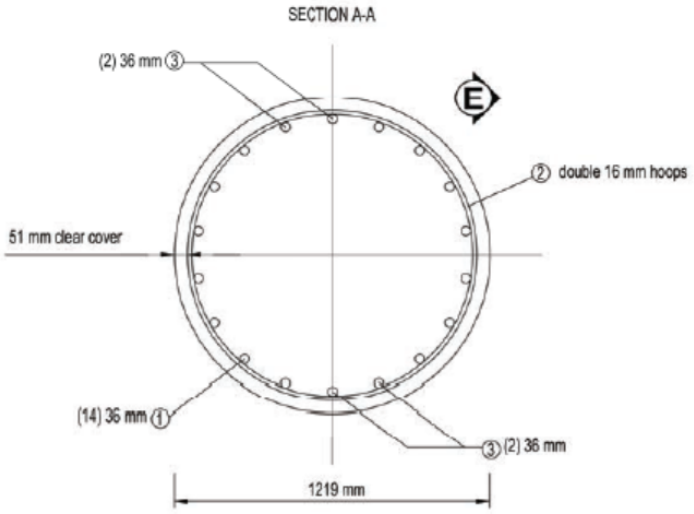

Figure 2.1: Pier Cross Section Details [2]

the maximum deflection that the column experienced during each of the simulated earthquakes. This allowed the different models to not only be compared with each other, but to be compared with the shake table response.

The software that was used for the computer analyses was the Open System for Earthquake Engineering Simulation (openSEES). This is a software that was initially developed by the University of California, Berkeley, and is now established as the primary computational platform for the Pacific Earthquake Engineering Research Center (PEER). It is an open-source platform that is used around the world for modeling the nonlinear response of structural systems subjected to dynamic loading.

The typical process for creating a model with openSEES is the engineer downloads a generic model from the community that resembles the system to be modeled (or begins with a model used previously). The generic model is then modified to match the desired dimensions, materials, conditions, etc. Right away, this presents a problem because there are several different models that could be chosen for the same structure. The different models range from simple, elastic analyses to advanced, nonlinear fiber models and FEA models.

This experiment consisted of a single cantilever column with a mass at the top,

which is just about the simplest structure one would ever need to analyze. Yet, even for this simple structure, there were several openSEES models that could be chosen and configured for the column. And if the same column was simulated in each of the different models, the resulting base reactions, deflections and internal stresses would be substantially different. This difference was the inspiration behind this work.

To compare the differences between models, five commonly available models were chosen. Table 2.1 shows the types of models used. Model 4 and model 5 each had 4 sub-models to compare different materials. Each model is discussed further in its respective section. Once the different models were built, identical loads were applied to each one. The acceleration load was obtained from the PEER experiment [2].

While the results of these models will be compared with the PEER test results [2], it is important to note that no attempt was made to "fit" the models to the test results. All of the models were created, run, and their results aggregated before being compared with the PEER test results. There were no parameters that were adjusted in attempt to improve the accuracy of the results. The intention was to create the models as if no test results were available, as would be the case in a design scenario.

Table 2.1: Model Types

Model	**Type of Analysis**	**No. of Elements**	**Type of Cross-Section**
Model 1	linear analysis	single element	solid cross-section
Model 2	linear analysis	multiple elements	solid cross-section
Model 3	nonlinear analysis	single element	solid cross-section
Model 4	nonlinear analysis	single element	fiber cross-section
Model 5	nonlinear analysis	single element	fiber cross-section

2.2 Model 1

Model 1 was the most basic model. It consisted of a single 24 foot tall element with a 16,211 slug mass at the top (applied in the model as 1.35 kip-s^2/in to convert to the appropriate units of inches, kips, and seconds) and the distributed mass of the column

itself along the length (0.00043 kip-s^2/in). This model used the elasticBeamColumn analysis element. This element had the limitation of a linear analysis even if the column stress exceeded the yield stress. Table 2.2 shows the parameters used in model 1. The primary parameter that had to be determined for this model was the moment of inertia. A composite moment of inertia was calculated, assuming a cracked cross-section, with all reinforcing bars intact (as opposed to selecting a state after some bars had yielded).

Table 2.2: Parameters used for Model 1

Parameter	**Value**
Model Name	model1
Number of Elements	1
Element Type	elasticBeamColumn
Fu	102 ksi
A	1810 in^2
E	3320 ksi
I	97600 in^4
mass	0.00043 kip-sec^2

2.3 Model 2

Model 2 was similar to model 1 in most aspects except the number of elements was increased from one to ten. This also required increasing the number of nodes from two to eleven. This number of elements was selected after running the model with several different numbers of elements and recording the maximum displacement in the column. It was observed that the change in max displacement decreased as the number of elements increased. Figure 2.2 illustrates how the maximum displacement of the model converged once the number of elements reached approximately ten.

Table 2.3 shows the parameters used in model 2.

Table 2.3: Parameters used for Model 2

Parameter	**Value**
Model Name	model2
Number of Elements	10
Element Type	elasticBeamColumn
Fu	102 ksi
A	1810 in^2
E	3320 ksi
I	97600 in^4
mass	0.00043 kip-sec^2

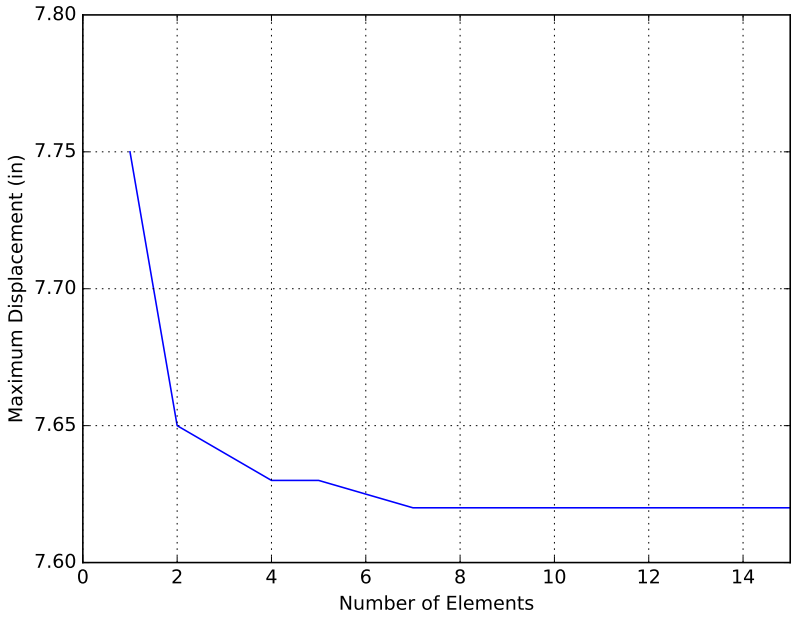

Figure 2.2: Comparison of maximum displacement and the number of elastic elements

2.4 Model 3

Model 3 was fundamentally different from model 1 and model 2 in that it utilized nonlinear analysis. It also used a composite material for the cross section. The material used was "Steel01". This material was chosen based on the assumption that the reinforced concrete behaves in a manner similar to steel in that it has a constant EI value up to a point and then loses stiffness and has a reduced EI beyond that point. The difference is the "kink" corresponds to the yielding of the individual rebars. This

was one area where an approximation had to be made. Since the column had a circular cross section, the reinforcing bars were not all a constant distance away from the neutral axis. Therefore, all of the reinforcing bars were not expected to yield simultaneously. Instead, as the internal moment in the column was increased, the steel furthest from the neutral axis would reach yielding first. Then, if the moment continued to increase, the next set of rebars would yield, and then the next, and so on. Unfortunately, there is not an opensees material that is designed to model this behavior explicitly. The "Steel01" material was chosen to be relatively similar to the actual behavior (albeit simplified). The "yield" point (point at which the slope of the moment-curvature plot abruptly changes) was determined to be 29800 in-kips based on a moment-curvature analysis of the column.

Table 2.4: Parameters used for Model 3

Parameter	**Value**
Model Name	model3
Number of Elements	1
Element Type	nonlinearBeamColumn
Number of Integration Points	10
f'c	6 ksi
A	1810 in^2
Ec	3320 ksi
I	97600 in^4
Yield Moment	29800 in-kip
Yield Curvature	0.63 x 10^{-4}
Cracked EI	324,000,000 in^2
Strain-Hardening ratio	0.04
mass	0.00043 kip-sec^2

The moment curvature plot was created by determining the moment and the curvature associated with the first concrete crack, the yield of the most extreme rebar, and then each subsequent rebar. The moment curvature plot is shown in Figure 2.3. The yield point was selected as the point at which the outermost 8 rebar yield, 29,800 in-kips.

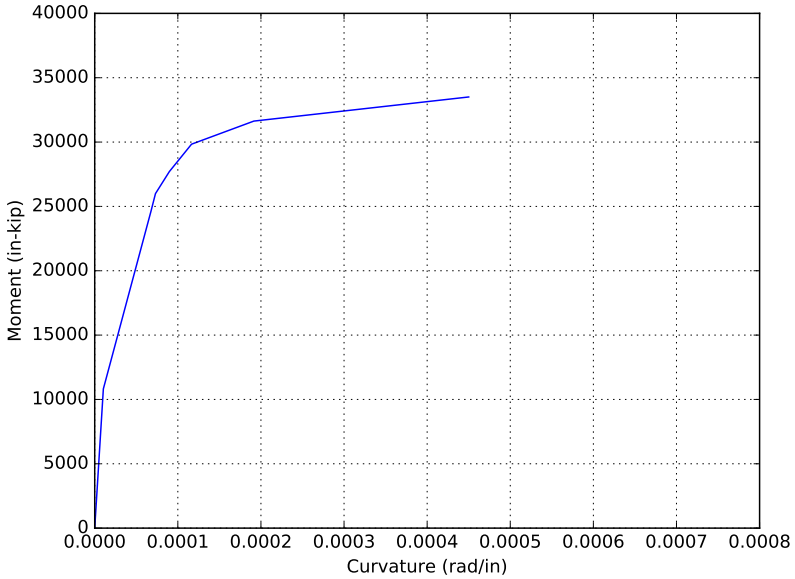

Figure 2.3: Moment-Curvature of Column at Different Loading Stages

Table 2.5: Moment-Curvature Data

Stage	**phi**	**M (in-kip)**
No Load	0	0
1st Crack	0.0000075	7790
2 Rebar Yield	0.0000639	22500
4 Rebar Yield	0.0000689	23800
6 Rebar Yield	0.0000843	25100
8 Rebar Yield	0.0001090	27300
10 Rebar Yield	0.0001730	28900
12 Rebar Yield	0.0003780	30600

The initial EI slope was input using the cracked moment of inertia of the column and the concrete modulus of elasticity. The cracked column moment of inertia was taken as 97600 in^4 and the modulus of elasticity was taken as 3320 ksi. The steel rebar areas were transformed to their equivalent concrete area when calculating composite modulii.

For the post yielding EI slope, a value of 0.04 x initial EI was used. The 0.04 value was chosen by comparing the slopes on the moment curvature plot. The element used in this model was 'nonlinearbeamcolumn'. Table 2.4 shows the parameters used in model 3.

2.5 Model 4

Model 4 also used the nonlinearBeamColumn element. However, the column was modeled using a fiber cross section instead of a uniform cross section, as it was in the previous models. There were still only two nodes and one element connecting them. The fiber cross section was created using three materials. The interior concrete (within the rebar cage), the exterior concrete (outside of the concrete cage), and the longitudinal reinforcing steel. The fiber cross section was built using the 'patch' and 'layer' commands in openSEES. The cross section was built using 20 angular divisions and 12 circumferential divisions, resulting in 240 total concrete fibers. Of these, 200 were within the rebar cage and 40 were outside the rebar cage.

The eighteen 36 mm (1.417 in) diameter longitudinal reinforcing bars were modeled using a steel area of 1.58 square inches per bar. The material parameters: yield strength, ultimate strength, initial modulus of elasticity, post strain hardening modulus of elasticity, strain at peak stress, and strain at initial strain hardening were taken directly from the PEER report. These values were provided as 75.2 ksi, 102.4 ksi, 28.4 ksi, 0.8 ksi, 12.2 percent, and 1.1 percent, respectively [2], as shown in Table 2.8.

There were four different variants of model 4 that were analyzed: model4a, model4b, model4c, and model4d. All of the models used the same concrete material for the inner concrete layers. However, they used different concrete materials for the outer concrete layers (outside of the rebar cage). The materials are given in Table 2.7

Table 2.6: Parameters used for Model 4

Parameter	**Value**
Model Name	model4
No. of Elements	1
Element Type	nonlinearBeamColumn
No. of Integration Points	6
mass	0.00043 kip-sec^2
No. of Steel Fibers	18
No. of Interior Conc. Fibers (Radial Direction)	10
No. of Interior Conc. Fibers (Circumf. Direction)	20
No. of Exterior Conc. Fibers (Radial Direction)	2
No. of Exterior Conc. Fibers (Circumf. Direction)	20
Area of Steel Fibers	1.58 in ^{2}

Table 2.7: Model 4 and Model 5 materials

Model	**Inner Concrete**	**Outer Concrete**	**Reinforcing Steel**
4a	concrete01	concrete01	ReinforcingSteel
4b	concrete01	concrete02	ReinforcingSteel
4c	concrete01	concrete03	ReinforcingSteel
4d	concrete01	concrete04	ReinforcingSteel
5a	concrete01	concrete01	ReinforcingSteel
5b	concrete01	concrete02	ReinforcingSteel
5c	concrete01	concrete03	ReinforcingSteel
5d	concrete01	concrete04	ReinforcingSteel

Table 2.8: Parameters used for fiber materials in model 4 and model 5

Parameter	**concrete01**	**concrete02**	**concrete03**	**concrete04**	**reinforcingSteel**
fpc	-6 ksi	-6 ksi	-6 ksi	-6 ksi	n/a
epsc0	-0.0026	-0.0026	-0.0026	-0.0026	n/a
fpcu	0	0	0	n/a	n/a
epsU	-0.005	-0.005	-0.005	-0.005	n/a
lambda	n/a	0.25	0.25	n/a	n/a
ft	n/a	0.580 ksi	0.580 ksi	0.580 ksi	n/a
Ets	n/a	733 ksi	n/a	n/a	n/a
epst0	n/a	n/a	0.00066	n/a	n/a
ft0	n/a	n/a	0.193 ksi	n/a	n/a
beta	n/a	n/a	-1	n/a	n/a
epstu	n/a	n/a	0.0021	n/a	n/a
Ec	n/a	n/a	n/a	3320 ksi	n/a
fct	n/a	n/a	n/a	0.0002	n/a
et	n/a	n/a	n/a	0.1	n/a
Fy	n/a	n/a	n/a	n/a	75.2 ksi
Fu	n/a	n/a	n/a	n/a	102.2 ksi
Es	n/a	n/a	n/a	n/a	28400
Esh	n/a	n/a	n/a	n/a	800
esh	n/a	n/a	n/a	n/a	1.1
eult	n/a	n/a	n/a	n/a	12.2

2.6 Concrete Materials

The material concrete01 considers the concrete to have zero tensile strength (see Figure 2.4).

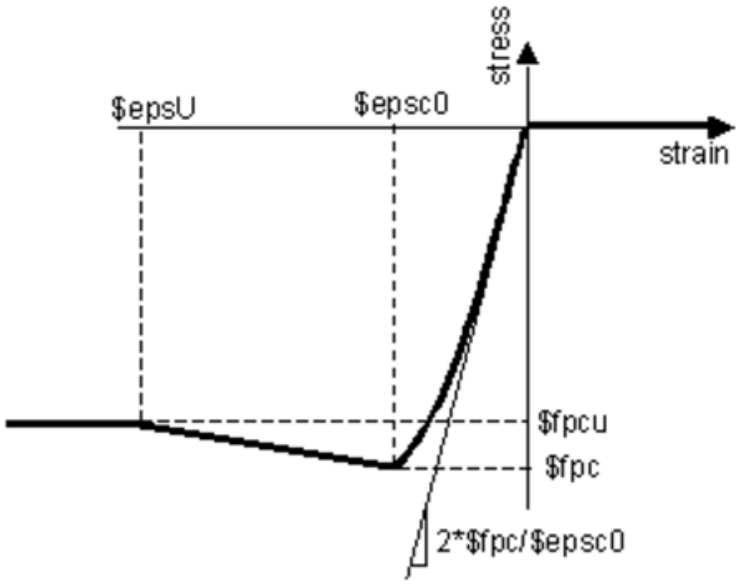

Figure 2.4: Concrete01 (Source: OpenSees documentation)

The concrete02 and concrete03 materials include parameters for the concrete tensile strength (see Figures 2.5 and 2.6). Concrete02 considers linear tension softening (based on the work of Yassin et al [7]) while concrete03 considers nonlinear tension softening.

The material concrete04 also considers concrete tensile strength with nonlinear tension softening, using the Popovics concrete model [8] (see Figure 2.7).

2.7 Model 5

Model 5 was a fiber model similar to model 4 except that it included parameters for strain penetration into the footing. The openSEES Bond-SP01 material was used to model this strain penetration. A zero length element at the column base was created and assigned the Bond-SP01 material. The reason for this element was to model the

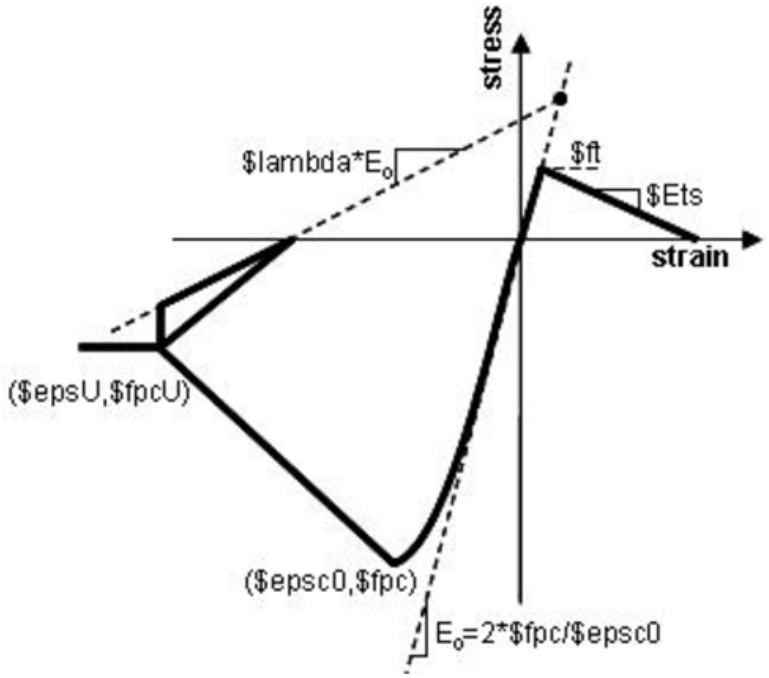

Figure 2.5: Concrete02 (Source: OpenSees documentation)

slip of the rebar in the column in the area where the reinforcing bars have not yet developed their full bond.

The parameters required for the Bond-SP01 material were: rebar yield strength (Fy), rebar slip under yield stress (Sy), rebar ultimate strength (Fu), rebar slip at ultimate strength (Su), initial hardening ratio (b), and pinching factor for the cyclic slip vs bar response (R). The parameter values are shown in Table 2.10.

The slip at yield stress, Sy, was calculated by the following equation taken from the opensees Bond-SP01 documentation, which is based on the work of Zhao and Sritharan [9].

$$Sy = 0.1 * \sqrt[a]{db/4000 * Fy/\sqrt{f'c} * (2a + 1)} + 0.013$$

In this equation, db represents the bar diameter, Fy is the yield stress of the

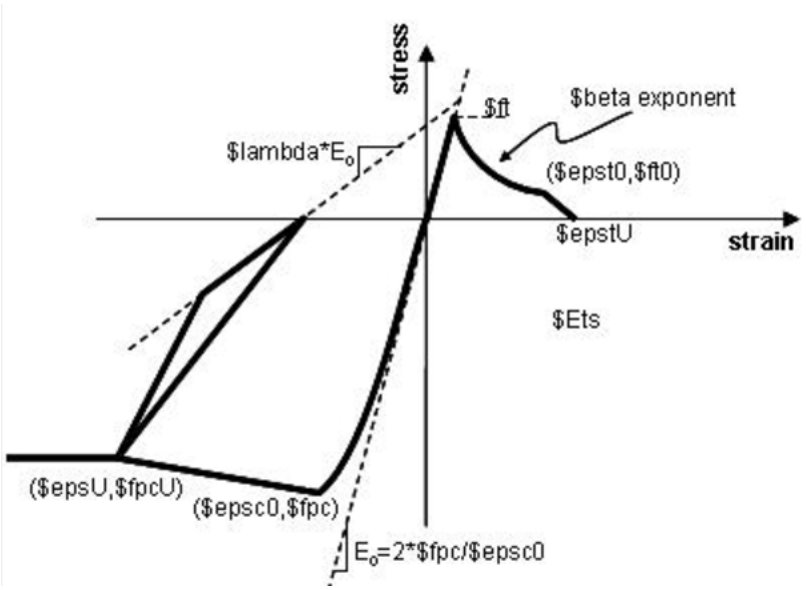

Figure 2.6: Concrete03 (Source: OpenSees documentation)

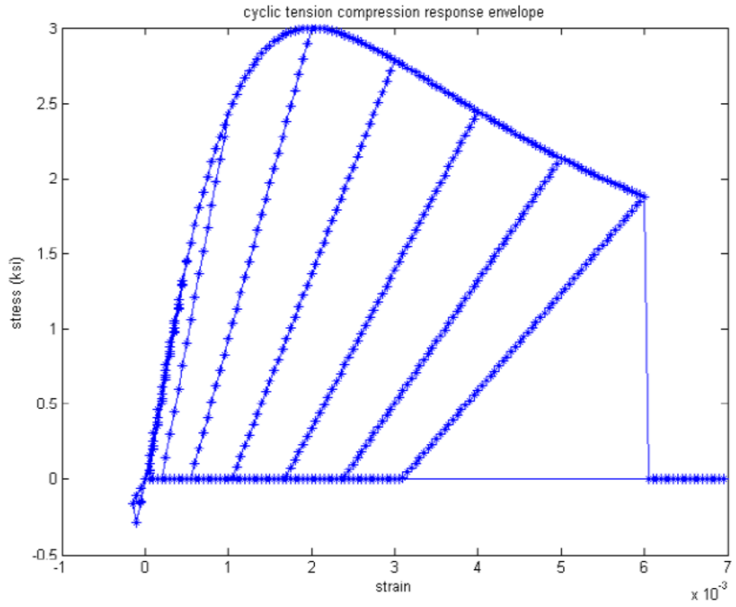

Figure 2.7: Concrete04 (Source: OpenSees documentation)

reinforcing steel, and f‘$_c$ is the compressive strength of the concrete. The variable ’a’ was taken as 0.4, per the CEB-FIB Model Code 90 [10]

The slip at ultimate stress was taken as 40 times the slip at yield [9], [11]. A range for typical initial hardening ratios, b, was given in the opensees documentation as 0.3 - 0.5. The median value of 0.4 was used in model 5. Similarly, a range for typical

Table 2.9: Parameters used for Model 5

Parameter	**Value**
Model Name	model5
No. of Elements	1
Element Type	nonlinearBeamColumn
No. of Integration Points	6
mass	0.00043 kip-sec^2
No. of Steel Fibers	18
No. of Interior Conc. Fibers (Radial Direction)	10
No. of Interior Conc. Fibers (Circumf. Direction)	20
No. of Exterior Conc. Fibers (Radial Direction)	2
No. of Exterior Conc. Fibers (Circumf. Direction)	20
Area of Steel Fibers	1.58 in ^{2}

Table 2.10: Parameters used for Bond-SP01 material

Parameter	**Value**
Fy	75 ksi
Fu	102 ksi
Sy	0.04 in
Su	1.6 in
b	0.4
R	0.7

pinching factors, R, was given in the opensees documentation as 0.5 - 1.0. The value used in model 5 was 0.7.

2.8 Number of Integration Points

It should be noted that the number of integration points was not held constant among the different concrete models. It would be ideal for this parameter to be constant, in order to have a better direct comparison of the different models' results. However, these models were very sensitive to this parameter and some of them would not converge unless a particular number of integration points was chosen.

The maximum number of integration points that the models were capable of running was 10. A trial and error approach was used to determine what number was

used. Each model was initially run with 10 integration points. If the model failed to converge using 10, the number was reduced by one until the model converged.

Chapter 3

Results

3.1 Excitation

The excitation input files for the openSEES models were obtained from DesignSafe (https://www.designsafe-ci.org/data/browser/public/nees.public/ NEES-2010-0987). The original experiment subjected the column to ten simulated earthquakes. The first nine were used in the openSEES models. The tenth was omitted because the column reached failure and hit the support structure.

The earthquake time histories were taken from two historical events: the 1989 earthquake in northern California near Loma Prieta and the 1995 earthquake in Kobe, Japan. Three different recordings of the Loma Prieta earthquake were taken from different monitoring stations in the San Francisco area. EQ1 was taken from the Agnew State Hospital station. The Corralitos Station record was used for EQ2 and again for EQ4. EQ3 and EQ6 were taken from the LGPC Station. Only one recording of the Kobe earthquake was used, but different scale factors were applied to create increasing amplitudes for the later excitations. EQ5 used the Kobe earthquake with a -0.8 scale factor. The scale factors for EQ7, EQ8, and EQ9 were +1.0, -1.2, and +1.2.

In the PEER experiment[2] , the same column was used for each of the earthquake simulations with no repairs being performed between excitations. This resulted in accumulated damage affecting the performance of the column for each subsequent excitation. The affect of cumulative damage can be seen by comparing the results of

EQ4 and EQ2 as well as the results of EQ6 and EQ3 and is discussed later in this chapter. Each of these excitation pairs used the same time history input but had notably different responses.

The accumulated damage was accounted for in the openSEES simulations by linking all of the excitations into a single input file and analyzing them in a single run. Each excitation was separated by enough time to allow all motion in the column to dissipate. The dead time between excitations was around 120-200 seconds between each earthquake. For comparison, each excitation was around 40 seconds in duration. While this differed from the actual experiment that spanned two days, it was not expected that the shortened dead time between excitations would affect the models.

The following sections describe the behavior of the models in terms of the base shear, base moment, and top deflection. The results from the PEER experiment were taken from [1].

The complete set of outputs from the openSEES models is included in the appendices. This includes the time history response of the deflection, base shear, and base moment of the column for each earthquake and each model.

3.2 Linear Elastic vs Nonlinear Models

Figures 3.1, 3.2, and 3.3 show the maximum shear force, bending moment and deflection for all models. Models 1 and 2 assumed linear elastic behavior, regardless of the stress in the column. This resulted in extremely large base shears and moments for the later earthquakes. These results were expected, as the excitations in the experimental test were chosen to ensure that the stresses in the column exceeded the linear stress range. The maximum deflections of the linear elastic models were also over-predicted, though not by as much of a margin as the base reactions. Even though the linear elastic models resulted in unrealistically high base reactions, they might still be useful as a sanity check for other models or to define limits for the

maximum values expected. This is, if other models give higher results, then it could be an indication of an error in the non-linear models.

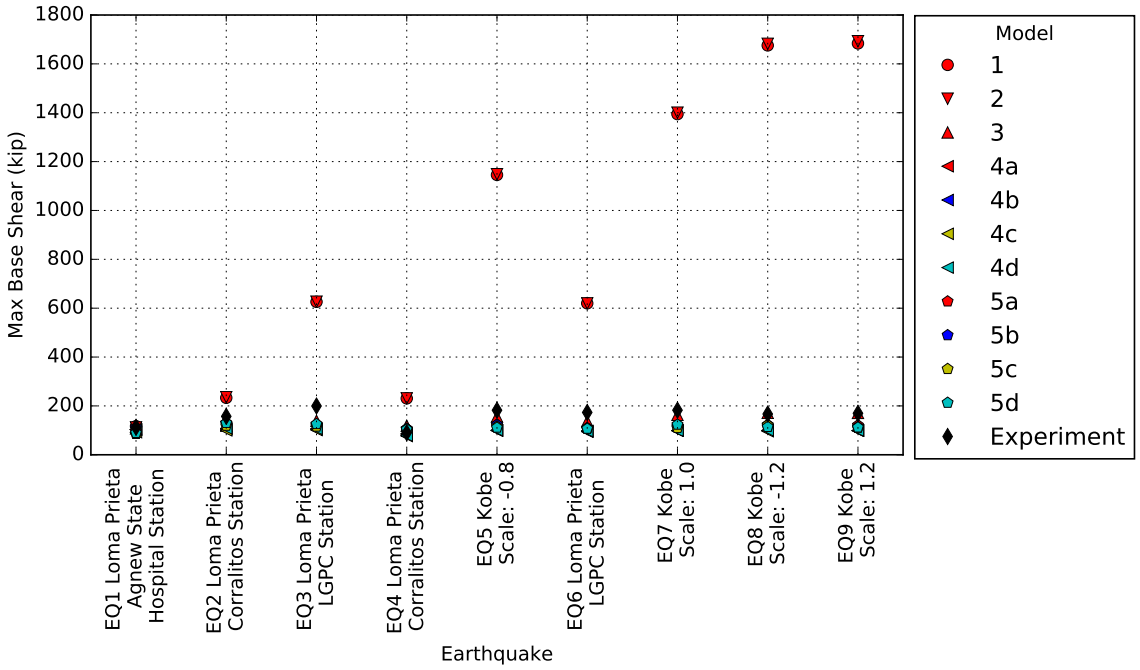

Figure 3.1: Maximum base shear of all models

Models 1 and 2 are linear models with the same type of element but different number of elements. Model 1 has only 1 beam element while model 2 has 10 elements. Figure 3.4 shows the time domain response of both models for EQ1 (Loma Prieta - Agnew State Hospital Station). As observed in this figure, the responses are very similar, with model 1 generally resulting in higher displacements throughout the excitation. Figure 3.5 shows the time domain response of both models for EQ5 (Kobe - scale -0.8). As observed in this figure, the responses are also similar, but model 2 generally resulted in higher displacements, except for the peak. Interestingly, model 1 still returned a higher peak displacement. Overall, based on the metrics defined by the blind test competition [1] it was observed that both models have very similar behavior, indicating that increasing the discretization to 10 elements did not make a big difference over using a single element in the linear elastic model.

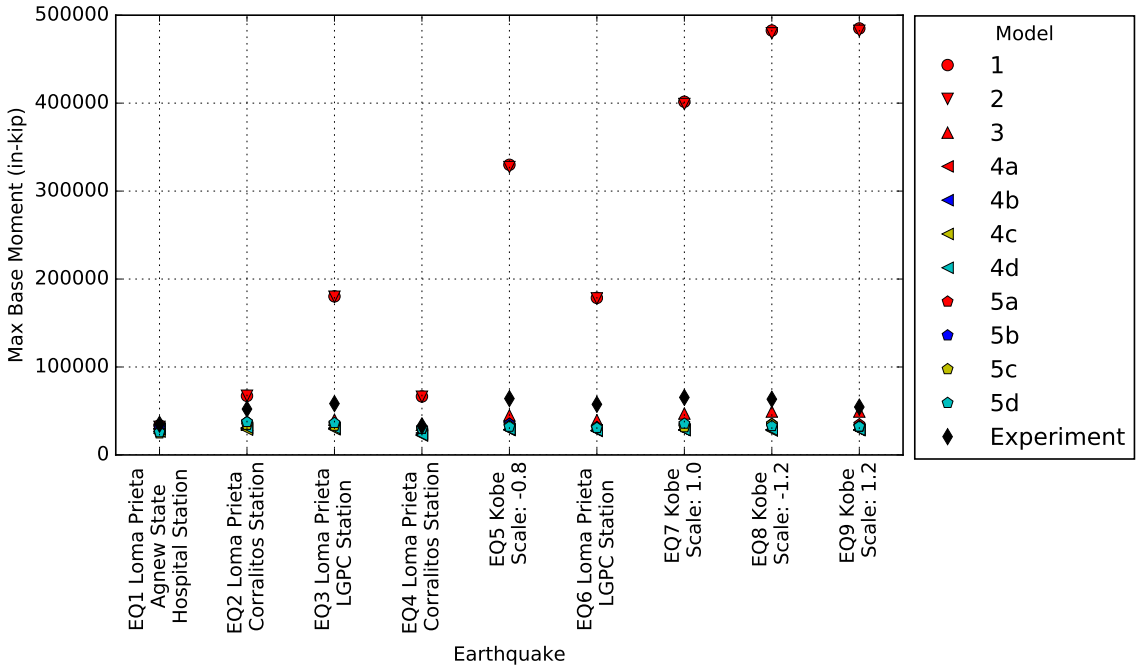

Figure 3.2: Maximum base moment of all models

Because of the high values of base shear, base moment and deflection from the linear models, it is easier to compare the results of the other models with each other if the model 1 and model 2 results are removed. Once the linear elastic models are removed, most of the models under-predict the base reactions. There are only three cases where the non linear models did not under-predict the base reactions: the maximum base shear and maximum base moment resulting from EQ4 and the maximum base moment resulting from EQ8. Of these, the base moment resulting from EQ 8 was only over-predicted by model 3. The fiber models (4 and 5) all under-predicted this reaction.

The following sections discuss in detail the behavior of the non-linear models.

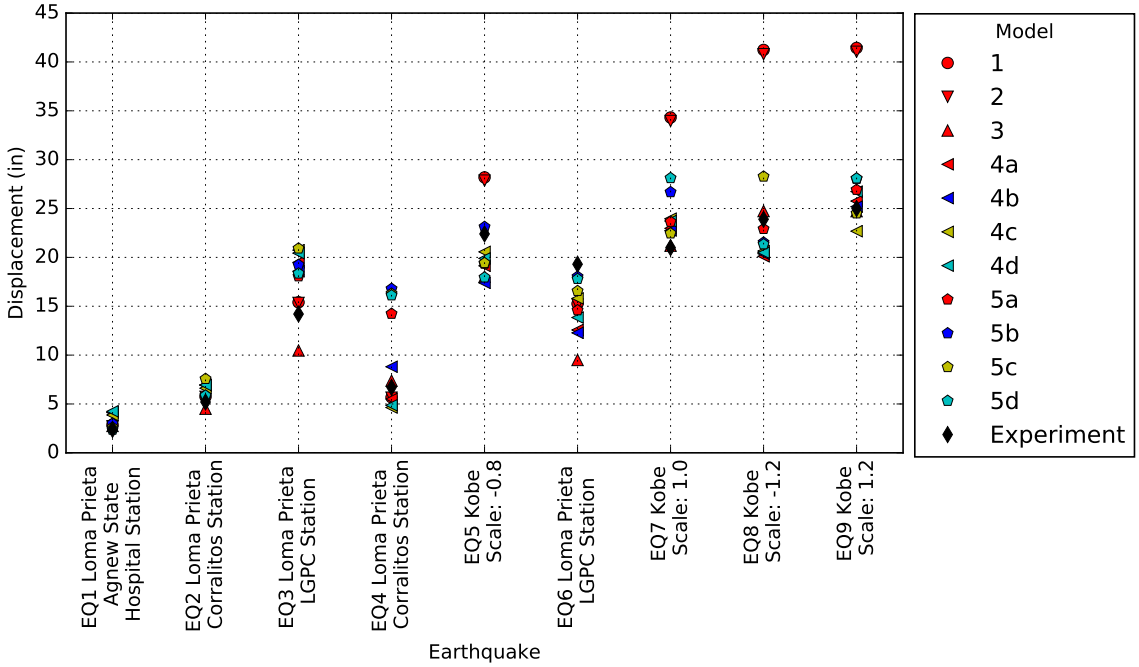

Figure 3.3: Maximum deflection of all models

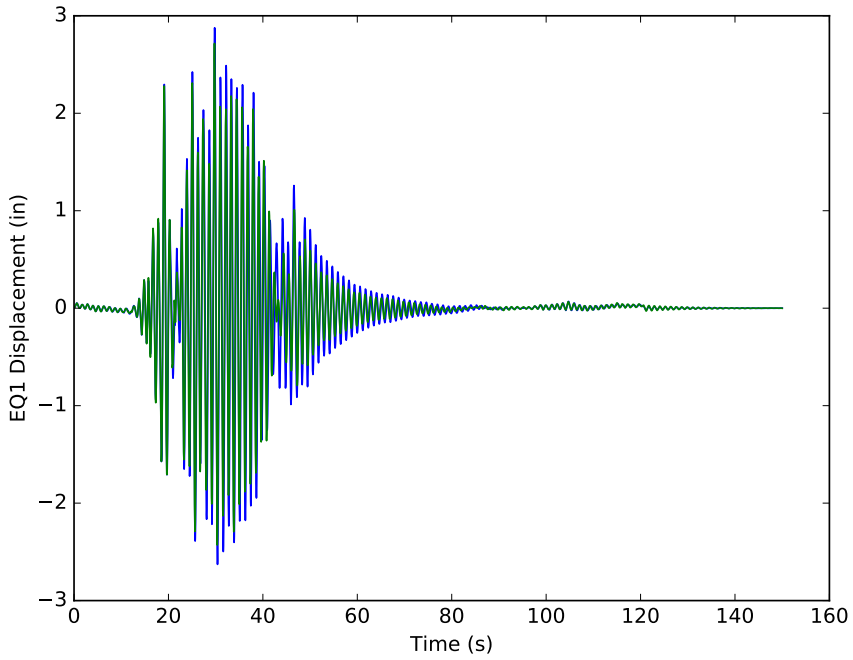

Figure 3.4: Comparing the time domain simulations of models 1 (blue) and 2 (green) for EQ 1

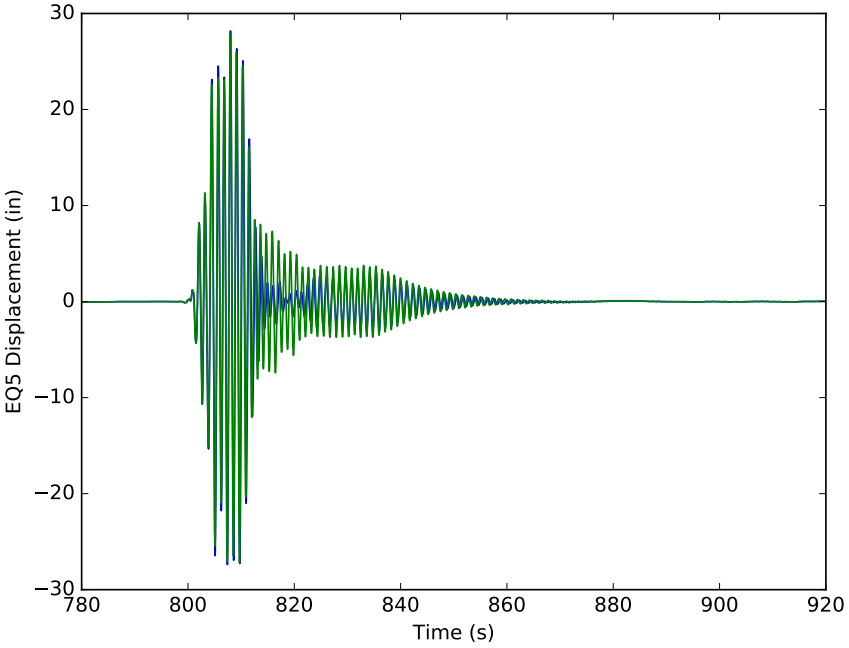

Figure 3.5: Comparing the time domain simulations of models 1 (blue) and 2(green) for EQ 5

3.3 Shear

Figure 3.6 displays the maximum base shear results from the different models grouped by excitation (earthquake).

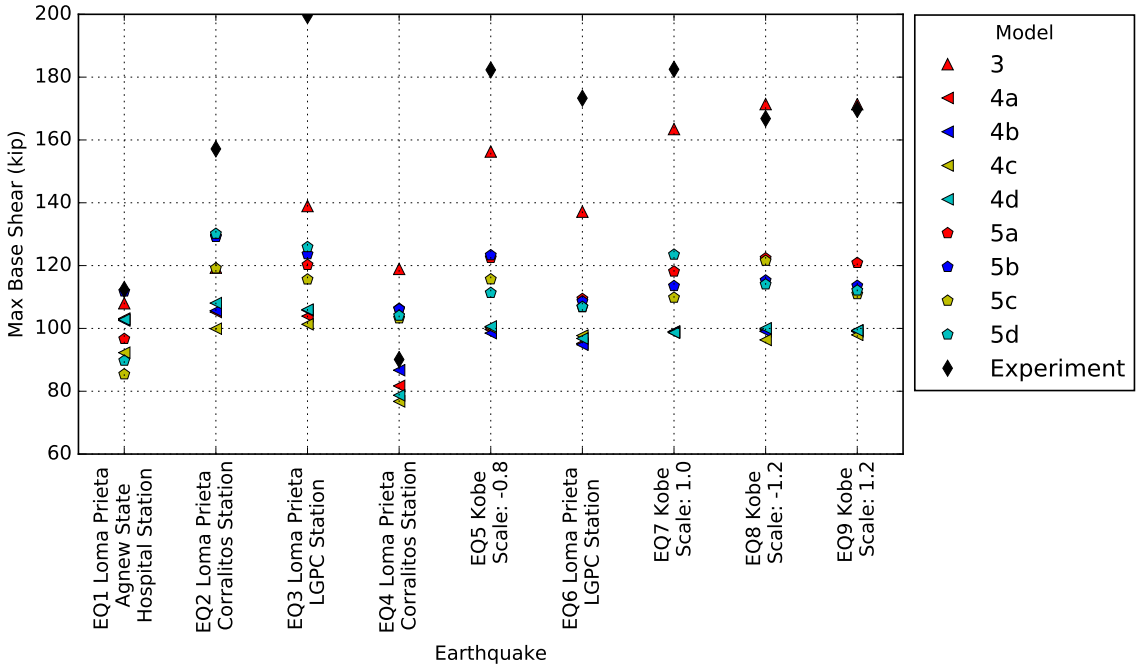

Figure 3.6: Maximum base shear omitting models 1 and 2

3.3.1 Shear - Model 3

Model 3 was similar to model 2 except that the material included parameters to account for nonlinear response when the internal stress exceeded a certain point. This resulted in more realistic base reactions and deflections than were obtained by the linear models.

Model 3 produced the most accurate predictions of the maximum base shear for all excitations except EQ2 and EQ4.

Model 3 under-predicted the maximum base shear for all excitations except EQ4 and EQ8.

Figure 3.7 shows the maximum base shear produced by model 3 compared with those obtained by the PEER experiment [2]. The results of some excitations were very accurate while others were quite far off. EQ1, EQ8, and EQ9 resulted in maximum shears very close to the experimental results - the model predicted max base shears within 4 percent of the experimentally obtained values. Conversely, EQ3 and EQ6 were much further off - the model under-predicted these values by 31 percent and 21 percent, respectively.

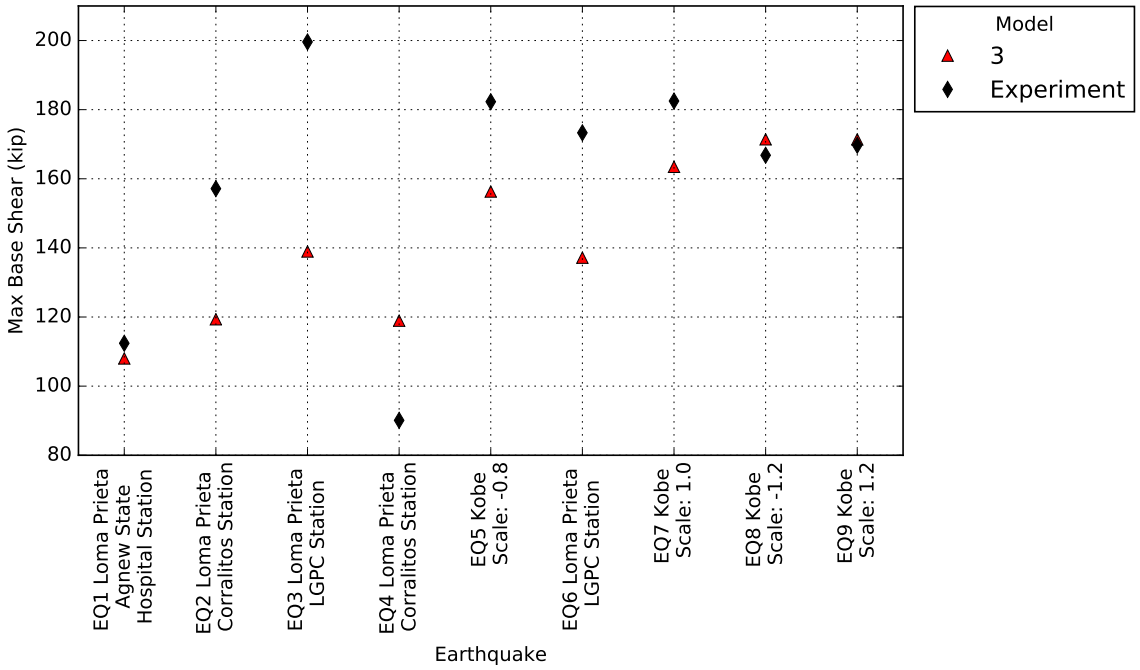

Figure 3.7: Maximum base shear of model 3 compared with the experimental results

3.3.2 Shear - Models 4 and 5

Models 4 and 5 were both fiber models. The only difference between the two model sets was that model 5 included parameters for strain penetration into the footing.

Model 5 produced more accurate maximum base shears than model 4 when compared with the experimental results for all excitations except EQ1 and EQ4.

Model 4 under-predicted the maximum base shear for all excitations. Likewise, model 5 also under-predicted the maximum base shear for all excitations.

The amount that these models under-predicted the base shear varied from model to model as well as from excitation to excitation. The most accurate prediction was from models 4a, 4b, and 4c during EQ1. These three models all predicted a max base shear within 9 percent of the experimentally obtained value. Conversely, the least accurate prediction was generated by model 4c during EQ3. This model predicted a maximum base shear of 101 kips, while the PEER experiment [2] returned a value of 200 kips for this excitation.

3.4 Moments

Figure 3.8 displays the maximum base moment results from the different models grouped by excitation (earthquake).

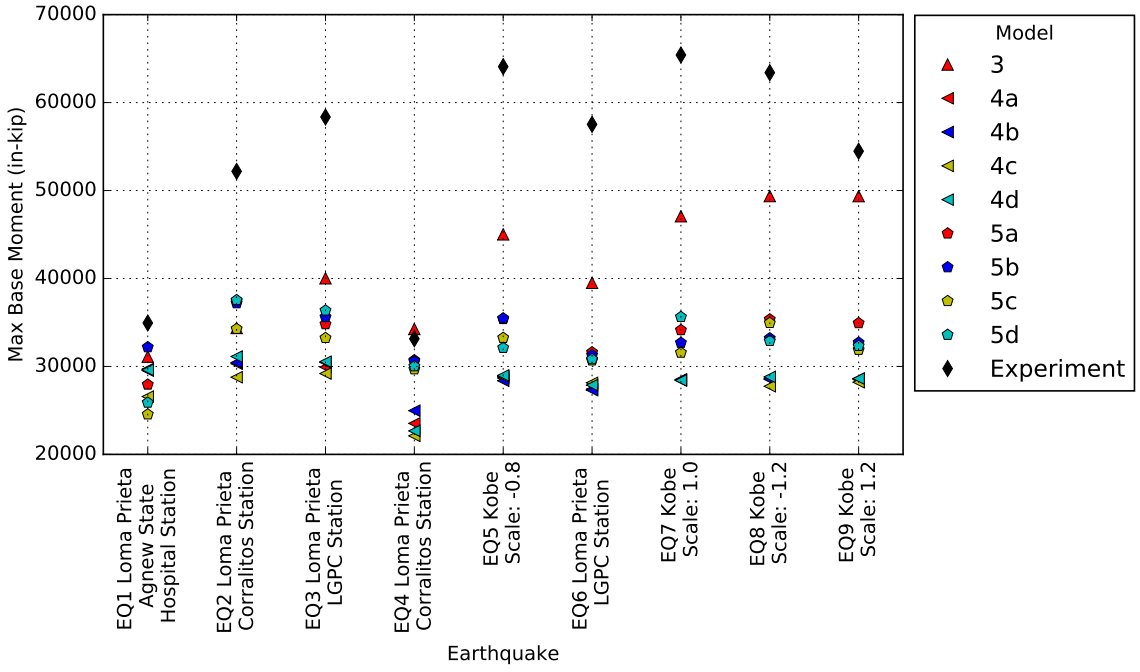

Figure 3.8: Maximum base moment omitting models 1 and 2

3.4.1 Moment - Model 3

Model 3 produced the most accurate predictions of the maximum base moment for all excitations except EQ1 and EQ2.

Model 3 under-predicted the maximum base moment for all excitations except EQ4.

Figure 3.9 shows the maximum base moments produced by model 3 compared with those obtained by the experiment. The results of some excitations were very accurate while others were quite far off. EQ1, EQ4, and EQ9 resulted in maximum base moments very close to the experimental results - the model predicted values within 12 percent of the experimentally obtained values. Conversely, EQ2, EQ3, and EQ5 were much further off - the model under-predicted these values by nearly 33 percent.

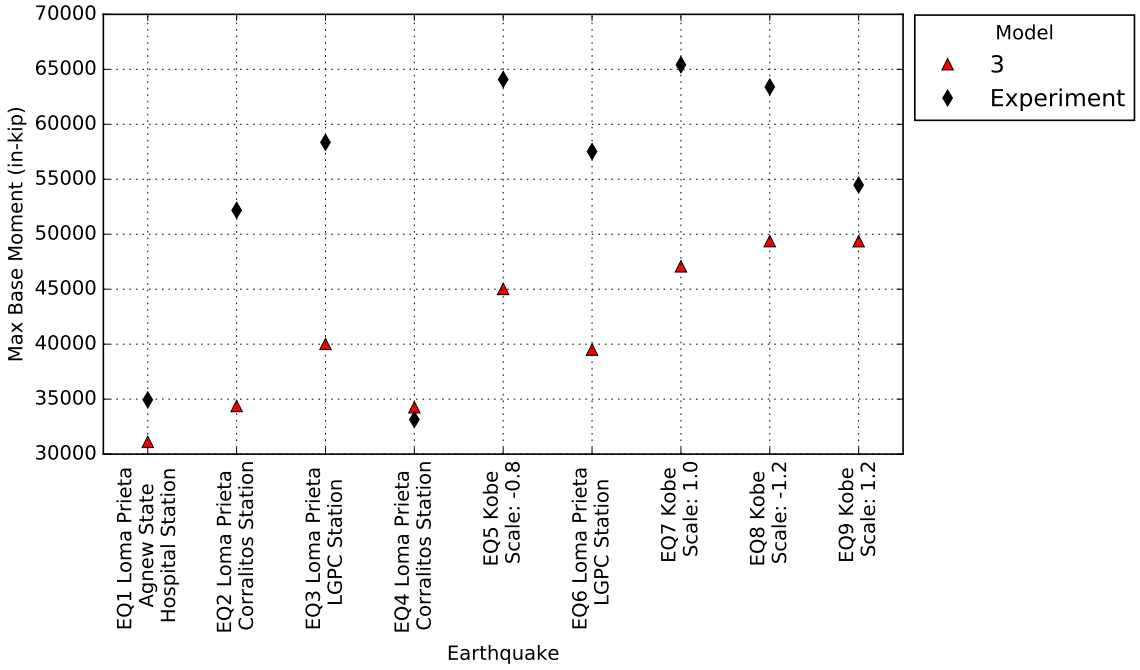

Figure 3.9: Maximum base moment of model 3 compared with the experimental results

3.4.2 Moments - Models 4 and 5

Model 5 produced more accurate maximum base moments than model 4 when compared with the experimental results for all excitations except EQ1.

Similar to the maximum base shears discussed previously, both models 4 and 5 under-predicted the maximum base moments for all excitations.

The amount that these models under-predicted the base moment varied from model to model as well as from excitation to excitation. The most accurate prediction was from model 5a during EQ4. This model predicted a max base moment within 8 percent of the experimentally obtained value. Conversely, the least accurate prediction was generated by model 4b during EQ5. This model predicted a max base moment (28371 in-kips) that was only 44 percent of the experimentally obtained value (64083 in-kips) [2].

3.5 Deflections

Figure 3.10 displays the maximum deflection results from the different models grouped by excitation (earthquake).

3.5.1 Deflections - Model 3

Model 3 produced the most accurate predictions of the maximum deflection for EQ2, EQ3, EQ4, EQ7, and EQ8. This was different than the max base shear and moment in that model 3 did not perform substantially better than models 4 or 5 in this aspect. It had the most accurate prediction only for about half of the excitations. In fact, model 3 had the least accurate prediction among the non-linear models for EQ6

Model 3 under-predicted the maximum deflection for 5 of the 9 excitations and over-predicted for the remaining 4.

Figure 3.11 shows the maximum deflections produced by model 3 compared with those obtained by the experiment. The results of some excitations were very accurate

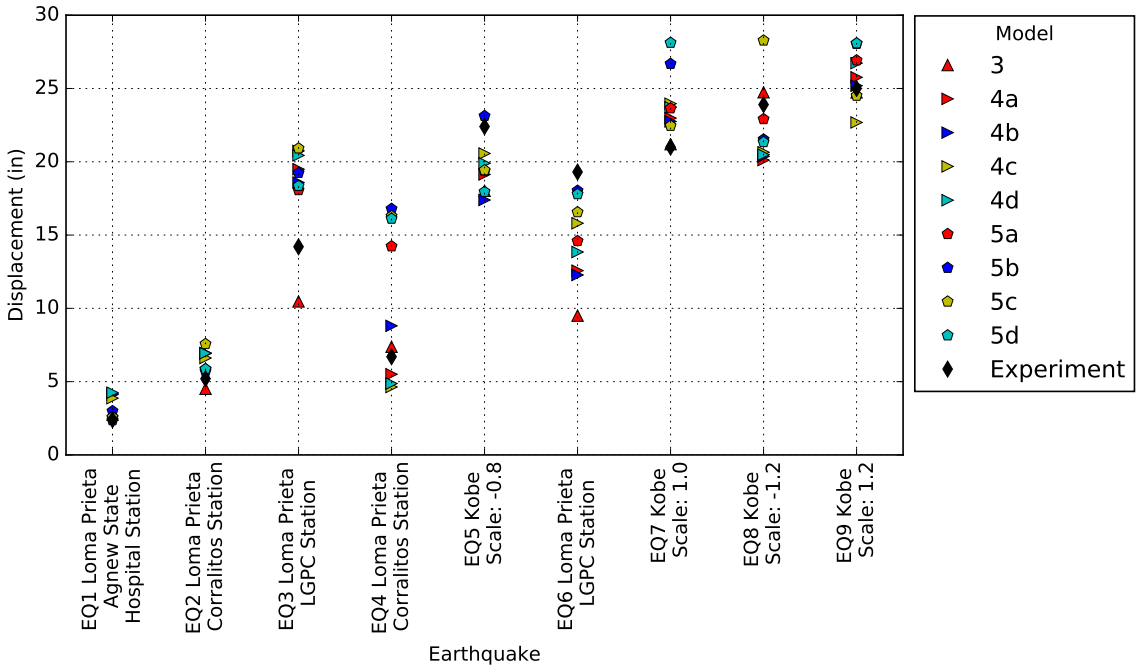

Figure 3.10: Maximum deflection omitting models 1 and 2

while others were quite far off. EQ7, EQ8, and EQ9 resulted in maximum deflections very close to the experimental results - the model predicted values within 3 percent of the experimentally obtained values. Conversely, EQ6 was much further off - the model under-predicted this value by nearly 50 percent.

3.5.2 Deflections - Models 4 and 5

With regards to accuracy, neither model 4 or model 5 performed better than the other. During EQ4, model 4 produced a more accurate maximum deflection prediction than model 5, but then during EQ6, model 5 produced a more accurate prediction. During the other 7 excitations, the predictions were intermixed, with neither model 4 or model 5 showing any advantage.

There was also no apparent trend to whether either model model under- or over-predicted the maximum deflections. This was markedly different than the base reactions. Nearly all of the maximum base reactions were under-predicted by the non-linear models, but the same cannot be said for the maximum deflections. Instead,

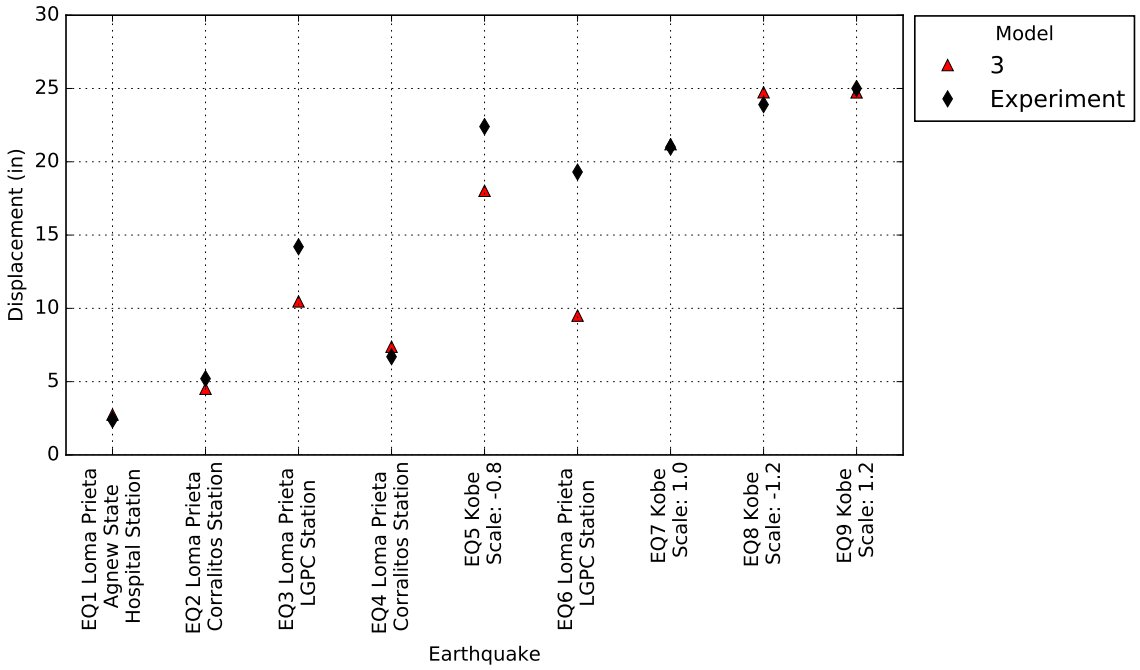

Figure 3.11: Maximum deflection of model 3 compared with the experimental results

both model 4 and model 5 under-predicted the max deflection for about half of the excitations, and over-predicted for about half of the excitations.

The amount that these models under- or over-predicted the maximum deflection varied from model to model as well as from excitation to excitation. The most accurate predictions were from models 5d (EQ1), 5b (EQ5), 5a (EQ8), 5c (EQ9), 4a (EQ9), and 4b (EQ9). These models all predicted max deflections within 5 percent of the experimentally obtained values. Conversely, the least accurate prediction was generated by model 5b during EQ4. This model predicted a max deflection (16.8 in) that was 250 percent of the experimentally obtained value (6.7 in) [2].

3.6 Effect of Different Concrete Materials

It was observed that the different materials used in models 4 and 5 did make a substantial difference in the maximum displacement, maximum base shear, and maximum base moment.

Figure 3.12, Figure 3.13, and Figure 3.14 compare the results of model4a, 4b, 4c, and 4d. The only difference in these models was the concrete material outside of the rebar cage. It can be seen in Figure 3.13 that the concrete material has the potential to affect the maximum base reactions. The range of maximum base moments produced by the different materials for EQ4 was about 11 percent. Although, on some excitations, the material had very little effect - as evident in Figure 3.13 and Figure 3.12 EQ7. The different materials had a similarly inconsistent effect on the maximum deflection of model 4. Figure 3.14 shows that on some excitations - EQ1, EQ2, & EQ8 - there was very little effect caused by the material changes, while EQ4, EQ6, & EQ9 show a substantial range of max deflections caused by the material changes.

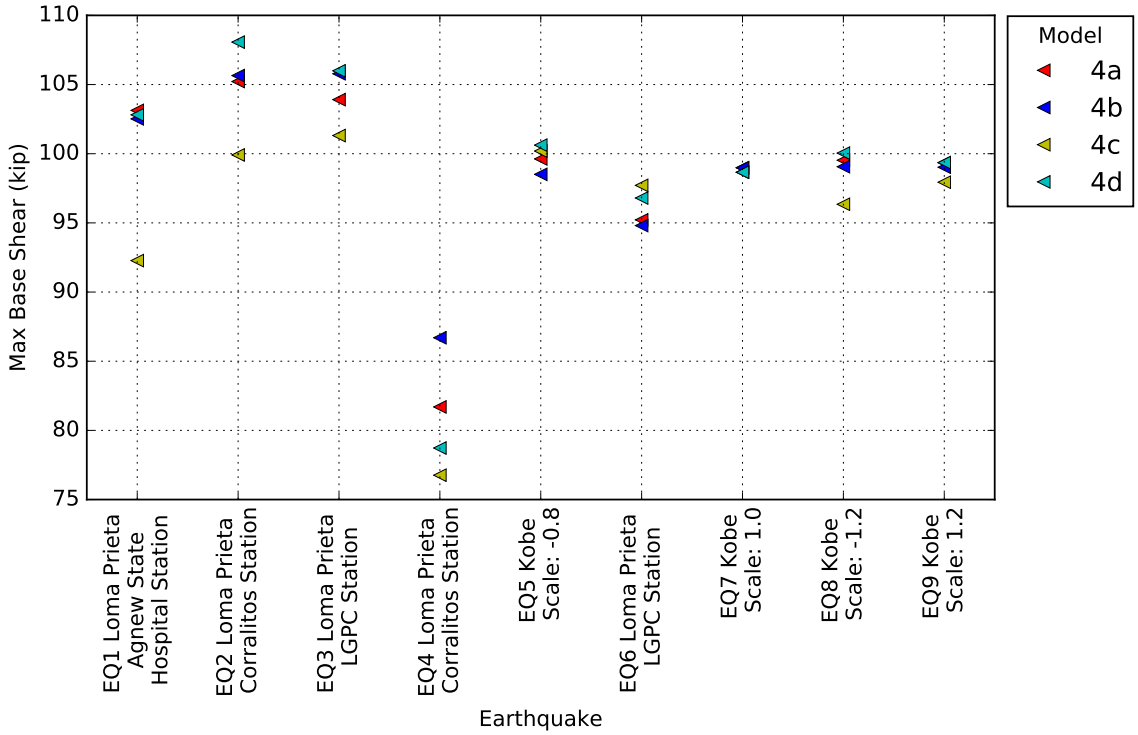

Figure 3.12: Comparing maximum base shear of models 4a, 4b, 4c, and 4d

Figure 3.15, Figure 3.16, and Figure 3.17 compare the results of model5a, 5b, 5c, and 5d. Similar to model4, the only difference in these models was the concrete material outside of the rebar cage. It can be seen in Figure 3.16 that the concrete material

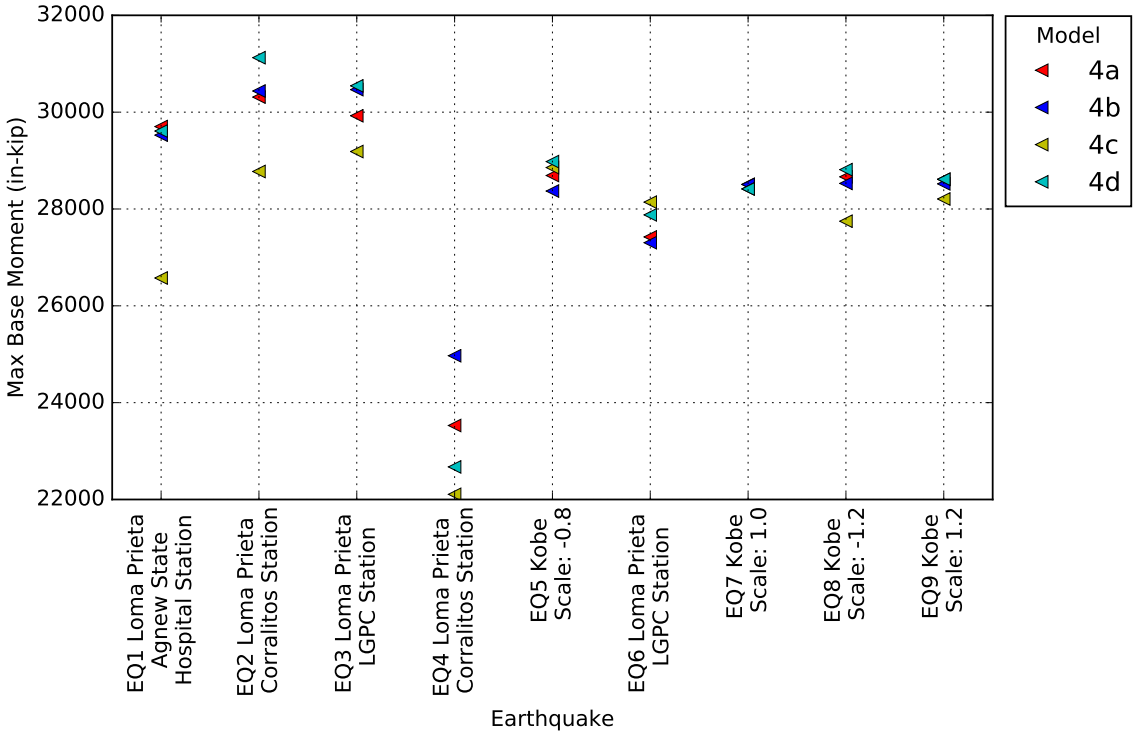

Figure 3.13: Comparing maximum base moment of models 4a, 4b, 4c, and 4d

has the potential to affect the maximum base reactions. The range of maximum base moments produced by the different materials for EQ1 was about 24 percent. Although, on some excitations, the material had a smaller effect - as evident in Figure 3.15 and Figure 3.16 EQ4 and EQ6. The different materials had a similarly inconsistent effect on the maximum deflection of model 5. Figure 3.17 shows that on some excitations, such as EQ1, there was very little effect caused by the material changes, while EQ6, EQ7, & EQ8 show a substantial range of max deflections caused by the material changes (nearly 25 percent).

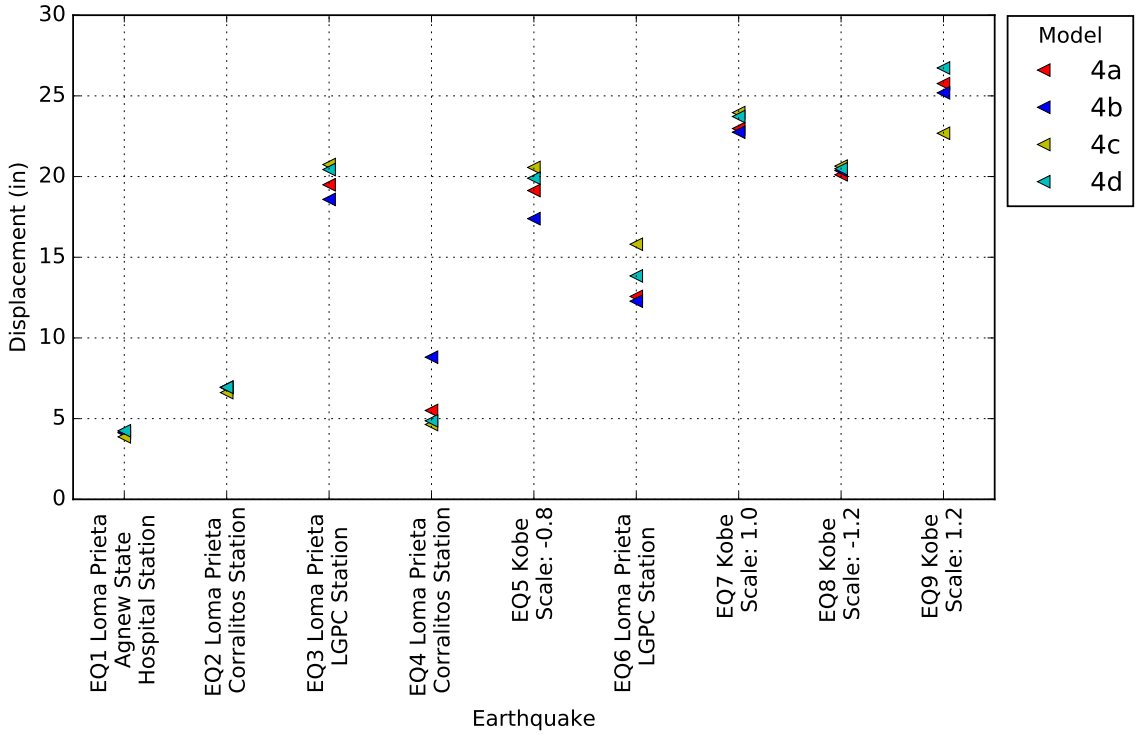

Figure 3.14: Comparing maximum deflection of models 4a, 4b, 4c, and 4d

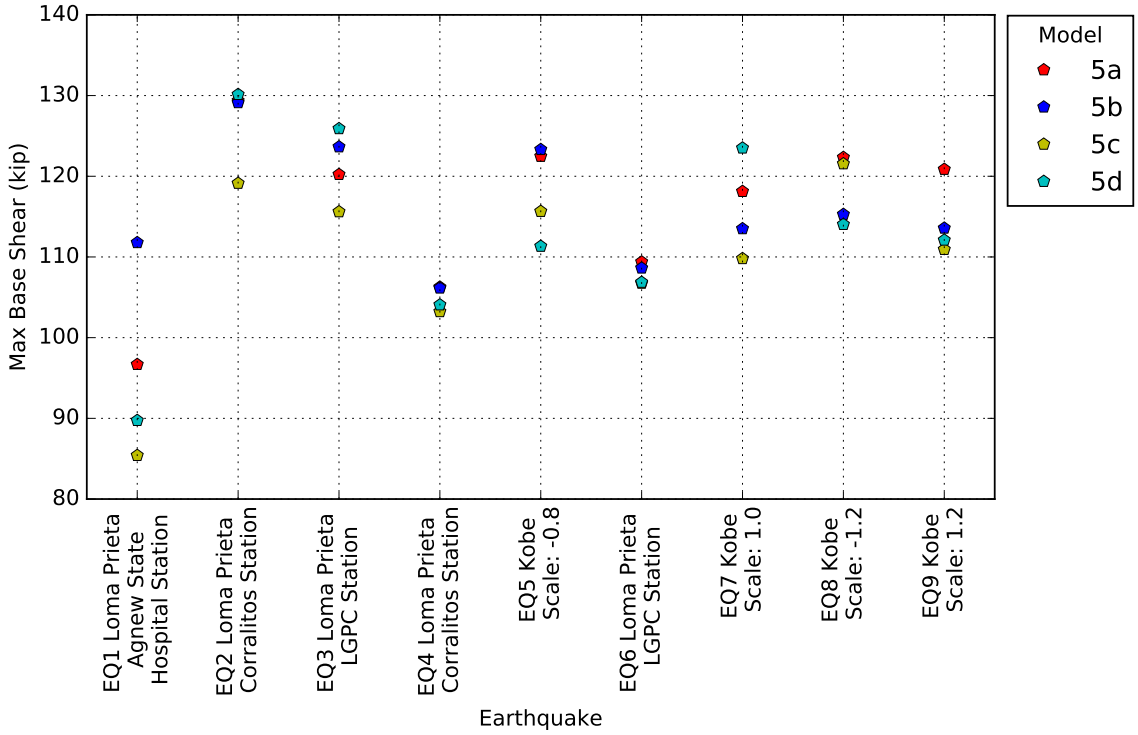

Figure 3.15: Comparing maximum base shear of models 5a, 5b, 5c, and 5d

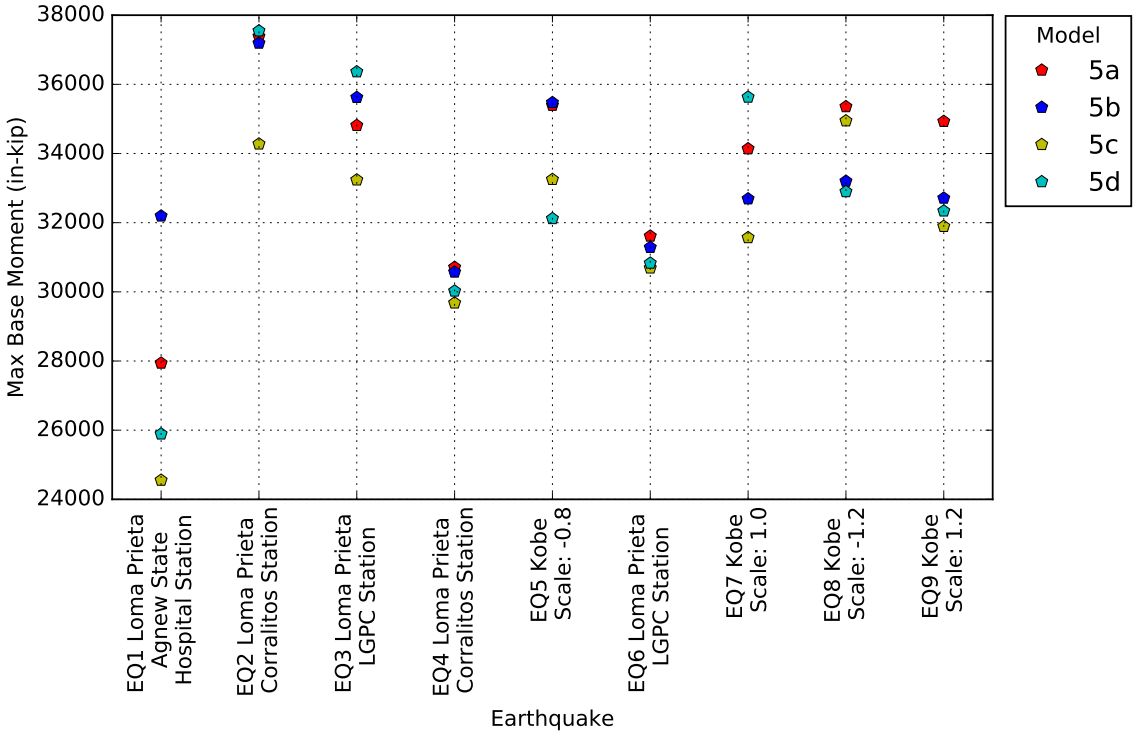

Figure 3.16: Comparing maximum base moment of models 5a, 5b, 5c, and 5d

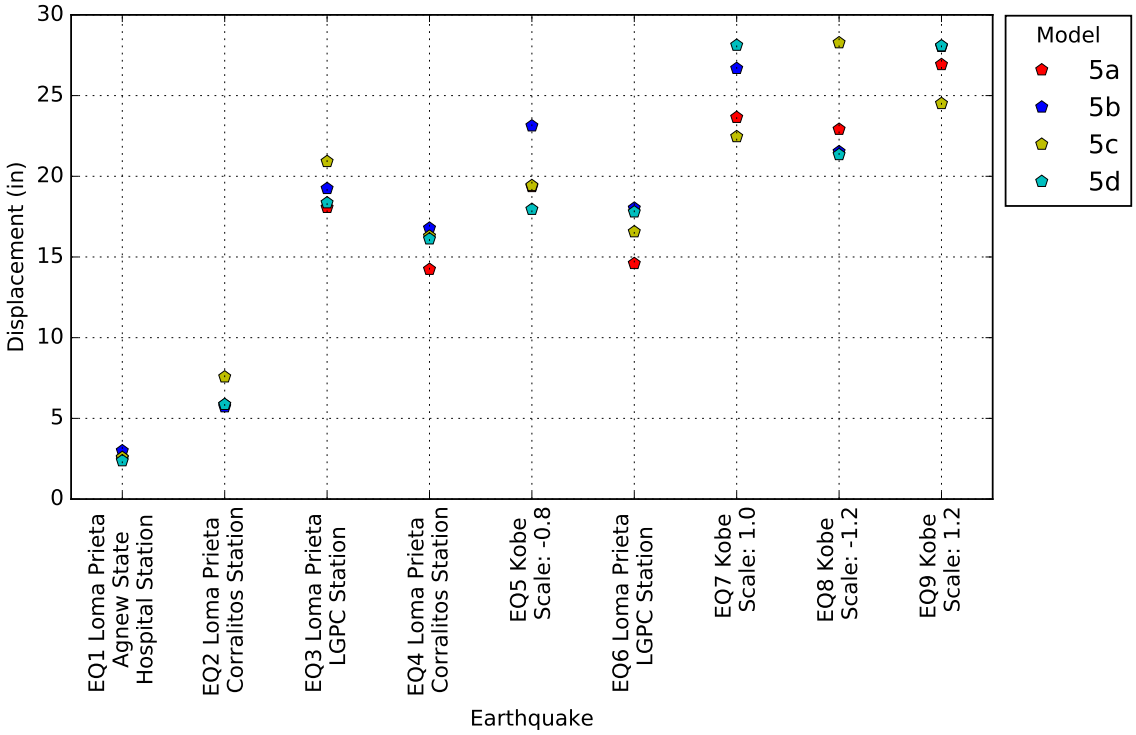

Figure 3.17: Comparing maximum deflection of models 5a, 5b, 5c, and 5d

3.7 Influence of the Excitation / Damage Accumulation

The input motion of EQ4 was recorded at the same station and earthquake as EQ2 (Corralitos Station, see Appendix A). It is interesting to note that even though the excitation was the same, the column did not produce the same response. The maximum base moment reaction for EQ2 was 52180 in-kips [2] while it was only 33143 in-kips for EQ4 [2]. Therefore, the base reaction produced from EQ4 was 36 percent lower than that produced from EQ2. The maximum deflection, on the other hand, increased 22 percent, 6.7 in during EQ4 compared to 5.2 in during EQ2 [2]. Since the input motion was similar for both excitations, the only difference was accumulated damage. This can also be observed in the moment-curvature plots for EQ2 and EQ3 that were generated from the PEER experiment [2] (Figure 3.18 and Figure 3.19)

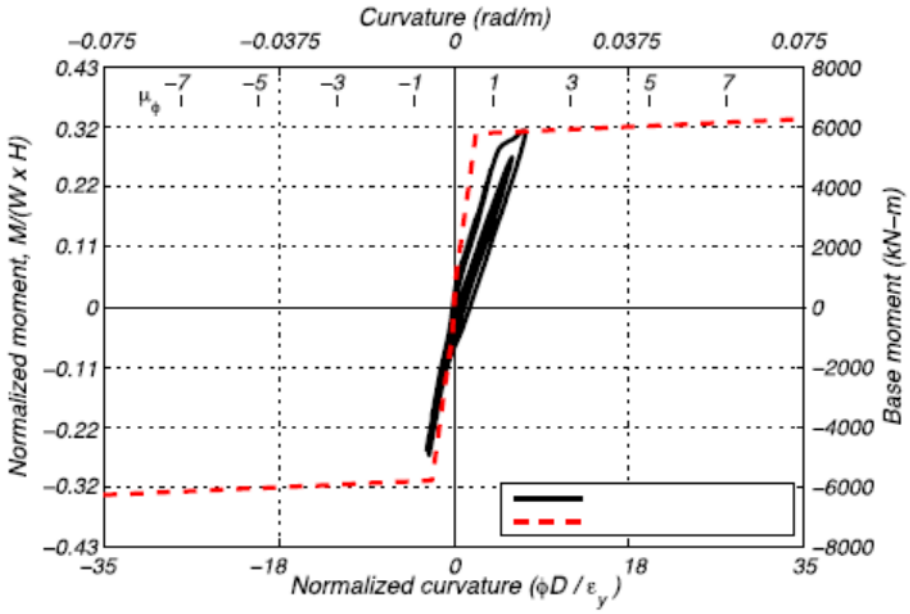

Figure 3.18: Moment-curvature plot of EQ2 generated from the PEER experiment [2]

Similarly, EQ6 was recorded at the same station and earthquake as EQ3 (LGPC Station, see Appendix A). The maximum base moment reaction for EQ3 was 58357 in-kips [2] which was similar to the 57525 in-kips generated from EQ6 [2]. However,

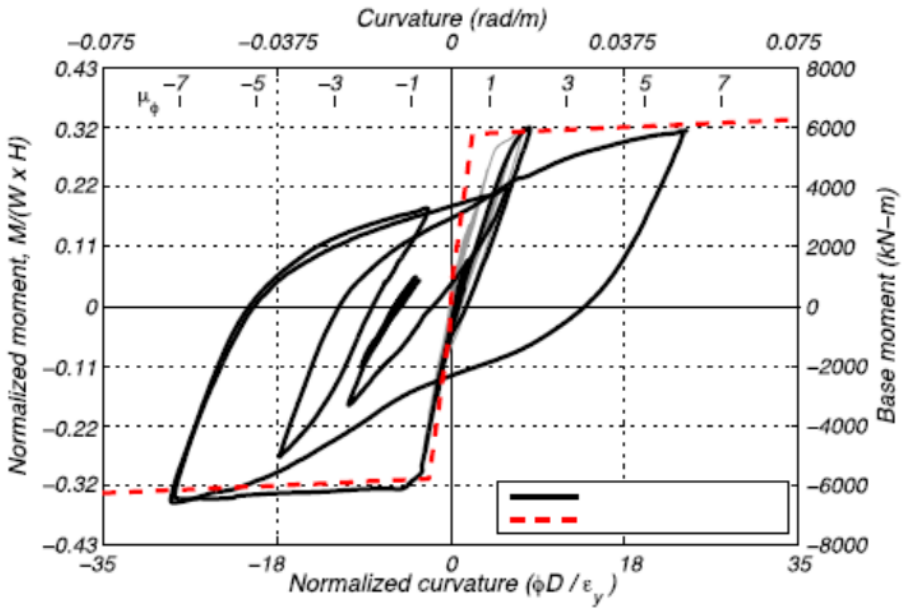

Figure 3.19: Moment-curvature plot of EQ3 generated from the PEER experiment [2]

the maximum deflection was 36 percent higher in EQ6 compared with EQ3, 19.3 in vs 14.2 in [2]. Again, since the input motion was similar for both excitations, the only difference was accumulated damage. This can also be observed in the moment-curvature plots for EQ4 and EQ5 that were generated from the PEER experiment [2] (Figure 3.20 and Figure 3.21)

The openSEES models showed different behavior when compared with the experimental test with regards to the effects of damage accumulation. In the linear elastic models, for example, there were negligible differences in both the base reactions and the deflections between EQ6/EQ3 and EQ4/EQ2. This was expected because damage occurs when the stress exceeds the elastic range, so if the model considers all stress as elastic, then there can be no damage accumulation.

In the nonlinear models, though, the effects of damage accumulation were evident. Figures 3.22, 3.23, 3.24 and 3.25 show the moment curvature plots generated from model 3 during EQ2, EQ3, EQ4, and EQ5 respectively. These can be compared with the moment curvature plots generated from the PEER experiment [2] shown

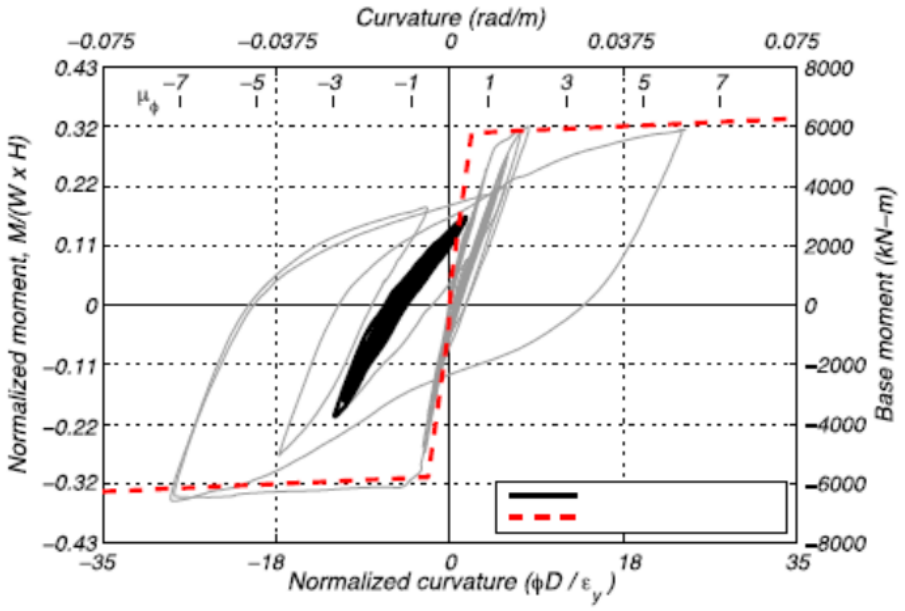

Figure 3.20: Moment-curvature plot of EQ4 generated from the PEER experiment [2]

in Figures 3.18, 3.19, 3.20, and 3.21. The plots generated from openSEES (Figures 3.22, 3.23, 3.24 and 3.25) demonstrate how damage is accumulating during each of the excitations. Since all of the nine excitations were combined and ran in a single simulation, each excitation begins exactly how the previous one left off, including any accumulated damage.

The effects of accumulated damage could also bee seen in the moment-curvature plots generated from models 4 and 5 (the fiber models). And since the fiber models were modeled using concrete and steel materials, they accounted for degradation in the column. Figures 3.26, & 3.27 show the moment-curvature responses from EQ4 and EQ5 generated from model 4a. The full set of moment-curvature plots for all excitations from all of the nonlinear models is included in the appendices.

Both the maximum base shear and moment decreased with the subsequent earthquakes (EQ4 and EQ6) compared with the earlier earthquakes (EQ2 and EQ3) in the openSEES simulations, which generally matches the response from the PEER experiment. However, the maximum deflection at the top of the column did not con-

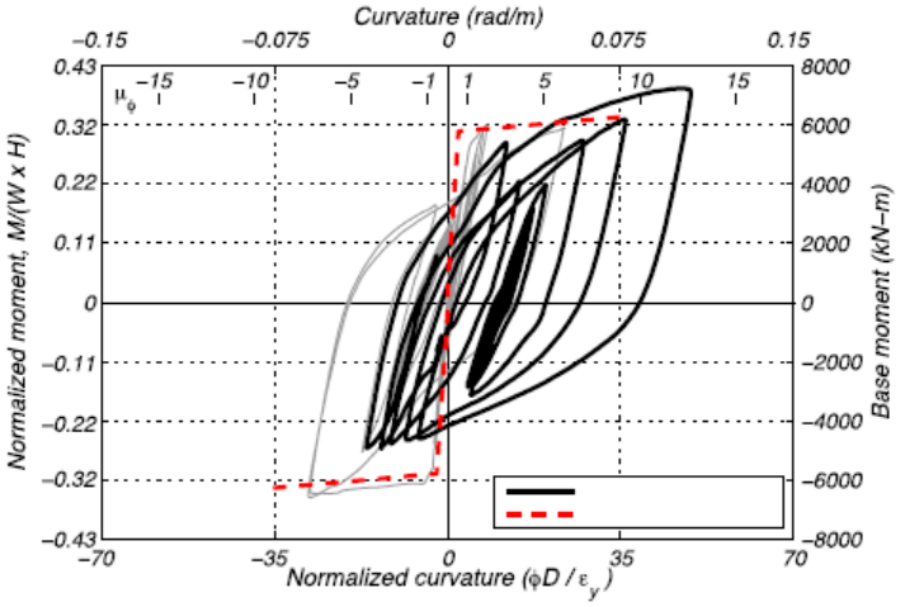

Figure 3.21: Moment-curvature plot of EQ5 generated from the PEER experiment [2]

sistently increase in the openSEES simulations as it did in the PEER experiment [2]. In fact, all of the openSEES models generated a smaller maximum deflection during EQ6 than they did during EQ3, which is the opposite of the shake table test results (Figure 3.10).

Table 3.1: Maximum Base Moment

Maximum Base Moment (in-kips)													
		Model											
		1	2	3	4a	4b	4c	4d	5a	5b	5c	5d	Experiment
Earthquake	EQ1	33674	31918	31110	29702	29525	26575	29610	27940	32193	24553	25890	34940
	EQ2	67155	67313	34372	30311	30437	28774	31125	37387	37192	34276	37546	52180
	EQ3	180282	179894	40023	29926	30465	29187	30544	34811	35621	33236	36363	58357
	EQ4	66474	66199	34257	23528	24969	22107	22673	30710	30572	29678	30023	33143
	EQ5	329898	327281	45019	28692	28371	28855	28979	35395	35473	33250	32118	64083
	EQ6	178561	177981	39506	27423	27303	28142	27878	31612	31286	30690	30830	57525
	EQ7	401593	398981	47078	28510	28506	28414	28414	34137	32689	31568	35630	65410
	EQ8	482567	479326	49370	28664	28528	27748	28812	35355	33199	34945	32897	63401
	EQ9	484933	482238	49364	28613	28518	28206	28615	34928	32709	31892	32338	54472

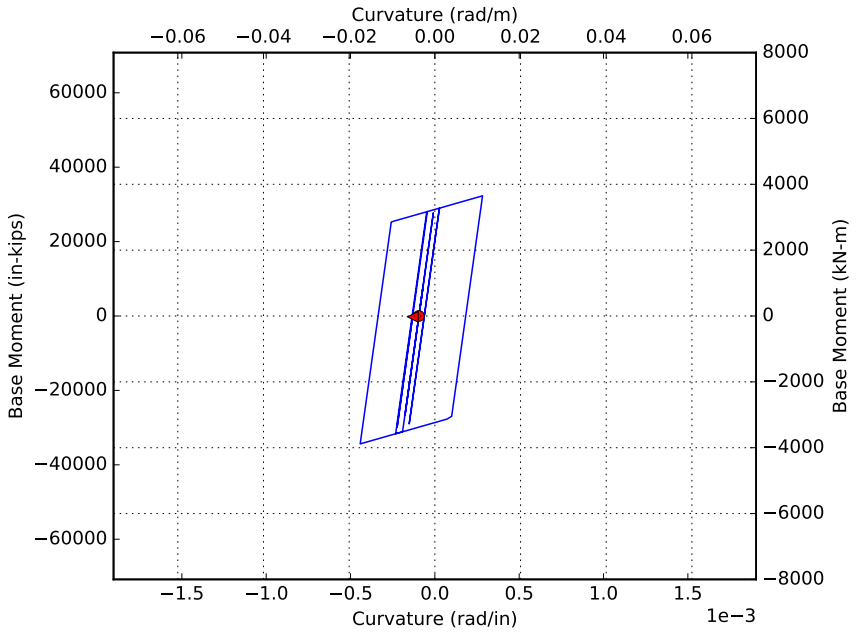

Figure 3.22: Moment-curvature plot of EQ2 generated from model 3

Table 3.2: Maximum Base Shear

Maximum Base Shear (kips)													
		Model											
		1	2	3	4a	4b	4c	4d	5a	5b	5c	5d	Experiment
Earthquake	EQ1	117	112	108	103	103	92	103	97	112	85	90	112
	EQ2	233	236	119	105	106	100	108	129	129	119	130	157
	EQ3	626	627	139	104	106	101	106	120	124	116	126	200
	EQ4	231	231	119	82	87	77	79	106	106	103	104	90
	EQ5	1145	1148	156	100	99	100	101	122	123	116	111	182
	EQ6	620	620	137	95	95	98	97	109	109	107	107	173
	EQ7	1394	1400	163	99	99	99	99	118	114	110	124	183
	EQ8	1676	1682	171	100	99	96	100	122	115	122	114	167
	EQ9	1684	1693	171	99	99	98	99	121	114	111	112	170

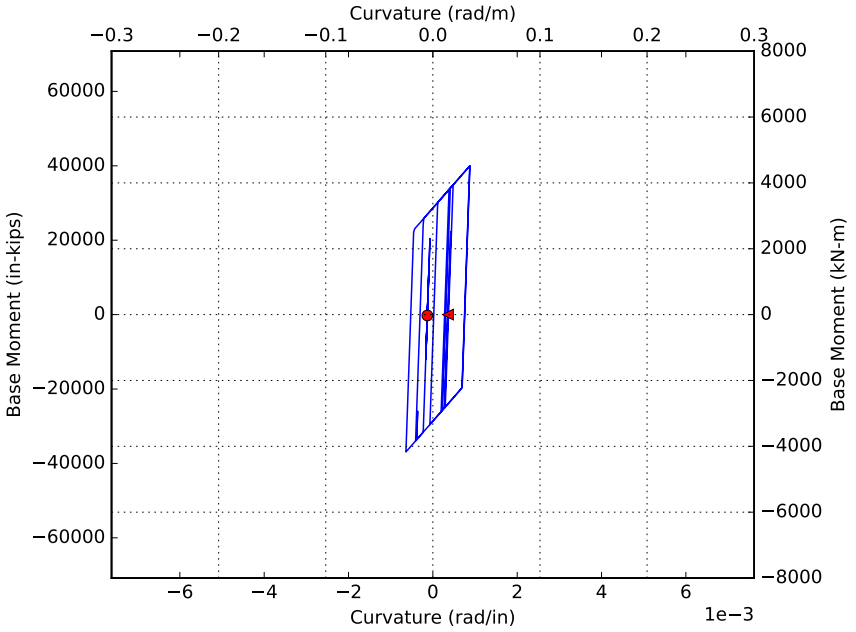

Figure 3.23: Moment-curvature plot of EQ3 generated from model 3

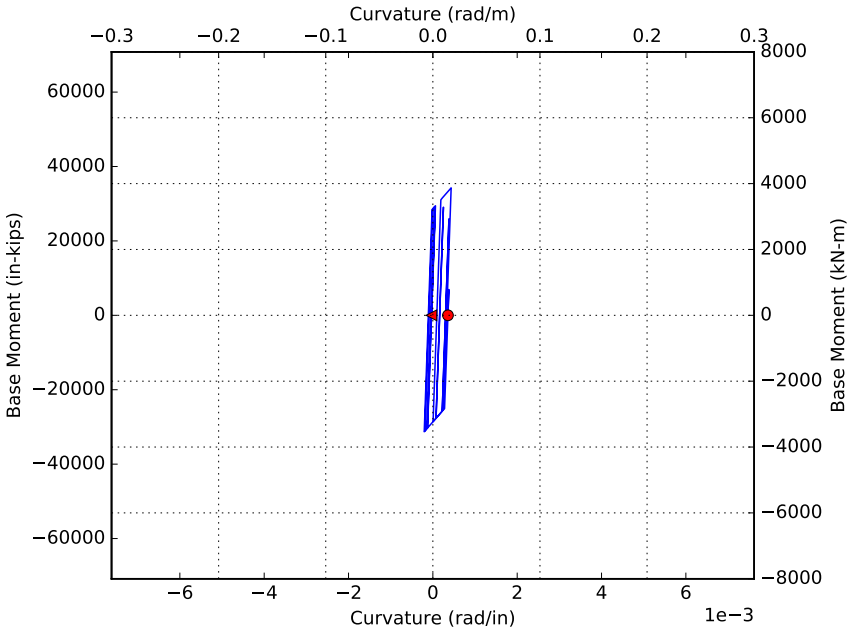

Figure 3.24: Moment-curvature plot of EQ4 generated from model 3

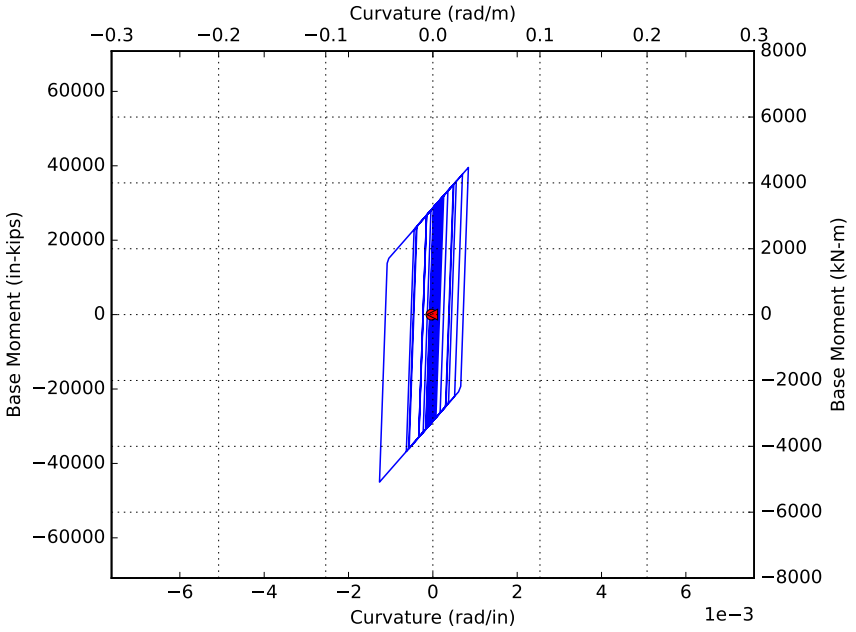

Figure 3.25: Moment-curvature plot of EQ5 generated from model 3

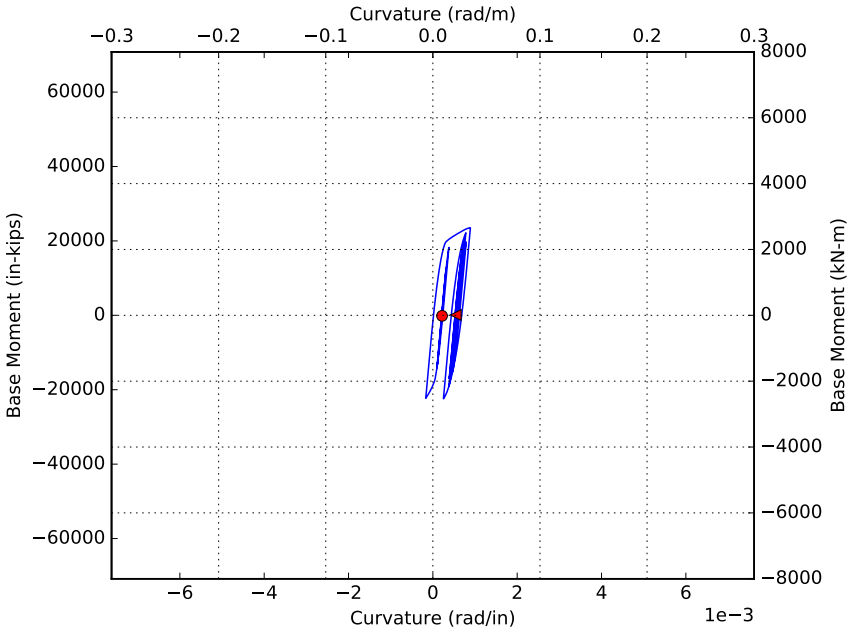

Figure 3.26: Moment-Curvature Plot of EQ4 generated from model 4a

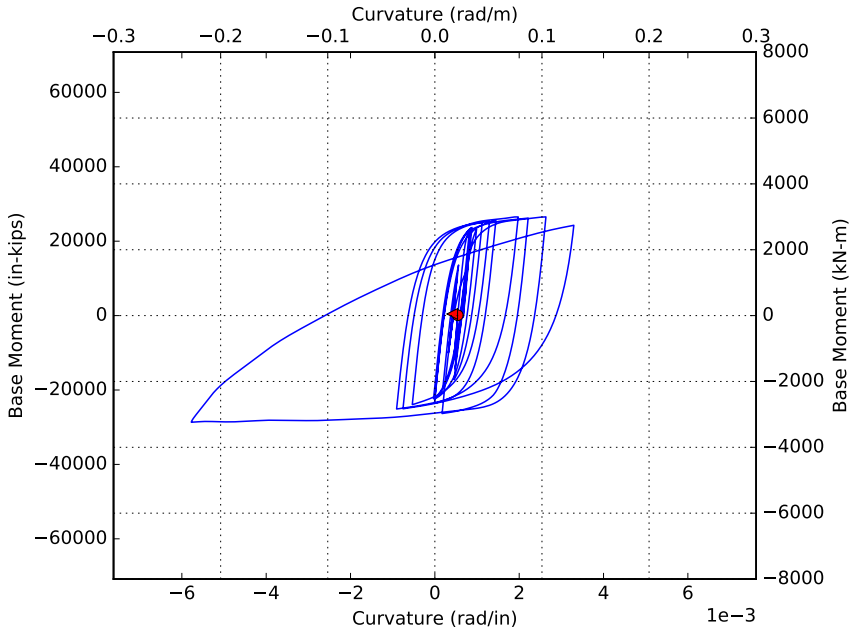

Figure 3.27: Moment-Curvature Plot of EQ5 generated from model 4a

Table 3.3: Maximum Deflection

Maximum Deflection (in)													
		Model											
		1	2	3	4a	4b	4c	4d	5a	5b	5c	5d	Experiment
Earthquake	EQ1	2.9	2.7	2.8	4.2	4.1	3.9	4.2	2.5	3.0	2.6	2.4	2.4
	EQ2	5.7	5.7	4.5	7.0	6.9	6.6	6.9	5.8	5.7	7.6	5.9	5.2
	EQ3	15.4	15.3	10.5	19.5	18.6	20.7	20.4	18.1	19.2	20.9	18.4	14.2
	EQ4	5.7	5.6	7.4	5.5	8.8	4.6	4.9	14.2	16.8	16.3	16.1	6.7
	EQ5	28.2	27.9	18.0	19.1	17.4	20.6	19.9	19.4	23.1	19.4	18.0	22.4
	EQ6	15.3	15.2	9.5	12.6	12.3	15.8	13.8	14.6	18.0	16.6	17.8	19.3
	EQ7	34.3	34.0	21.2	23.0	22.8	24.0	23.7	23.7	26.7	22.5	28.1	21.0
	EQ8	41.2	40.8	24.7	20.1	20.4	20.6	20.5	22.9	21.5	28.3	21.3	23.9
	EQ9	41.4	41.0	24.7	25.8	25.2	22.7	26.7	26.9	28.0	24.5	28.1	25.0

3.8 Combination of Results

It can be seen that different openSEES models generate considerably different column responses. For the designer trying to select a model to use, it can be difficult to determine which model will generate the most accurate response, particularly since full scale test results for the structure are usually not available when the model is being created.

One potential solution to this problem is for the designer to run multiple models and combine the results probabilistically to generate a probability density function as output.

Figure 3.28 shows a plot of the maximum base shears generated from models 4a, 4b, 4c, and 4d. The only difference between these four models was the concrete material used outside of the rebar cage. When the results of these models were compared with the results of the PEER experiment [2], it was not evident that one material generated a more accurate response than the others. Instead of choosing one material and using the resulting base reaction from that model, all four models could be analyzed and the resulting maximum base shears combined to generate a probabilistic result instead of a single number output.

Combining the result of the models can be performed within a Bayesian framework. Here, probability is understood as state of knowledge rather than the frequentist view of the chances of an event occurring [12]. Within this framework one can propose a probability distribution for the base shear, moment, etc that has been informed by the results of the models. The engineer performing the analysis can express their belief on these models by providing different weights to each model and expressing an uncertainty in the value of the estimation. Although this is not a prior predictive distribution, as defined in the literature [13], it is within the spirit of this distribution.

Figure 3.29 shows a violin plot of this combination, along with the experimental

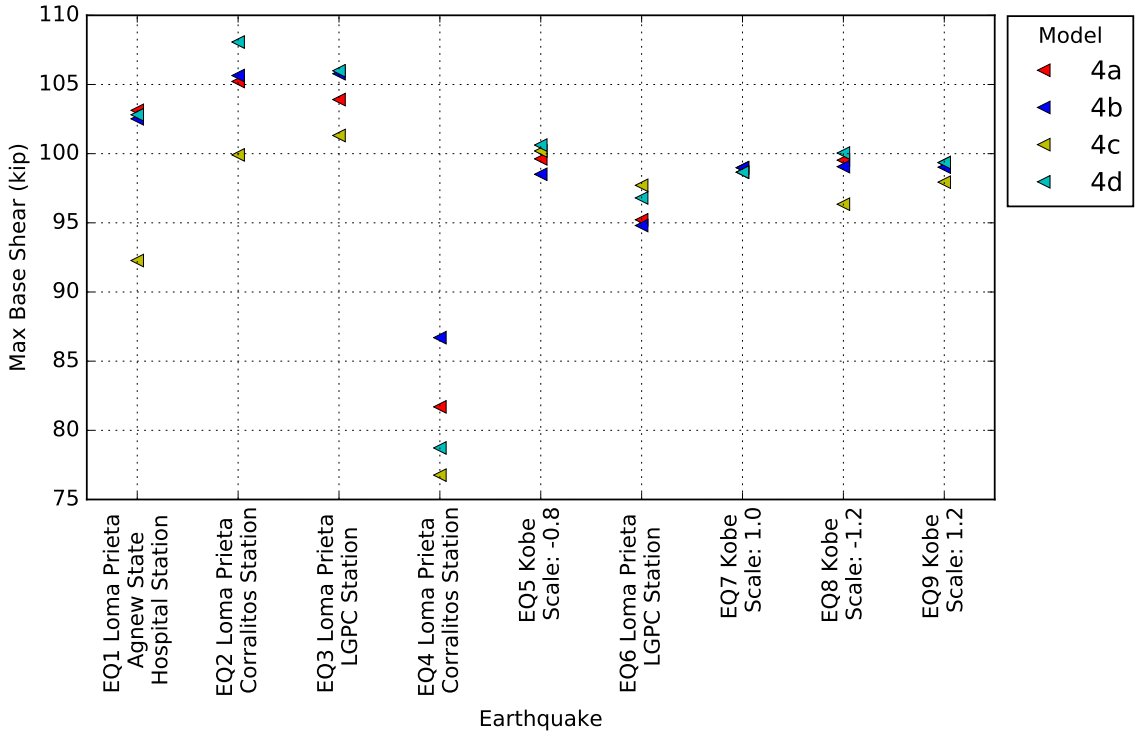

Figure 3.28: Comparing maximum base shear of models 4a, 4b, 4c, and 4d

results. This plot took the base shears from each model into consideration along with a relative weight and standard deviation for each model. For simplicity, a Gaussian distribution was assumed for each quantity of interest (base shear, base moment, top displacement) The weight was a numerical value assigned to each model representing the engineer's confidence in that model relative to the others, based on their own prior experience modeling structural systems. The standard deviation was assigned based on the modeler's expectation on the precision of the results. The relative weight and standard deviation were selected qualitatively, not calculated. The weight and standard deviation values used are shown in Table 3.4. Equal weights were used for each of the model 4 variants (4a, 4b, 4c, & 4d). Similarly, the standard deviation was also set equal for each of the four models (5 kips).

Figure 3.30 shows a similar violin plot for the maximum base moment for models 4a, 4b, 4c, and 4d. Figures 3.31 and 3.32 show similar plots, except using the results

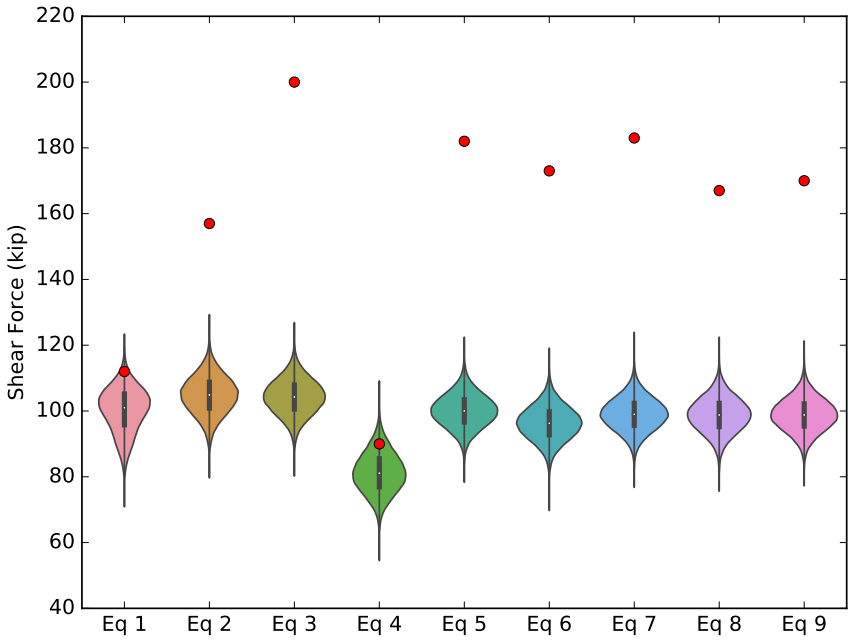

Figure 3.29: Prior prediction combination of maximum base shear generated from models 4a, 4b, 4c, and 4d. Red markers indicate experimental results.

of models 5a, 5b, 5c, and 5d. Models 4 and 5 were very similar, the only difference being model 5 included the effect of strain penetration into the footing. They were both reasonable models that could be selected to analyze the column. Therefore, the results from both of the models could also be combined into a single probabilistic result. Figures 3.33 and 3.34 show the resulting combination of the base shears and base moments of models 4a, 4b, 4c, 4d, 5a, 5b, 5c, and 5d. For these combinations, equal relative weights were not used for all of the models. Instead, a higher relative weight was assigned to the model 5 variants to account for the fact the they included the extra analysis parameters. A weight of 50 was used for models 5a, 5b, 5c, and 5d and 25 was used for models 4a, 4b, 4c, and 4d.

This method of combining model results together to come up with a probabilistic response could be expanded to include even more models. However, each additional model has the possibility of increasing the size of the resulting violin plots due to the additional uncertainty of the column response.

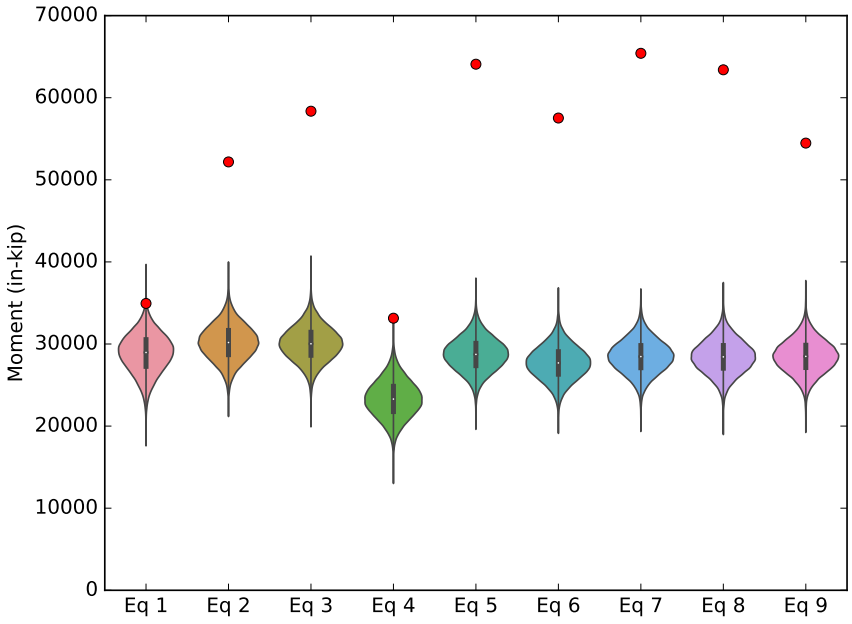

Figure 3.30: Prior prediction combination of maximum base moment generated from models 4a, 4b, 4c, and 4d. Red markers indicate experimental results.

Figures 3.35 and 3.36 combine the results of all the nonlinear models into a single probabilistic output. For these combinations, a relative weight of 100 was assigned to model 3, indicating it was expected to generate the most accurate response, 50 was assigned to the model 5 variants, and 25 was assigned to the model 4 variants. It can be seen that as more models were added, the size of the band increased, representing the increased uncertainty of the column response. It can be observed that even though the prior prediction, as used in this work, is able to express uncertainty in the results, the results were still biased when compared with the experimental data. Updating the model based on experimental data of the material, or adding additional observations about the column should be investigated as a way to reduce this bias.

Table 3.4: Relative weights assigned to the openSEES models

Model	**Weight**	**Standard Deviation**
3	100	5
4	25	5
5	50	5

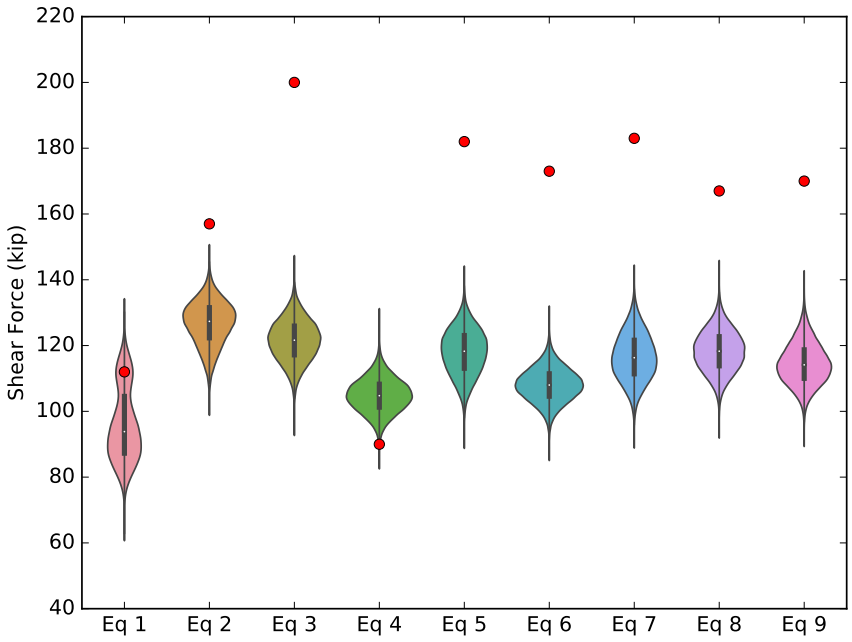

Figure 3.31: Prior prediction combination of maximum base shear generated from models 5a, 5b, 5c, and 5d. Red markers indicate experimental results.

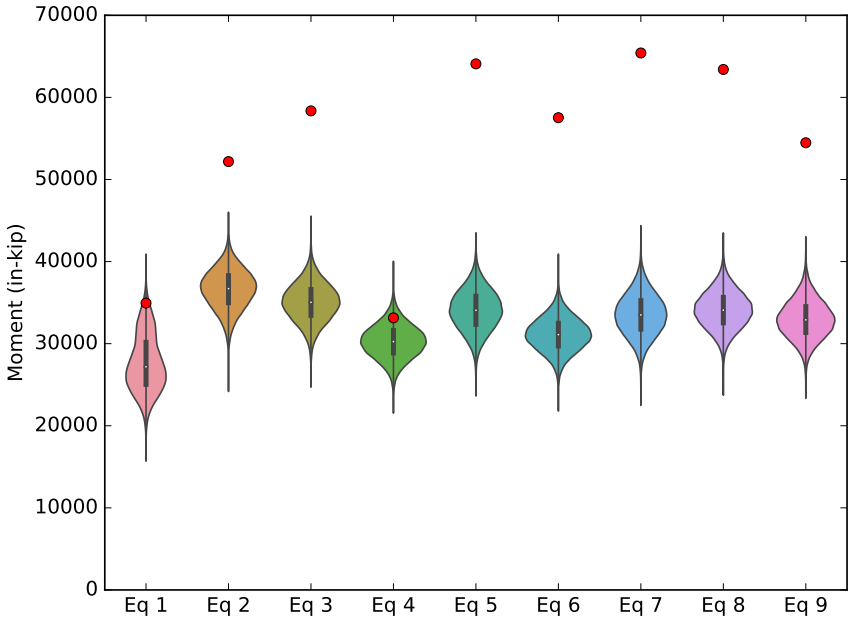

Figure 3.32: Prior prediction combination of maximum base moment generated from models 5a, 5b, 5c, and 5d. Red markers indicate experimental results.

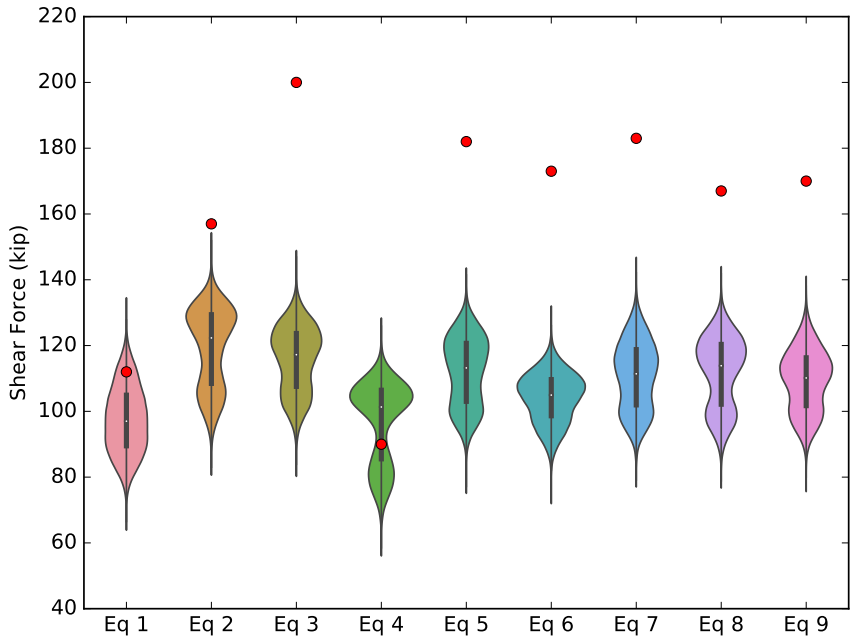

Figure 3.33: Prior prediction combination of maximum base shear generated from models 4a, 4b, 4c, 4d, 5a, 5b, 5c, and 5d. Red markers indicate experimental results.

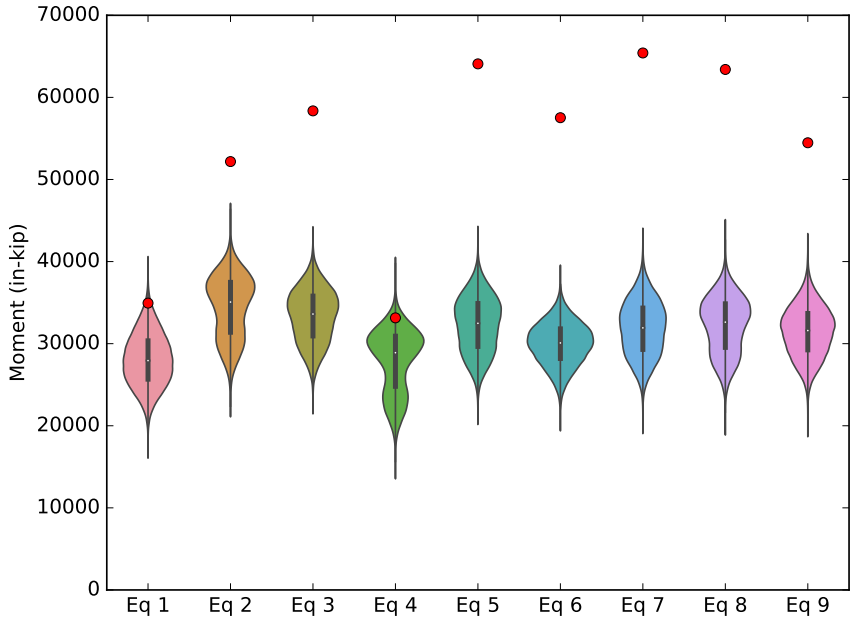

Figure 3.34: Prior prediction combination of maximum base moment generated from models 4a, 4b, 4c, 4d, 5a, 5b, 5c, and 5d. Red markers indicate experimental results.

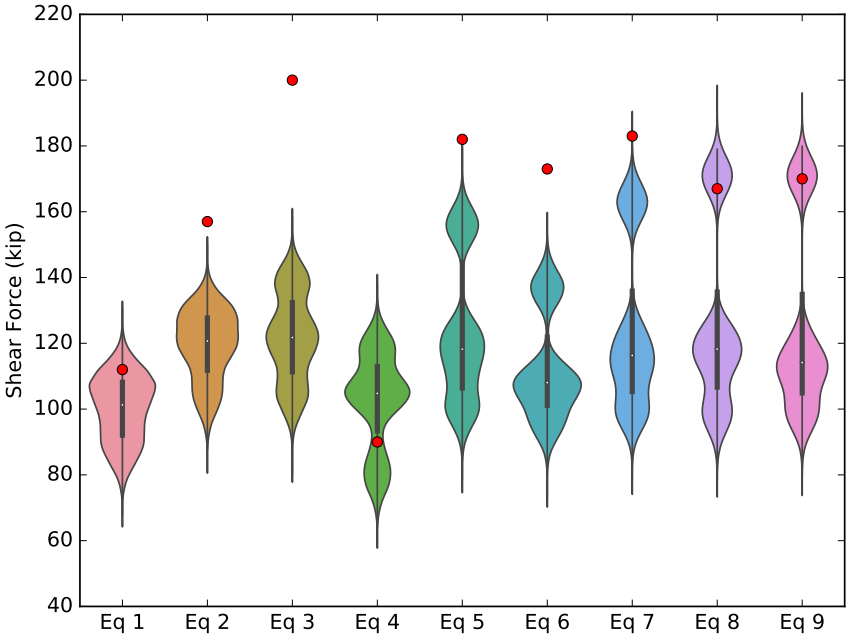

Figure 3.35: Prior prediction combination of maximum base shear generated from models 3, 4a, 4b, 4c, 4d, 5a, 5b, 5c, and 5d. Red markers indicate experimental results.

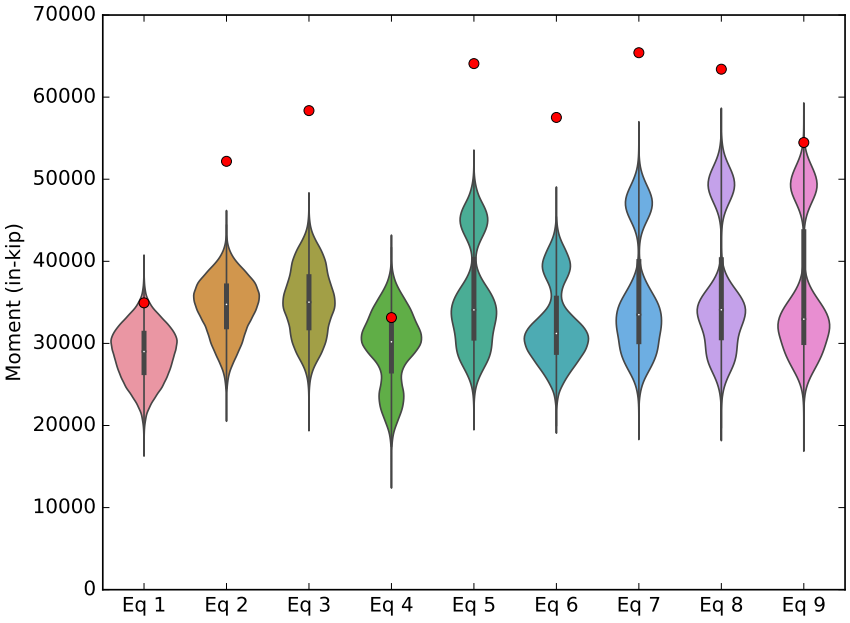

Figure 3.36: Prior prediction combination of maximum base moment generated from models 3, 4a, 4b, 4c, 4d, 5a, 5b, 5c, and 5d. Red markers indicate experimental results.

3.9 Hand Calculation Method for Baseline Reference

In addition to the openSEES models, some basic hand calculations were performed to compare with the openSEES model results of earthquakes 1, 2, and 3 using techniques described in [14] and [15]. Figures 3.37, 3.38, and 3.39 show the pseudo acceleration and displacement response spectra as given in the shake table report [3] at a 1% damping ratio. The parameters used in the calculations are given in Table 3.5 and Table 3.6 and the resulting base reactions and displacements are shown in Table 3.7. The linear hand method returned base reactions and deflections very similar to the linear openSEES models (Table 3.8).

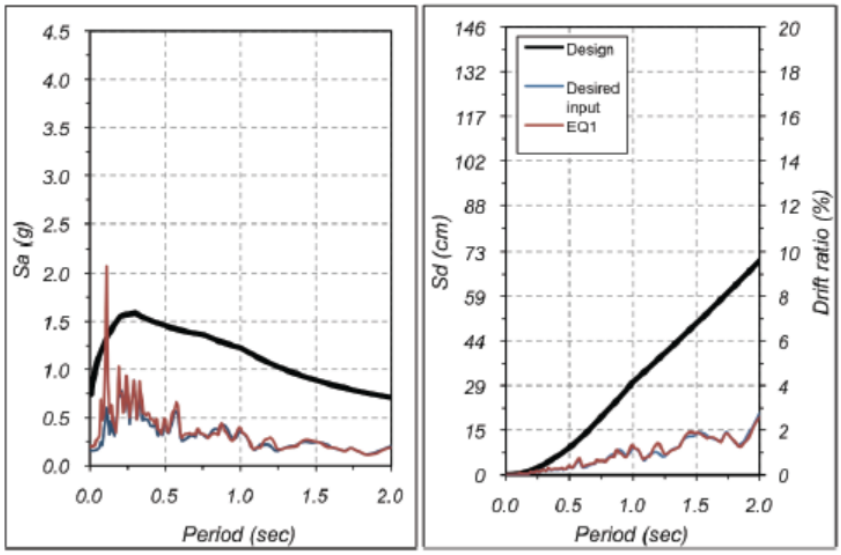

Figure 3.37: EQ1 pseudo-acceleration and displacement response spectra at 1% damping ratio [3]

Table 3.5: Parameters used to estimate the column response using hand methods

Parameter	**Value**
k	40.7 kip/in
m	1.352 (kip-s^2)/in
f_n	0.873 1/sec
T_n	1.146 s

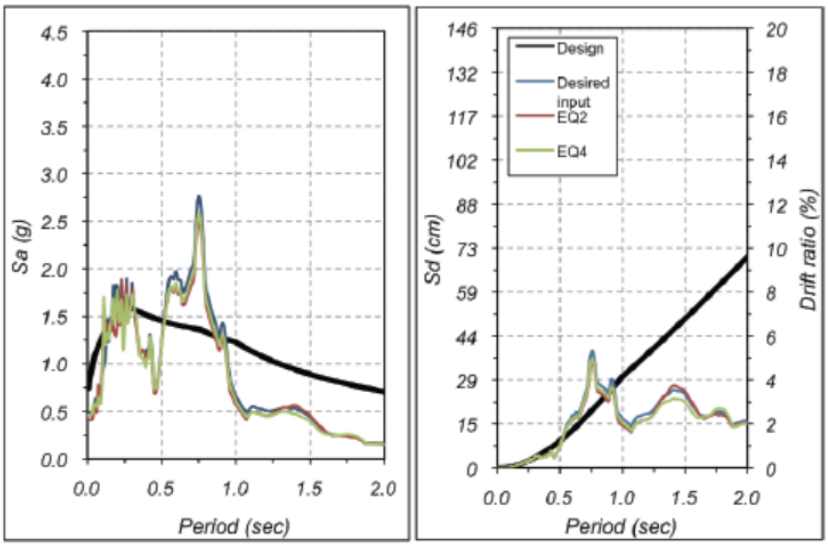

Figure 3.38: EQ2 pseudo-acceleration and displacement response spectra at 1% damping ratio [3]

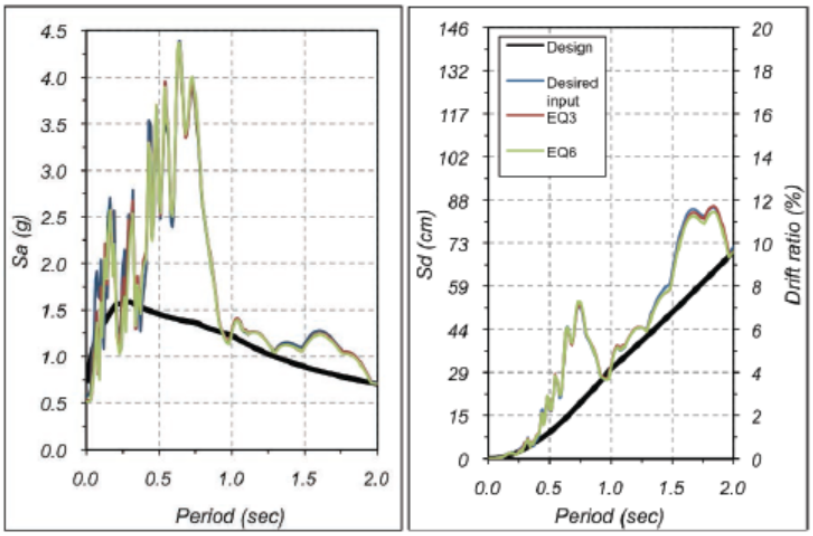

Figure 3.39: EQ3 pseudo-acceleration and displacement response spectra at 1% damping ratio [3]

Table 3.6: S_a and S_d values for $T_n = 1.15$ from Figures 3.37, 3.38, and 3.39

EQ	**S_a**	**S_d**
1	0.25 g	7.5 cm
2	0.50 g	15 cm
3	1.25 g	37 cm

Table 3.7: Resulting Base Reactions from EQ 1, 2, & 3 based on linear single degree of freedom model [14], [15]

EQ	**Base Shear (kips)**	**Base Moment (in-kips)**	**Deflection (in)**
1	130	37,600	3
2	261	75,200	5.9
3	652	188,000	14.6

Table 3.8: Column response to EQ 1, 2, & 3 based on openSEES model 2

EQ	**Base Shear (kips)**	**Base Moment (in-kips)**	**Deflection (in)**
1	112	31,918	2.8
2	236	67,313	4.5
3	627	179,894	10.5

Chapter 4

Conclusions and Future Work

4.1 Modeling From a Practitioner Point of View

The following comments are made from a practitioner point of view. They are based on the experience I have had working in industry as a structural engineer.

From a professional design standpoint, models 1 and 2 were relatively easy to create. The most difficult part was determining an appropriate moment of inertia to describe the composite behavior of the reinforced concrete section. But even this step was achievable using basic engineering knowledge that any practicing structural engineer should possess or be able to obtain with minimal research.

Model 3 was the most difficult of the five to create. This is primarily due to the need to model the composite action of the circular cross-section reinforced concrete member using the parameters for a basic steel material. The moment-curvature action of the column had to be investigated and plotted. Then a "yield point", and post yield behavior had to be estimated from the shape of the moment-curvature plot. This is something that many practicing engineers do not do on a daily basis and may find to be difficult without specific training or extensive research that they may not have time to perform.

Model 4 was not as difficult to create as model 3, but did pose its own challenges. It was not difficult to create the fiber cross sections using the openSEES commands, but the accuracy of the model depends heavily on the material chosen and the parameters used. This particular model had the benefit of having the PEER report [2] available

that contained the results of project specific material testing. So the model was able to use the actual yield and ultimate stress and strain values of the reinforcing bars. A design engineer would typically not have this information and would need to estimate these values. Similarly, the PEER report had the results of concrete cylinder tests that provided some of the concrete parameters. It is likely that a design engineer would use the design parameters of the material being specified, which are minimum values that are often exceeded by the steel mill/concrete plant.

Then there is the issue of which concrete material to use. Four concrete materials were compared here and none of them produced results that were more accurate than the others. The concrete01 material was pretty simple because it assumed no tensile strength and only required parameters that could be reasonably estimated by a practicing engineer. The other concrete materials (concrete02, concrete03, concrete04), however, included parameters for tensile strength degradation that had to be estimated.

Model 5 included all of the challenges described for model 4 but with the additional complexity of needing to model the strain penetration parameters.

All of these descriptions neglect the learning curve of openSEES itself. There were some idiosyncrasies of the program (failing to converge, sensitivity to the number of integration points, etc) that created challenges with some of the models. However, the same could be said about most software packages.

4.2 Model Conclusions

Model 3 was the most reliable of the models tested for estimating the base reactions, followed by model 5 and then model 4. Conversely, none of the models performed consistently better than the others at predicting the maximum column deflection. There was also not a trend to either over-predict or under-predict the deflection.

Model 3 produced the most accurate predictions of the maximum base shear

compared to the other models for all excitations except EQ2 and EQ4. However, even model 3 did not produce consistently accurate results. For example, the maximum base shear was within 4 percent of the actual test results for some excitations but off by 31 percent for others. It was also seen that the effect of damage accumulation can be difficult to predict and leads to additional uncertainty.

It is interesting to see that the fiber models did not generate more accurate base reactions than model 3, when they used actual concrete and reinforcing steel materials and model 3 was simplified to a conform to a purely bilinear steel material. Although, perhaps related, out of the four concrete materials used for the fiber models, there was no single material that produced consistently better results.

It's important to note that every possible openSEES model type was not tested in this comparison. For instance, there was not a model that used a lumped plasticity element - such as beamWithHinges. The element used in models 3, 4, and 5 was a distributed plasticity element

It is also interesting to see that the maximum base reaction predictions from nearly all of the models were too low. Figures 4.1 and 4.2 show the maximum base reactions of all the nonlinear models. These results clearly seem to be biased. A similar bias is seen in the PEER blind prediction contest [1] where there were more base reaction predictions below the shake table results than above (Figure 1.2). Since a variety of analysis software was used amongst the contest entrants, this is evidence that the bias exists in most design software. This can result in non-conservative designs because in reality, many practicing engineers fail to recognize the degree of uncertainty in seismic analyses.

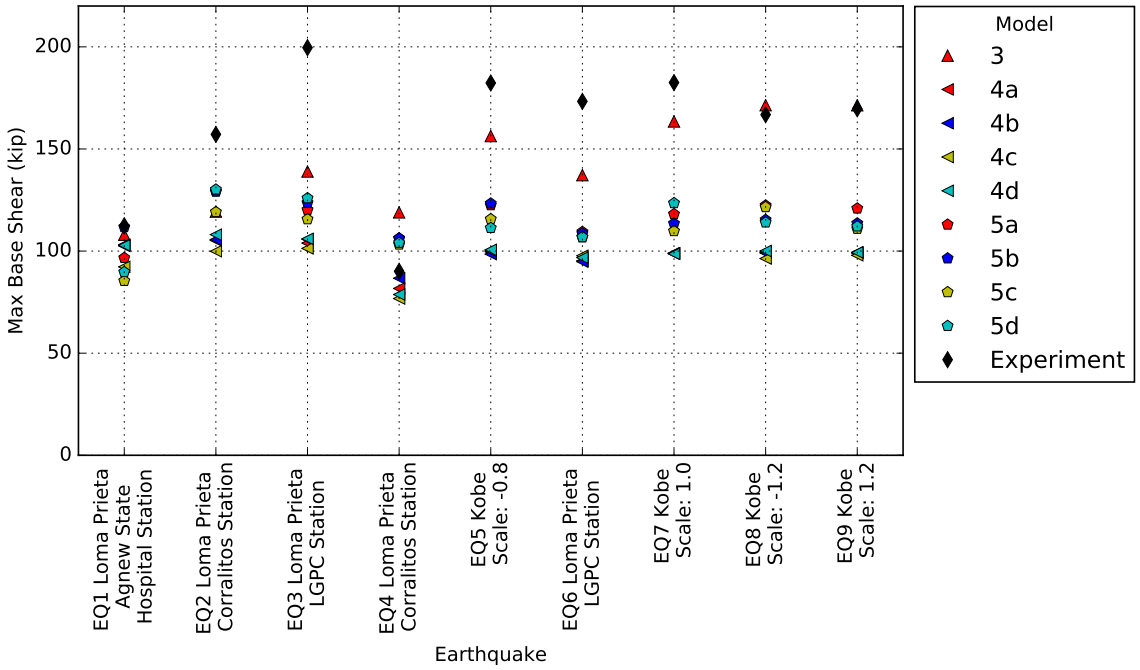

Figure 4.1: Maximum Base Shear omitting models 1 and 2

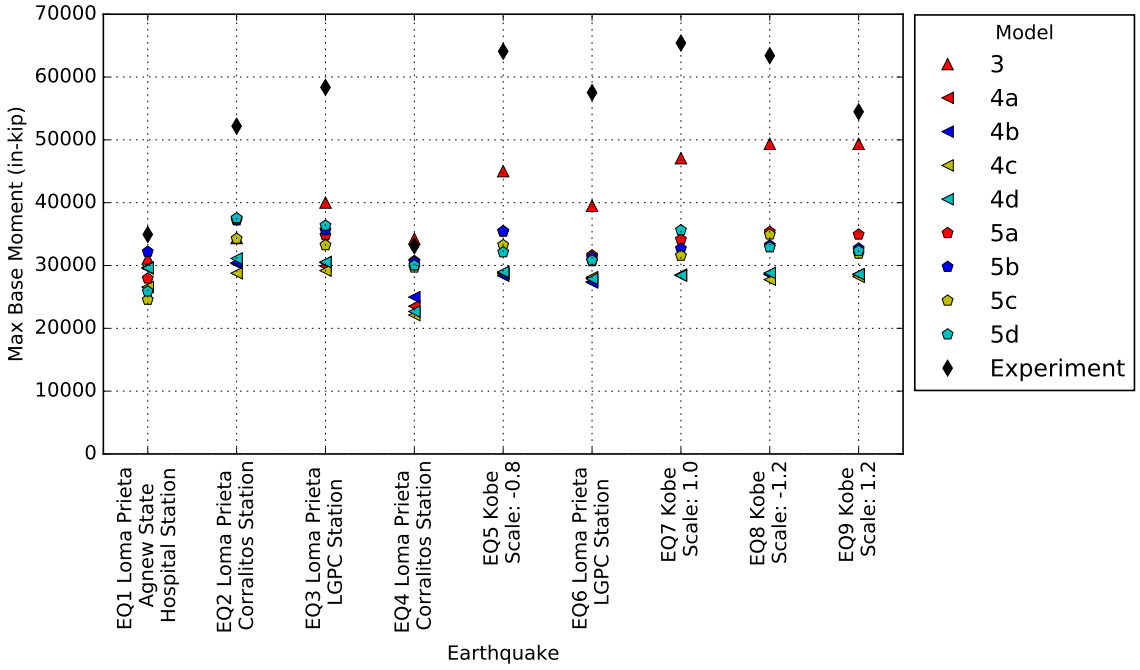

Figure 4.2: Maximum Base Moment omitting models 1 and 2

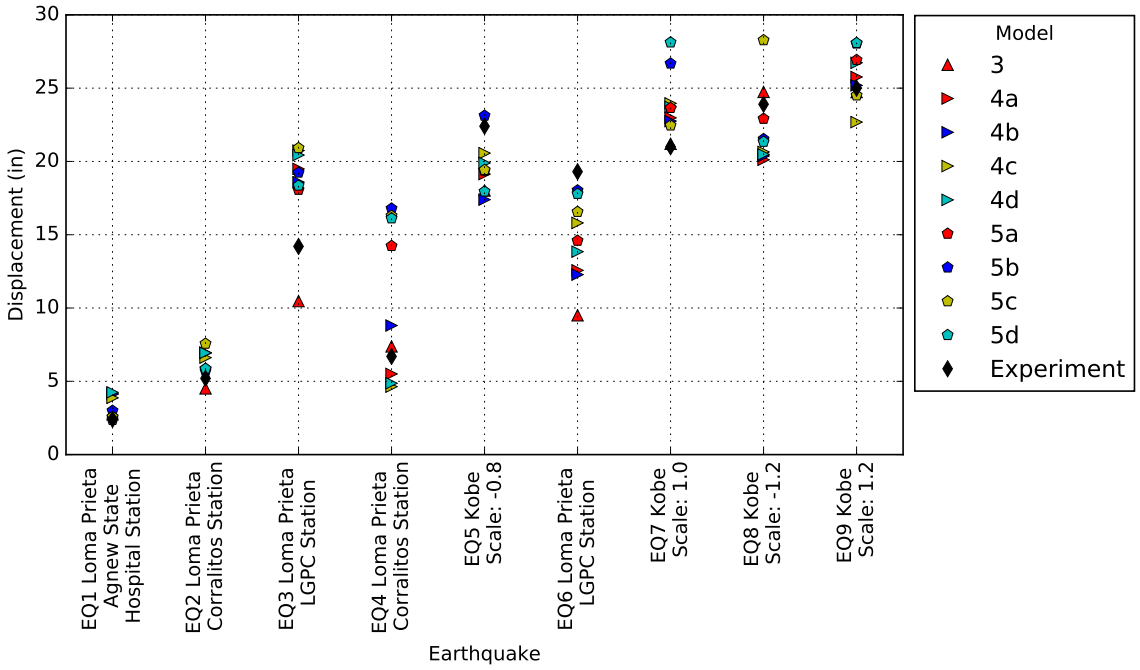

Figure 4.3: Maximum Column Deflection omitting models 1 and 2

4.3 Future Work

All possible models were not tested in this comparison. There are more model types and more element types that could be used to model the column. Further investigations could also expand the scope to include more complicated structures than a simple cantilevered column - such as a moment frame or braced frame. This comparison was limited to a single cantilevered column because there were full scale test results readily available for this structure.

There are also additional element types that could be chosen to model the same column. One of these is the beamWithHinges element, which is a nonlinear beam-column element with lumped plasticity. The PEER experiment test results [2] were deliberately not studied until after the models for this thesis were chosen and ran. After reviewing the test results, though, it appears that the beamWithHinges element may be a good fit.

Another element type that should be investigated is the dispBeamColumn element. This is also a nonlinear beam-column element, but is a displacement based element instead of a force based element (the element used in model 3 was a force based element). After the model results were reviewed and it was realized that model 3 (nonlinearBeamColumn) provided the best fit for most excitations, a preliminary model was created and ran using the same parameters as model 3 except with the element type changed to dispBeamColumn. This element resulted in higher maximum reactions (base shear and base moment) for all excitations. Since model 3 underpredicted the base reactions for most excitations, this appeared to result in improved accuracy compared with the nonlinearBeamColumn element.

The maximum displacement predictions from the dispBeamColumn element were not as clear as the base reactions, though. Some excitations resulted in a slightly more accurate maximum displacement with the dispBeamColumn element, while other excitations resulted in slightly less accurate predictions.

4.4 Application

One method to attempt to improve the accuracy of a deterministic model that has a degree of uncertainty is to create multiple models and combine the responses into a single probabilistic model, as discussed in Chapter 3.

This is good in theory but poses a few problems from a practical design standpoint. The first problem is the time required to create multiple models. A structural engineer in a design role is usually under some degree of time pressure. Increasing the number of models the engineer needs to create has the potential to significantly increase the engineer's workload and increase the time/cost of the design. This time increase will be further exacerbated when you consider that most design projects are somewhat iterative in nature. As design changes are implemented, the engineer must go back and update the model to verify the adequacy of each new configuration. If there are multiple models that must be updated, the potential to make an error greatly increases.

One potential solution for this problem would be to develop a software package that runs multiple analytical models based on a single geometric model. The engineer could then just create a single model of the structure and have the software perform multiple analyses of the structure using different parameters. The software could then combine the responses of these different analyses and produce a single probabilistic response for the structure. This eliminates the potential issue of needing the engineer to update multiple models each time the design evolves.

Since each analysis relies on different parameters, and since each parameter has a degree of uncertainty associated with it, the result would effectively be a range of potential responses. This type of output might seem desirable from a purely academic point of view, because academics recognize and appreciate the uncertainty in analytical models. In engineering practice, however, there is generally a different atmosphere, and a probabilistic output from a design package may not be readily

accepted.

If a single model is analyzed and a deterministic response produced, the engineer moves forward with confidence that this is "the number" to design for. But if several models are analyzed and the results combined in a probabilistic form, the designer has less confidence in a single number to design for. The designer does, however, now have a more realistic sense of the uncertainty in the models and will be forced to apply engineering judgment in order to determine whether or not the structure is adequate.

It could easily turn into a situation where even though a range of reactions or stresses are returned, the engineer only uses the value at the top of the range. As an example, a software package might analyze a model and return as an output that there is a 95 % probability that the maximum reaction at the base of a particular column is within a particular range. The engineer would likely just design the column, connection, and foundation for the value at the top of the range. To design for any value less than that places the engineer in a position of increased legal risk and potentially raises ethical questions. The engineer has an obligation to design the structure for the maximum stresses induced by the design loads.

If the engineer designs the structural element for less than the value at the top of the range for any reason, it would also open the door to potential lawsuits. It would be tough to defend a design if the engineer's analysis indicates a potential moment of one number, but the engineer designed the connection for a smaller moment, even if the smaller moment was within the probable range of maximum moments.

In this respect, there is little benefit to returning a probabilistic output, and the software could simply return the value at the top of the band (most conservative result).

Uncertainty in design is not a new concept, however, and has been amply discussed as well as addressed within building codes. There is uncertainty in construction mate-

rials, uncertainty in construction methods, uncertainty in live loads, and uncertainty in environmental loads. All of these are currently addressed by the use of safety factors and load factors. For a probabilistic analysis to become useful, it would need to also be addressed in the building codes.

These allow the use of individual, deterministic models. This method is easy to defend as well - the column was designed to withstand the maximum moment, therefore it is a safe design. However the adequacy of the model depends on the engineer's education, experience, ability to use the correct assumptions and the parameters that are built into the software. There is currently no "safety factor" that addresses the type of analysis performed; it is left to the judgment of the engineer.

This issue is highlighted by the PEER blind contest [1] that invited engineers and academic researchers to submit their best attempt, using any tool available to them, to predict the response of the simple, cantilever column subjected to a known excitation. Many of the submissions were quite far off. Many of them under-predicted the reactions, as well, which is particularly alarming.

Bibliography

[1] V. Terzic, M. J. Schoettler, J. I. Restrepo, and S. A. Mahin, "Concrete column blind prediction contest 2010: outcomes and observations," *PEER Report*, vol. 1, 2015.

[2] M. Schoettler, J. Restrepo, G. Guerrini, D. Duck, and F. Carrea, "Peer report no. 2015/02: A full-scale, single-column bridge bent tested by shake-table excitation.," *Pacific Earthquake Engineering Research Center, University of California, Berkeley, CA*, 2015.

[3] M. Schoettler, J. Restrepo, G. Guerrini, D. Duck, and F. Carrea, "A full-scale, single-column bridge bent tested by shake-table excitation," *Center for Civil Engineering Earthquake Research, Department of Civil Engineering, University of Nevada*, 2012.

[4] N. Pereira, X. Romão, and R. Delgado, "Epistemic uncertainty of the structural response of reinforced concrete members under cyclic loading due to different material modelling choices," in *15th World Conference on Earthquake Engineering, WCEE 2012*, 2012.

[5] W.-H. Pan, M.-X. Tao, J.-G. Nie, and D.-X. Yang, "Fiber beam-column model considering reinforcement slip effect for simulation of an rc bridge column shake-table test,"

[6] W.-H. Pan, M.-X. Tao, and J.-G. Nie, "Fiber beam–column element model considering reinforcement anchorage slip in the footing," *Bulletin of Earthquake Engineering*, vol. 15, no. 3, pp. 991–1018, 2017.

[7] M. H. M. Yassin, *Nonlinear analysis of prestressed concrete sructures under monotonic and cyclic loads*. University of California, Berkeley, 1994.

[8] S. Popovics, "A numerical approach to the complete stress-strain curve of concrete," *Cement and concrete research*, vol. 3, no. 5, pp. 583–599, 1973.

[9] J. Zhao and S. Sritharan, "Modeling of strain penetration effects in fiber-based

analysis of reinforced concrete structures," *ACI structural journal*, vol. 104, no. 2, p. 133, 2007.

[10] M. CEB-FIP, "90, design of concrete structures. ceb-fip model code 1990," *British Standard Institution, London*, 1993.

[11] K. K. Moridani and P. Zarfam, "Nonlinear analysis of reinforced concrete joints with bond-slip effect consideration in opensees," *Nonlinear Analysis*, vol. 3, no. 6, pp. 362–367, 2013.

[12] M. J. Bayarri and J. O. Berger, "The interplay of bayesian and frequentist analysis," *Statistical Science*, pp. 58–80, 2004.

[13] E. T. Jaynes, *Probability theory: The logic of science*. Cambridge university press, 2003.

[14] A. K. Chopra *et al.*, *Dynamics of structures*, vol. 3. Prentice hall New Jersey, 1995.

[15] A. K. Chopra and C. Chintanapakdee, "Inelastic deformation ratios for design and evaluation of structures: single-degree-of-freedom bilinear systems," *Journal of structural engineering*, vol. 130, no. 9, pp. 1309–1319, 2004.

Appendix A

Excitations

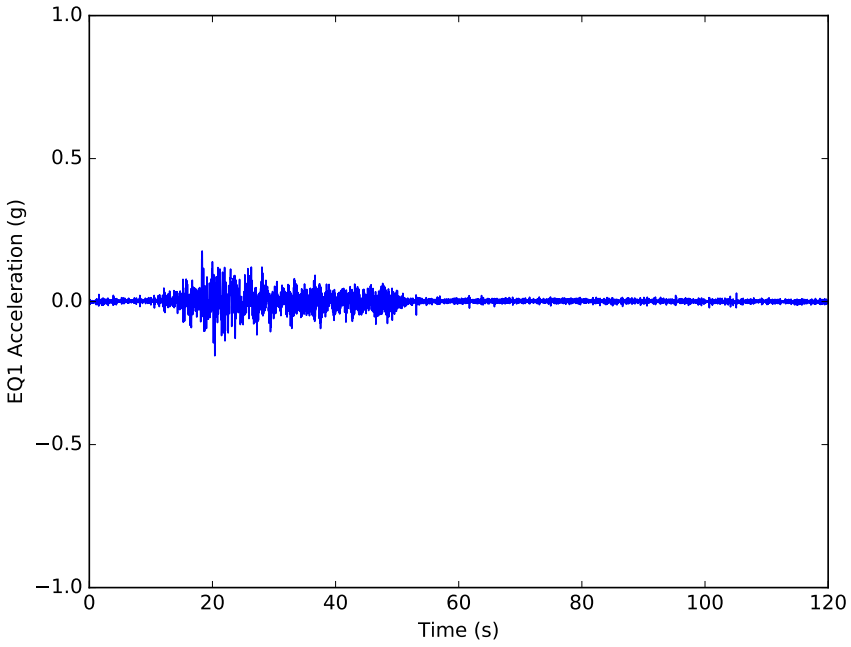

Figure A.1: Input excitation for EQ1 [1]

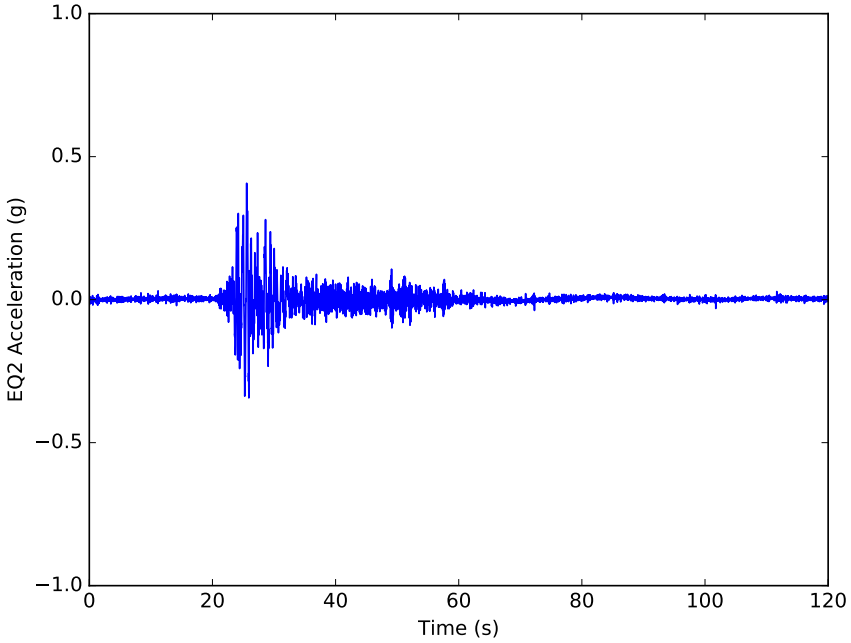

Figure A.2: Input excitation for EQ2 [1]

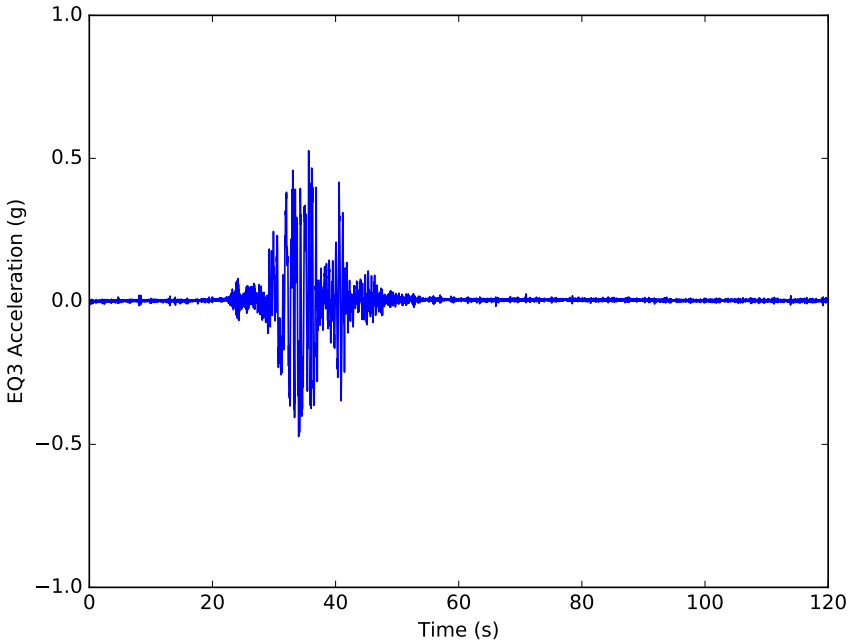

Figure A.3: Input excitation for EQ3 [1]

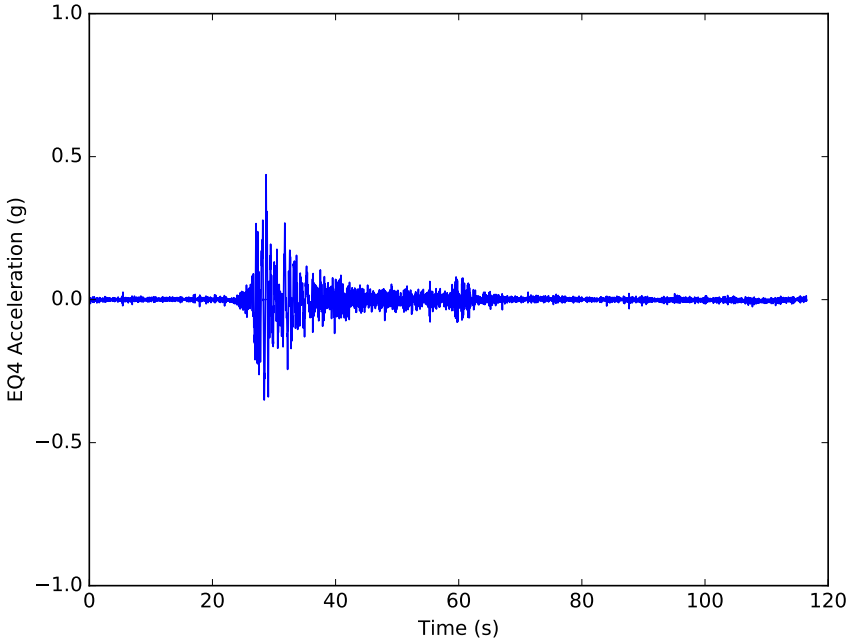

Figure A.4: Input excitation for EQ4 [1]

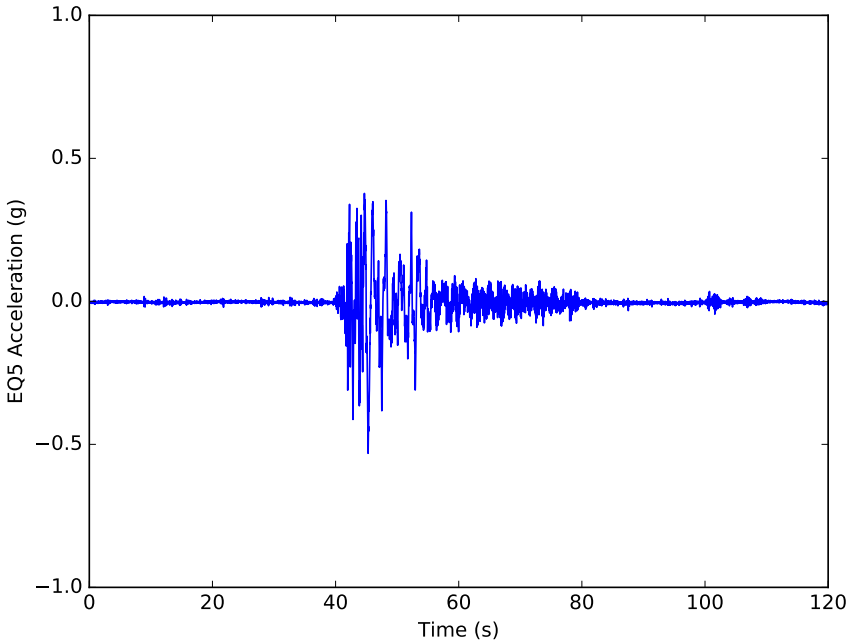

Figure A.5: Input excitation for EQ5 [1]

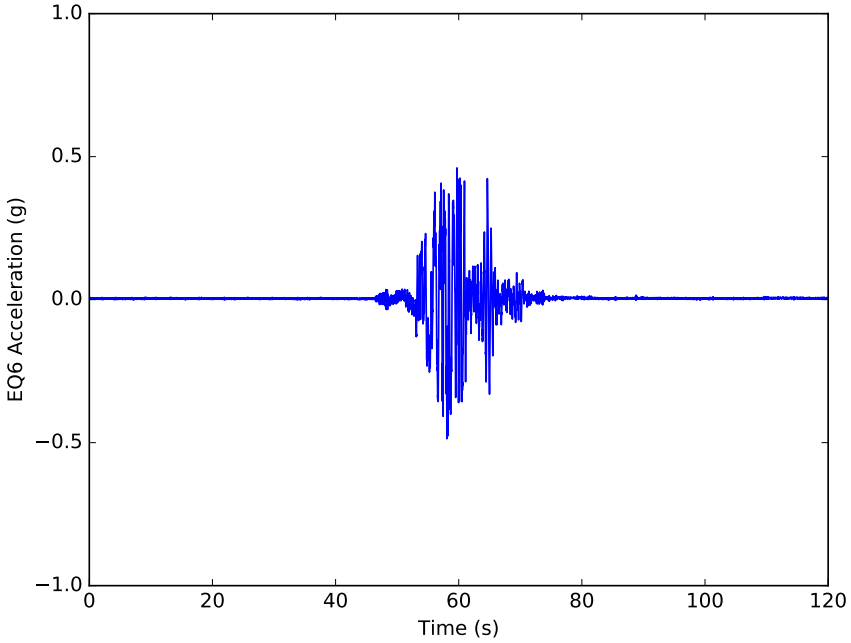

Figure A.6: Input excitation for EQ6 [1]

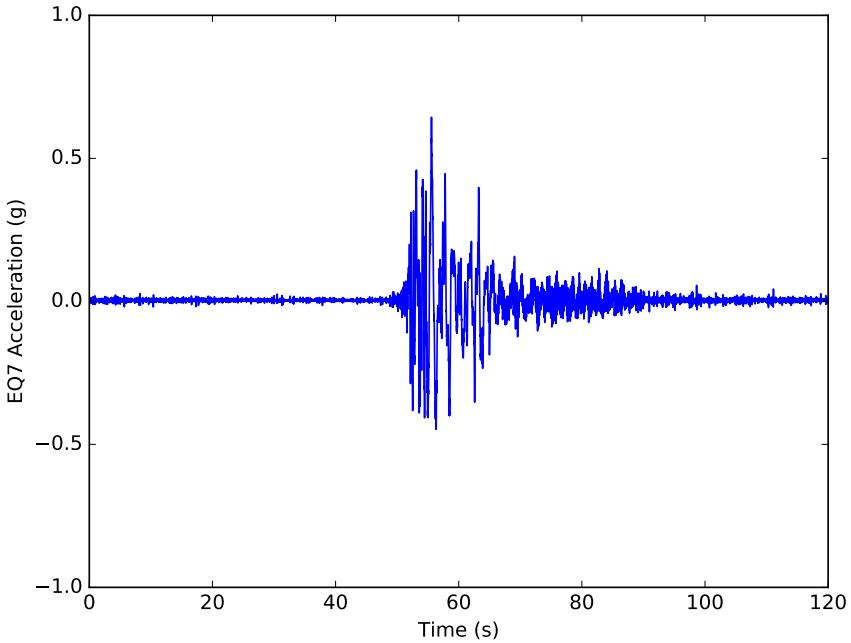

Figure A.7: Input excitation for EQ7 [1]

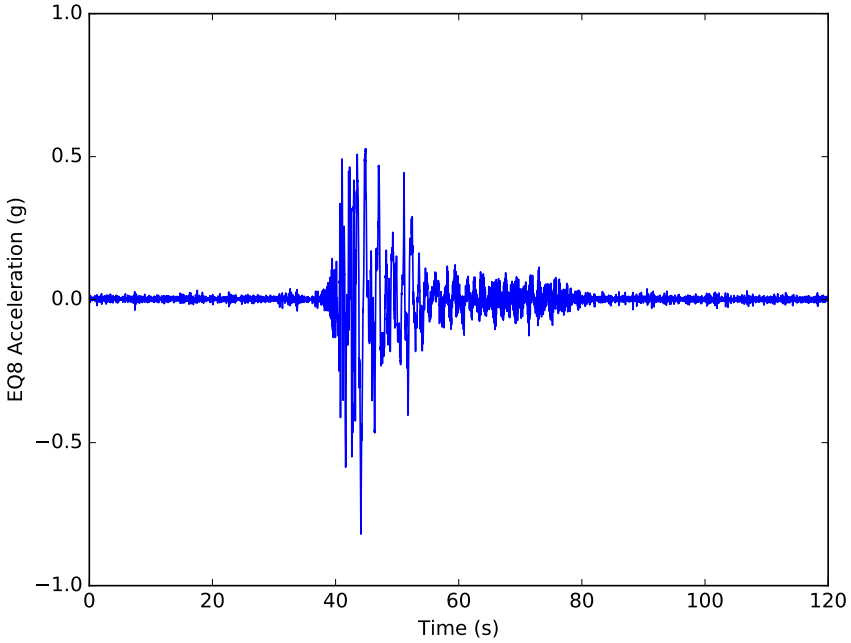

Figure A.8: Input excitation for EQ8 [1]

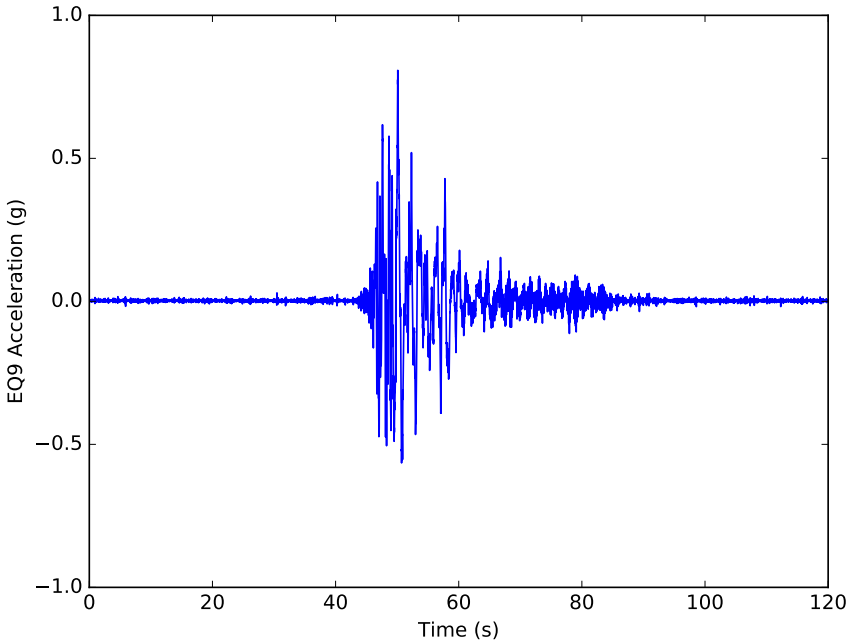

Figure A.9: Input excitation for EQ9 [1]

Appendix B

Model 1 Output

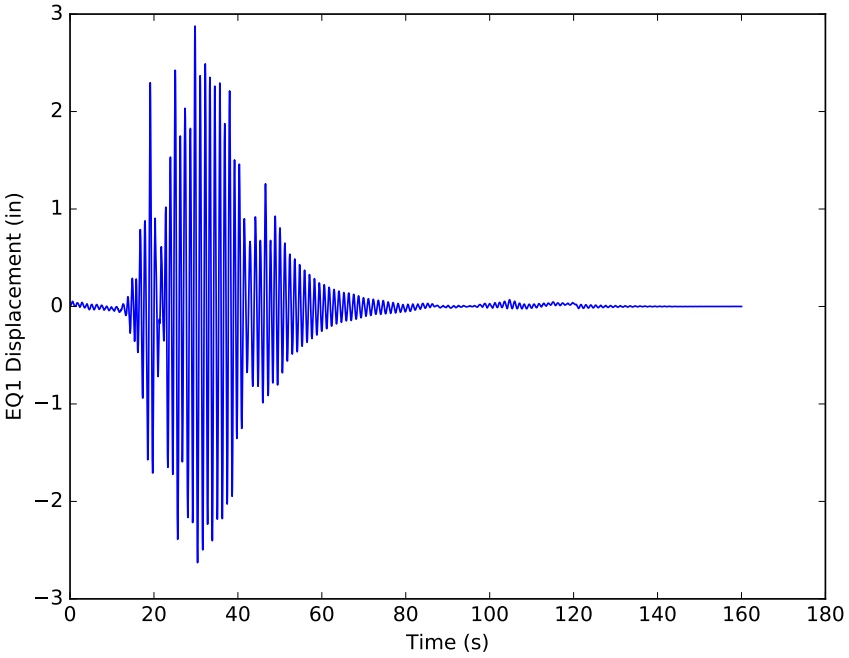

Figure B.1: Displacement response of model 1 for EQ1

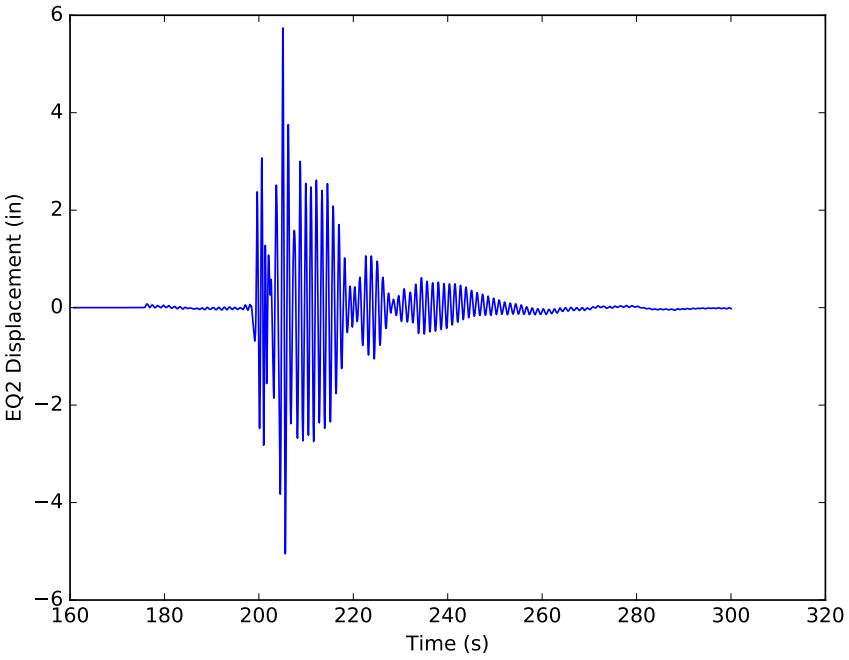

Figure B.2: Displacement response of model 1 for EQ2

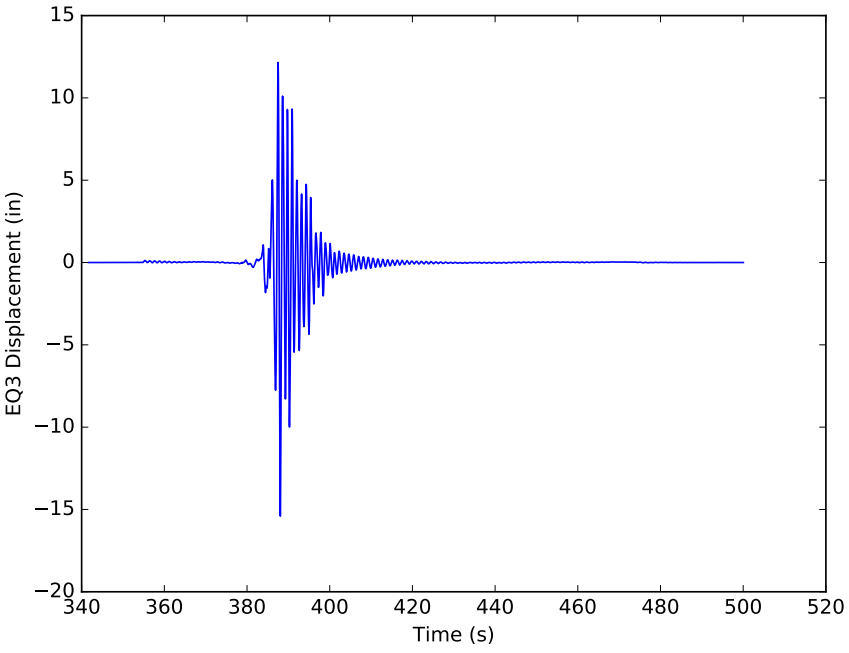

Figure B.3: Displacement response of model 1 for EQ3

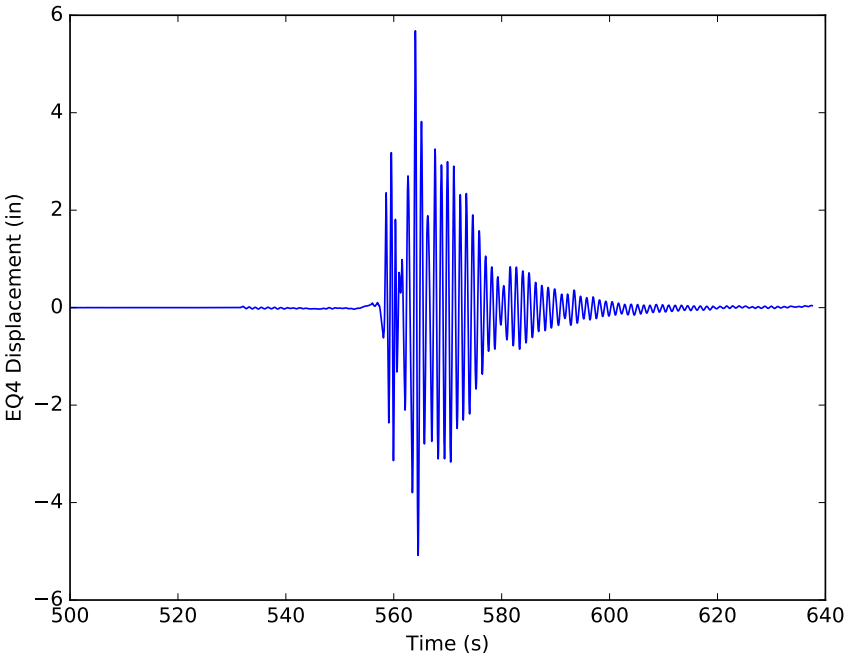

Figure B.4: Displacement response of model 1 for EQ4

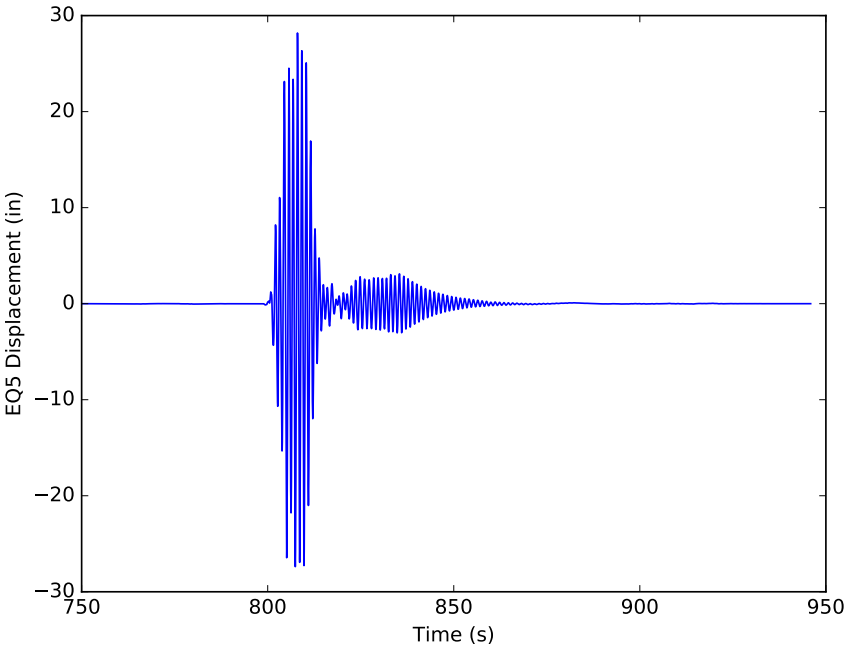

Figure B.5: Displacement response of model 1 for EQ5

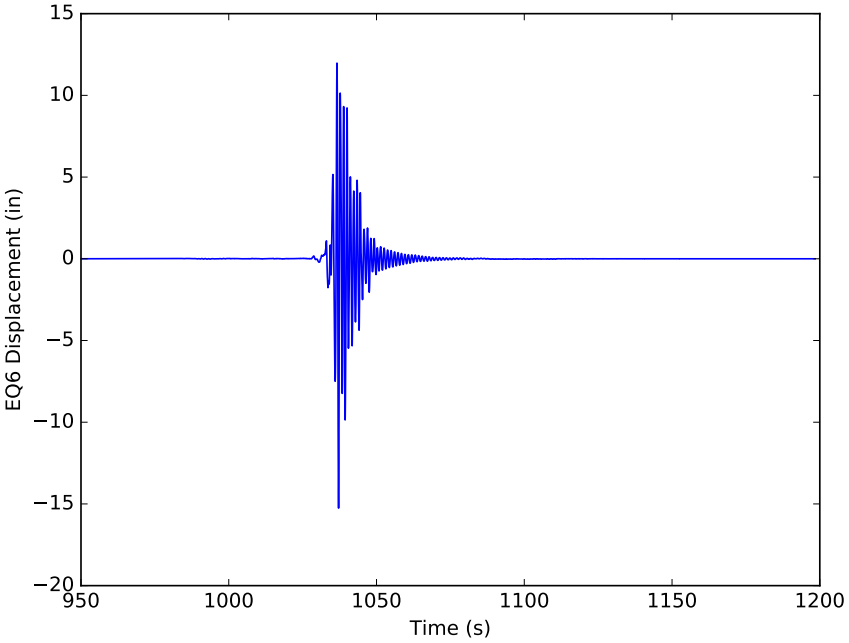

Figure B.6: Displacement response of model 1 for EQ6

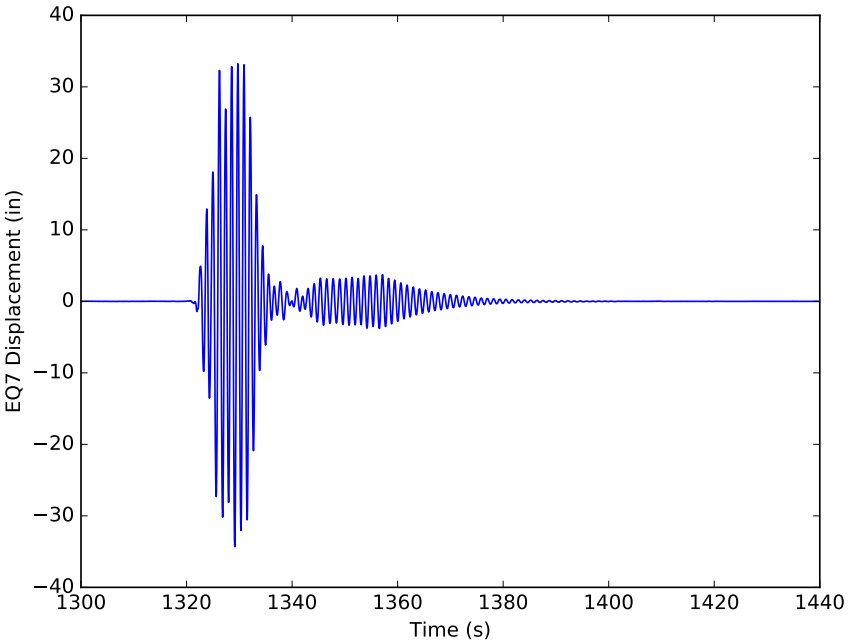

Figure B.7: Displacement response of model 1 for EQ7

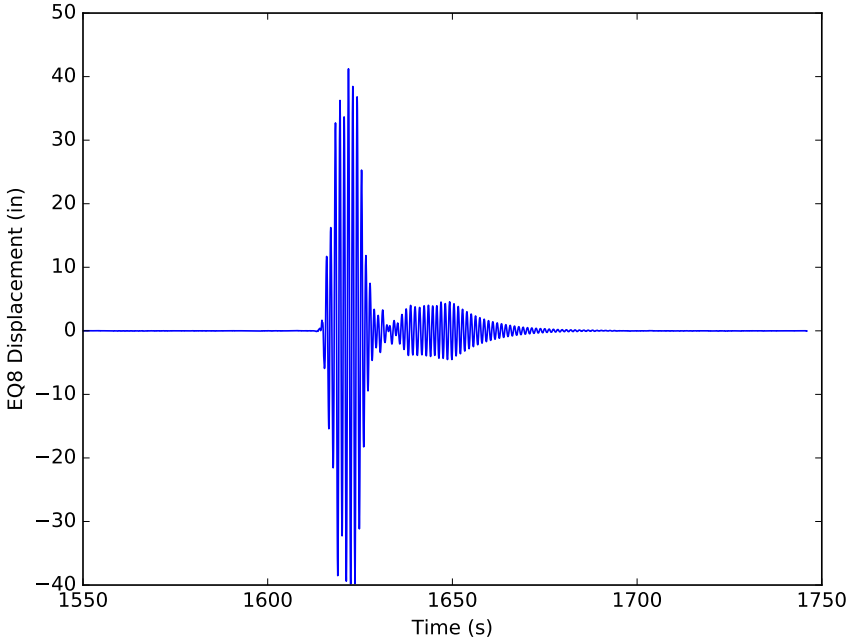

Figure B.8: Displacement response of model 1 for EQ8

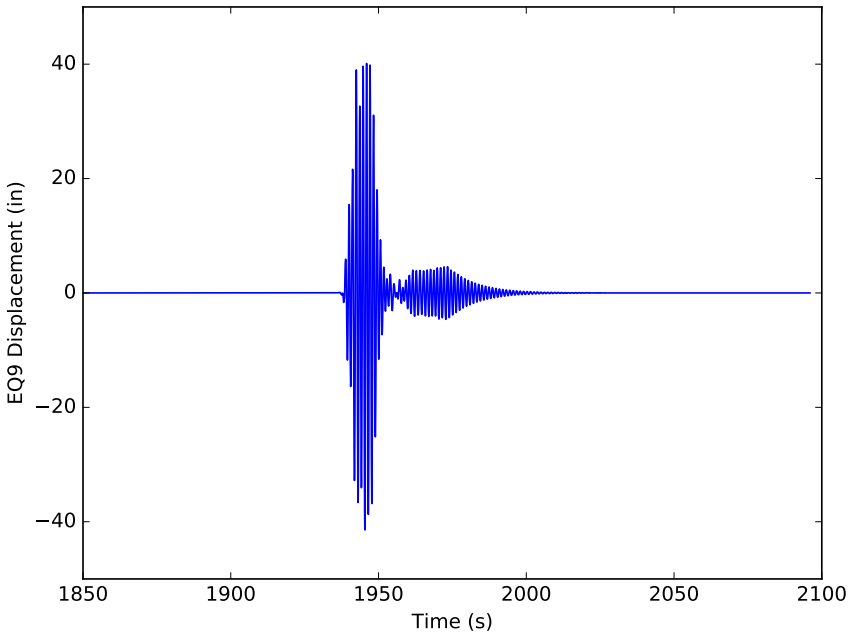

Figure B.9: Displacement response of model 1 for EQ9

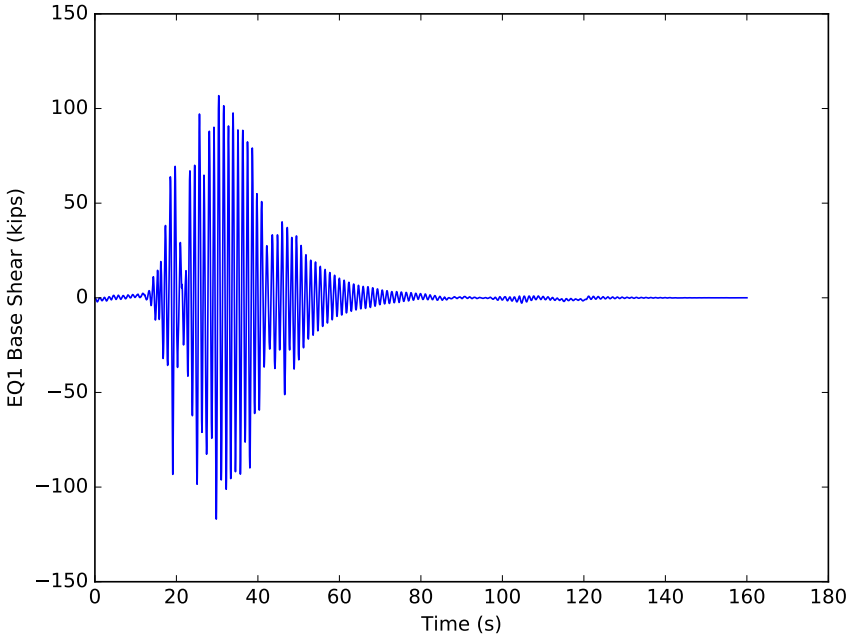

Figure B.10: Fx response of model 1 for EQ1

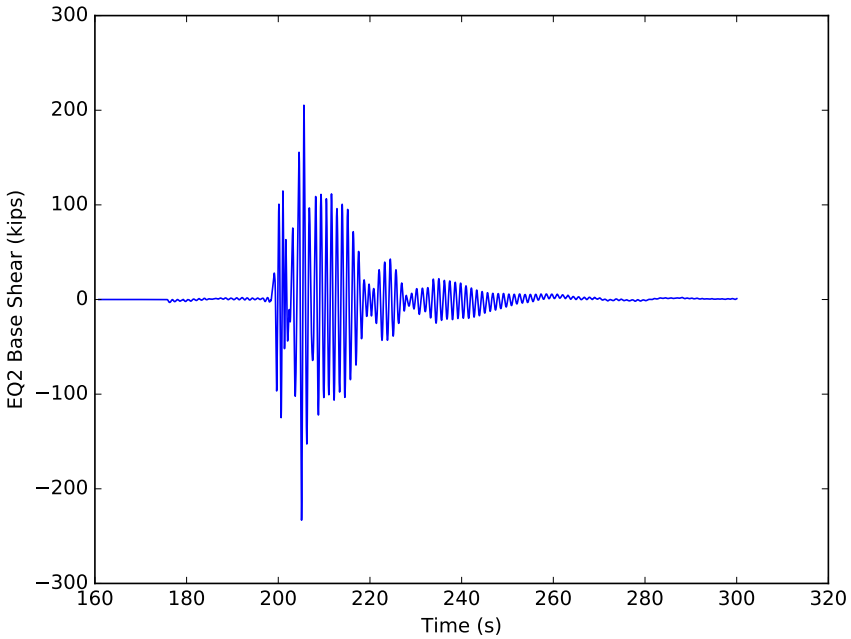

Figure B.11: Fx response of model 1 for EQ2

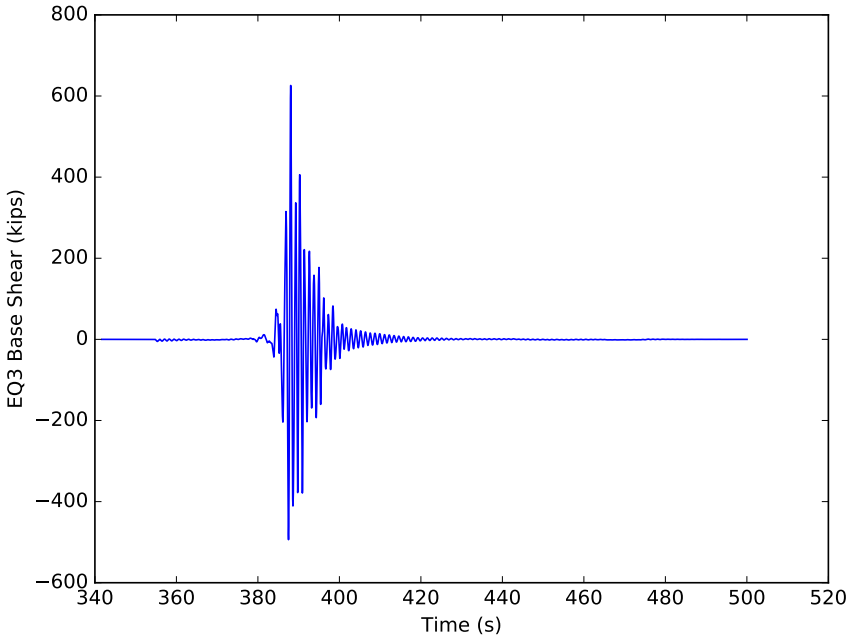

Figure B.12: Fx response of model 1 for EQ3

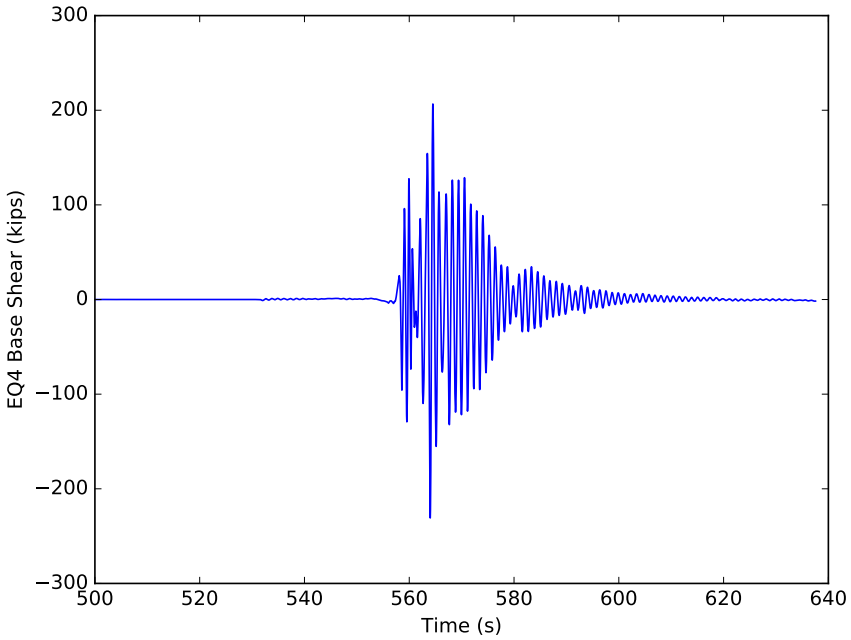

Figure B.13: Fx response of model 1 for EQ4

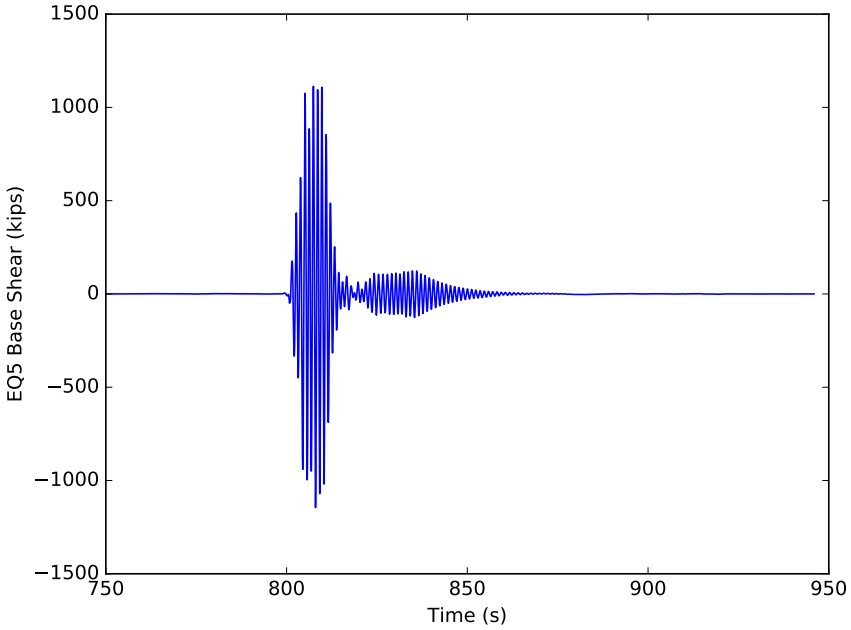

Figure B.14: Fx response of model 1 for EQ5

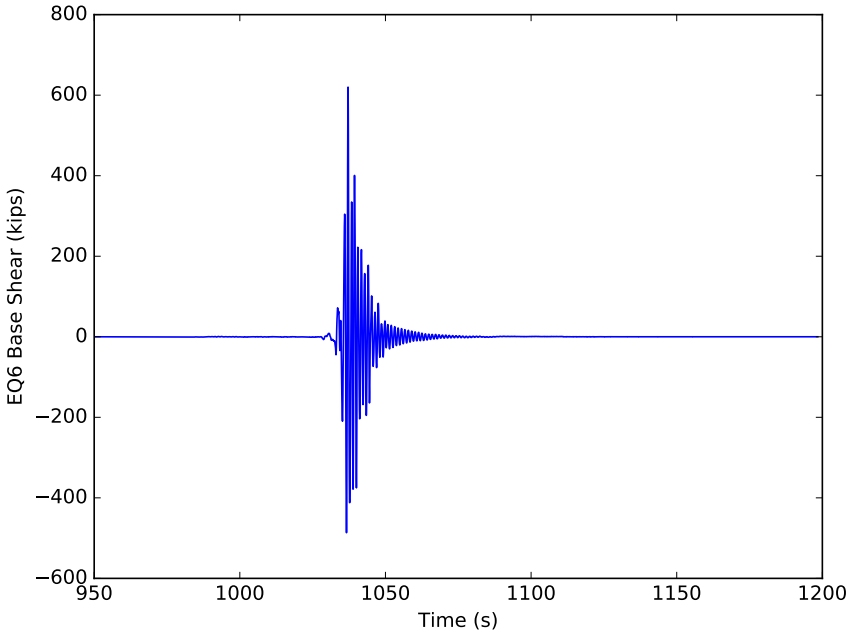

Figure B.15: Fx response of model 1 for EQ6

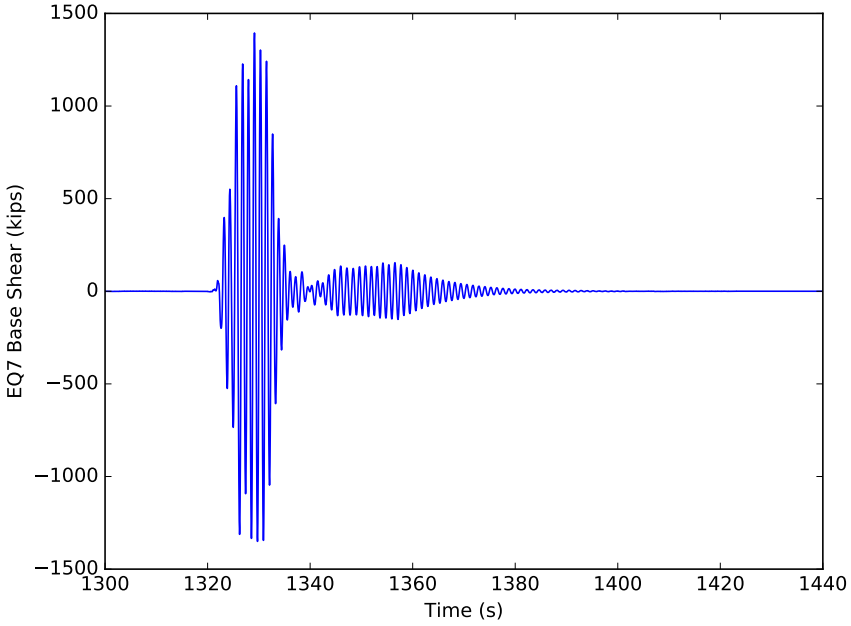

Figure B.16: Fx response of model 1 for EQ7

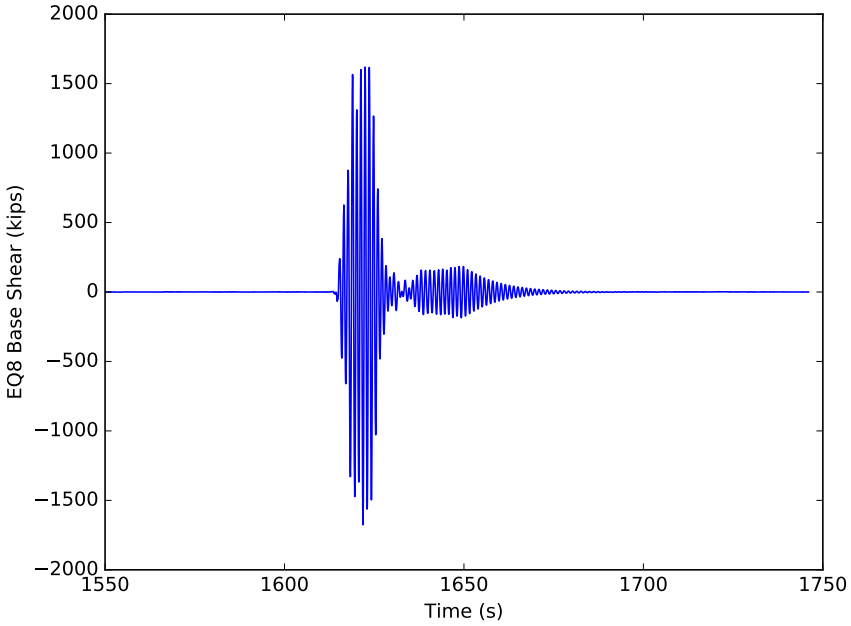

Figure B.17: Fx response of model 1 for EQ8

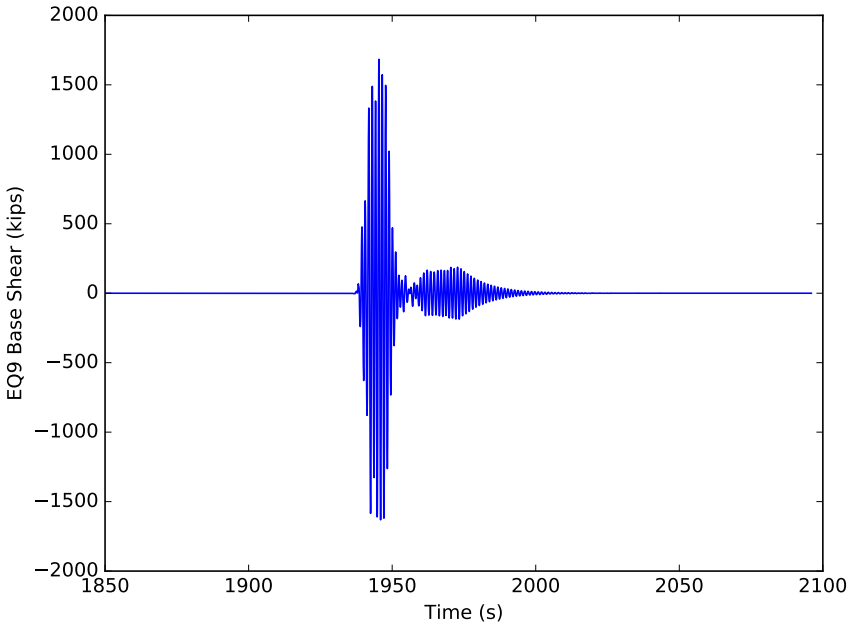

Figure B.18: Fx response of model 1 for EQ9

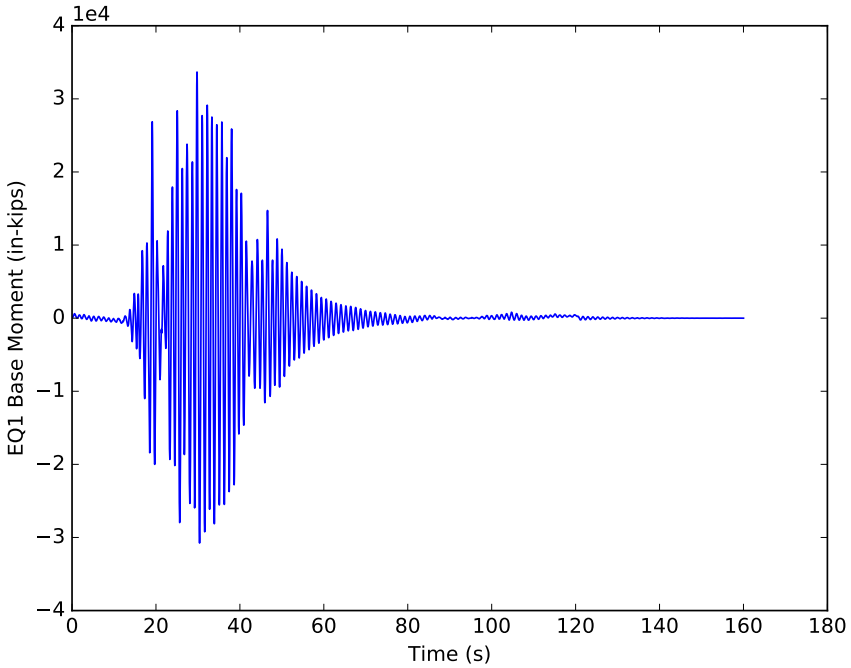

Figure B.19: Mz response of model 1 for EQ1

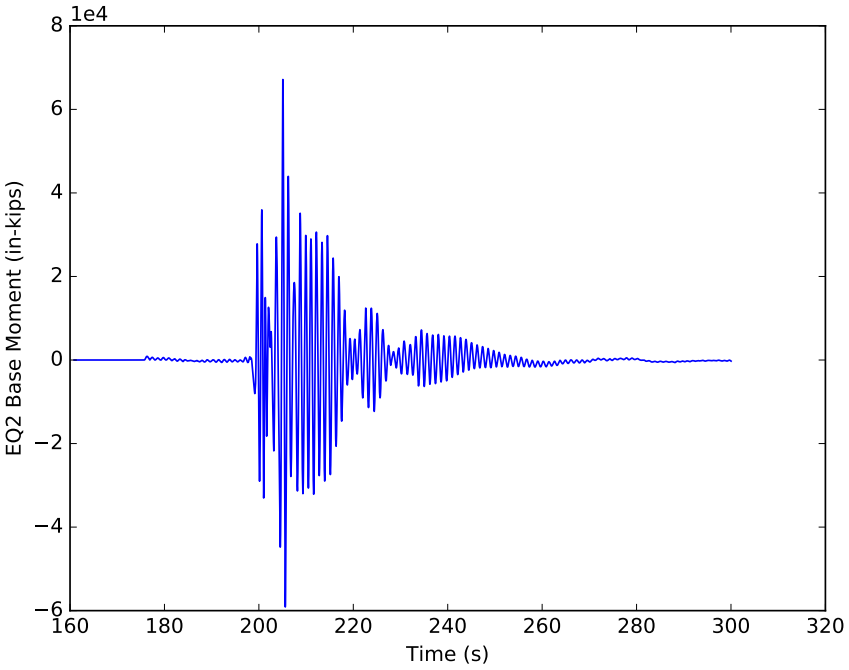

Figure B.20: Mz response of model 1 for EQ2

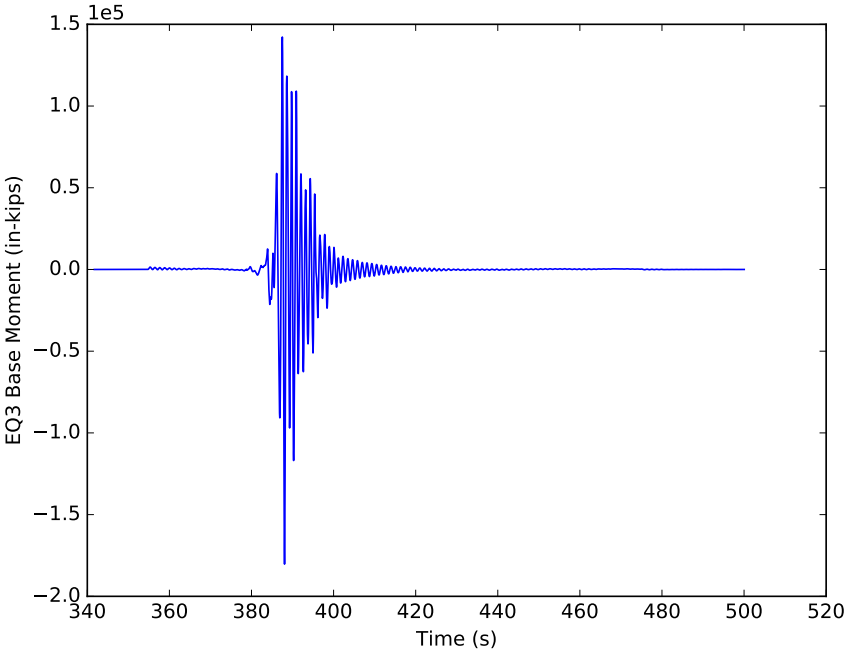

Figure B.21: Mz response of model 1 for EQ3

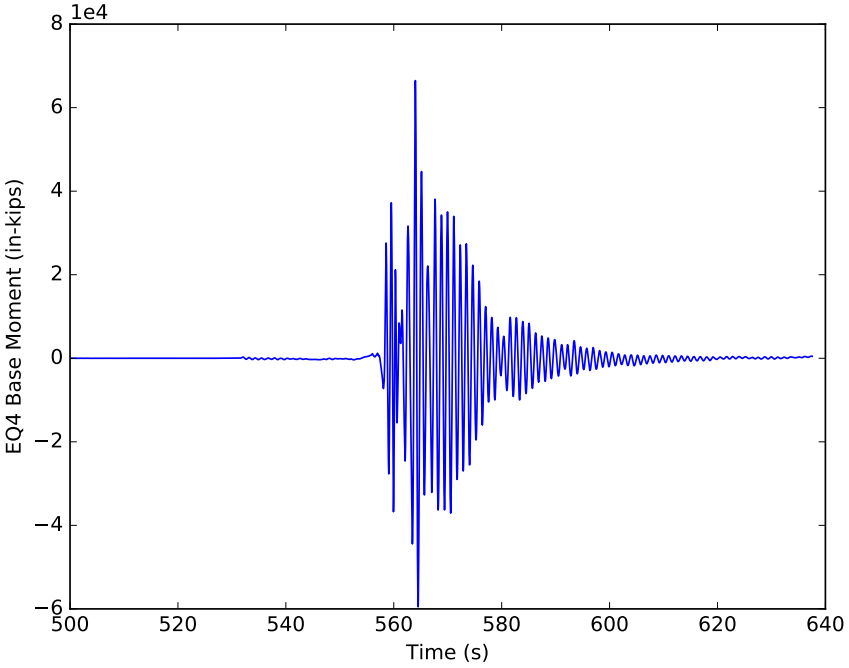

Figure B.22: Mz response of model 1 for EQ4

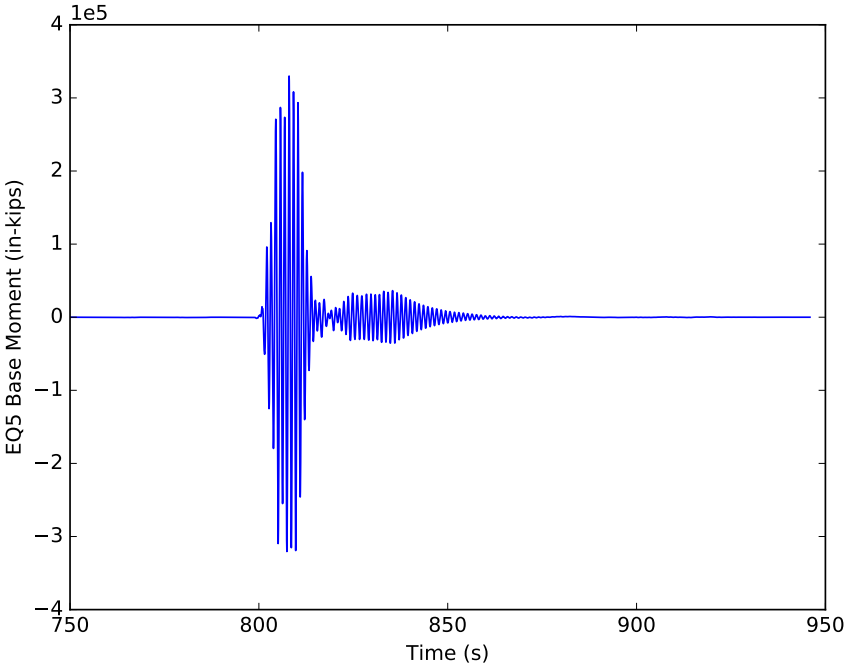

Figure B.23: Mz response of model 1 for EQ5

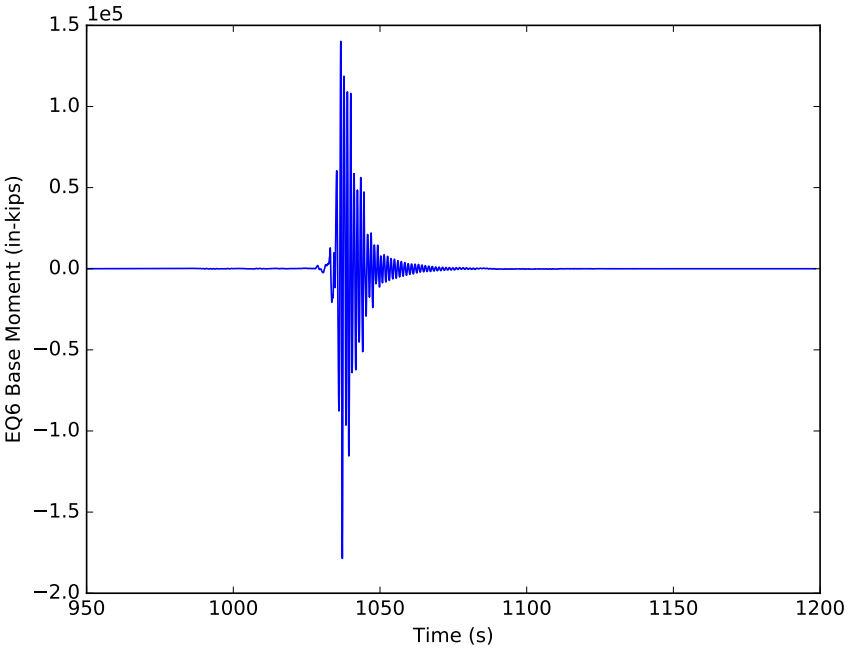

Figure B.24: Mz response of model 1 for EQ6

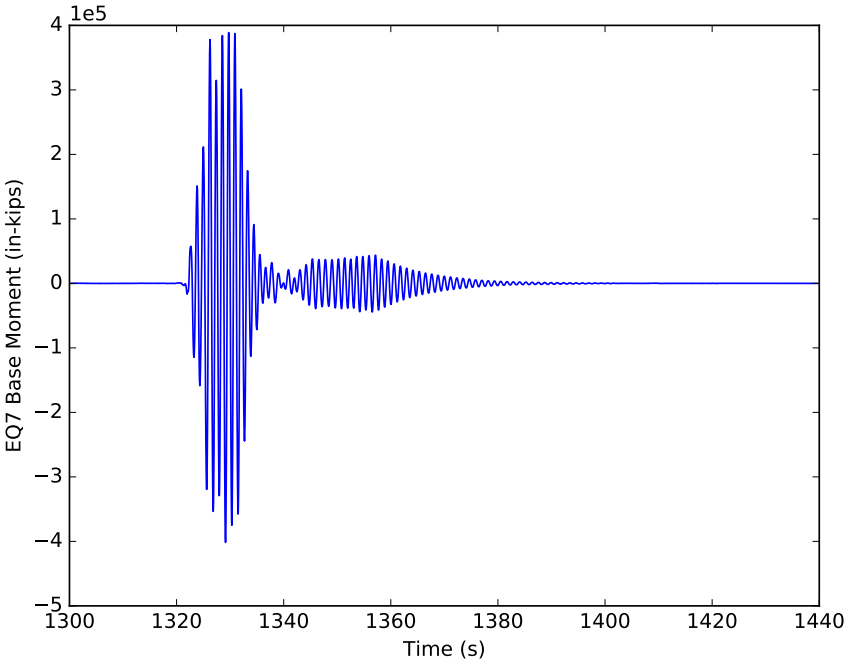

Figure B.25: Mz response of model 1 for EQ7

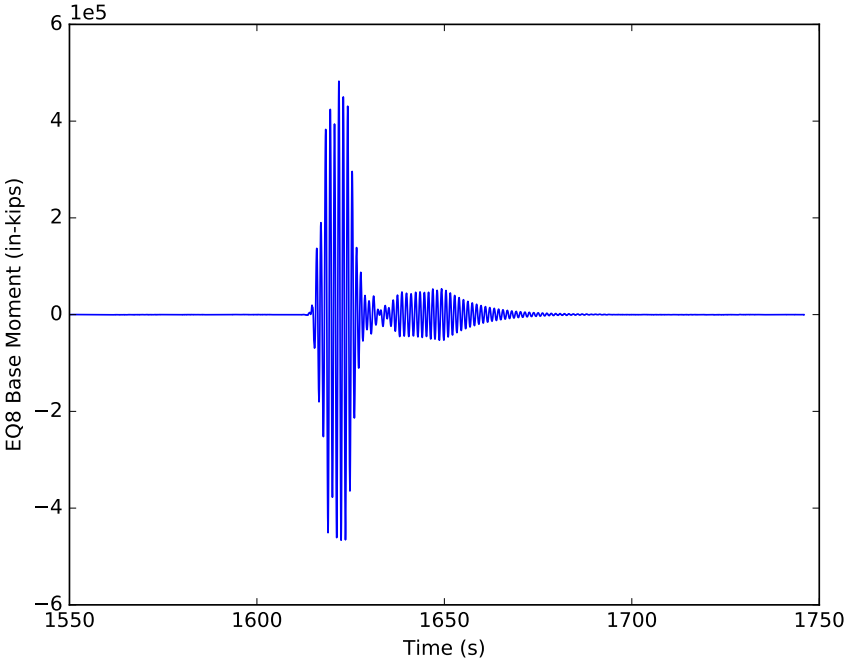

Figure B.26: Mz response of model 1 for EQ8

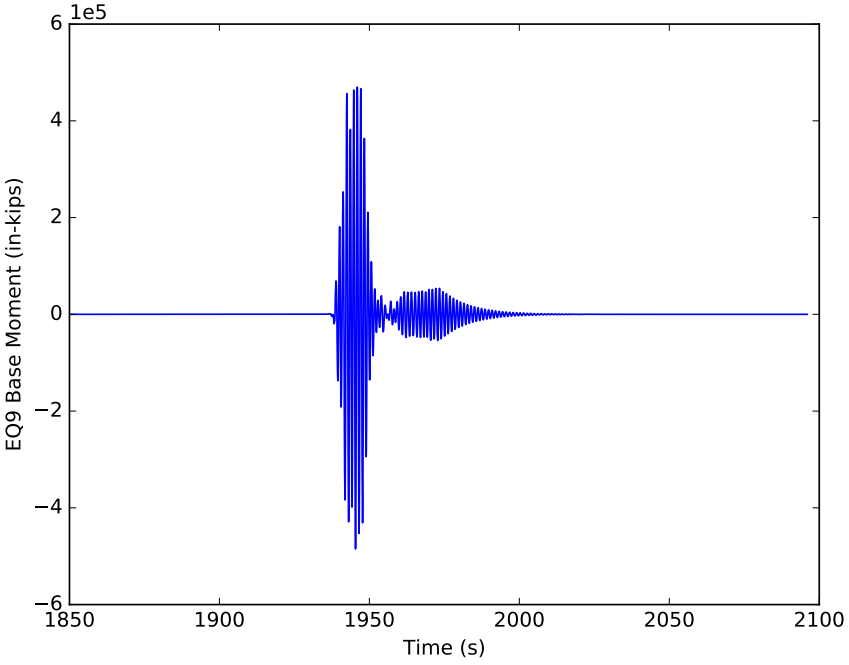

Figure B.27: Mz response of model 1 for EQ9

Appendix C

Model 2 Output

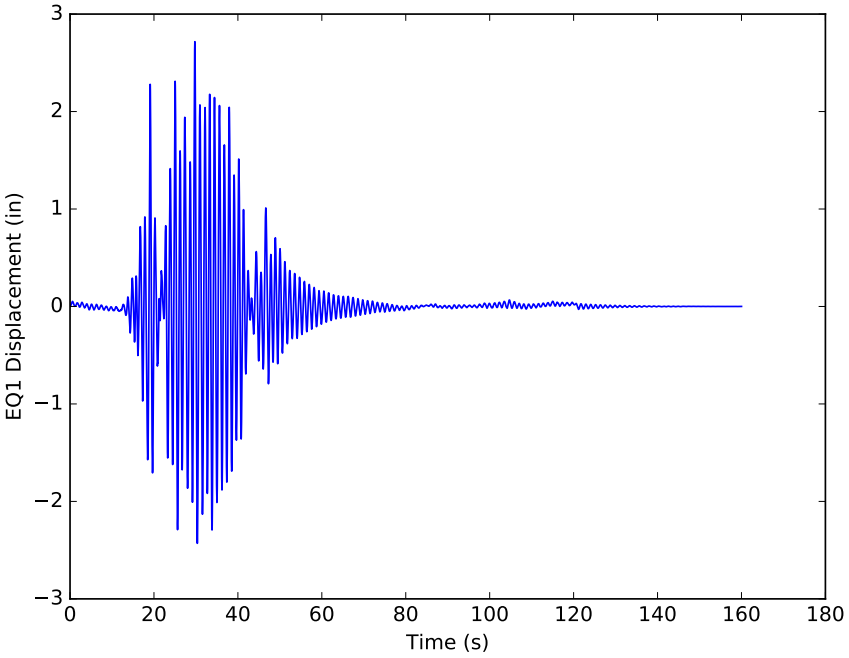

Figure C.1: Displacement response of model 2 for EQ1

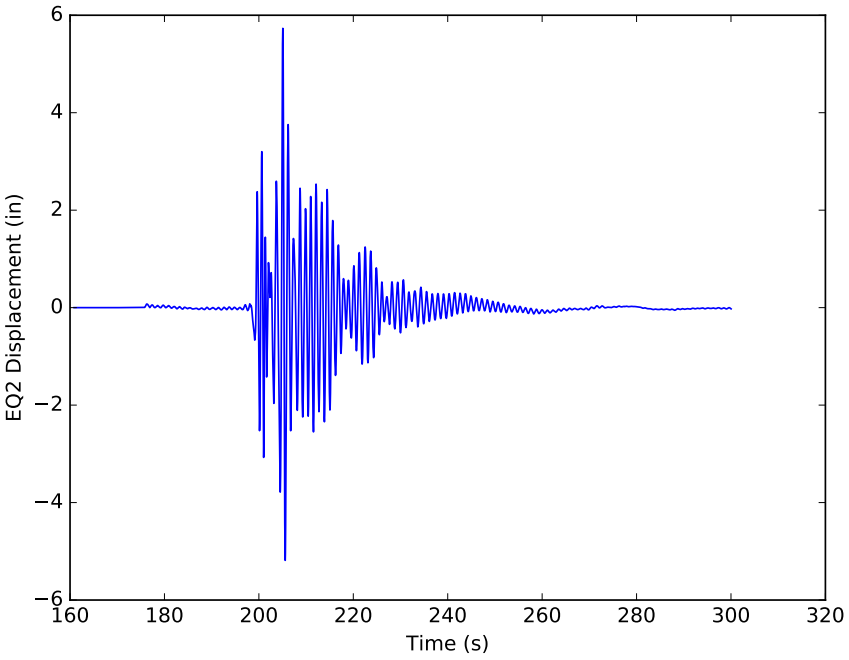

Figure C.2: Displacement response of model 2 for EQ2

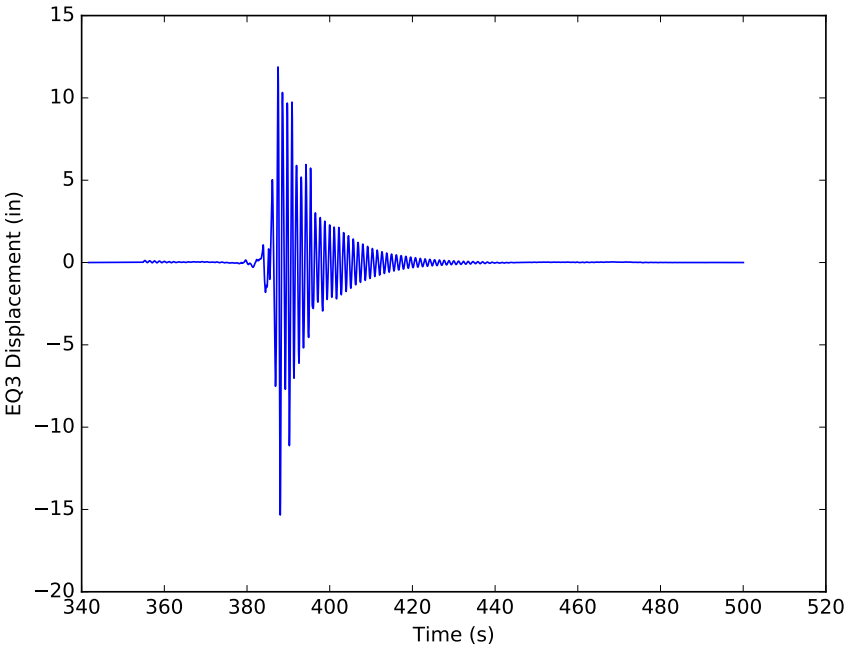

Figure C.3: Displacement response of model 2 for EQ3

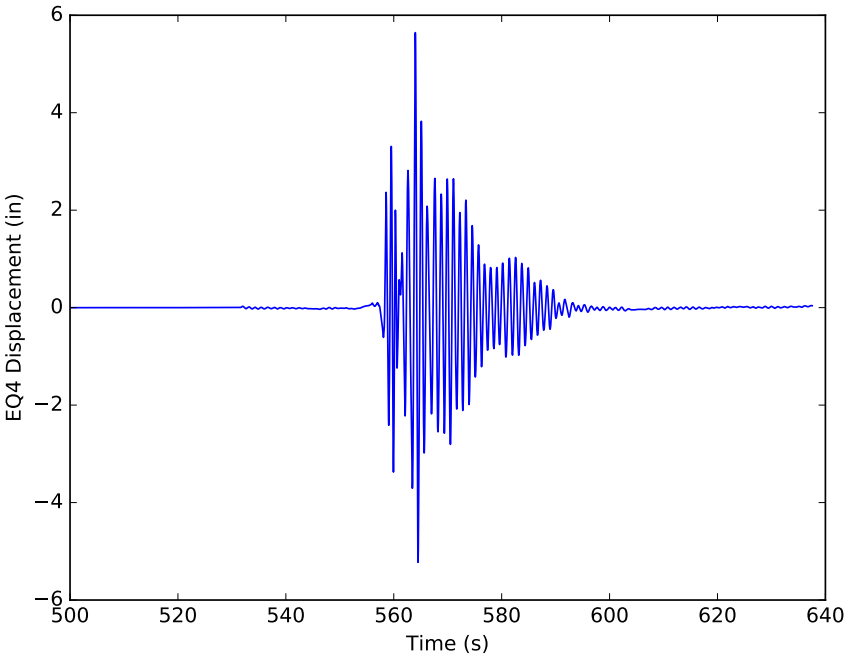

Figure C.4: Displacement response of model 2 for EQ4

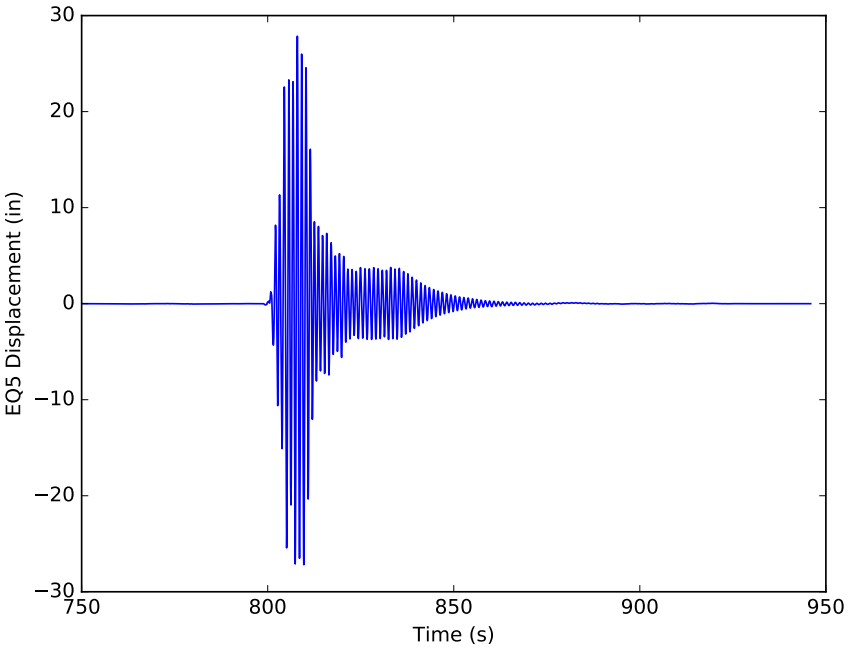

Figure C.5: Displacement response of model 2 for EQ5

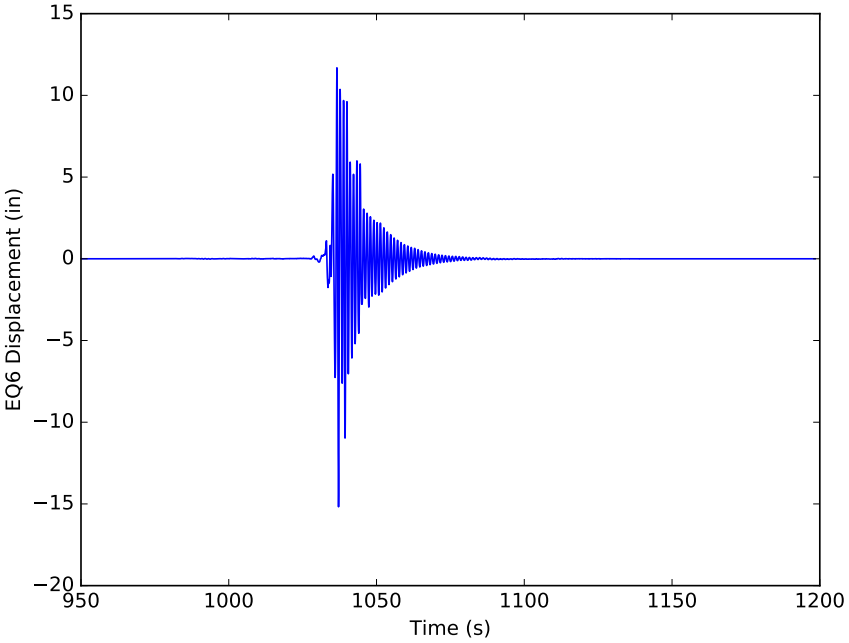

Figure C.6: Displacement response of model 2 for EQ6

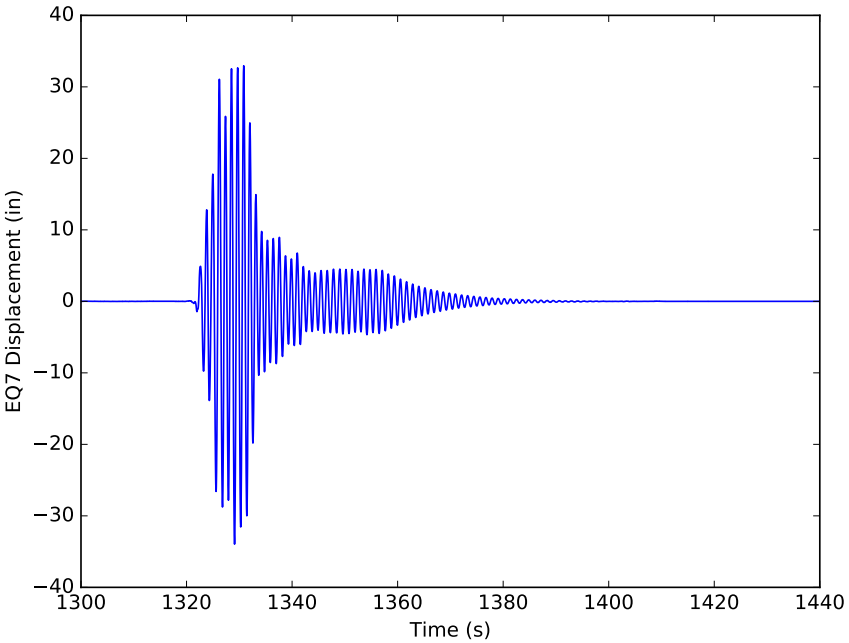

Figure C.7: Displacement response of model 2 for EQ7

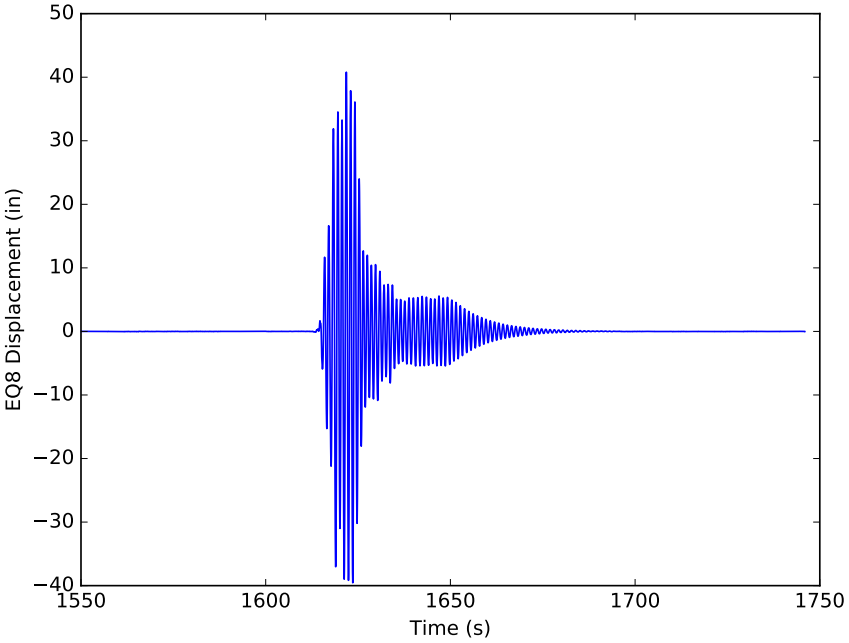

Figure C.8: Displacement response of model 2 for EQ8

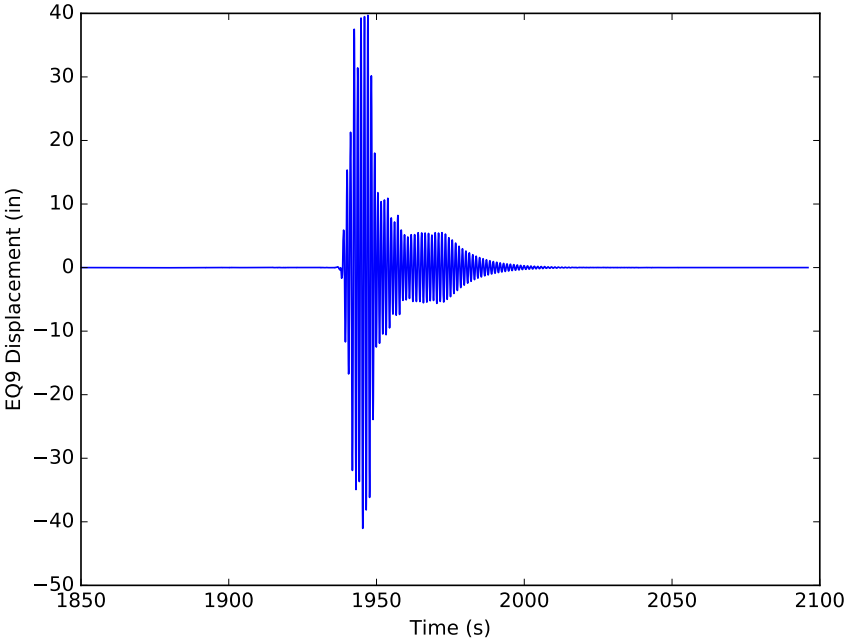

Figure C.9: Displacement response of model 2 for EQ9

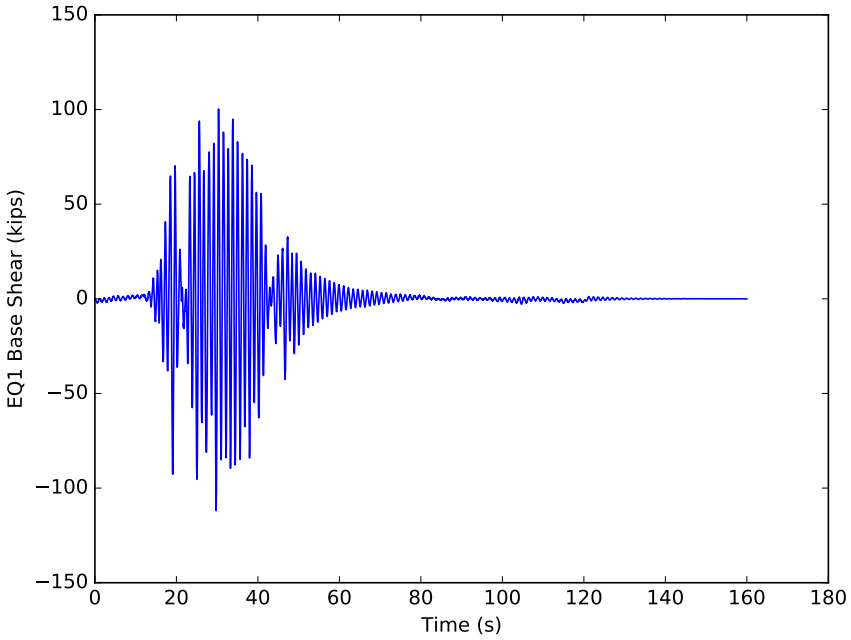

Figure C.10: Fx response of model 2 for EQ1

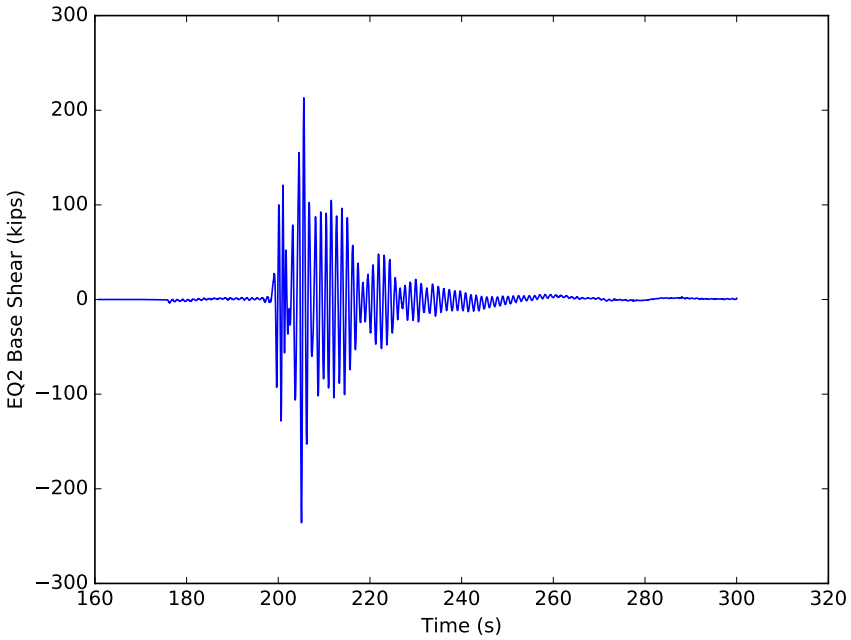

Figure C.11: Fx response of model 2 for EQ2

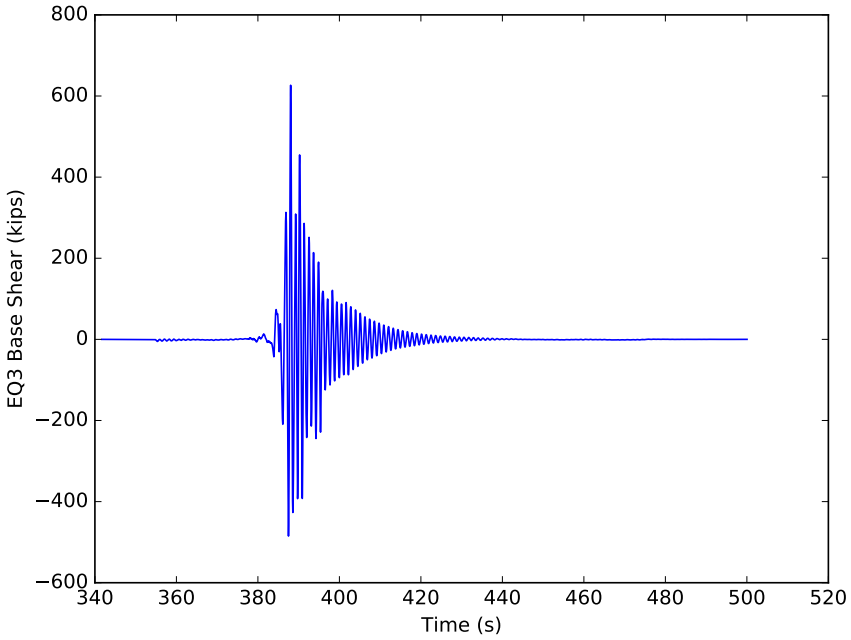

Figure C.12: Fx response of model 2 for EQ3

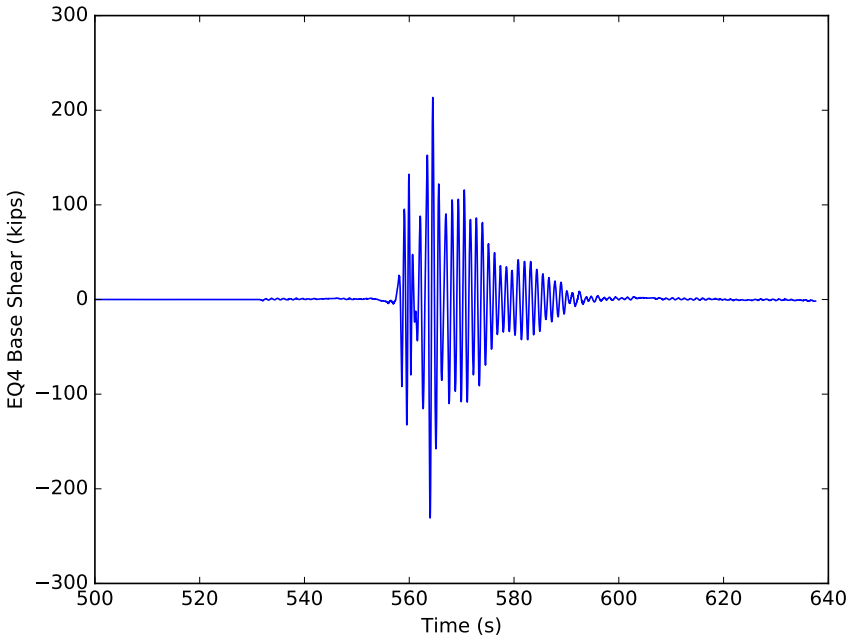

Figure C.13: Fx response of model 2 for EQ4

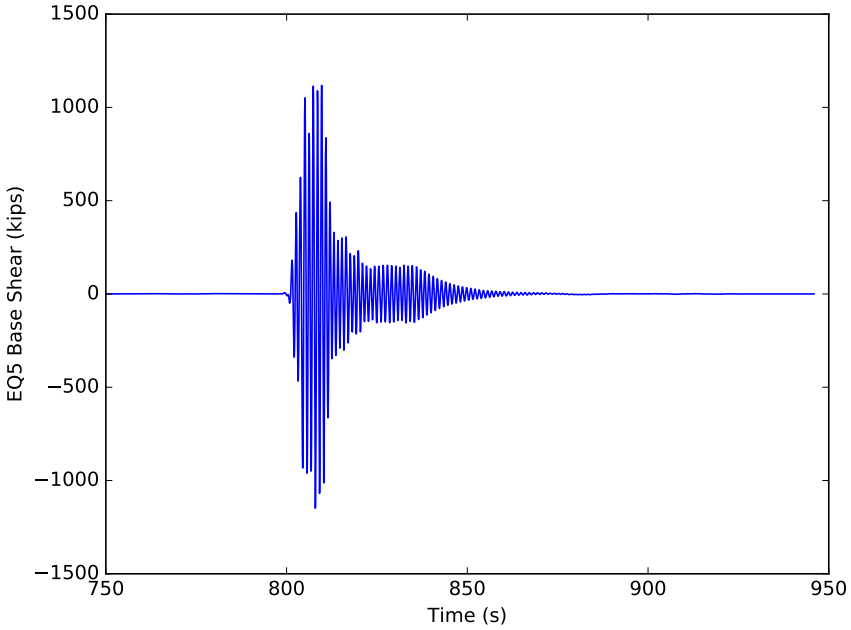

Figure C.14: Fx response of model 2 for EQ5

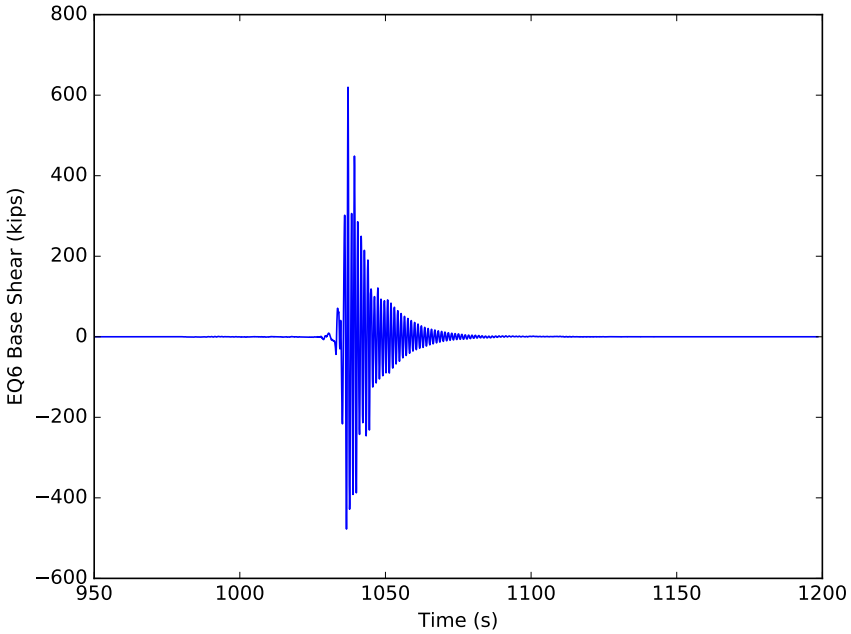

Figure C.15: Fx response of model 2 for EQ6

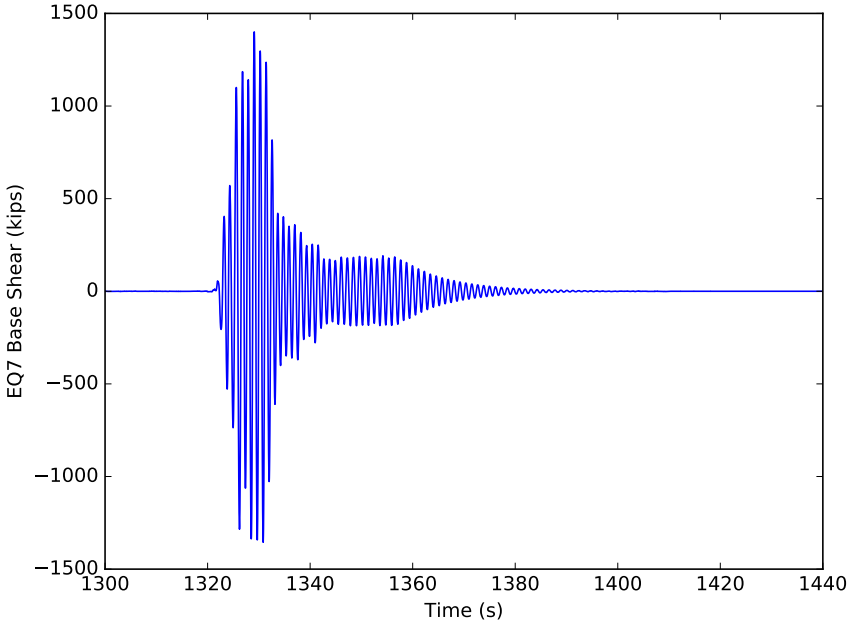

Figure C.16: Fx response of model 2 for EQ7

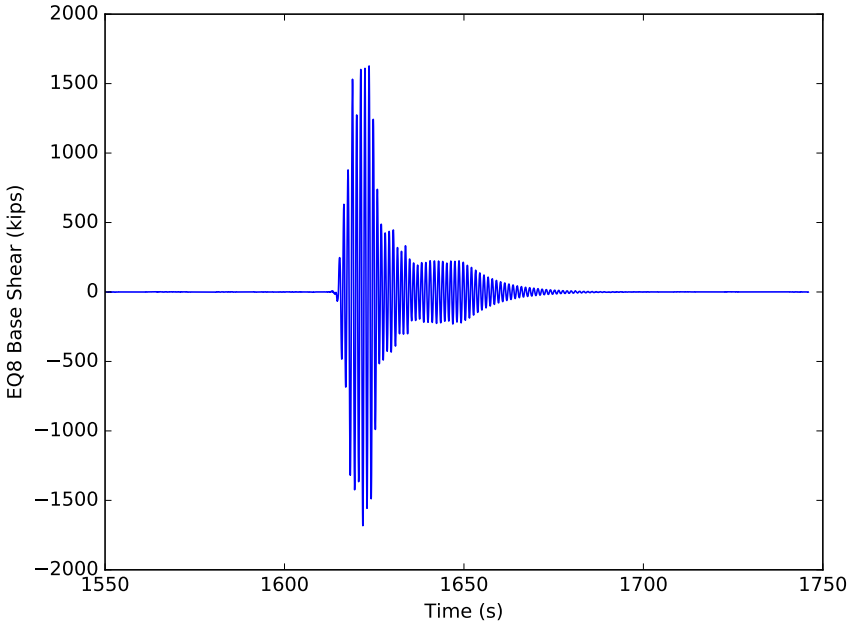

Figure C.17: Fx response of model 2 for EQ8

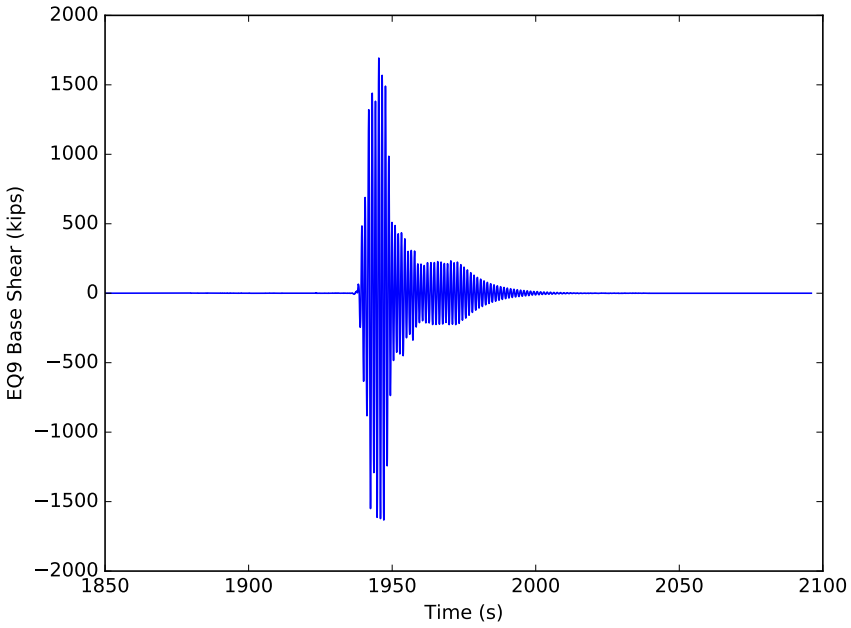

Figure C.18: Fx response of model 2 for EQ9

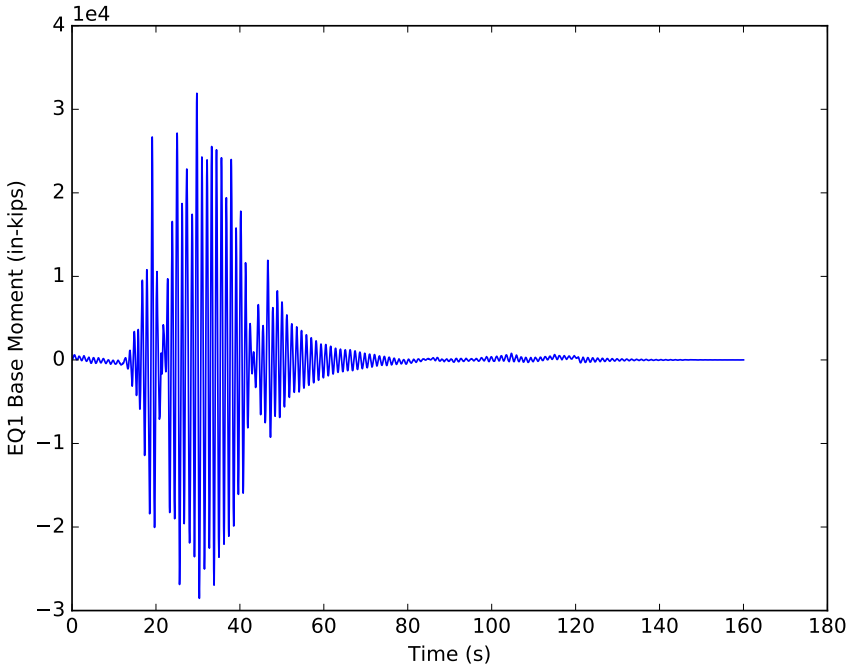

Figure C.19: Mz response of model 2 for EQ1

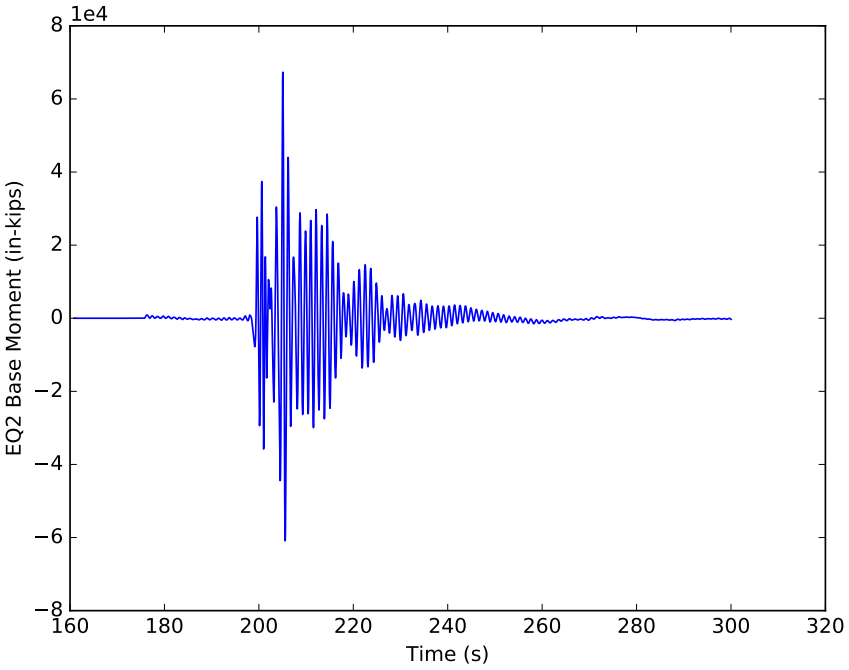

Figure C.20: Mz response of model 2 for EQ2

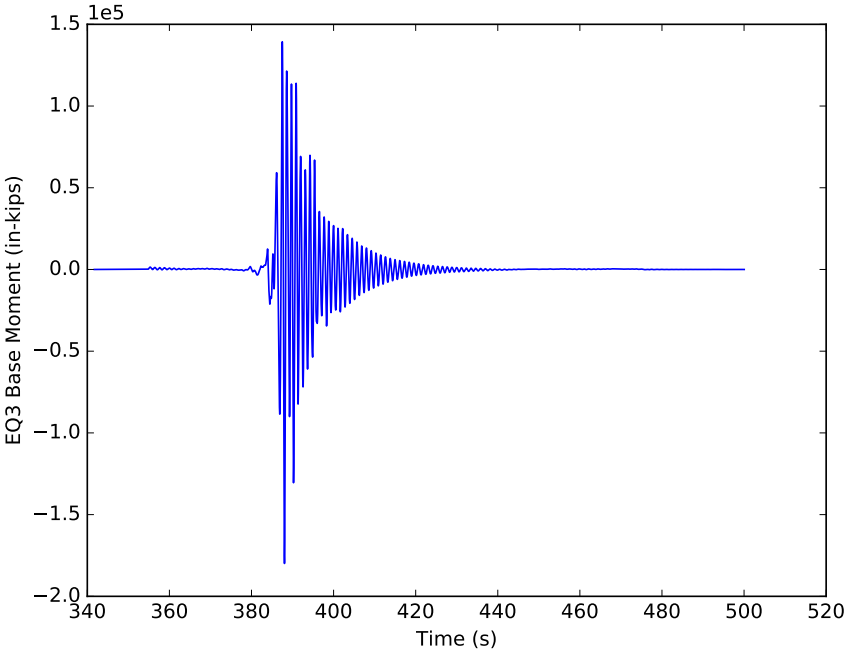

Figure C.21: Mz response of model 2 for EQ3

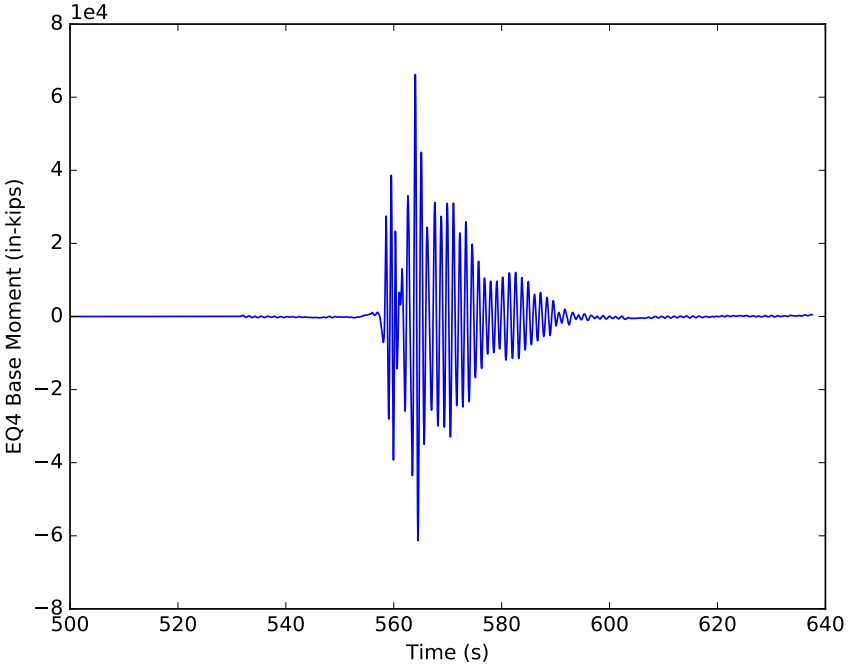

Figure C.22: Mz response of model 2 for EQ4

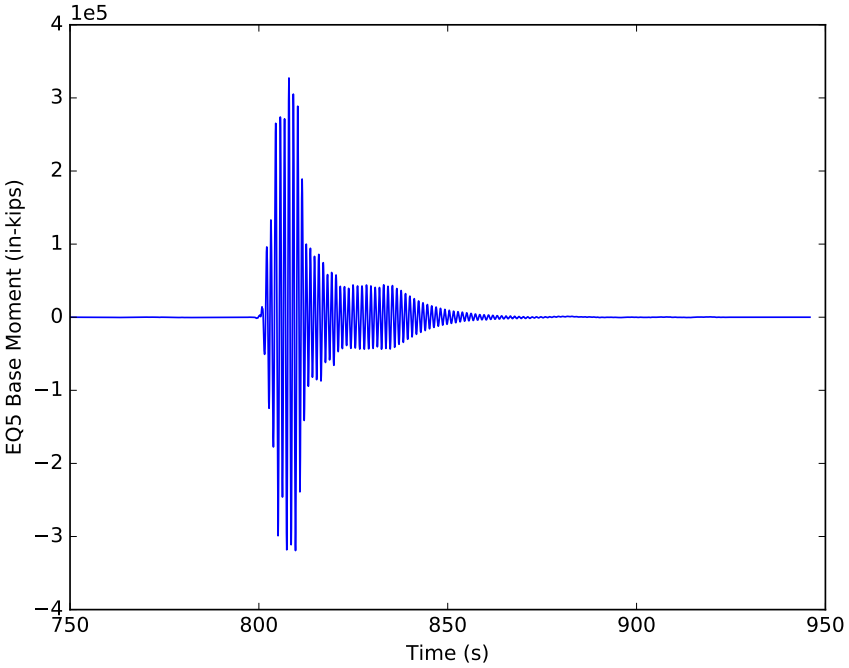

Figure C.23: Mz response of model 2 for EQ5

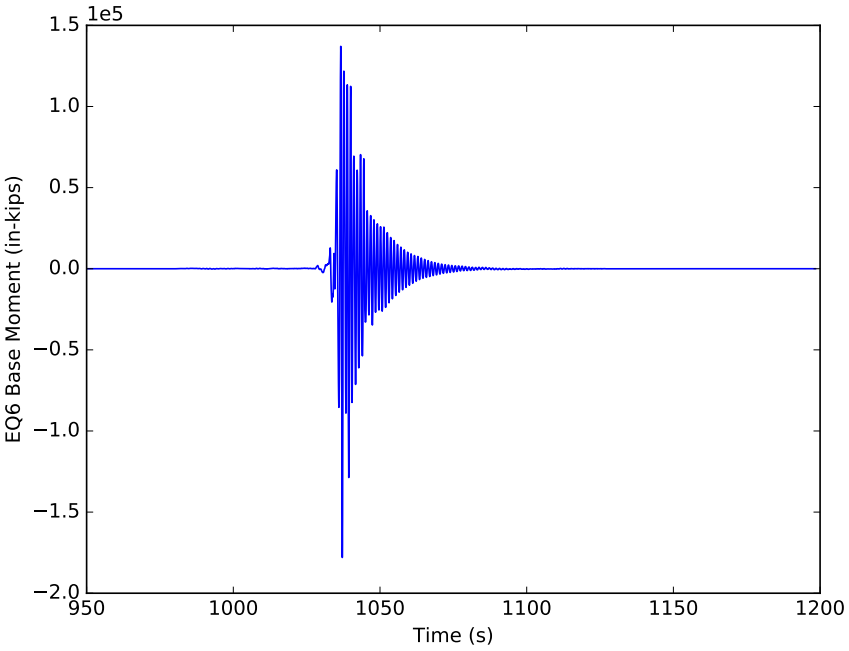

Figure C.24: Mz response of model 2 for EQ6

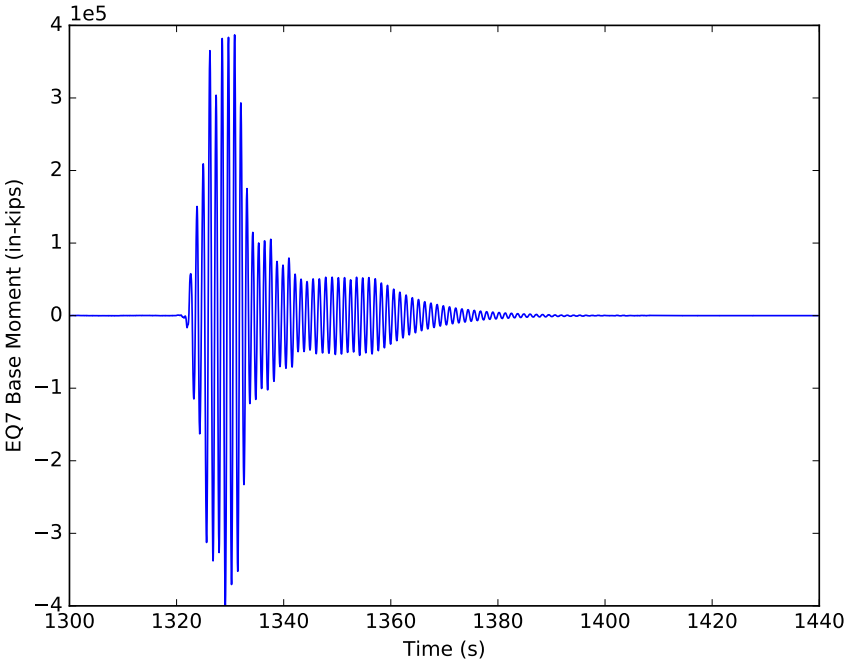

Figure C.25: Mz response of model 2 for EQ7

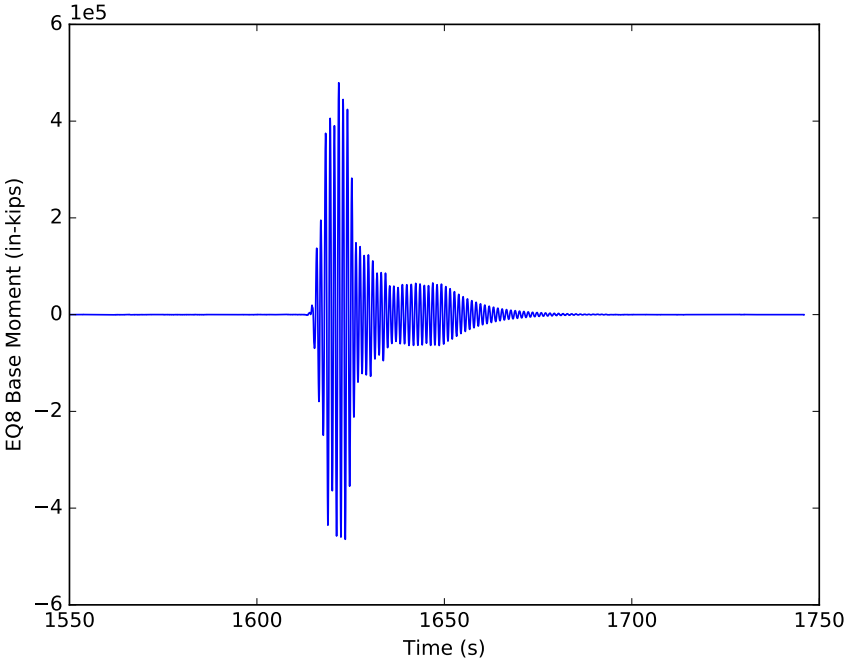

Figure C.26: Mz response of model 2 for EQ8

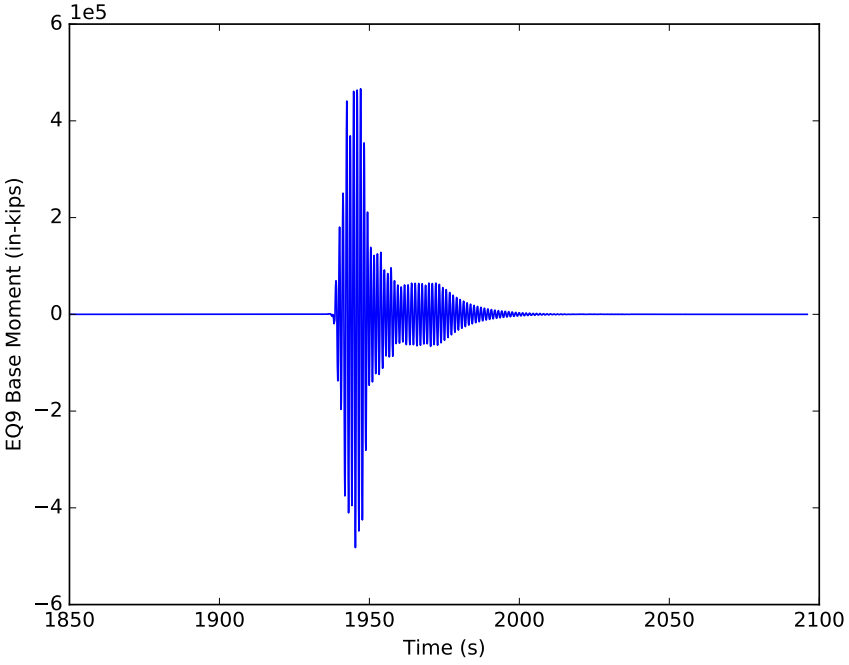

Figure C.27: Mz response of model 2 for EQ9

Appendix D

Model 3 Output

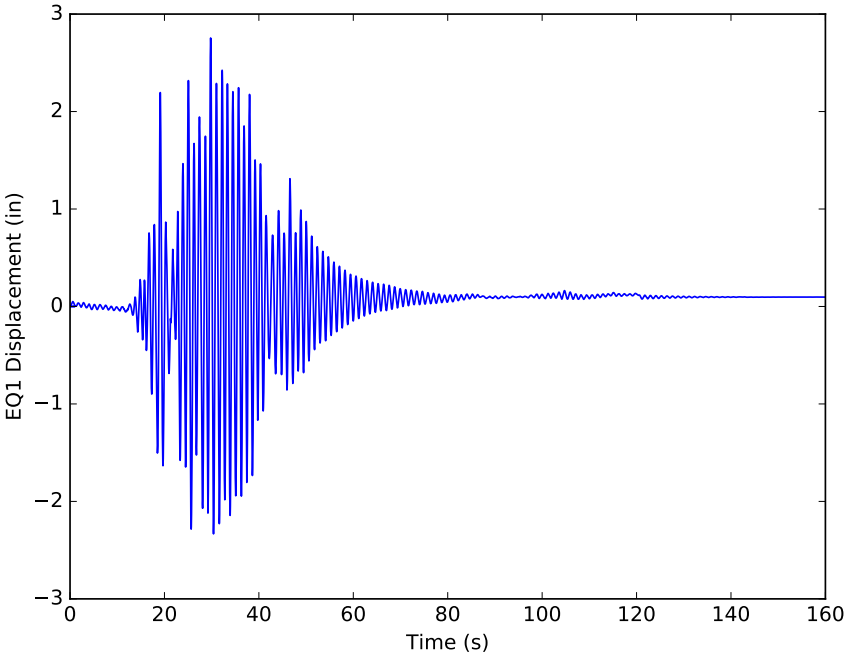

Figure D.1: Displacement response of model 3 for EQ1

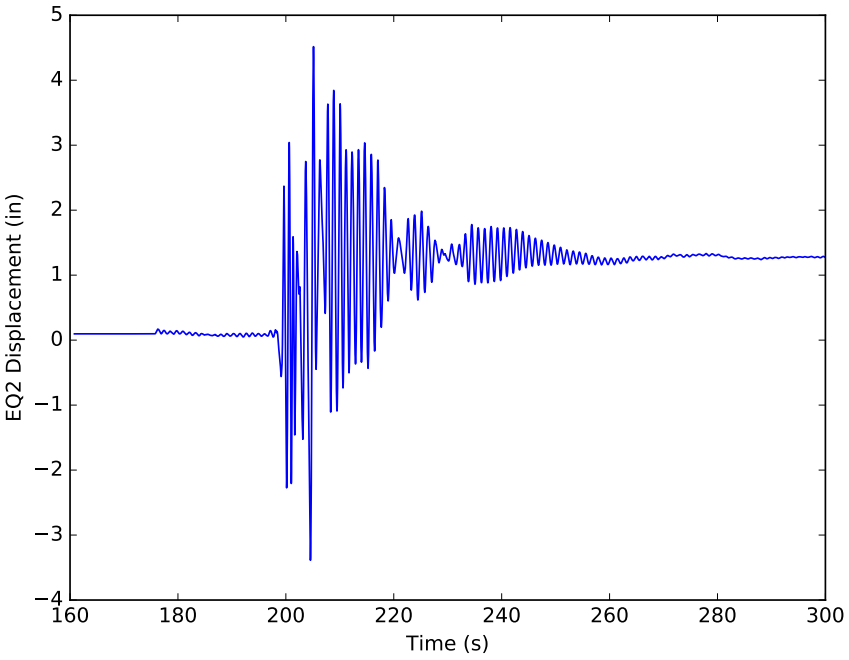

Figure D.2: Displacement response of model 3 for EQ2

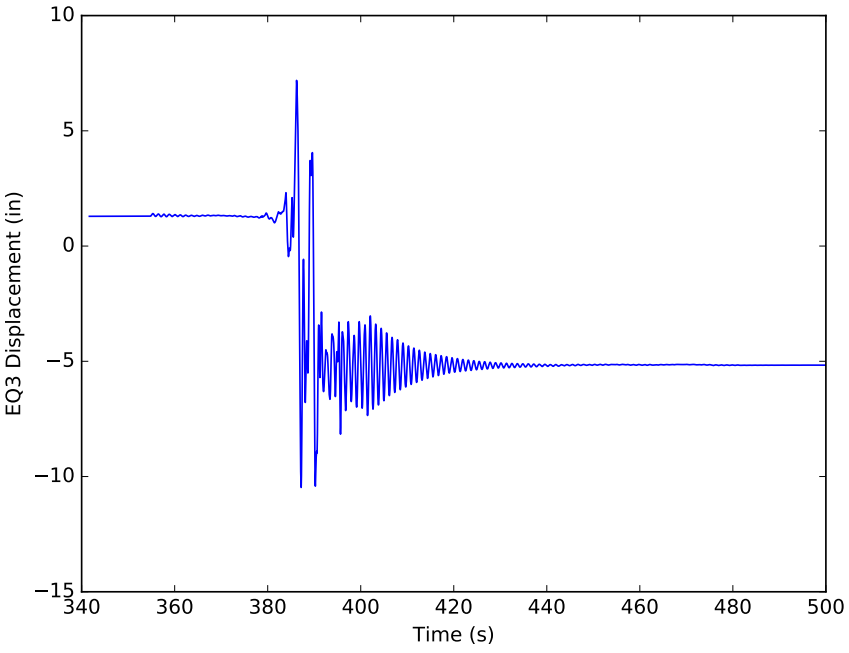

Figure D.3: Displacement response of model 3 for EQ3

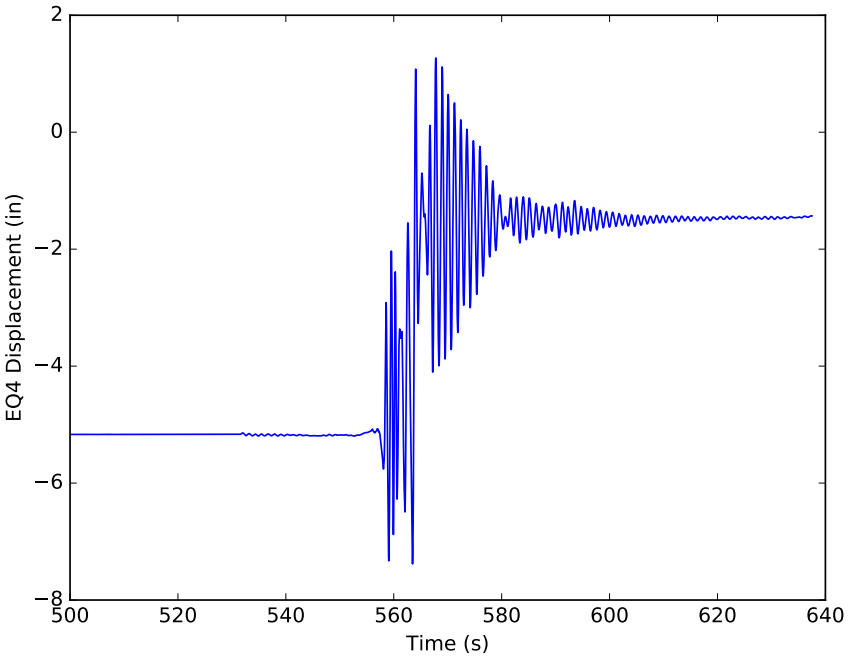

Figure D.4: Displacement response of model 3 for EQ4

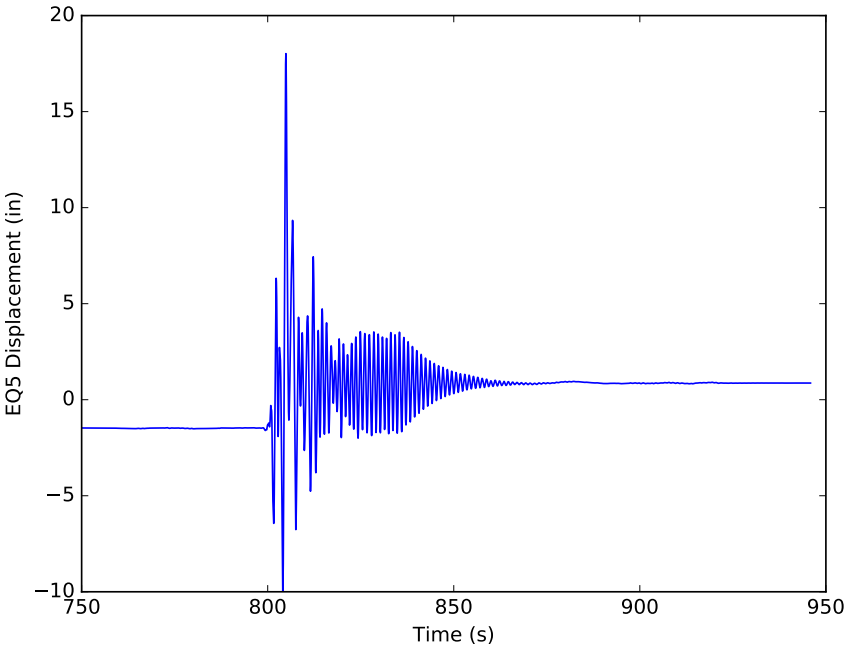

Figure D.5: Displacement response of model 3 for EQ5

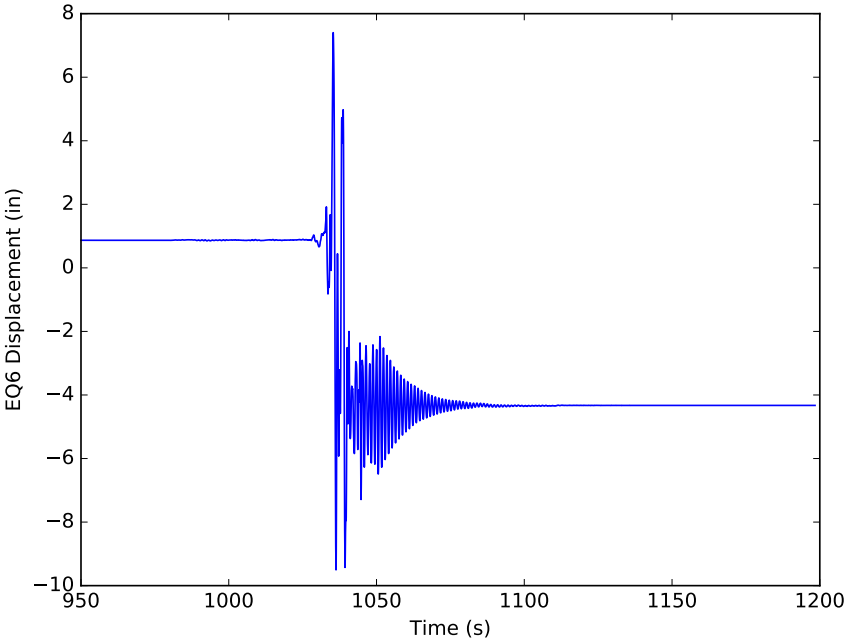

Figure D.6: Displacement response of model 3 for EQ6

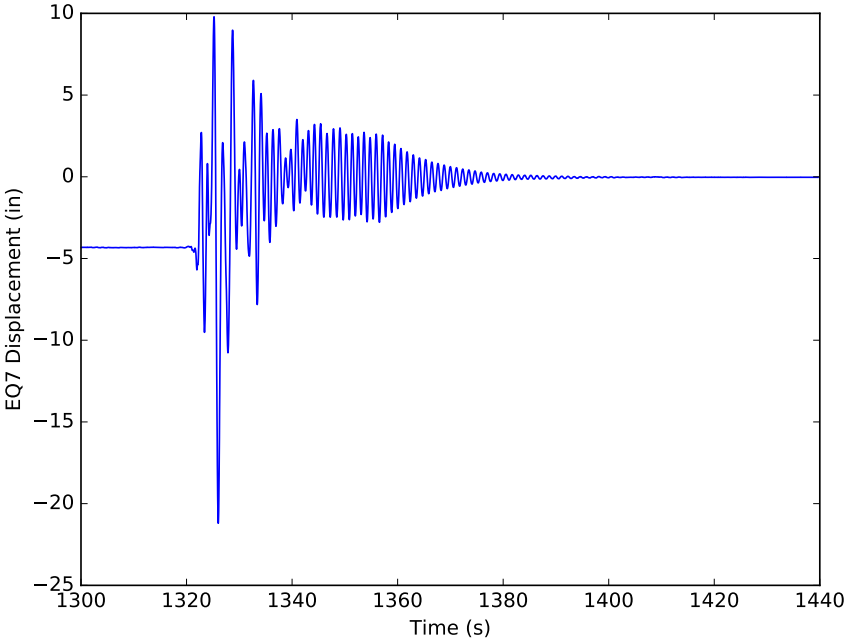

Figure D.7: Displacement response of model 3 for EQ7

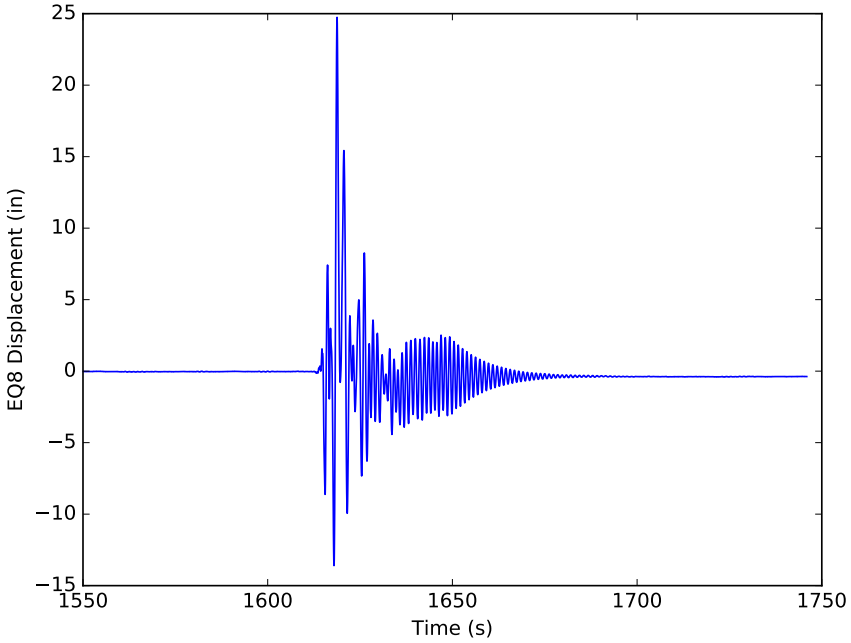

Figure D.8: Displacement response of model 3 for EQ8

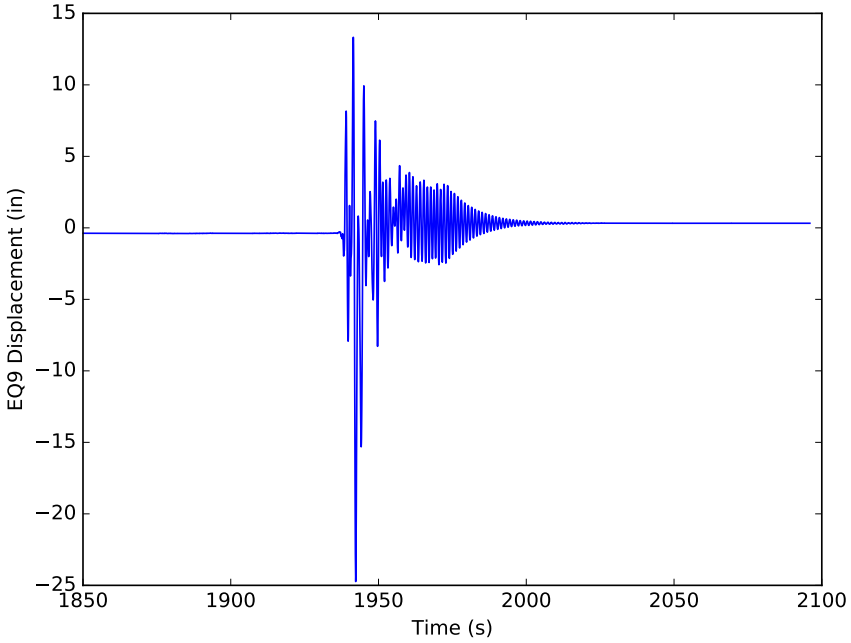

Figure D.9: Displacement response of model 3 for EQ9

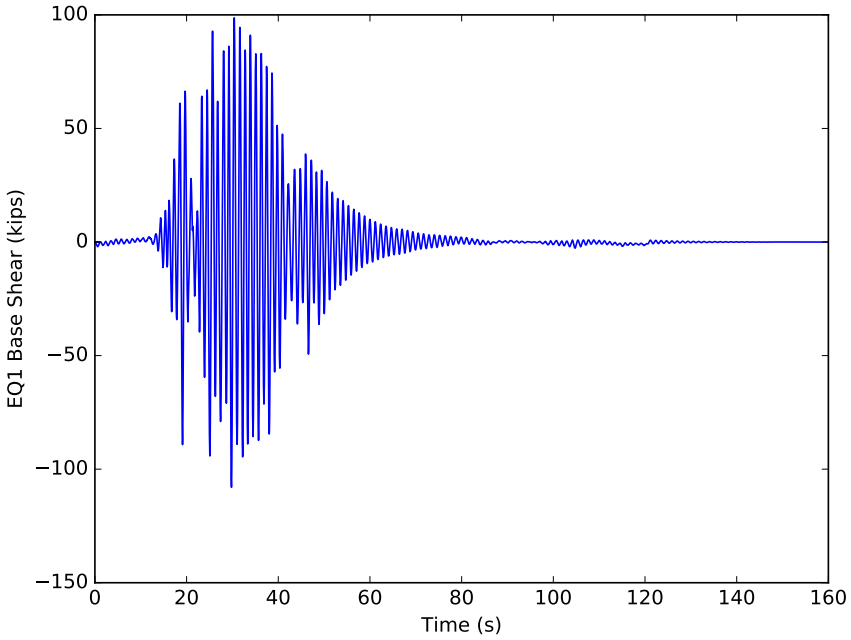

Figure D.10: Fx response of model 3 for EQ1

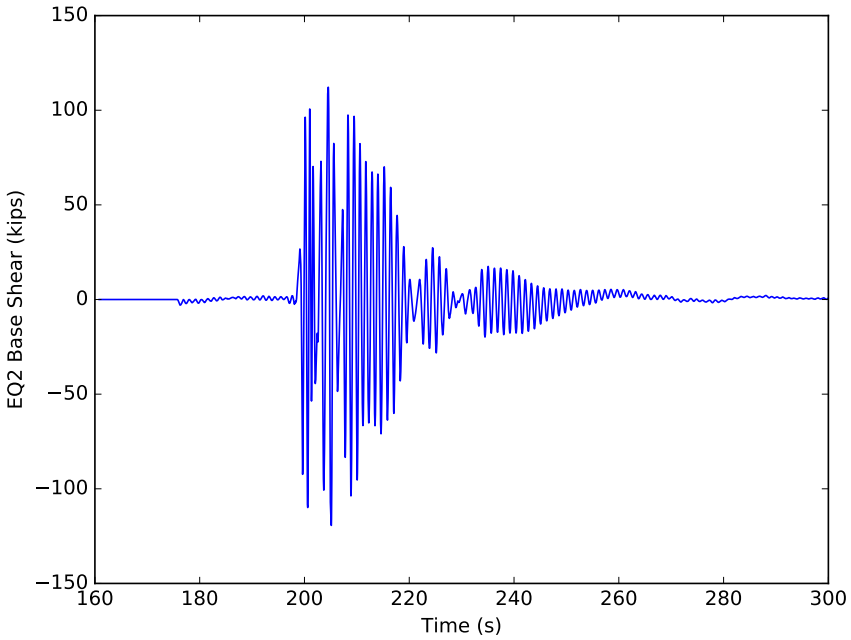

Figure D.11: Fx response of model 3 for EQ2

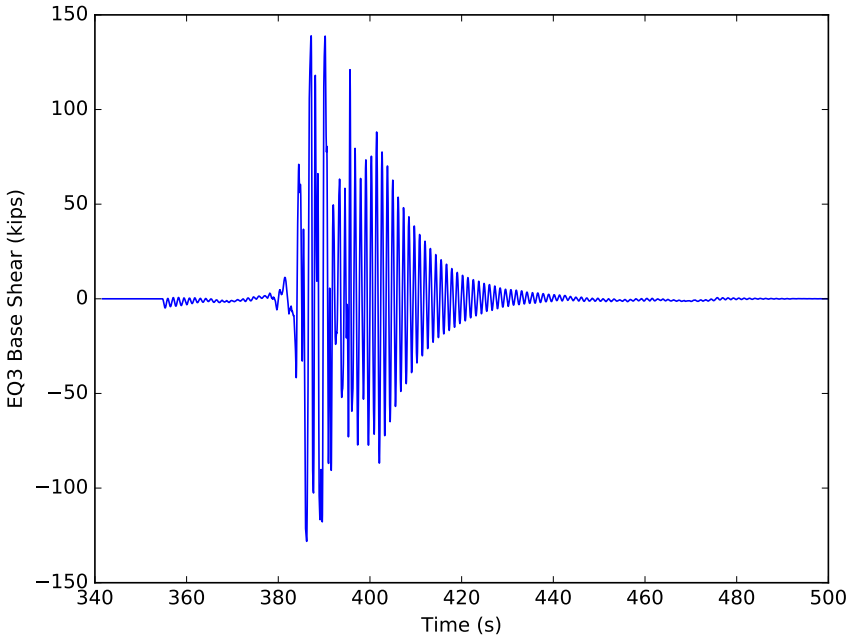

Figure D.12: Fx response of model 3 for EQ3

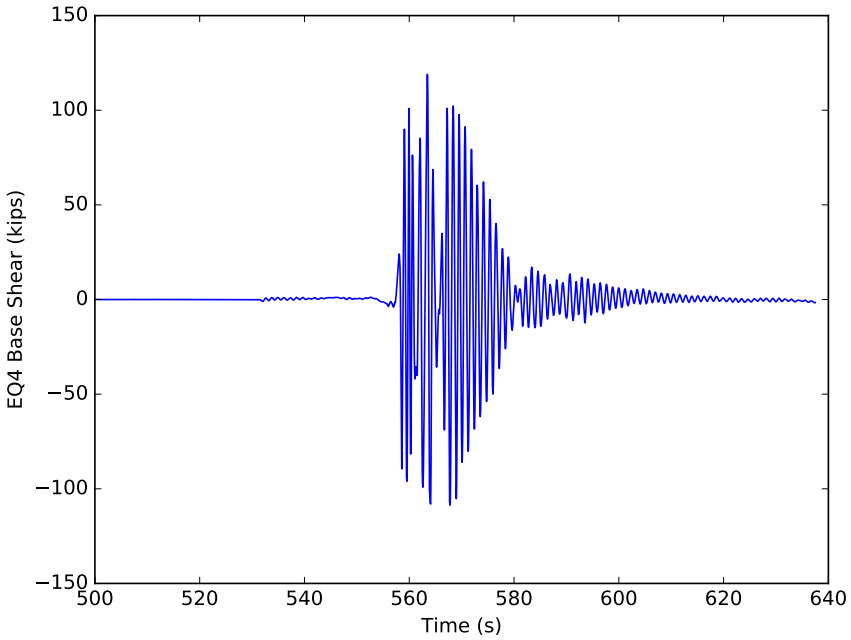

Figure D.13: Fx response of model 3 for EQ4

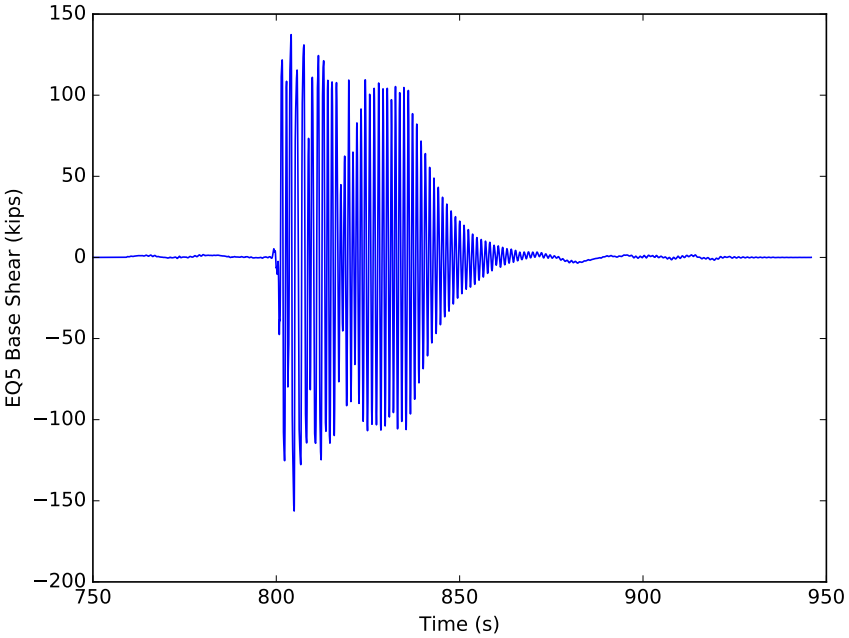

Figure D.14: Fx response of model 3 for EQ5

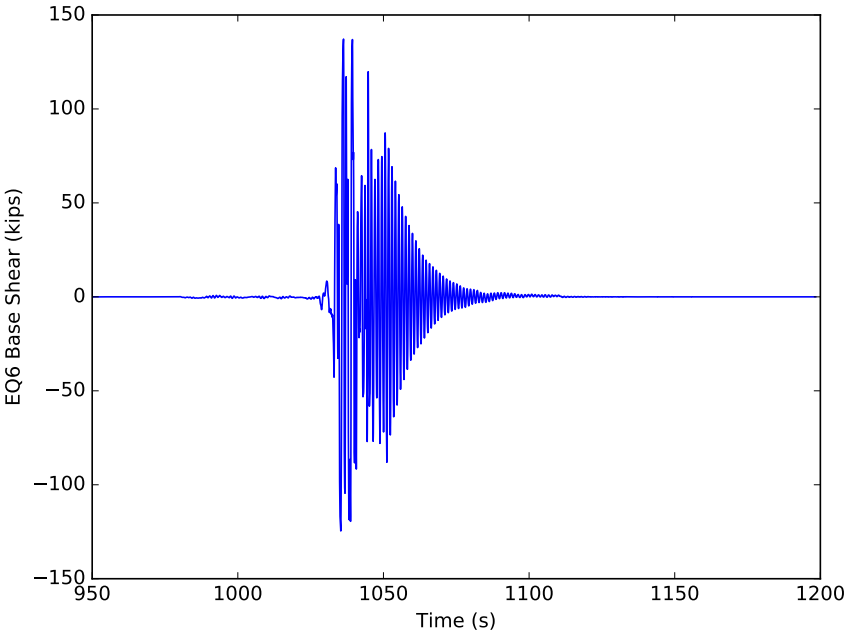

Figure D.15: Fx response of model 3 for EQ6

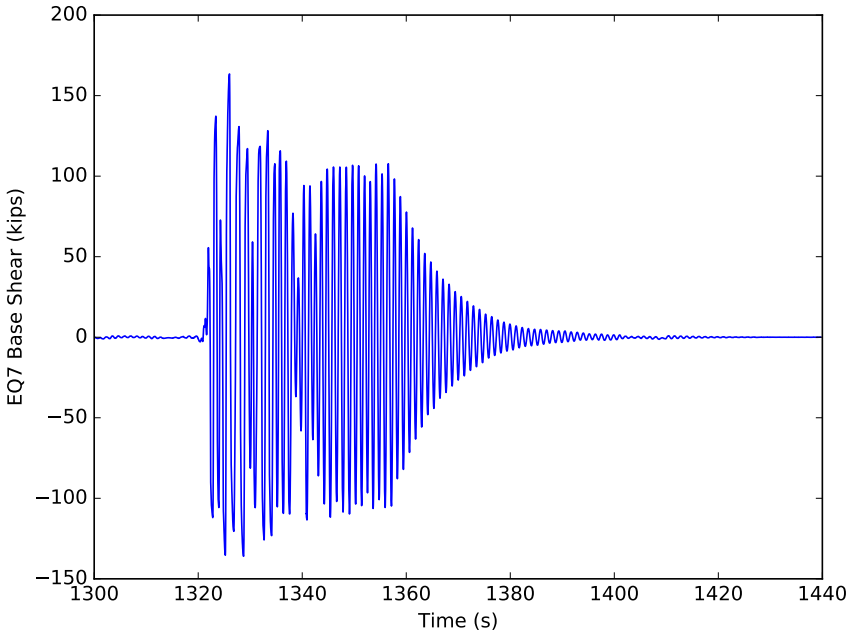

Figure D.16: Fx response of model 3 for EQ7

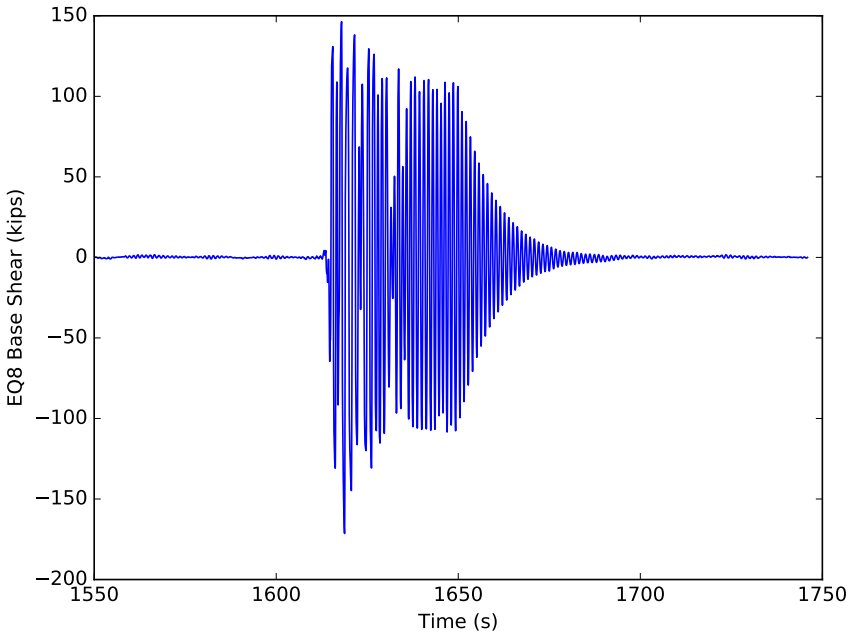

Figure D.17: Fx response of model 3 for EQ8

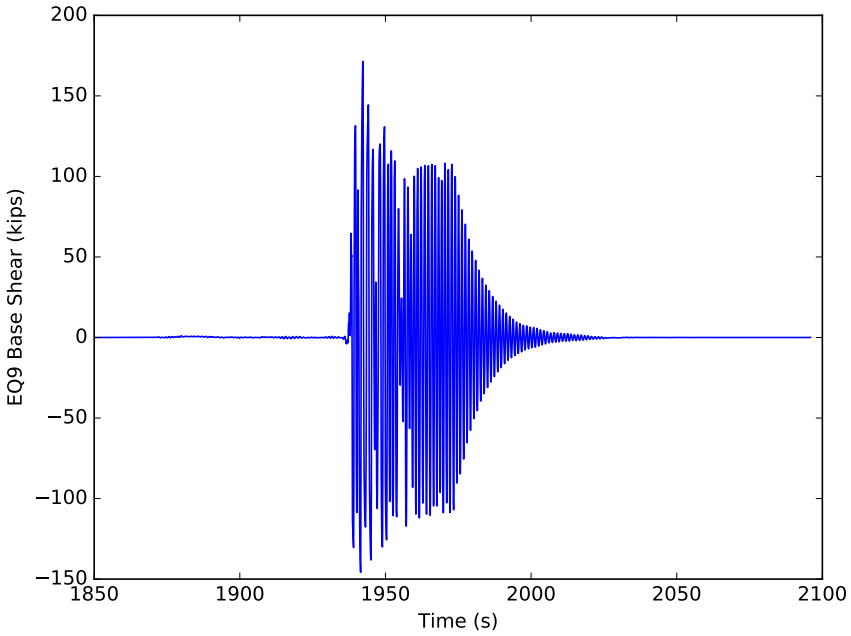

Figure D.18: Fx response of model 3 for EQ9

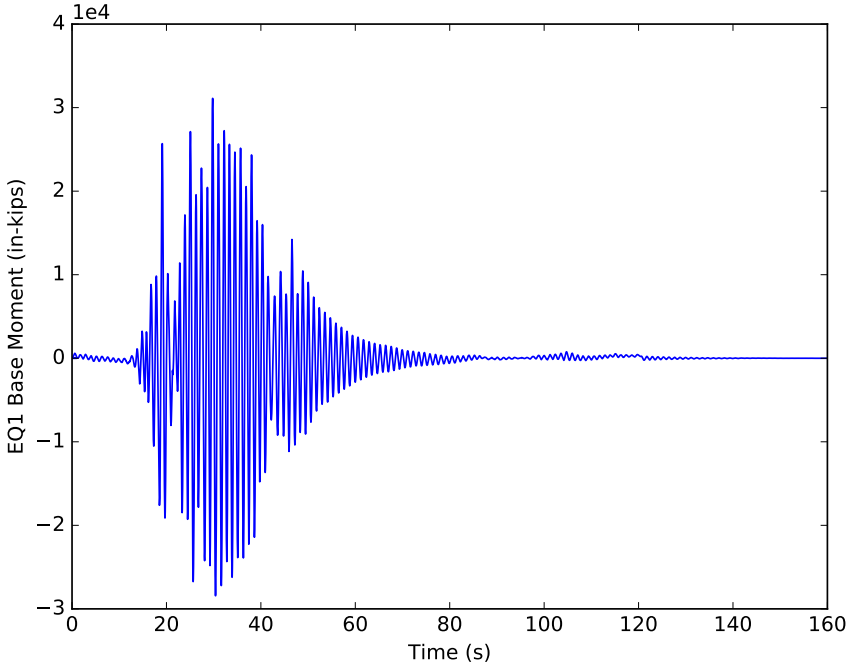

Figure D.19: Mz response of model 3 for EQ1

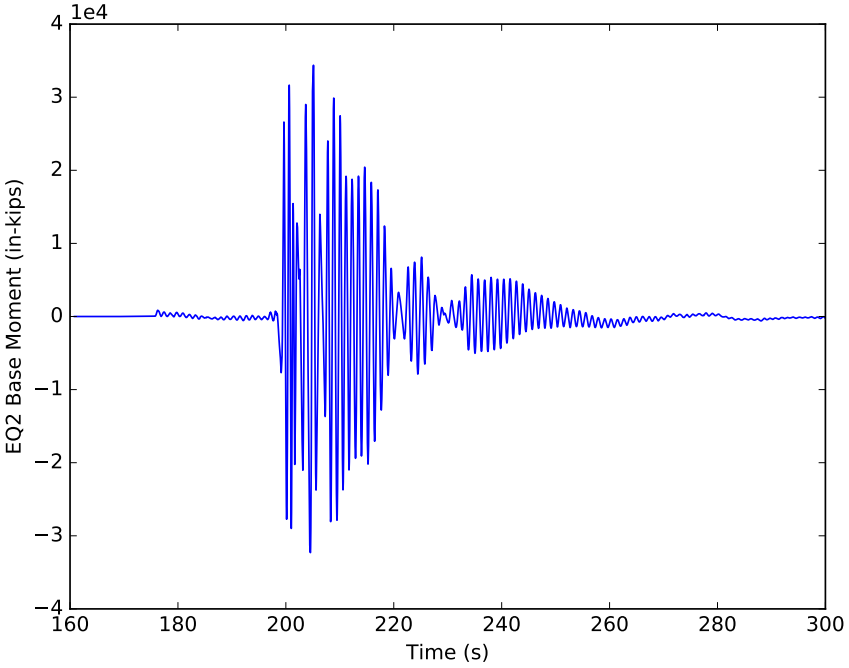

Figure D.20: Mz response of model 3 for EQ2

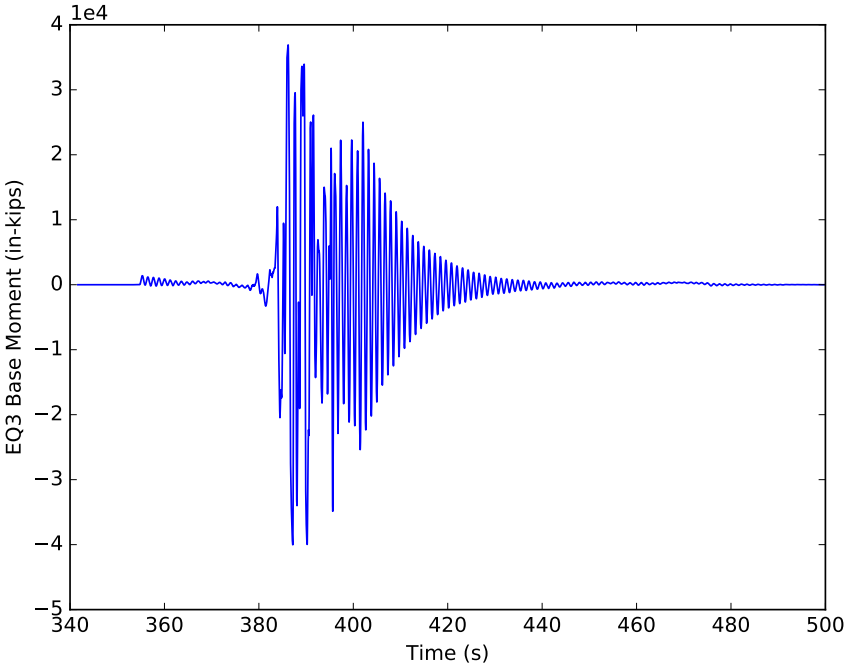

Figure D.21: Mz response of model 3 for EQ3

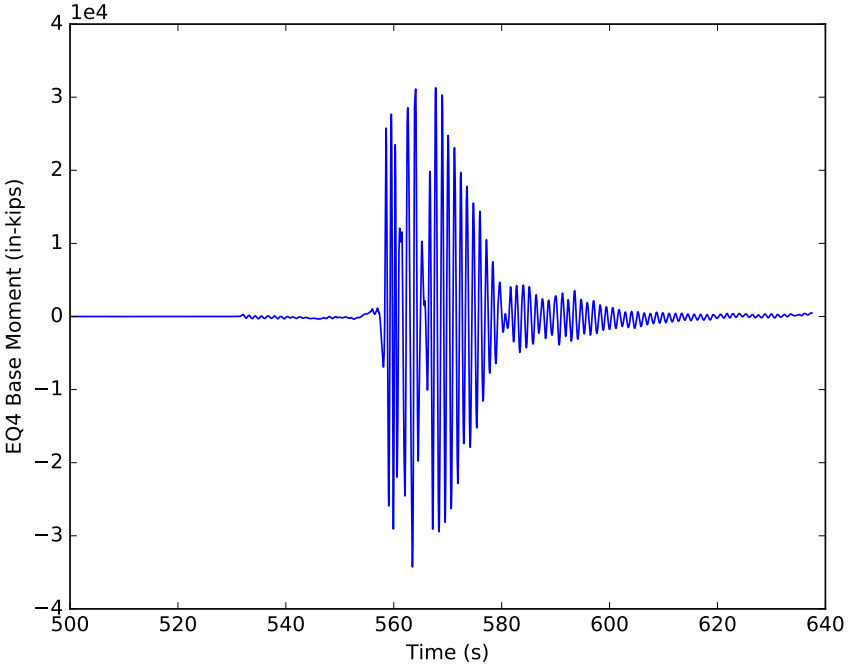

Figure D.22: Mz response of model 3 for EQ4

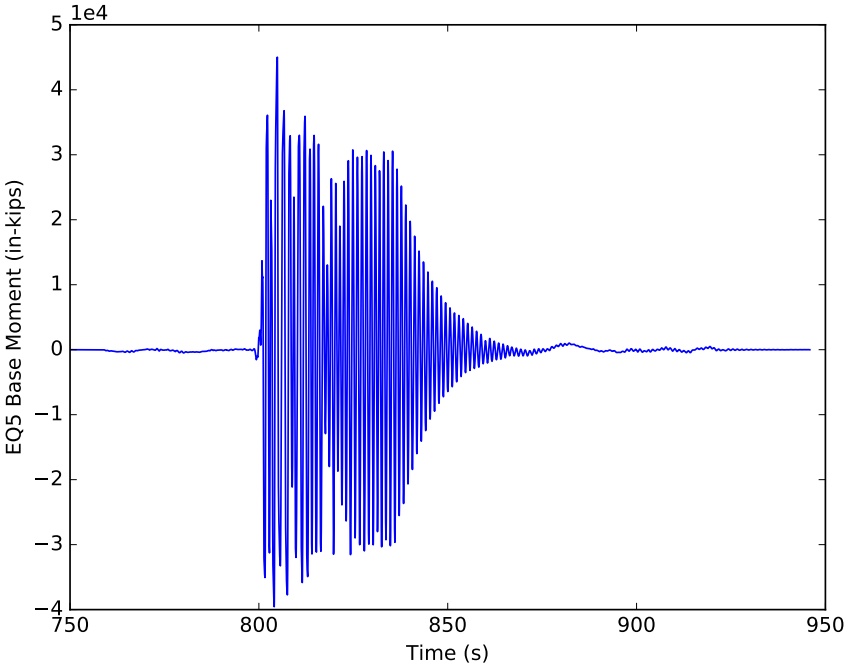

Figure D.23: Mz response of model 3 for EQ5

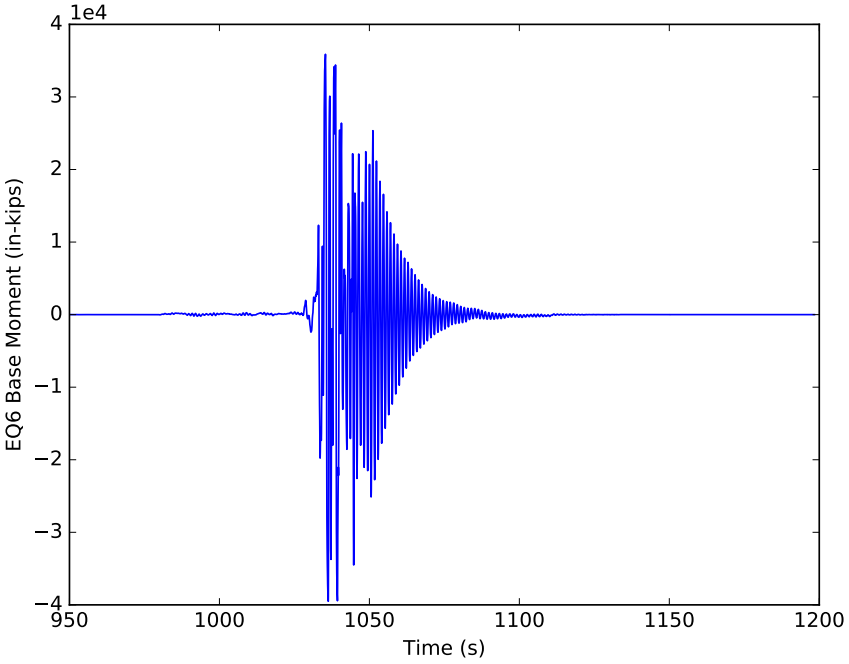

Figure D.24: Mz response of model 3 for EQ6

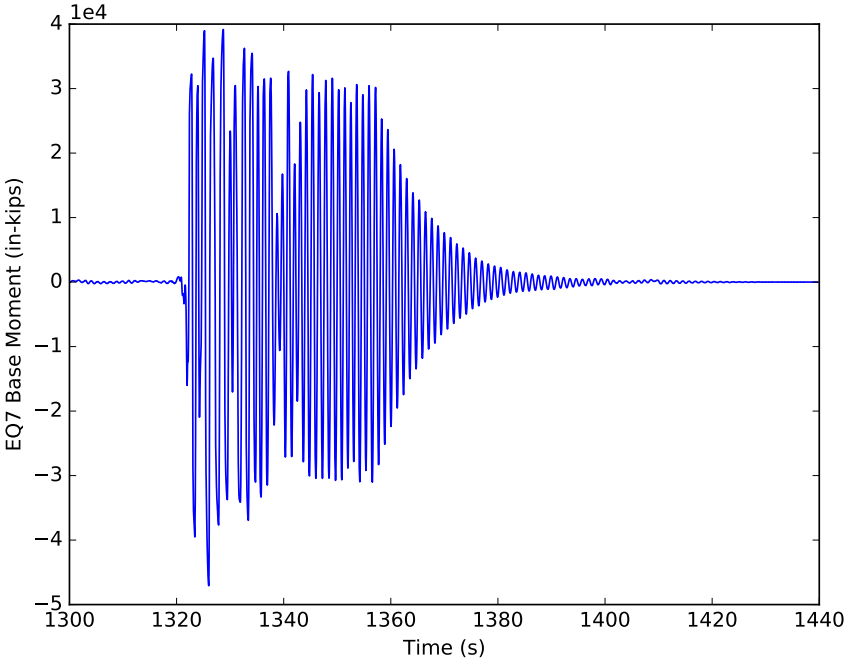

Figure D.25: Mz response of model 3 for EQ7

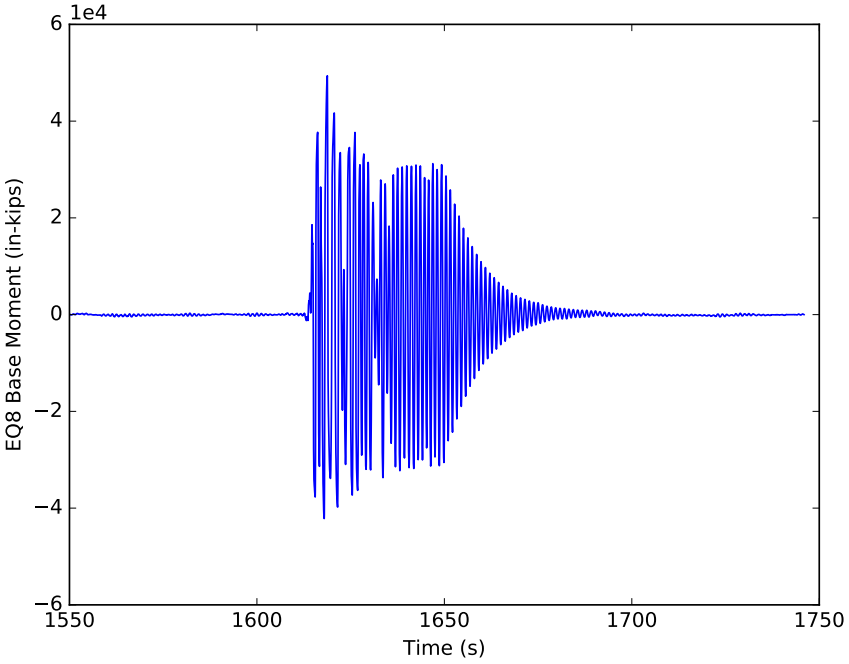

Figure D.26: Mz response of model 3 for EQ8

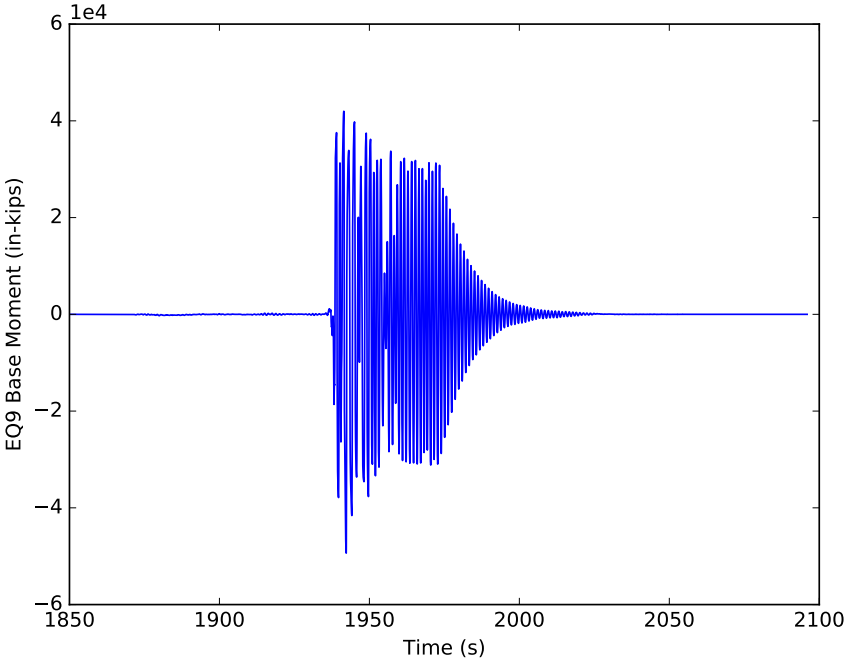

Figure D.27: Mz response of model 3 for EQ9

Appendix E

Model 4a Output

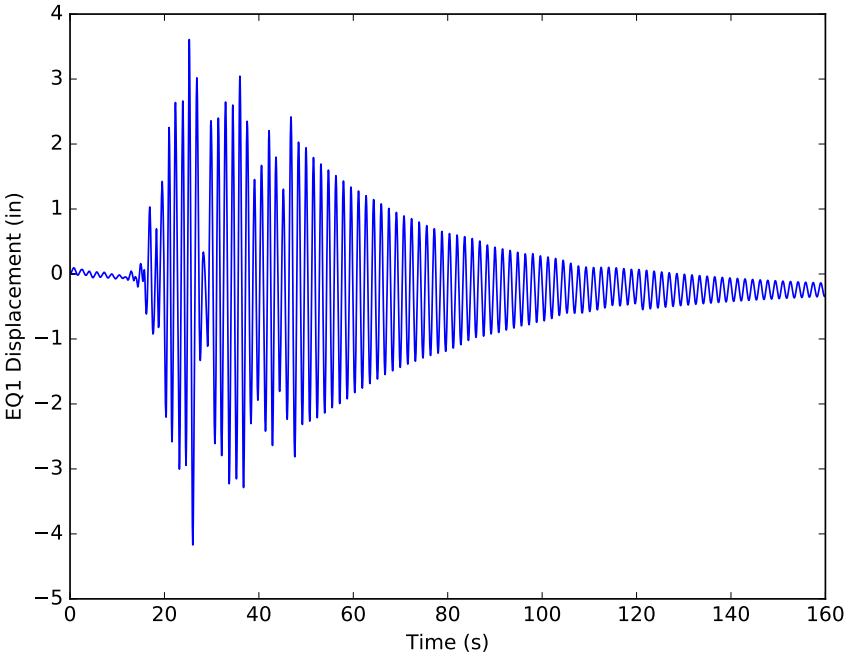

Figure E.1: Displacement response of model 4a for EQ1

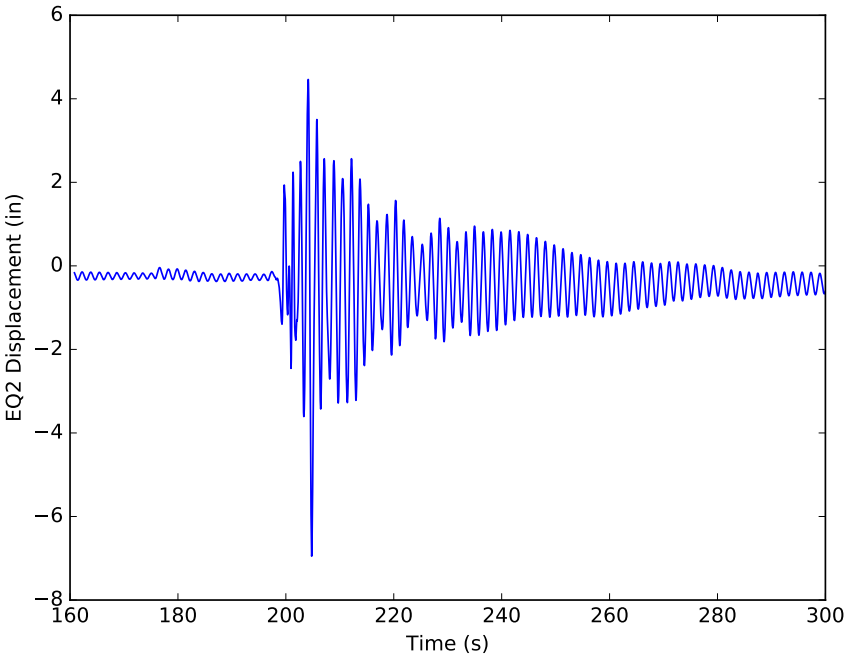

Figure E.2: Displacement response of model 4a for EQ2

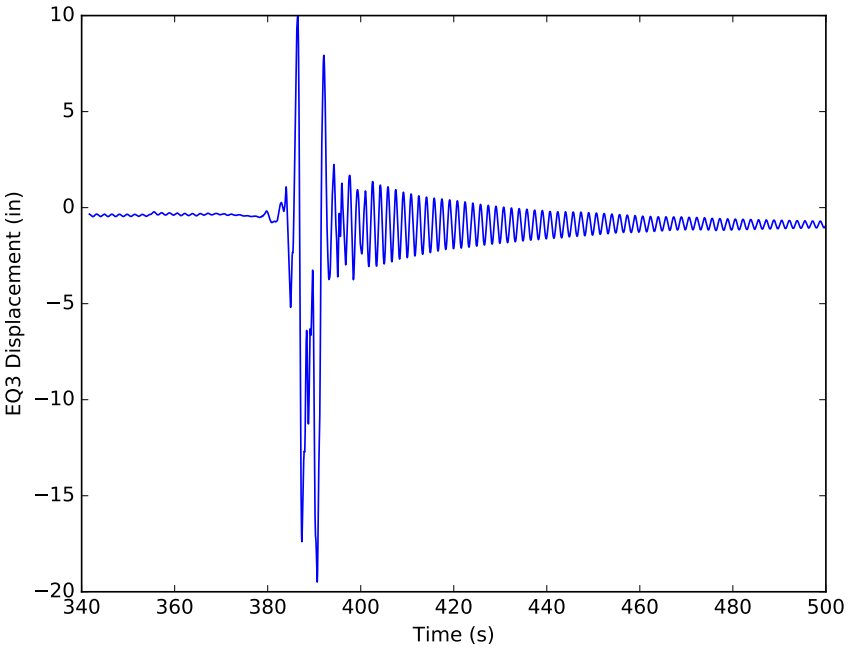

Figure E.3: Displacement response of model 4a for EQ3

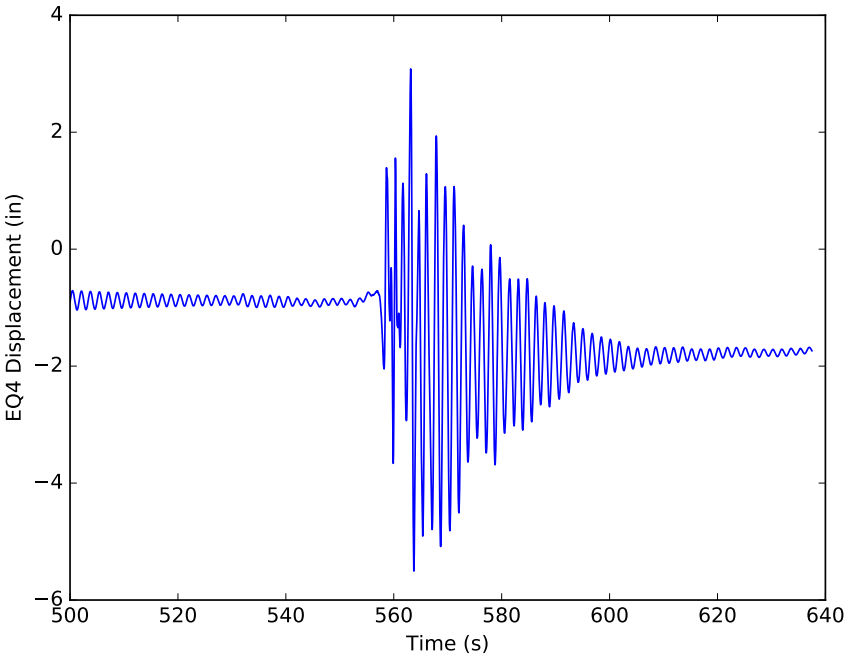

Figure E.4: Displacement response of model 4a for EQ4

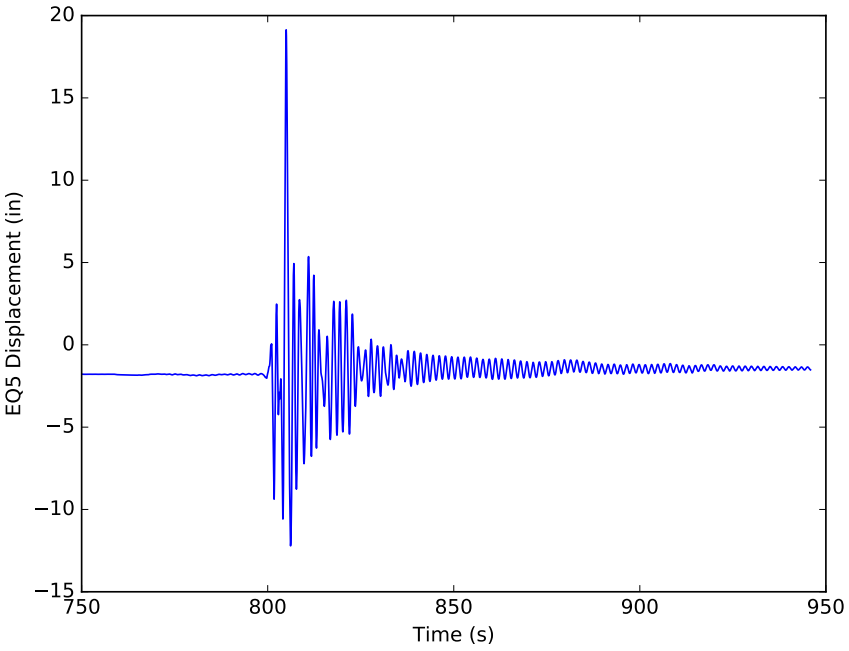

Figure E.5: Displacement response of model 4a for EQ5

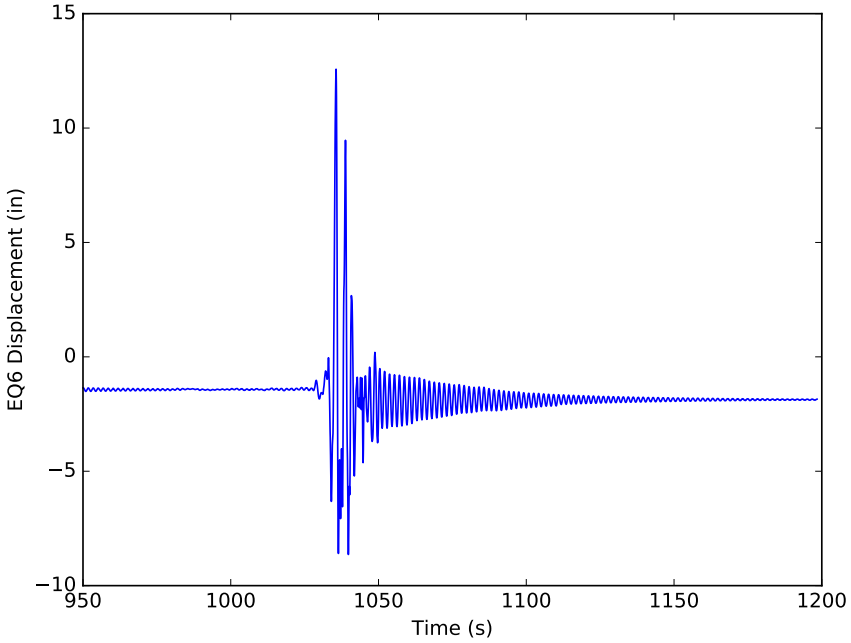

Figure E.6: Displacement response of model 4a for EQ6

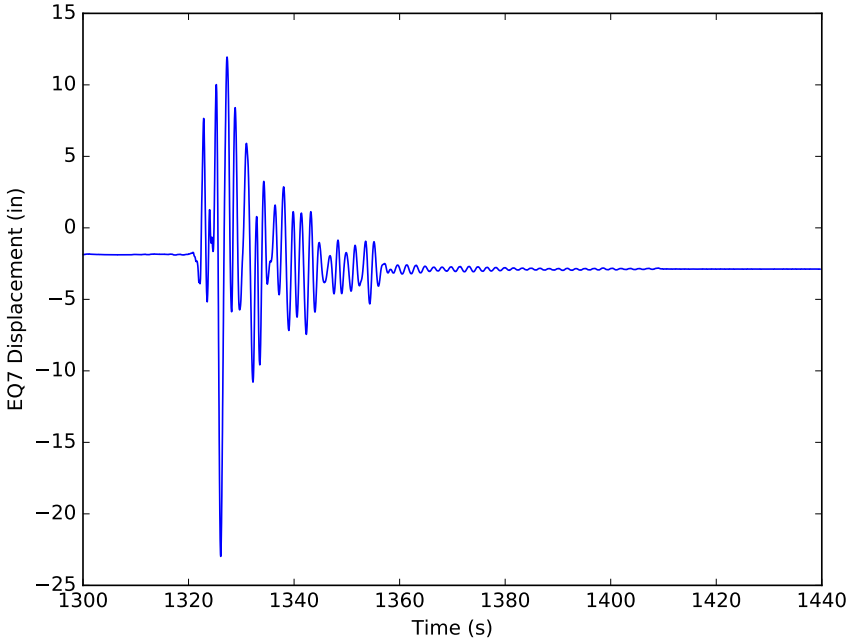

Figure E.7: Displacement response of model 4a for EQ7

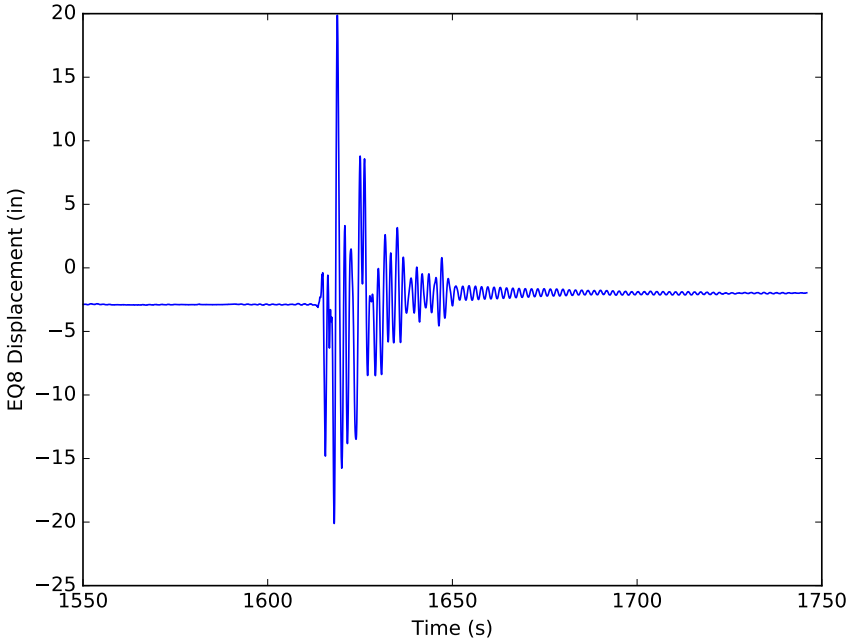

Figure E.8: Displacement response of model 4a for EQ8

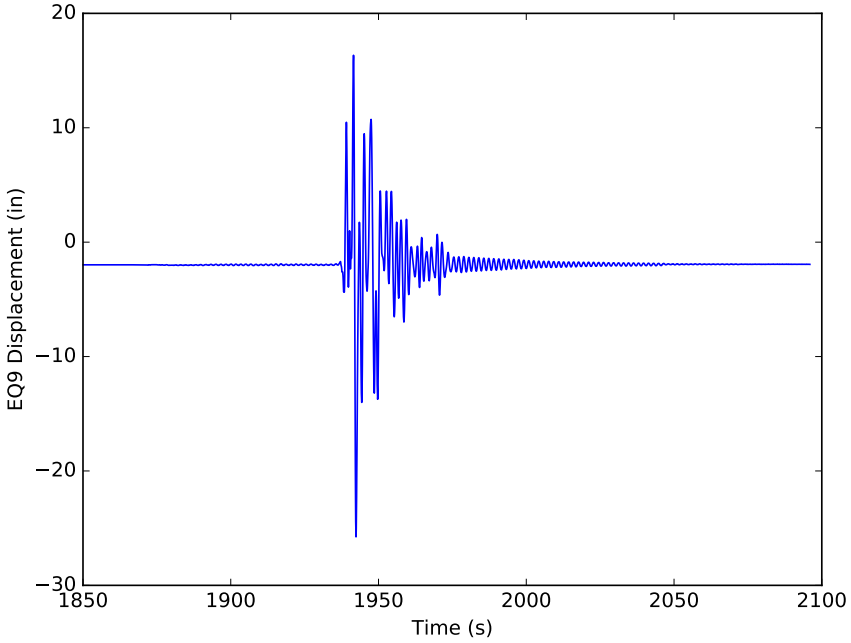

Figure E.9: Displacement response of model 4a for EQ9

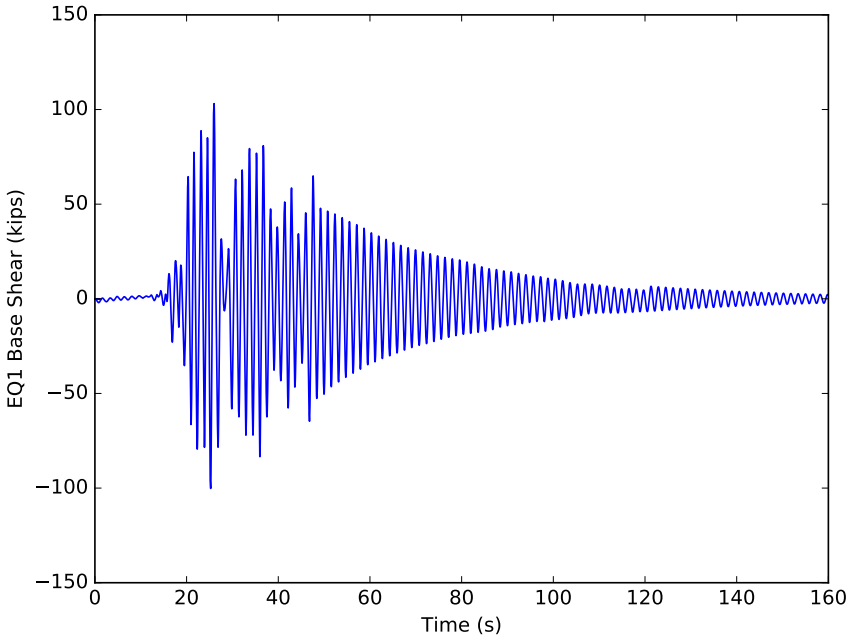

Figure E.10: Fx response of model 4a for EQ1

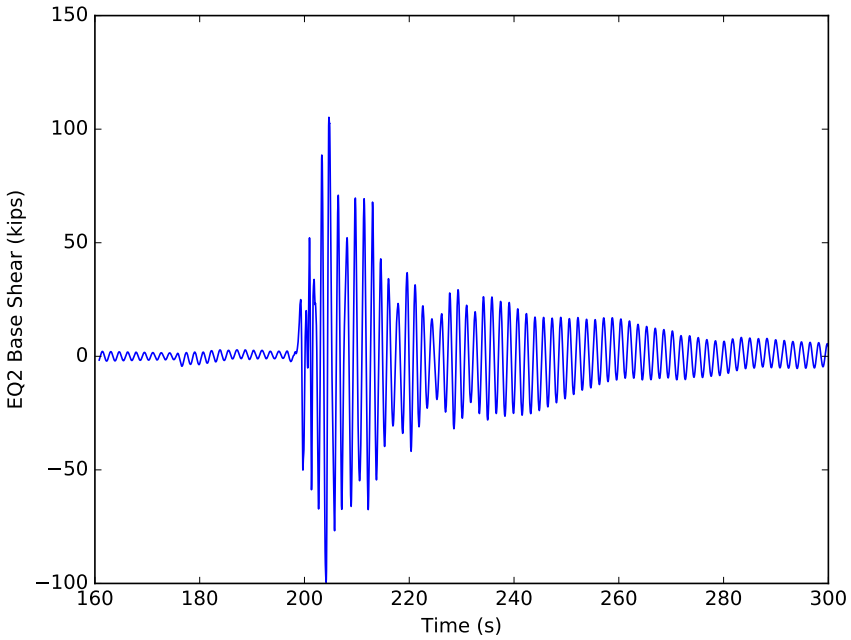

Figure E.11: Fx response of model 4a for EQ2

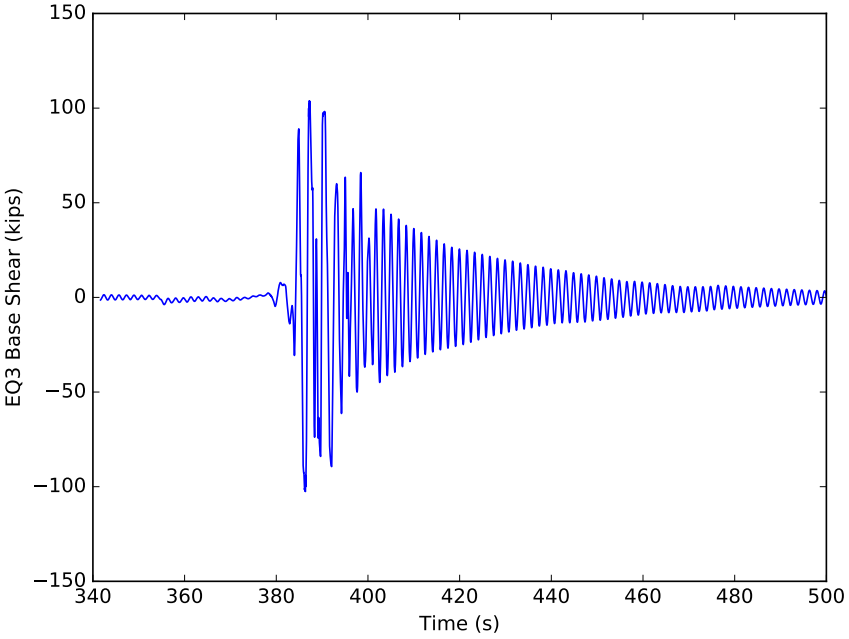

Figure E.12: Fx response of model 4a for EQ3

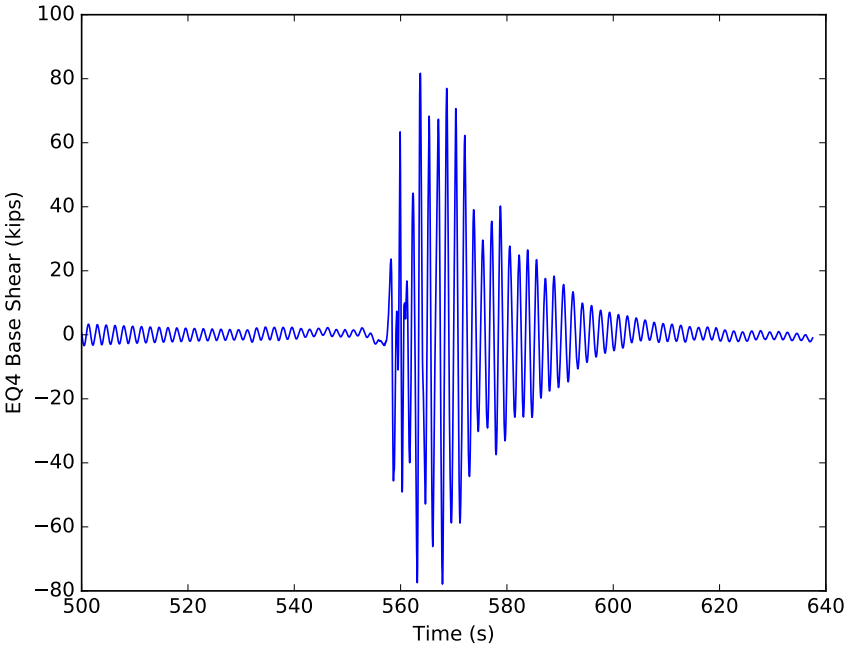

Figure E.13: Fx response of model 4a for EQ4

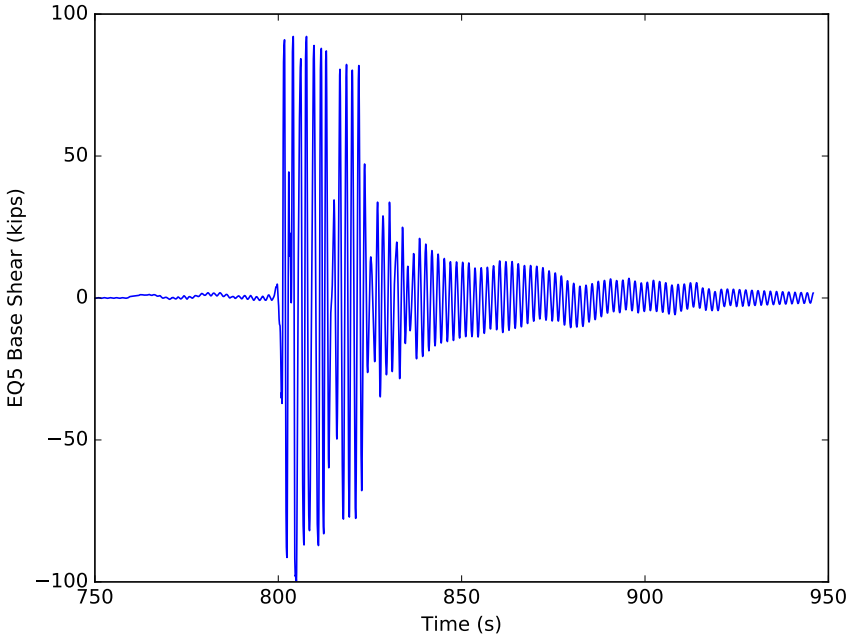

Figure E.14: Fx response of model 4a for EQ5

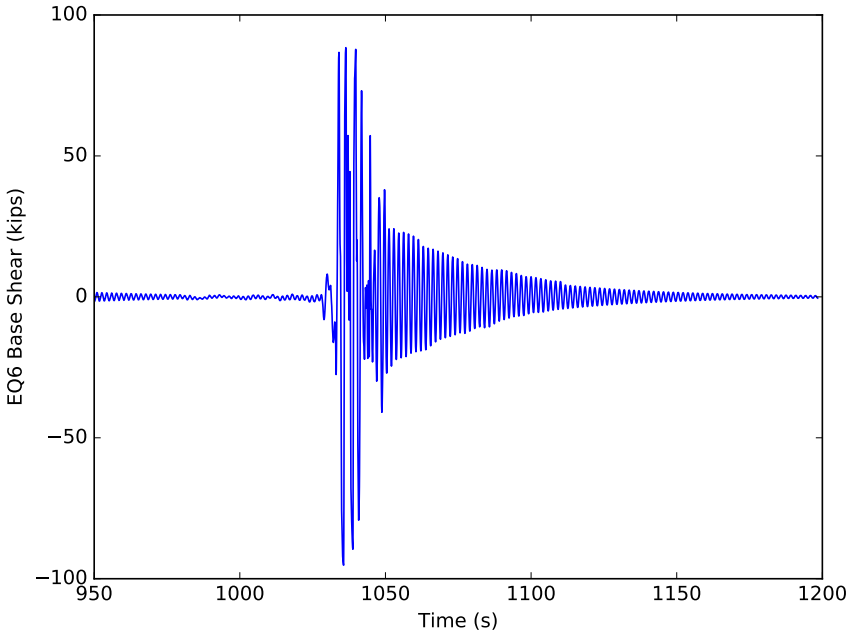

Figure E.15: Fx response of model 4a for EQ6

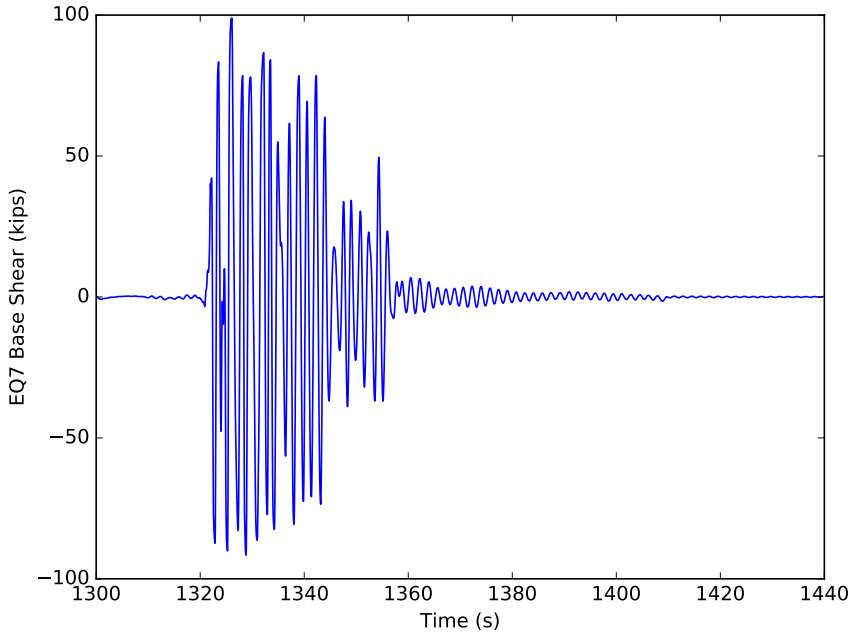

Figure E.16: Fx response of model 4a for EQ7

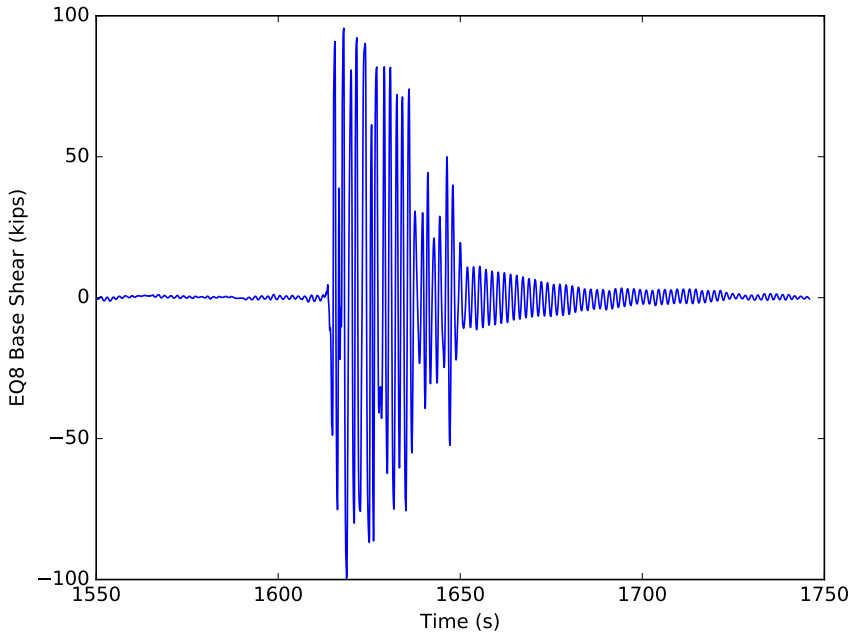

Figure E.17: Fx response of model 4a for EQ8

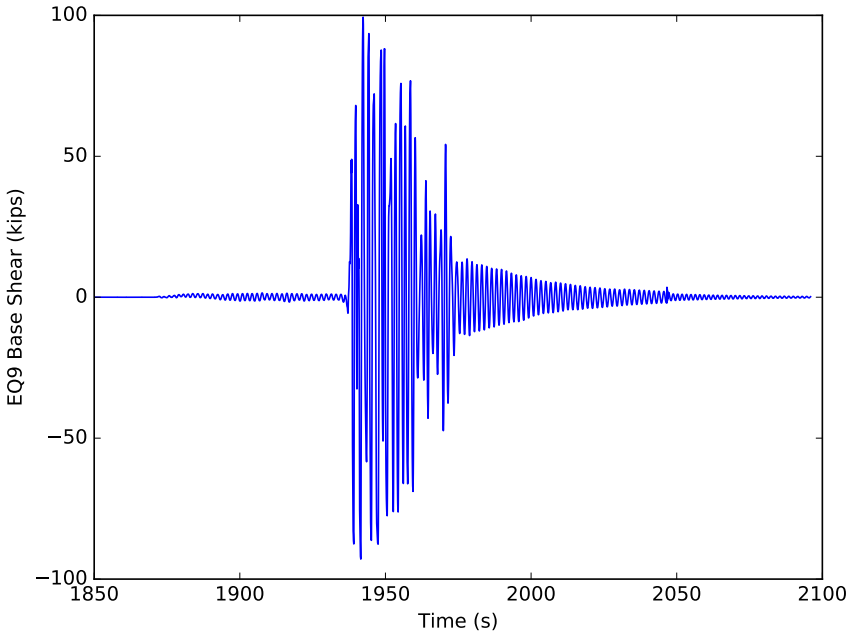

Figure E.18: Fx response of model 4a for EQ9

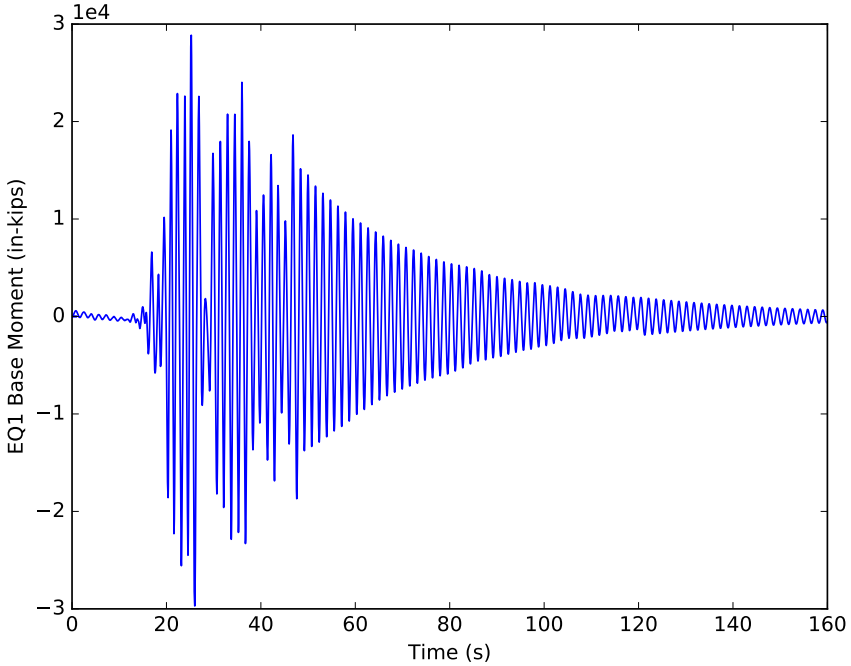

Figure E.19: Mz response of model 4a for EQ1

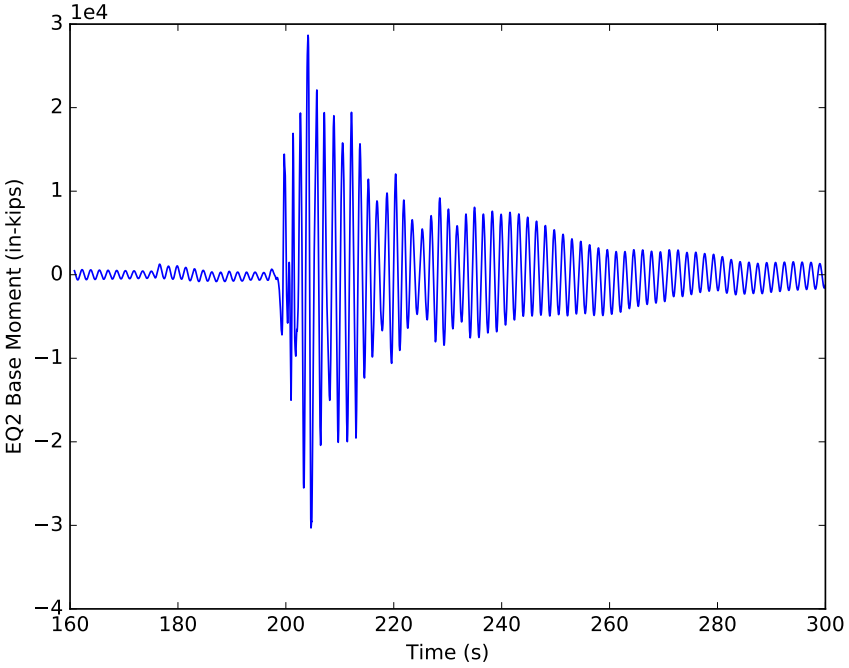

Figure E.20: Mz response of model 4a for EQ2

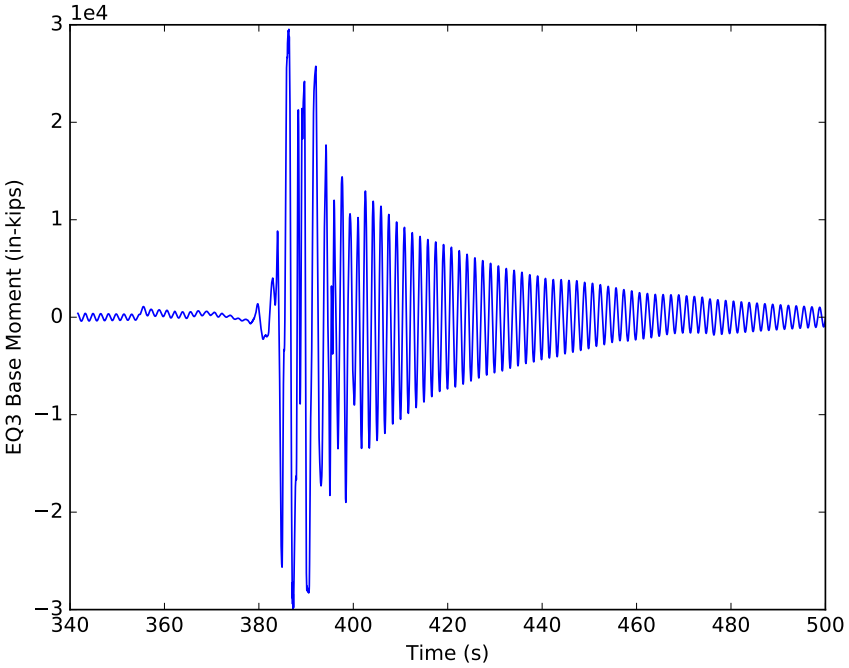

Figure E.21: Mz response of model 4a for EQ3

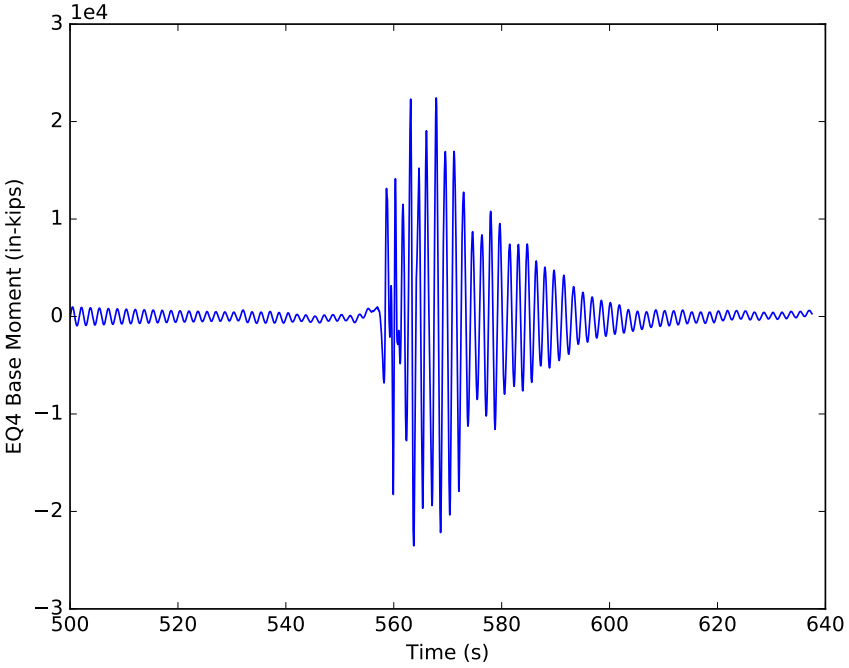

Figure E.22: Mz response of model 4a for EQ4

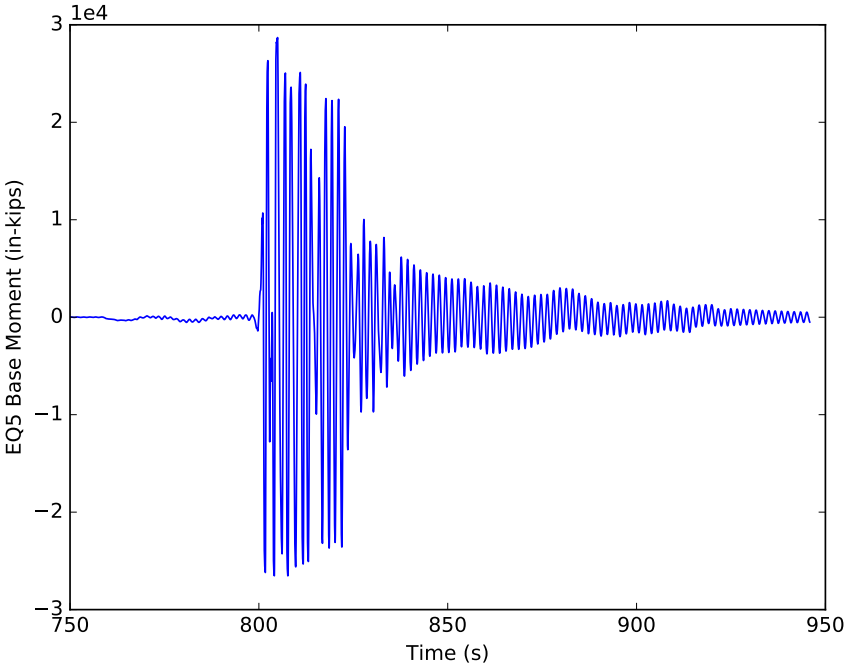

Figure E.23: Mz response of model 4a for EQ5

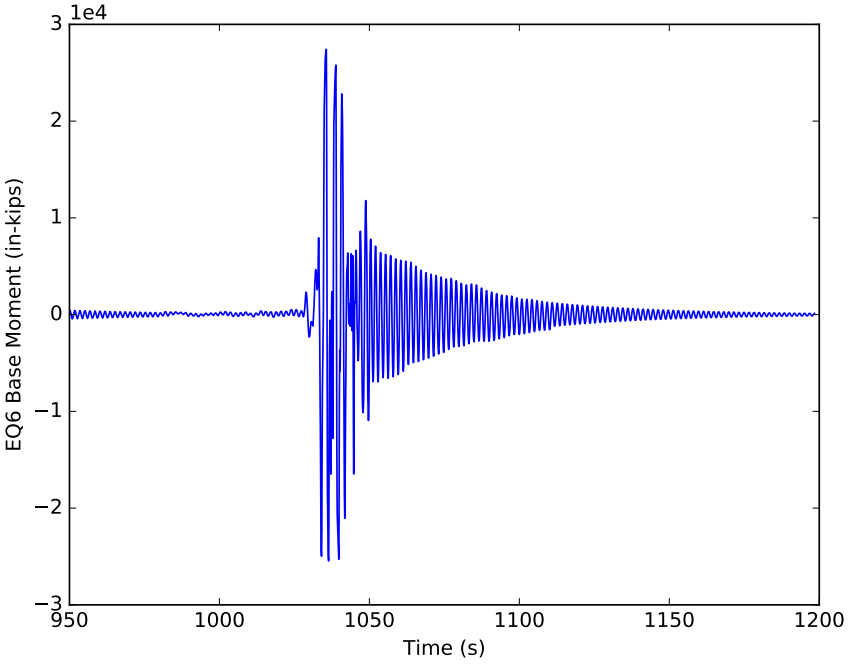

Figure E.24: Mz response of model 4a for EQ6

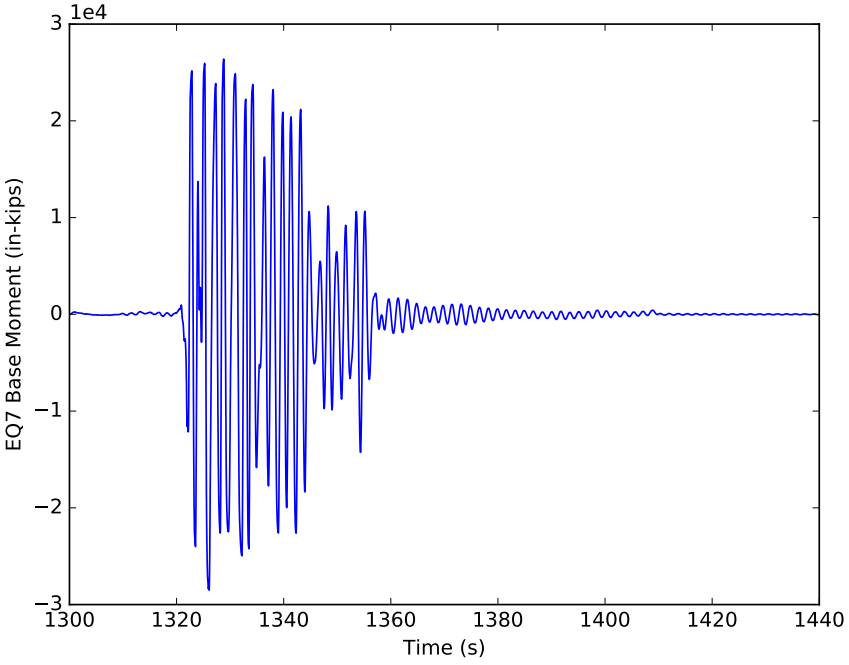

Figure E.25: Mz response of model 4a for EQ7

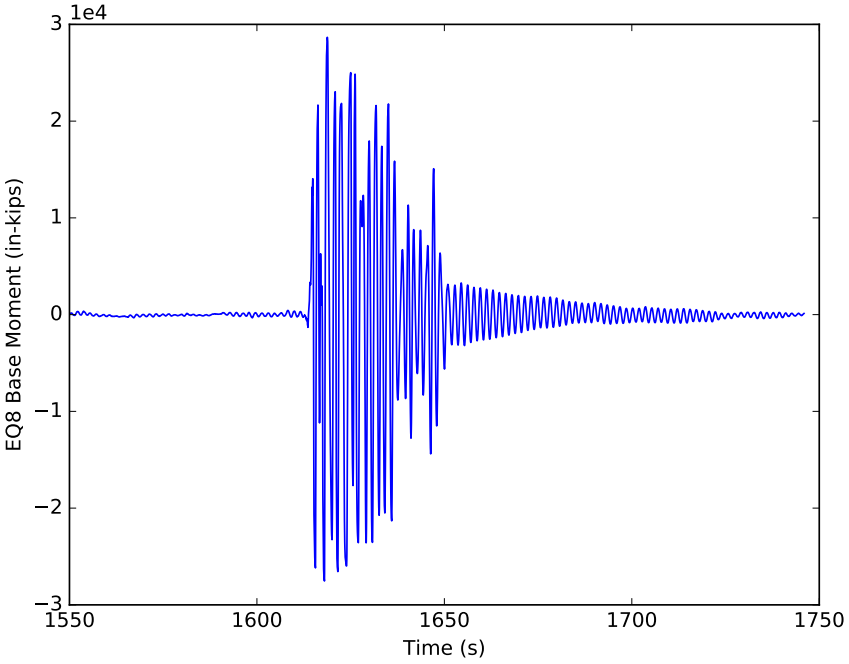

Figure E.26: Mz response of model 4a for EQ8

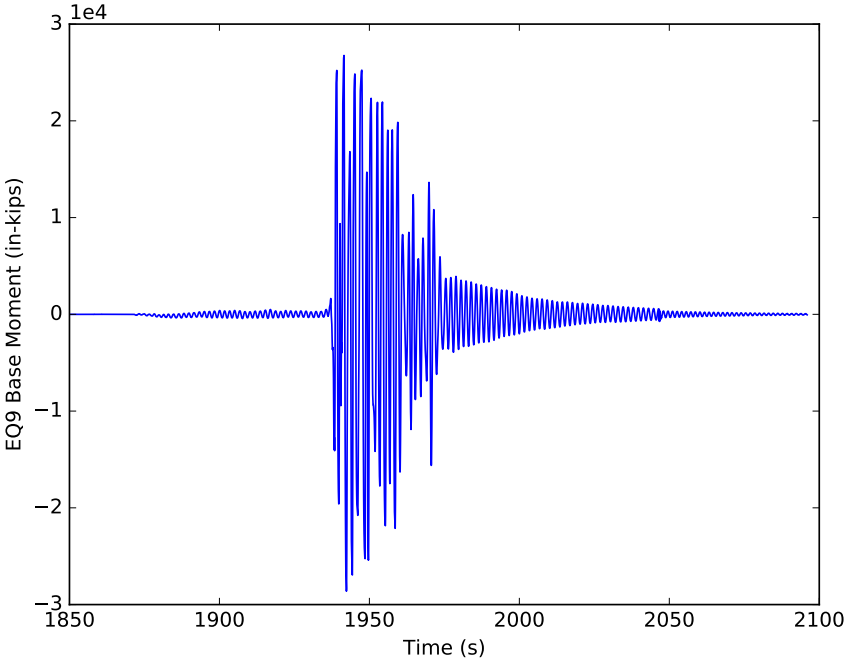

Figure E.27: Mz response of model 4a for EQ9

Appendix F

Model 4b Output

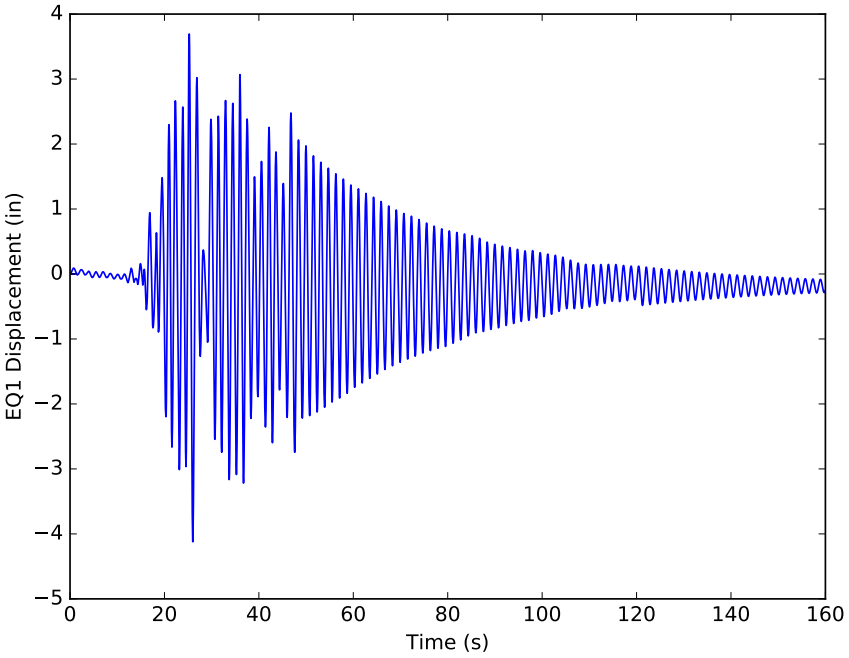

Figure F.1: Displacement response of model 4b for EQ1

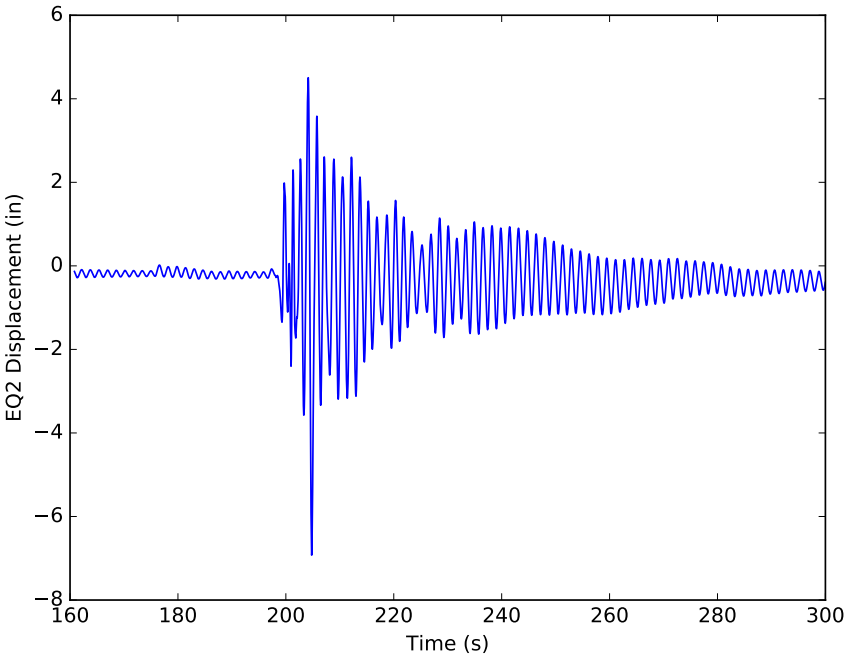

Figure F.2: Displacement response of model 4b for EQ2

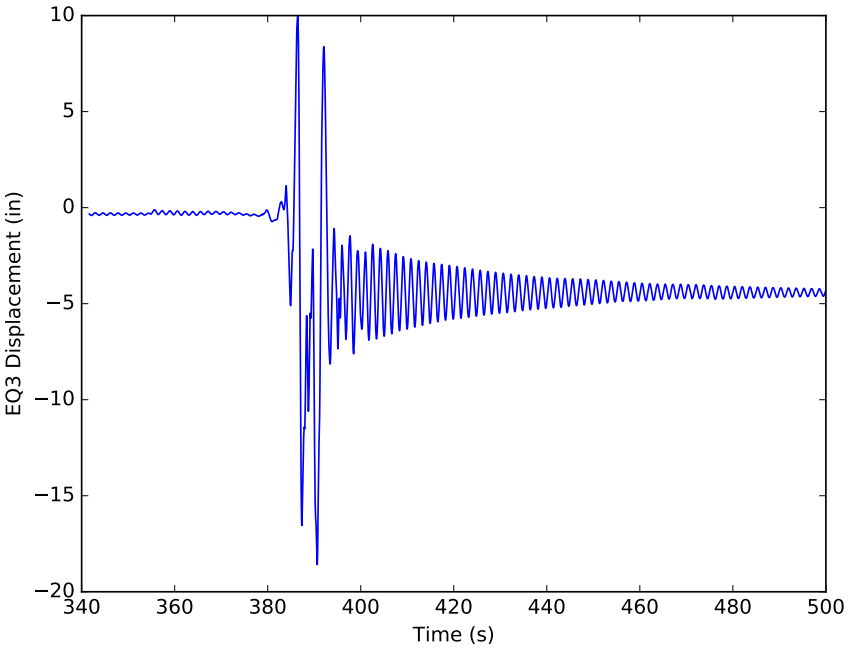

Figure F.3: Displacement response of model 4b for EQ3

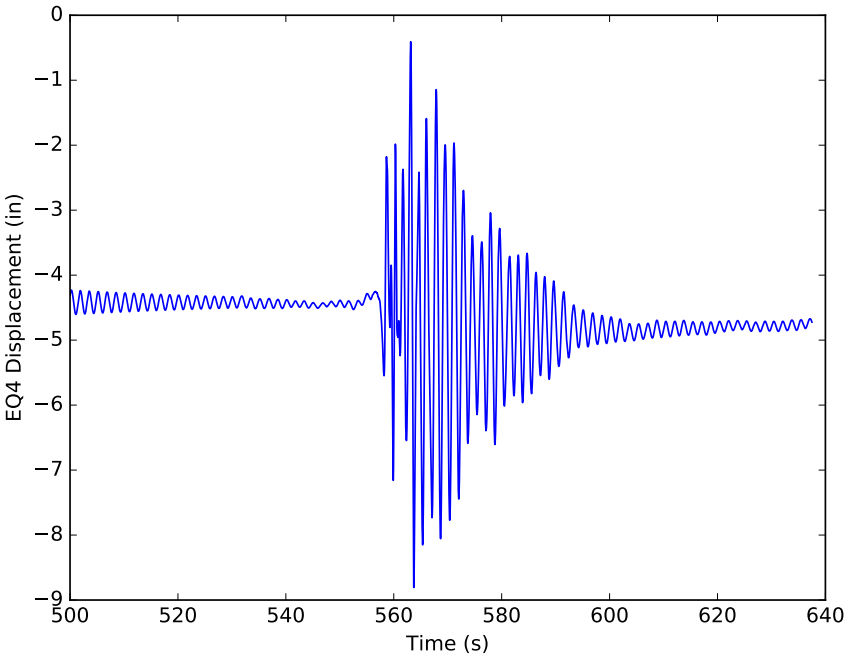

Figure F.4: Displacement response of model 4b for EQ4

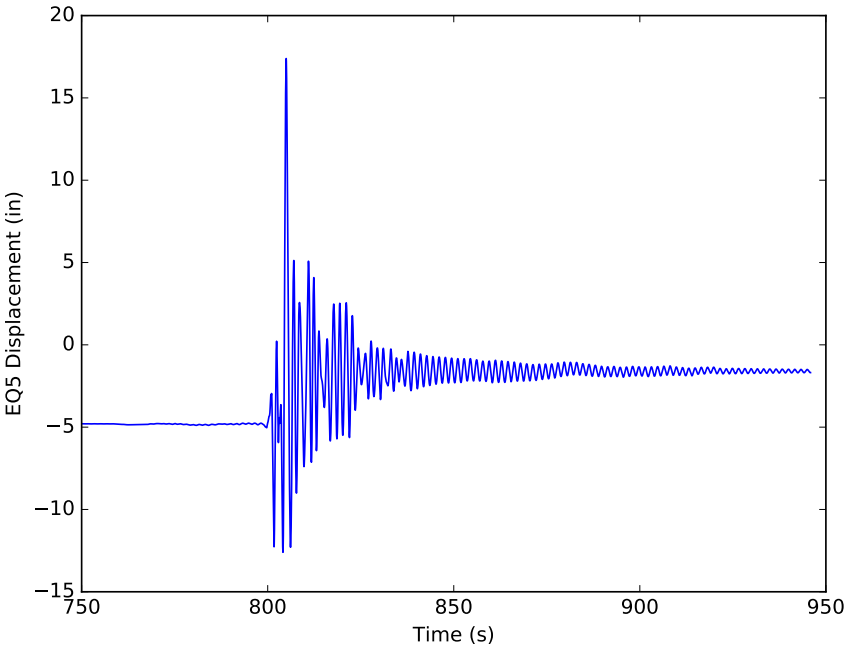

Figure F.5: Displacement response of model 4b for EQ5

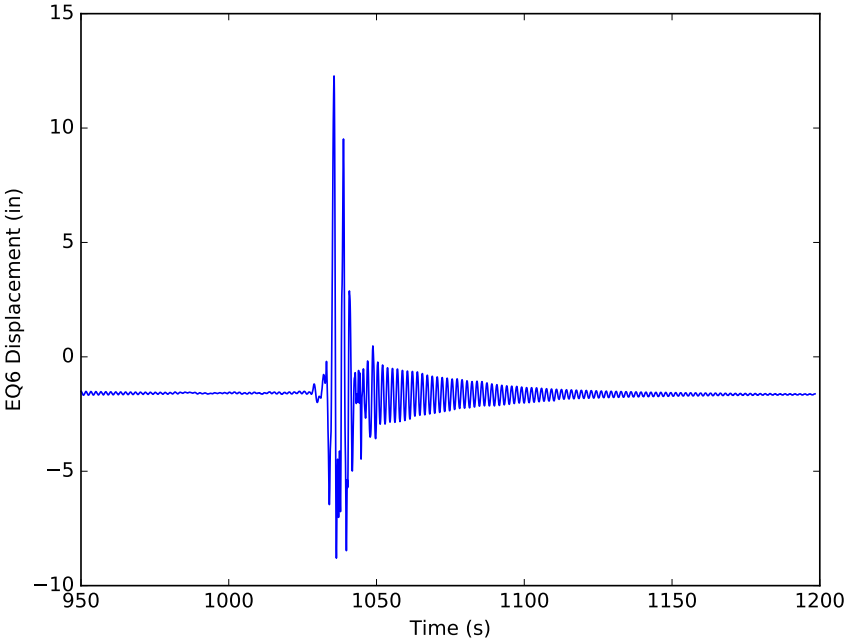

Figure F.6: Displacement response of model 4b for EQ6

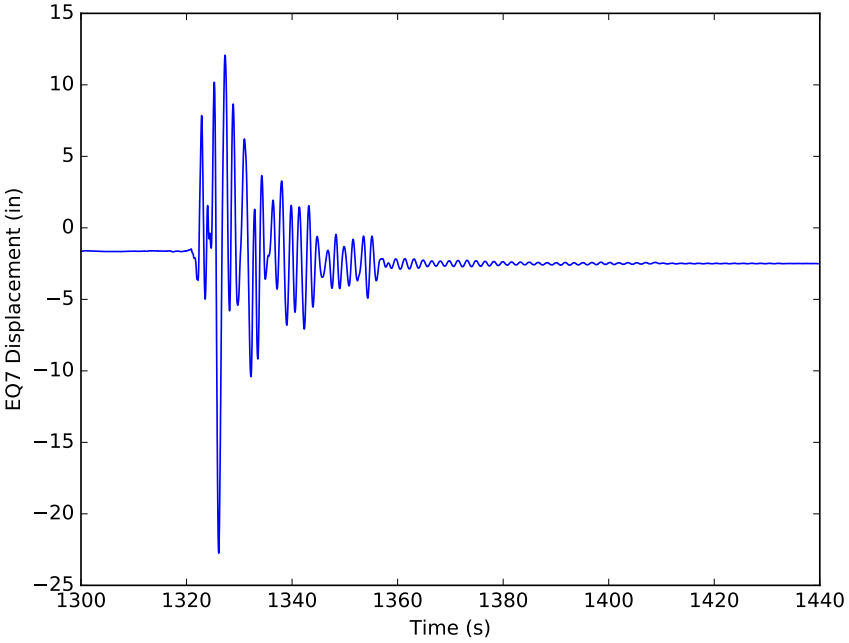

Figure F.7: Displacement response of model 4b for EQ7

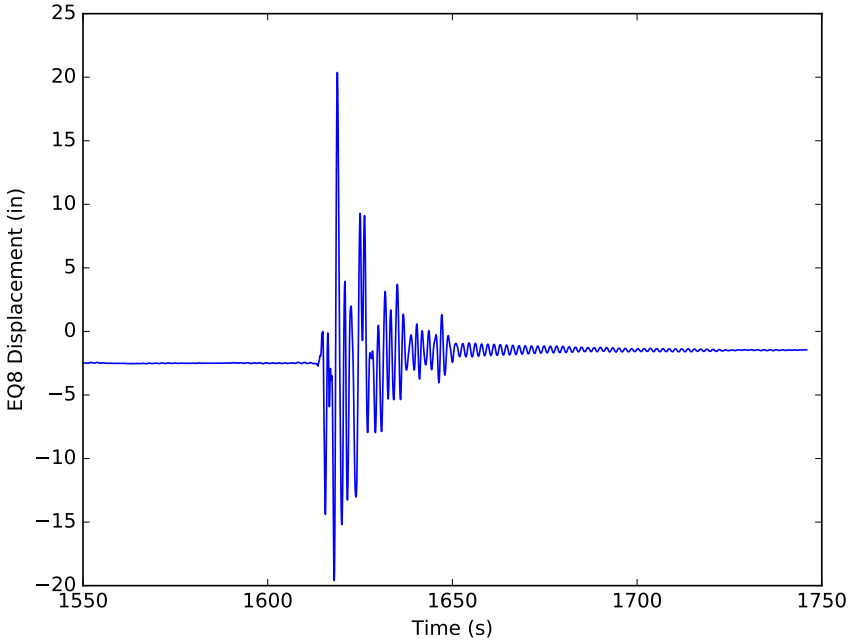

Figure F.8: Displacement response of model 4b for EQ8

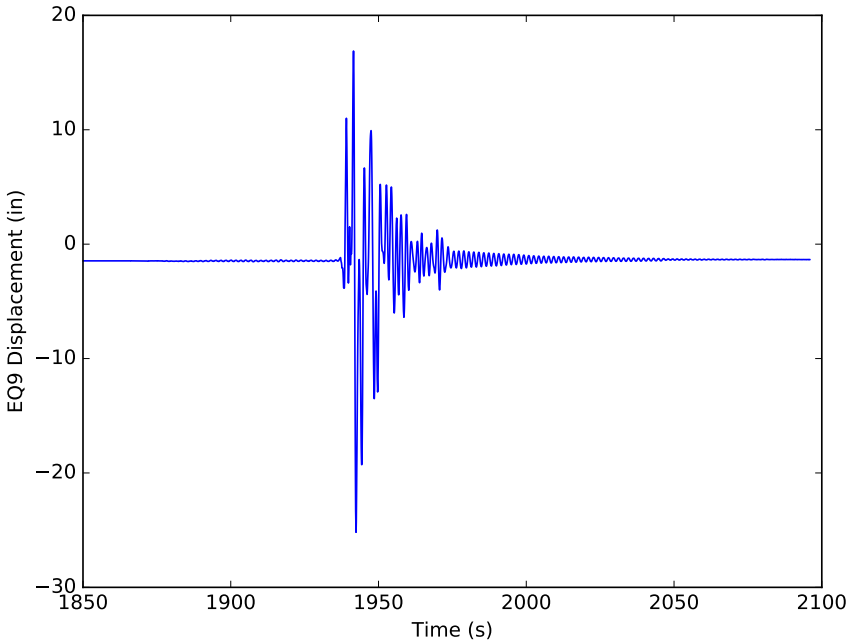

Figure F.9: Displacement response of model 4b for EQ9

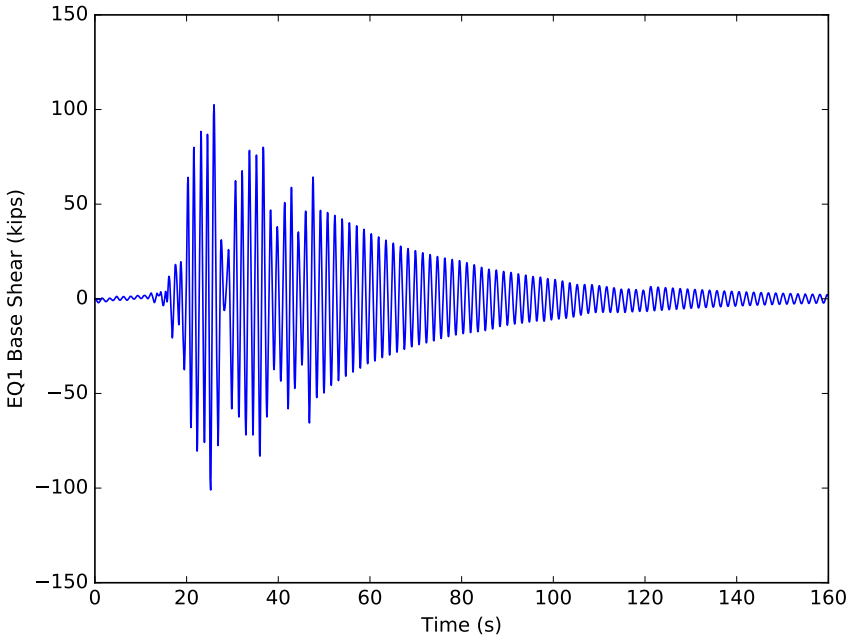

Figure F.10: Fx response of model 4b for EQ1

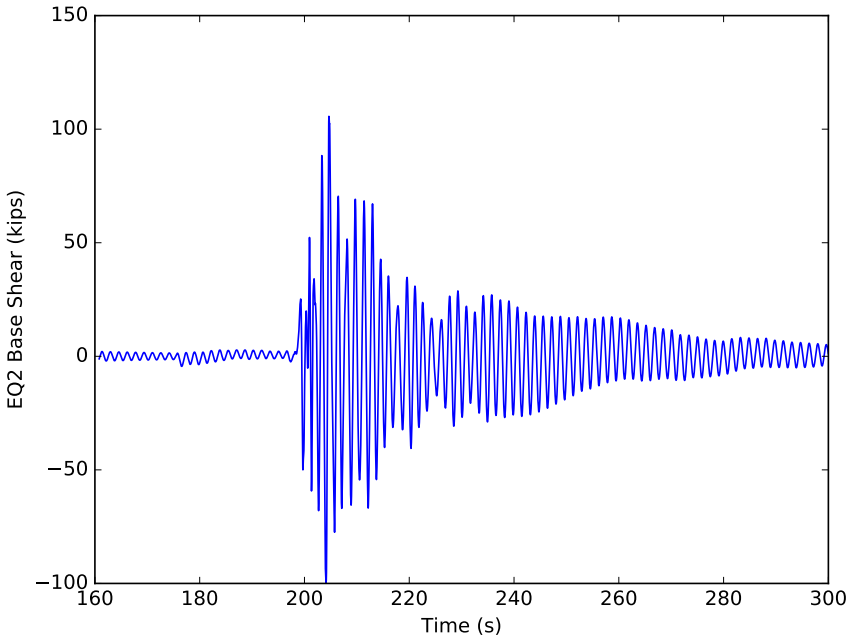

Figure F.11: Fx response of model 4b for EQ2

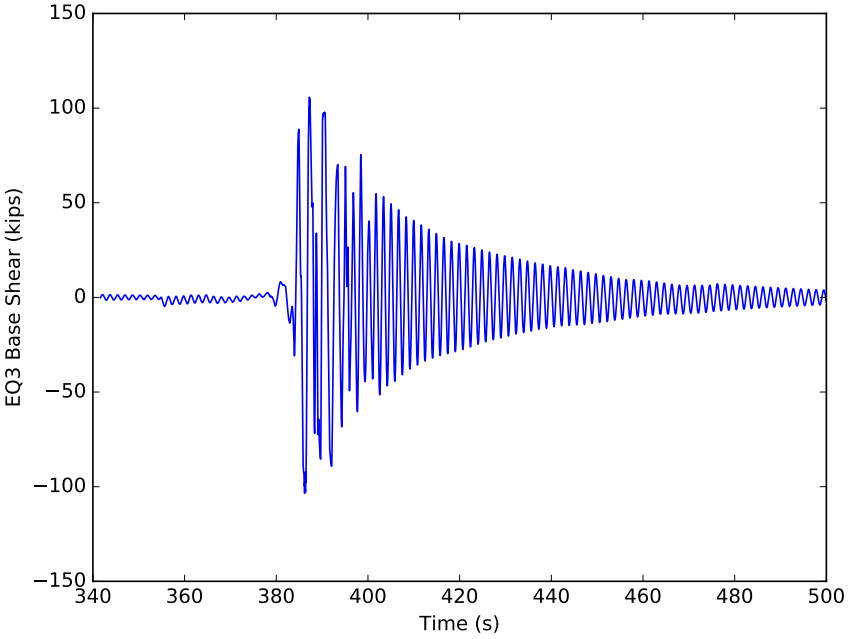

Figure F.12: Fx response of model 4b for EQ3

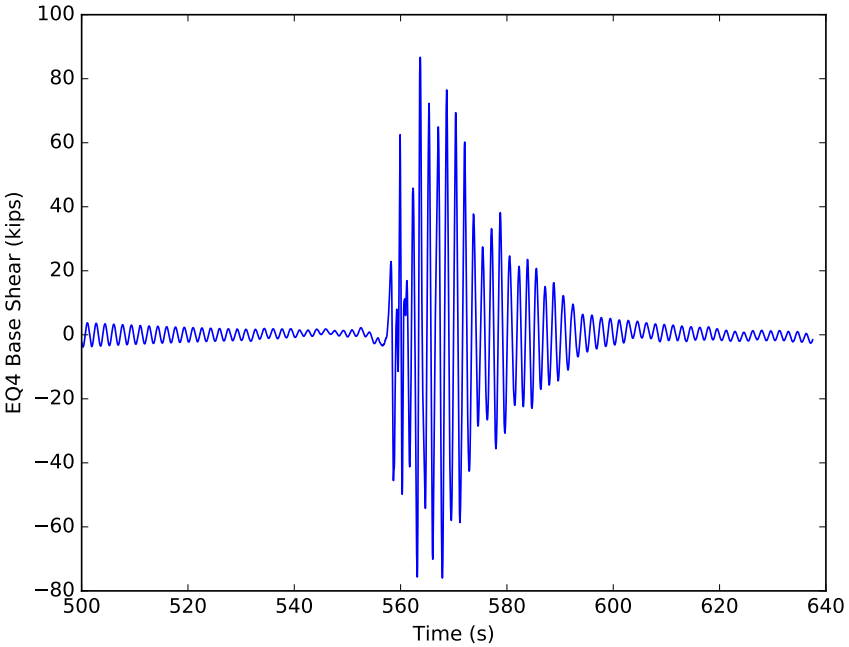

Figure F.13: Fx response of model 4b for EQ4

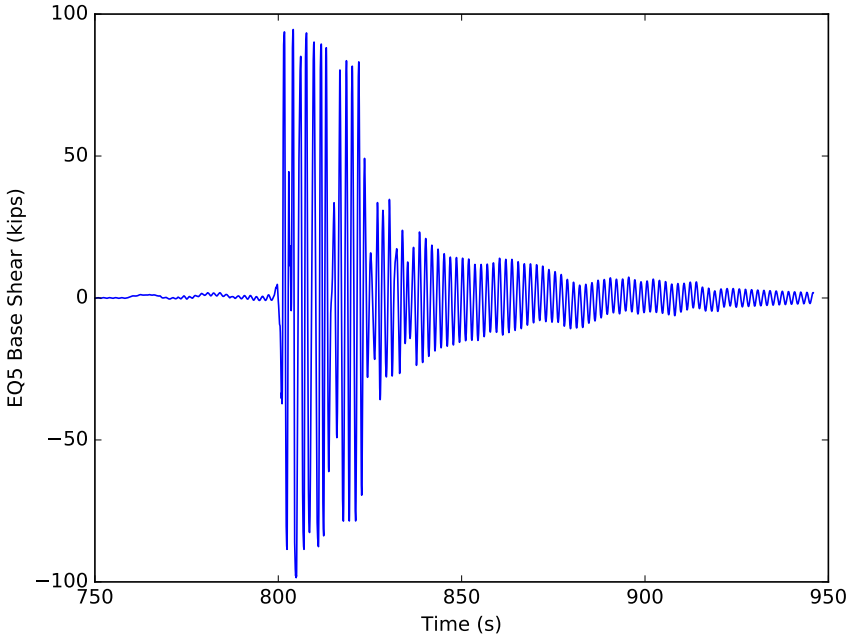

Figure F.14: Fx response of model 4b for EQ5

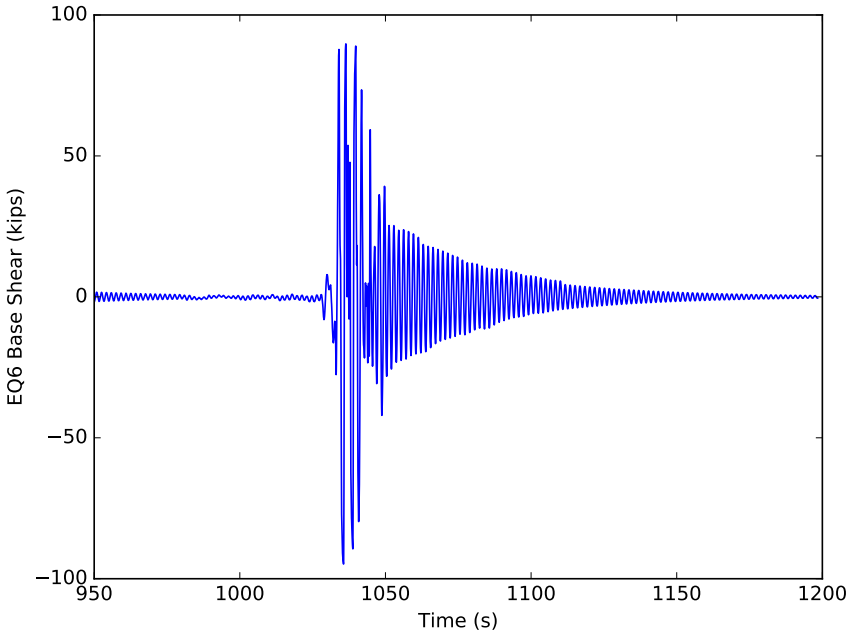

Figure F.15: Fx response of model 4b for EQ6

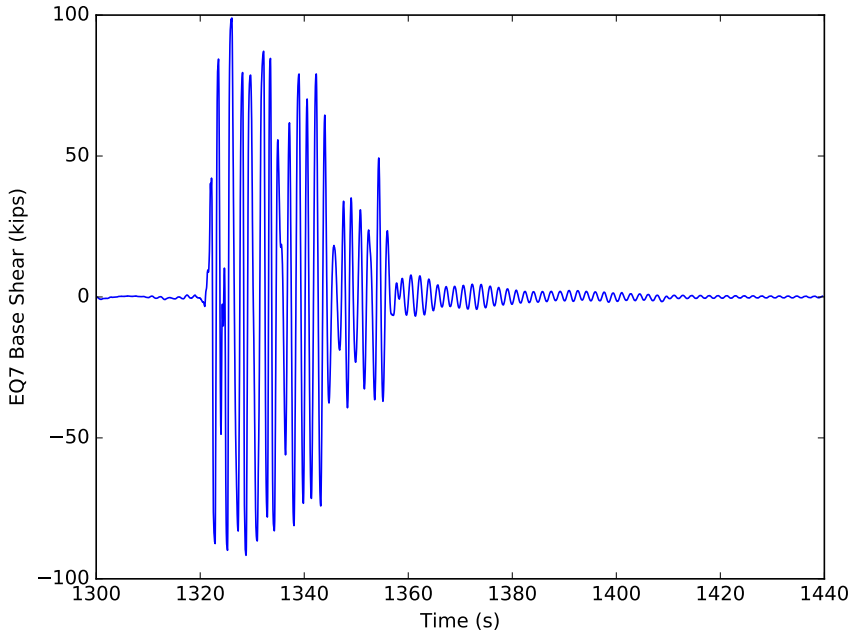

Figure F.16: Fx response of model 4b for EQ7

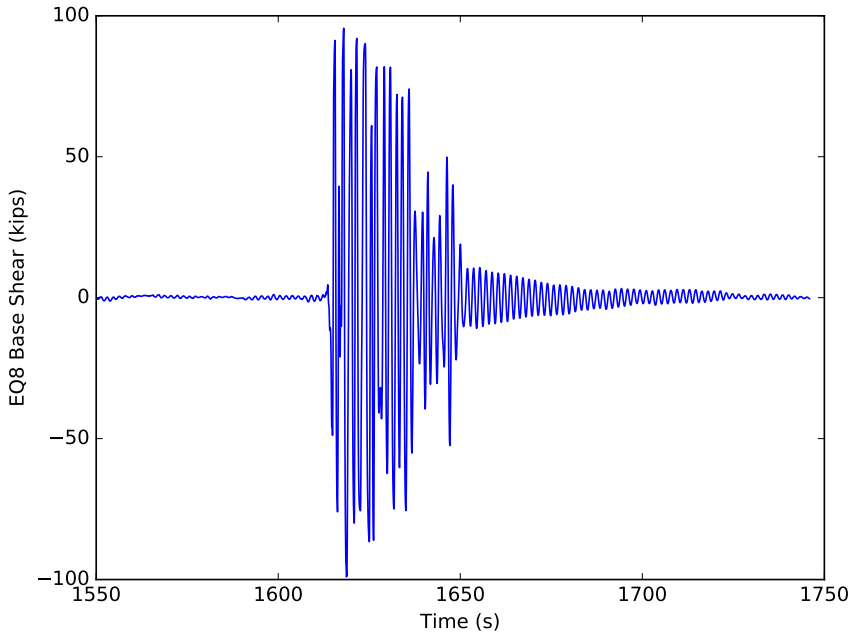

Figure F.17: Fx response of model 4b for EQ8

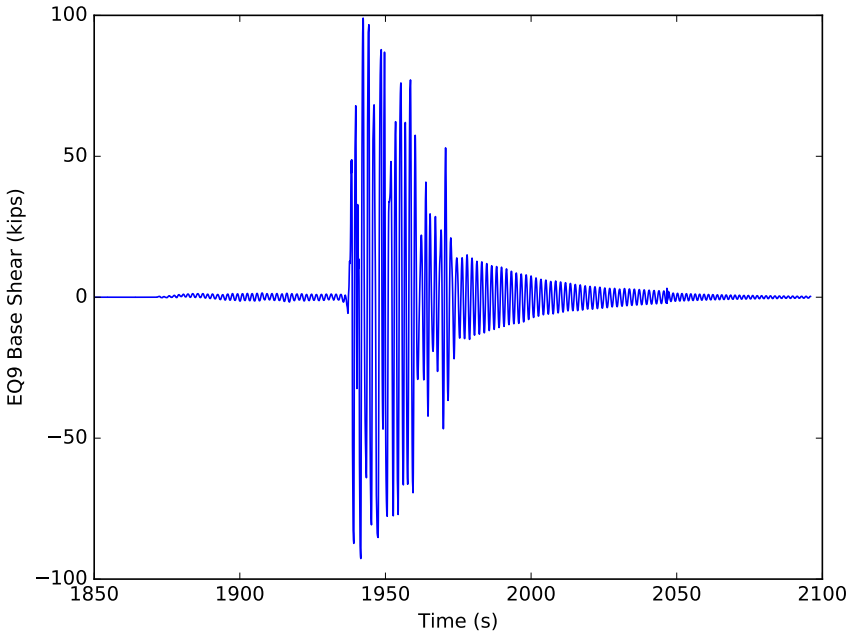

Figure F.18: Fx response of model 4b for EQ9

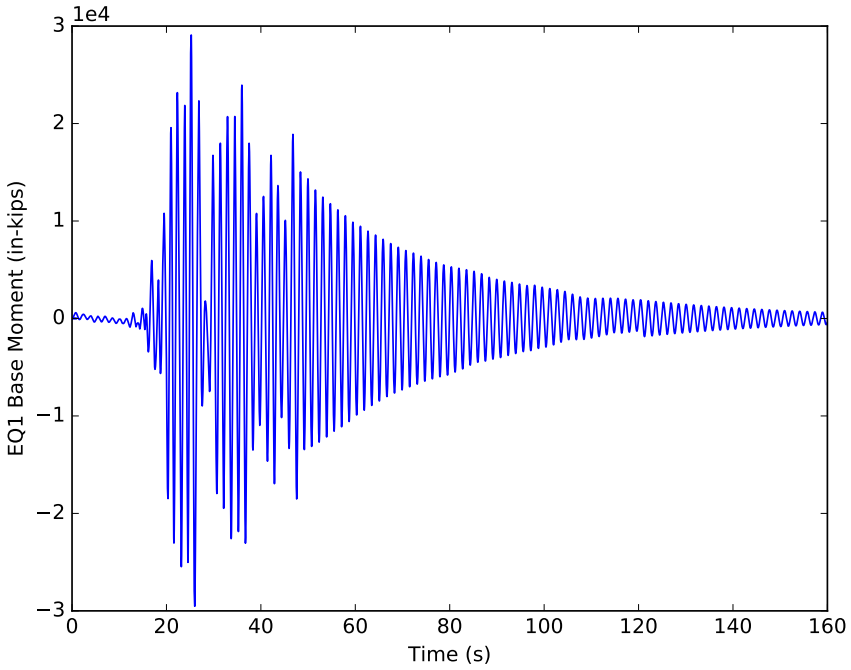

Figure F.19: Mz response of model 4b for EQ1

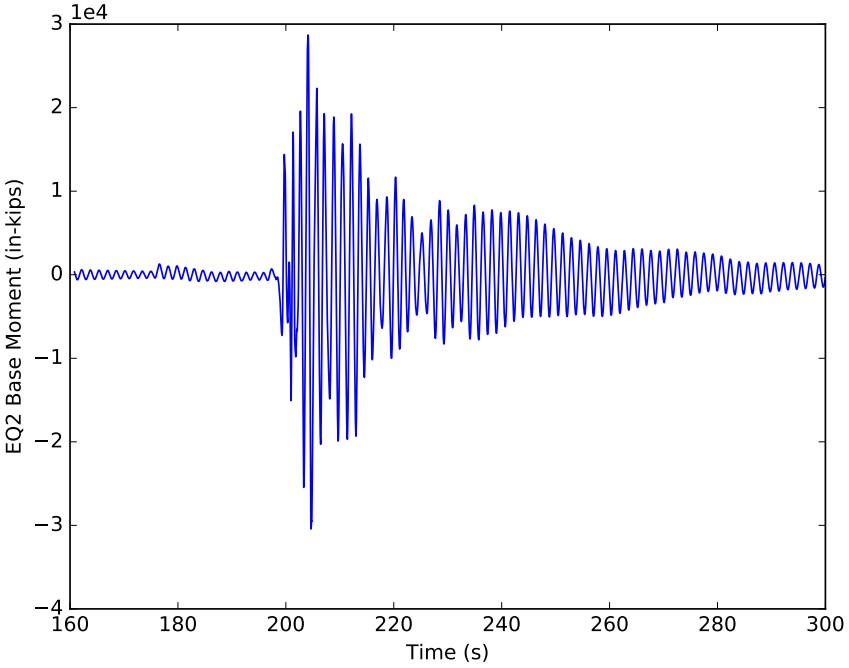

Figure F.20: Mz response of model 4b for EQ2

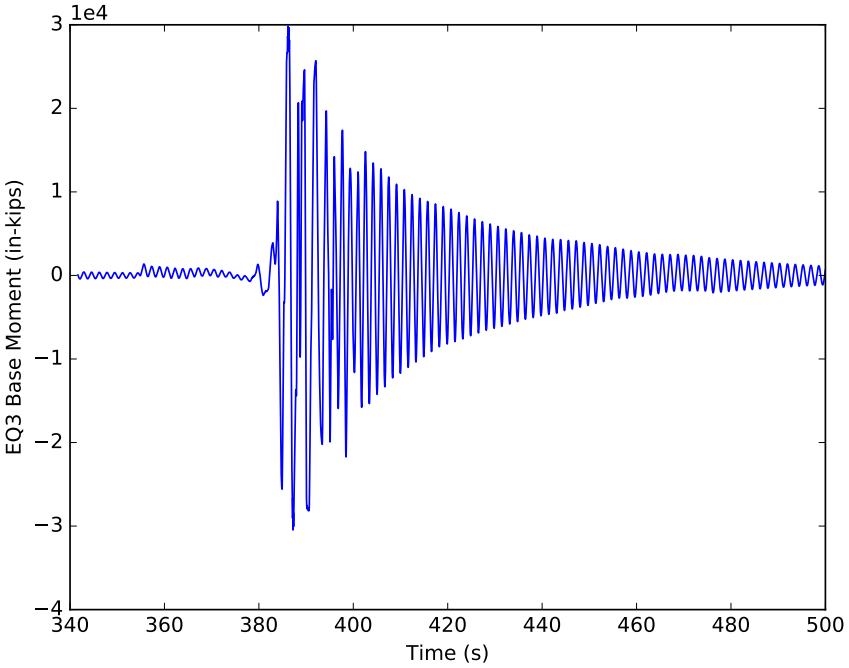

Figure F.21: Mz response of model 4b for EQ3

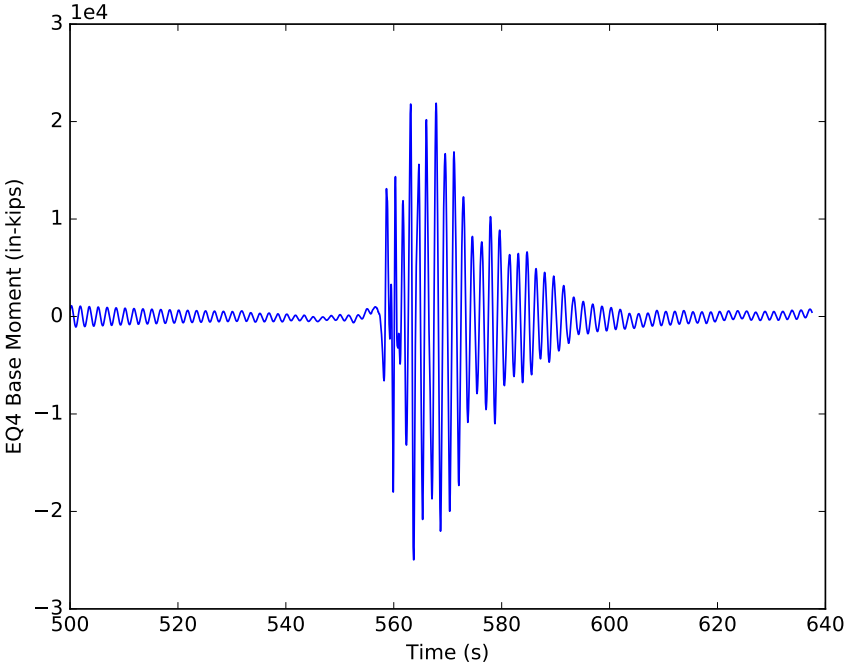

Figure F.22: Mz response of model 4b for EQ4

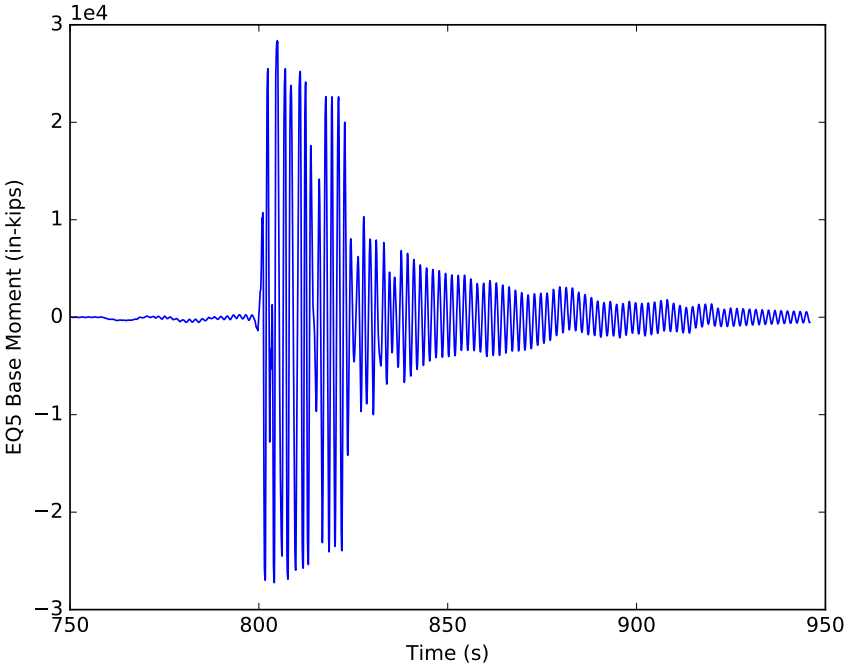

Figure F.23: Mz response of model 4b for EQ5

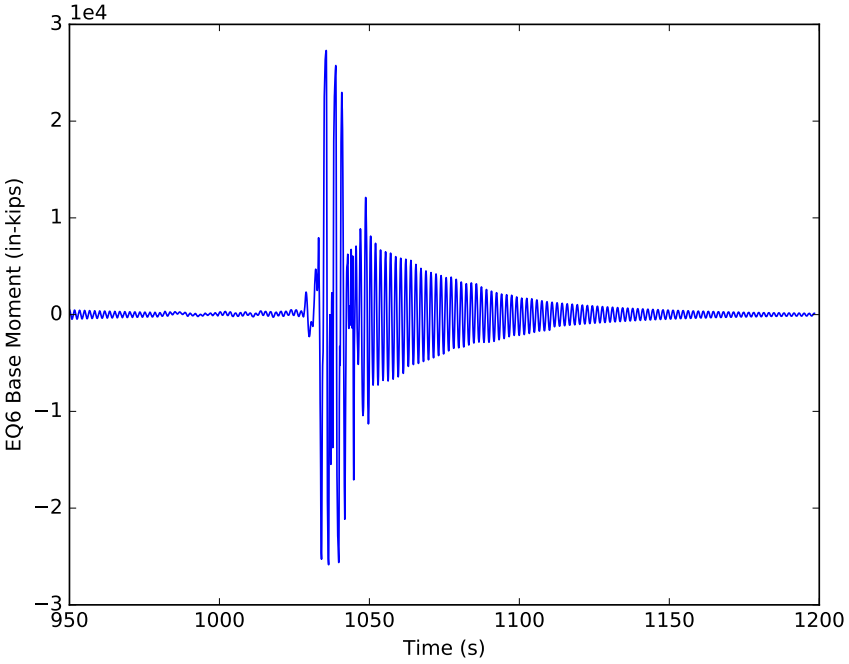

Figure F.24: Mz response of model 4b for EQ6

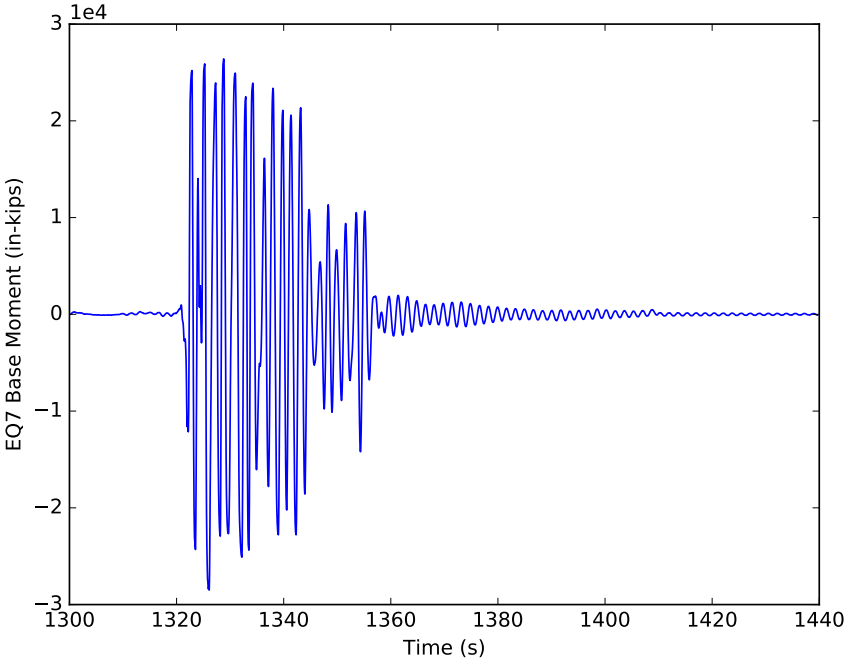

Figure F.25: Mz response of model 4b for EQ7

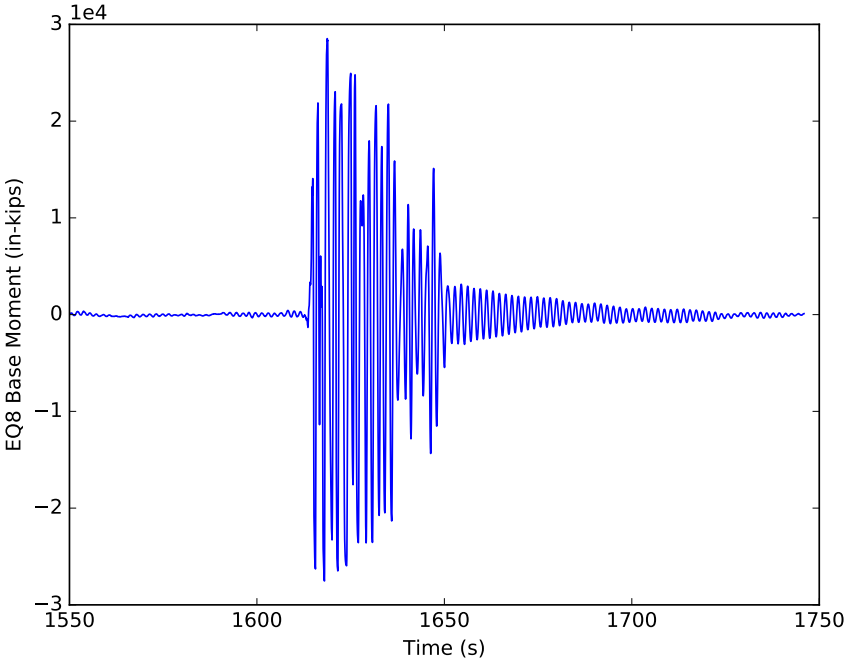

Figure F.26: Mz response of model 4b for EQ8

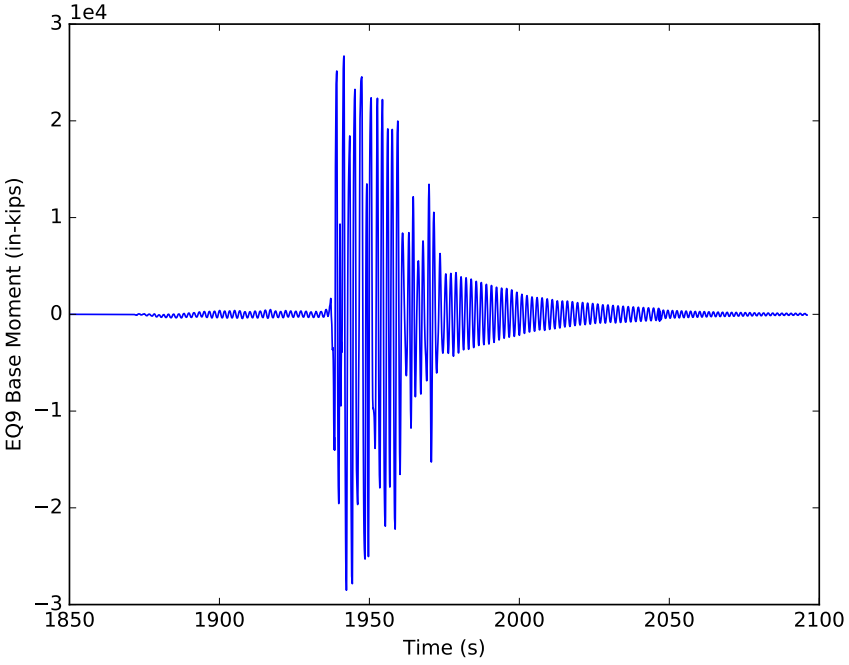

Figure F.27: Mz response of model 4b for EQ9

Appendix G

Model 4c Output

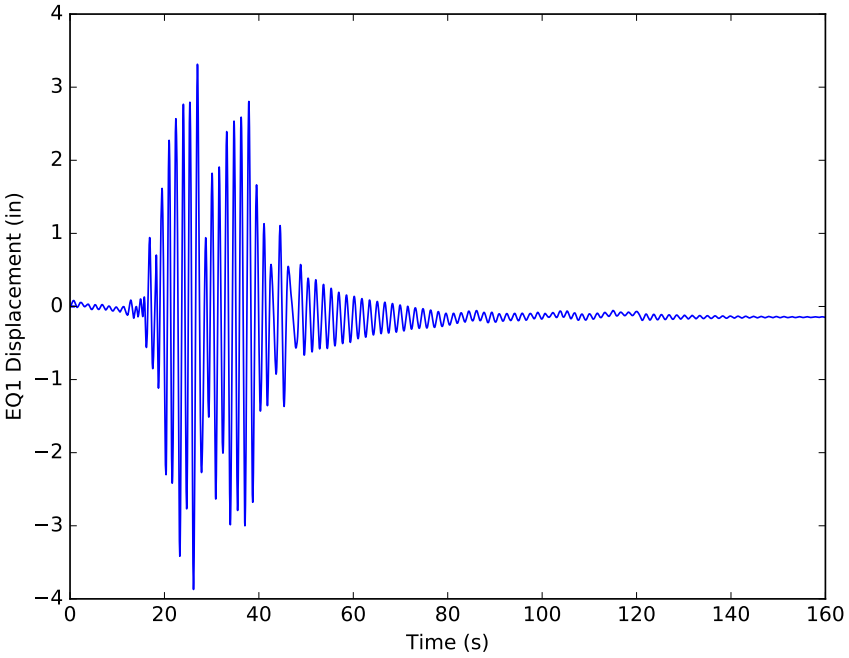

Figure G.1: Displacement response of model 4c for EQ1

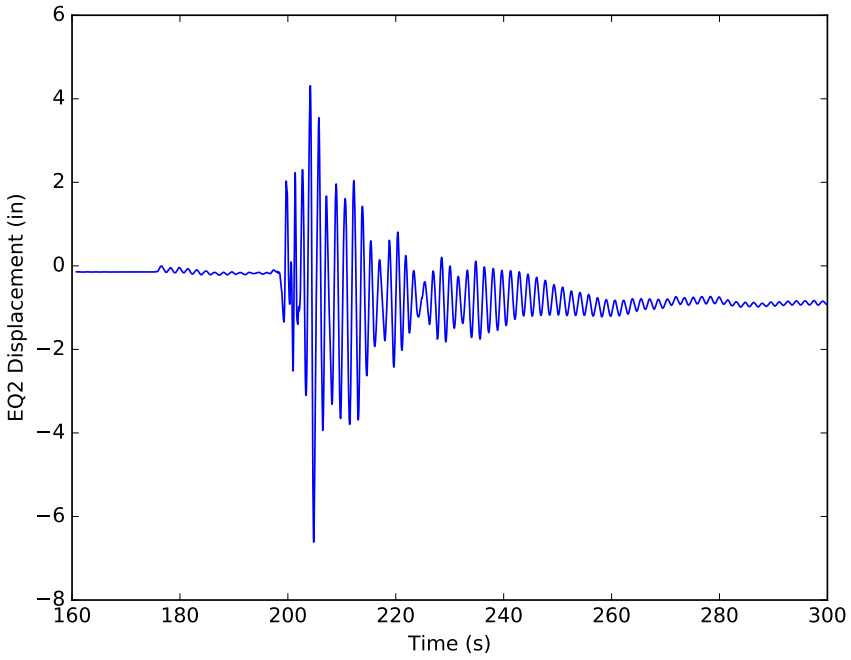

Figure G.2: Displacement response of model 4c for EQ2

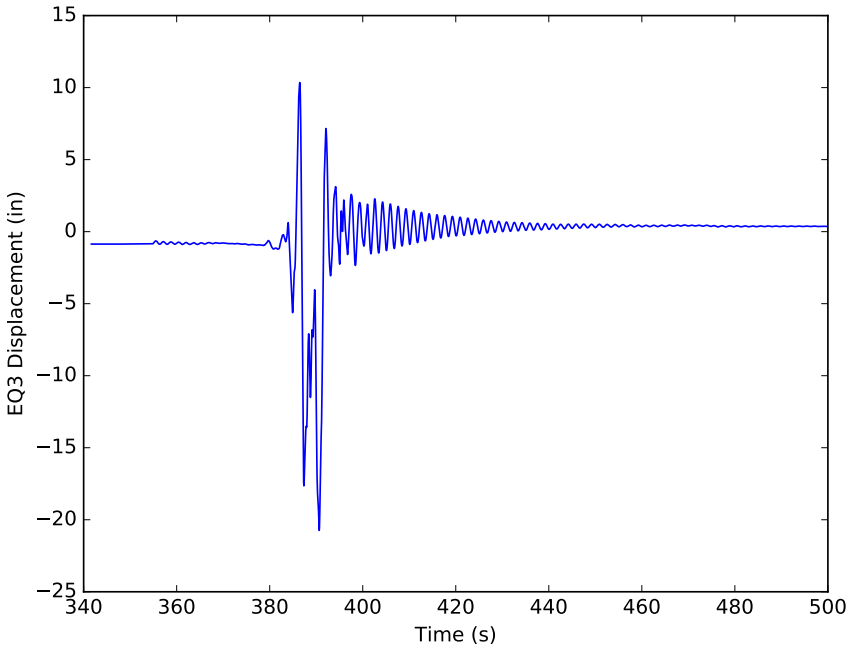

Figure G.3: Displacement response of model 4c for EQ3

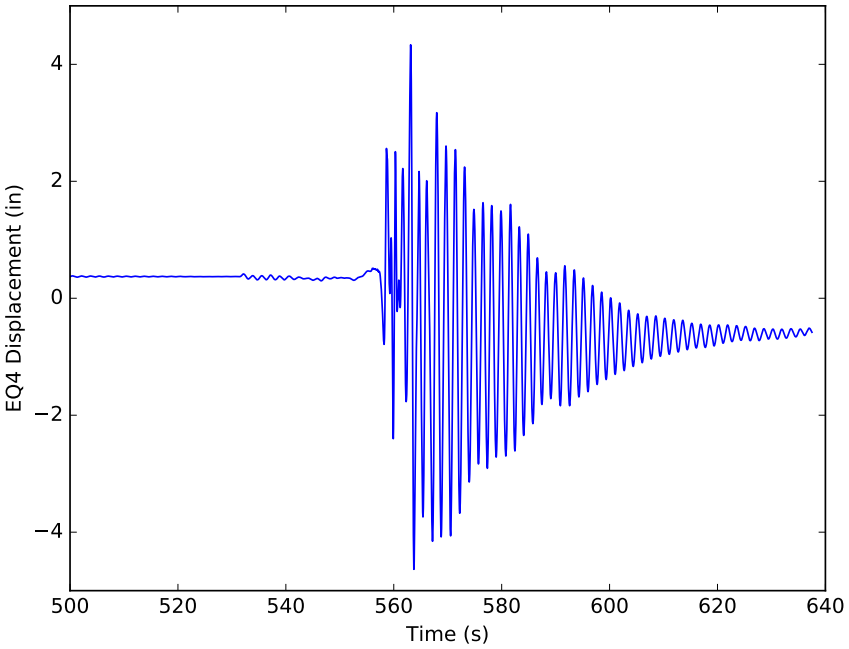

Figure G.4: Displacement response of model 4c for EQ4

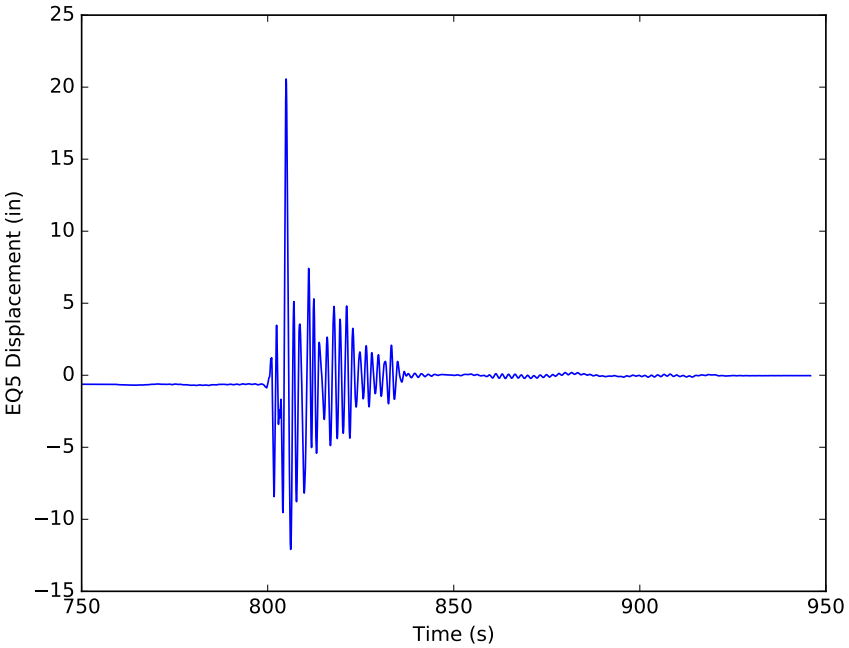

Figure G.5: Displacement response of model 4c for EQ5

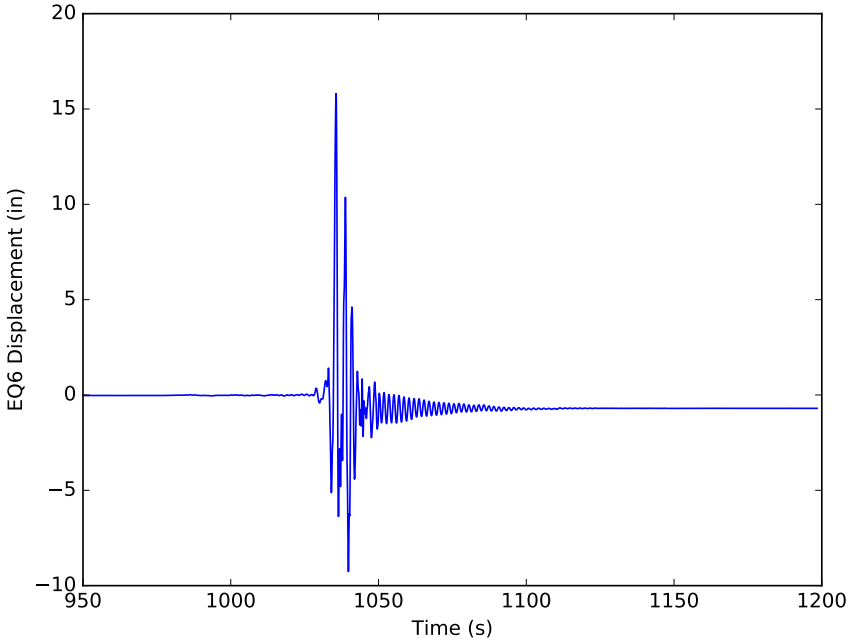

Figure G.6: Displacement response of model 4c for EQ6

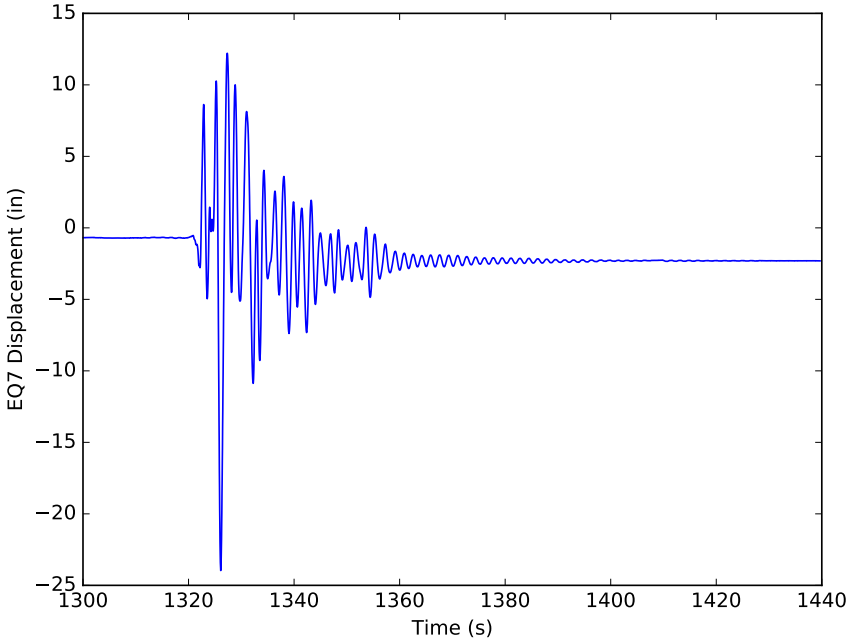

Figure G.7: Displacement response of model 4c for EQ7

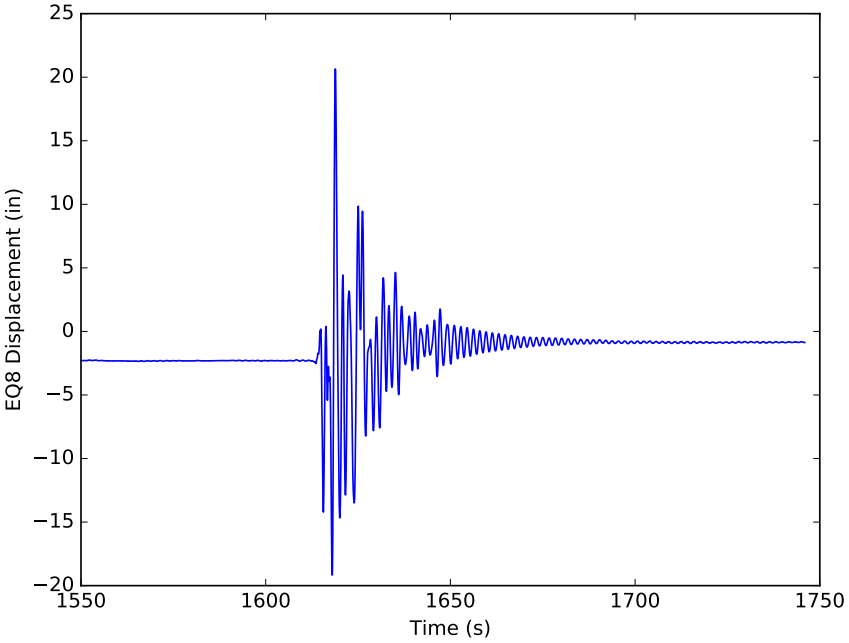

Figure G.8: Displacement response of model 4c for EQ8

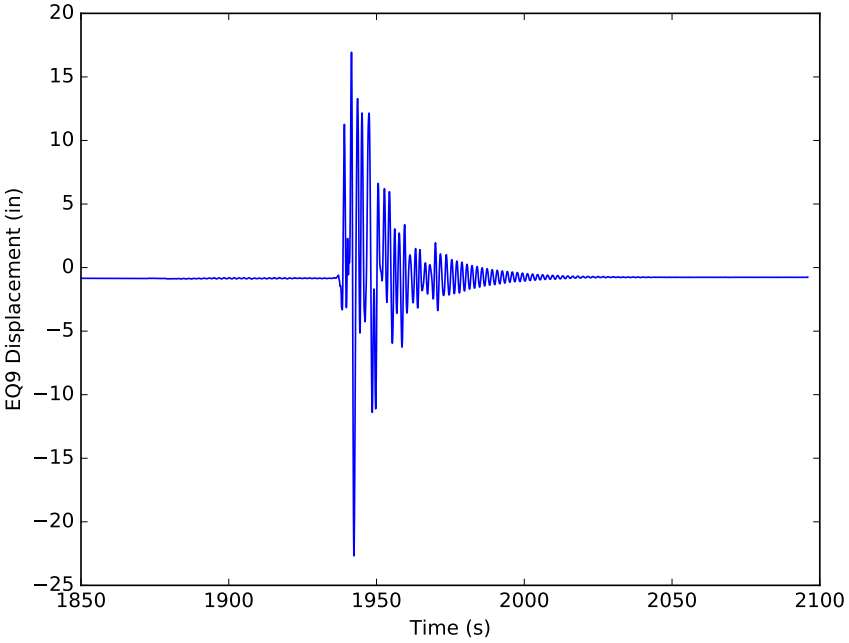

Figure G.9: Displacement response of model 4c for EQ9

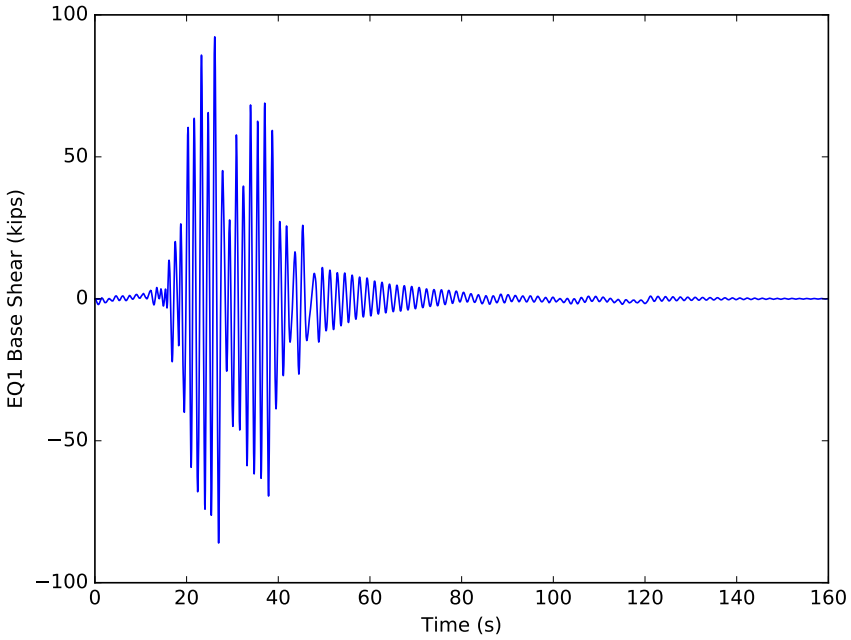

Figure G.10: Fx response of model 4c for EQ1

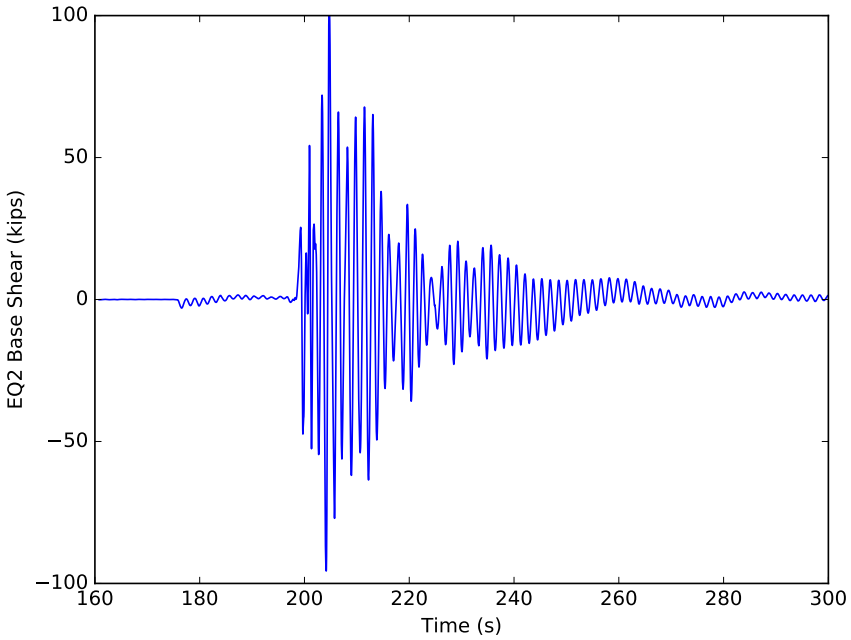

Figure G.11: Fx response of model 4c for EQ2

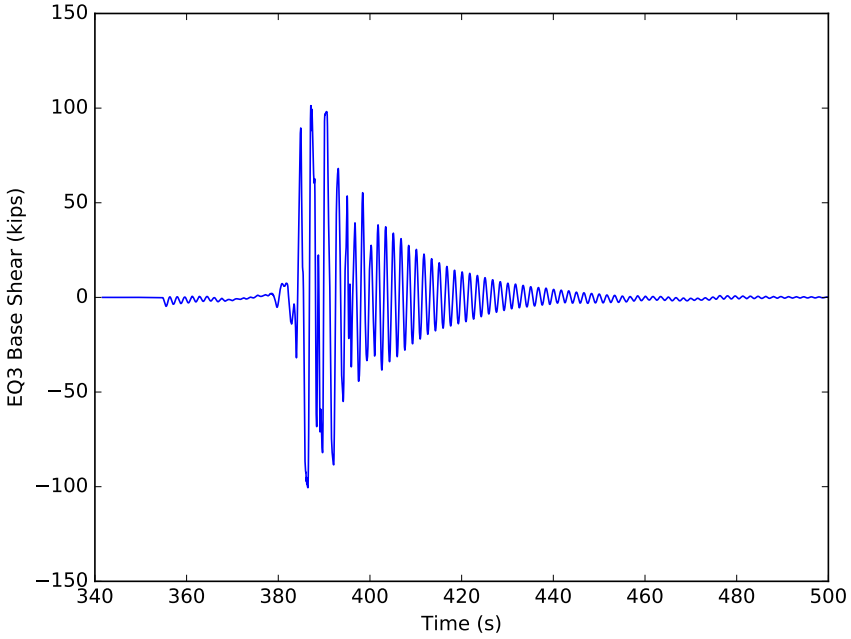

Figure G.12: Fx response of model 4c for EQ3

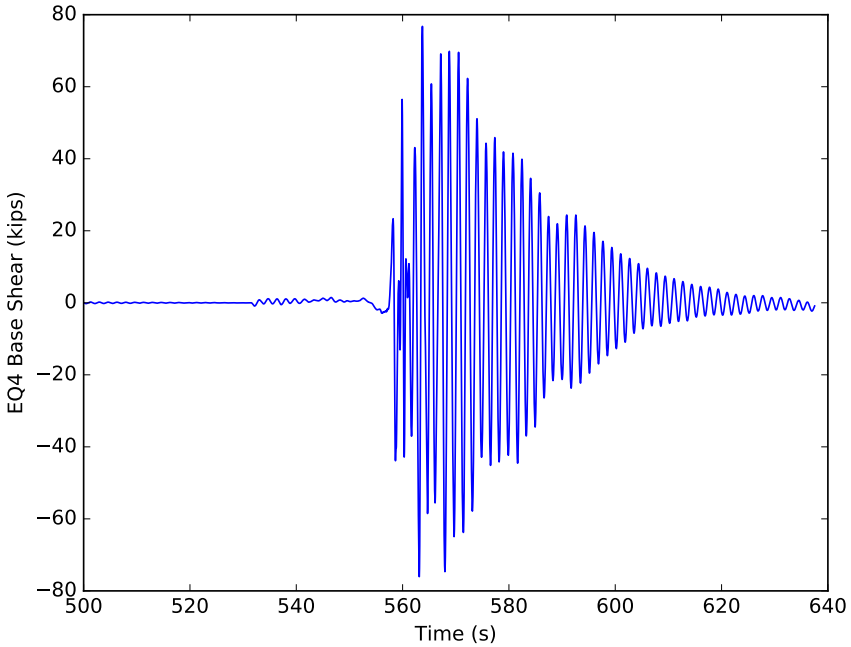

Figure G.13: Fx response of model 4c for EQ4

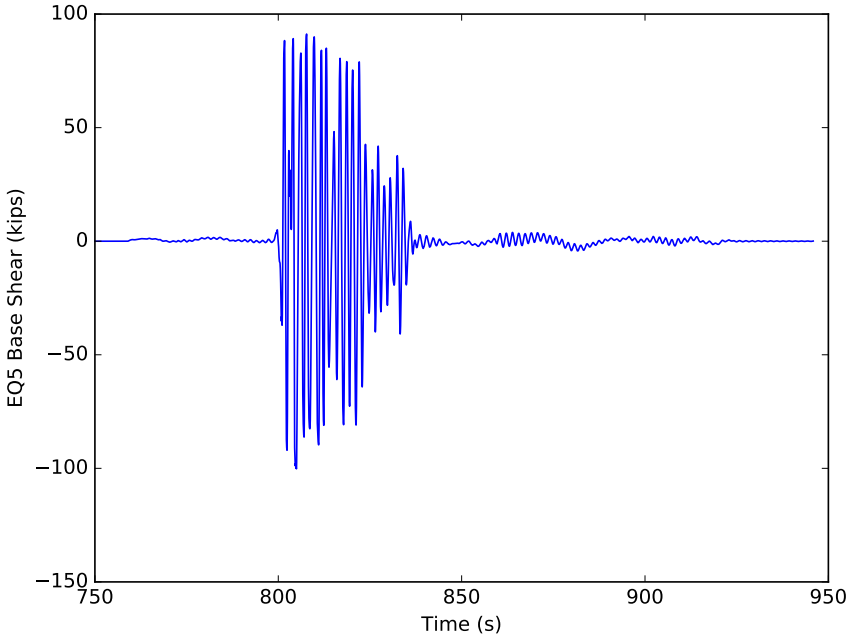

Figure G.14: Fx response of model 4c for EQ5

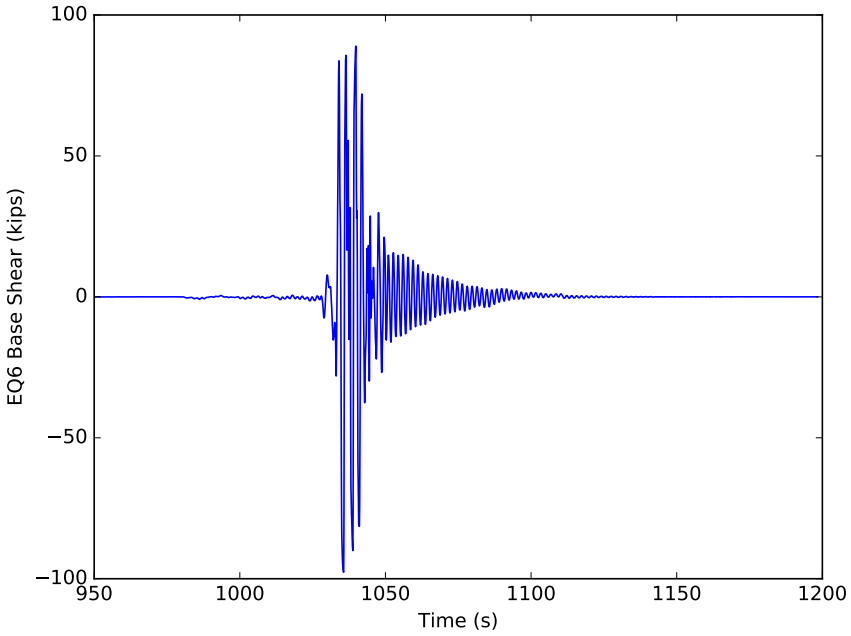

Figure G.15: Fx response of model 4c for EQ6

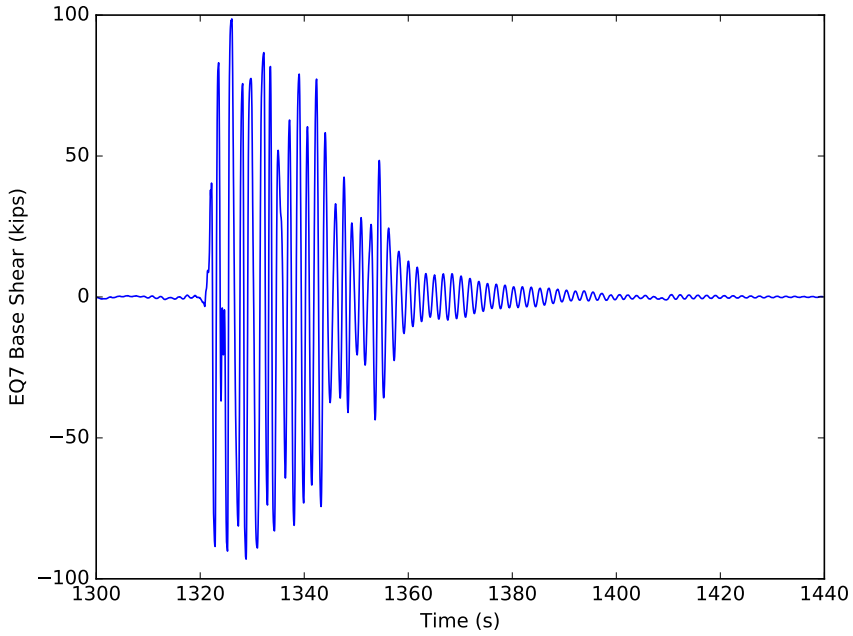

Figure G.16: Fx response of model 4c for EQ7

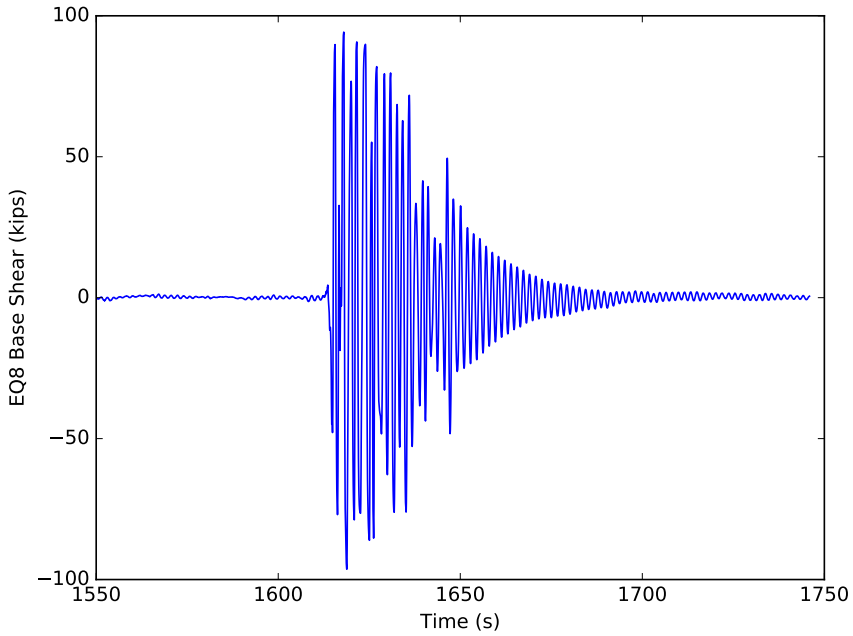

Figure G.17: Fx response of model 4c for EQ8

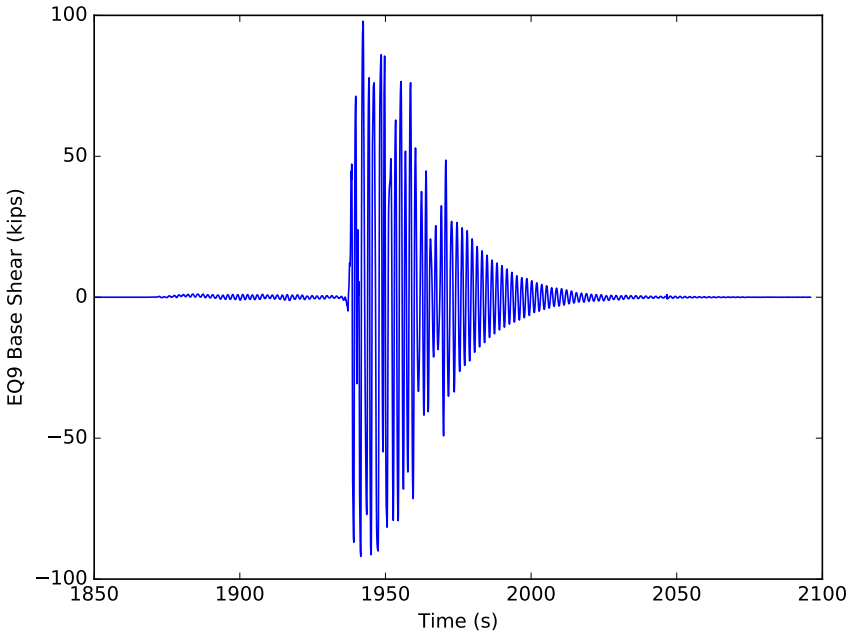

Figure G.18: Fx response of model 4c for EQ9

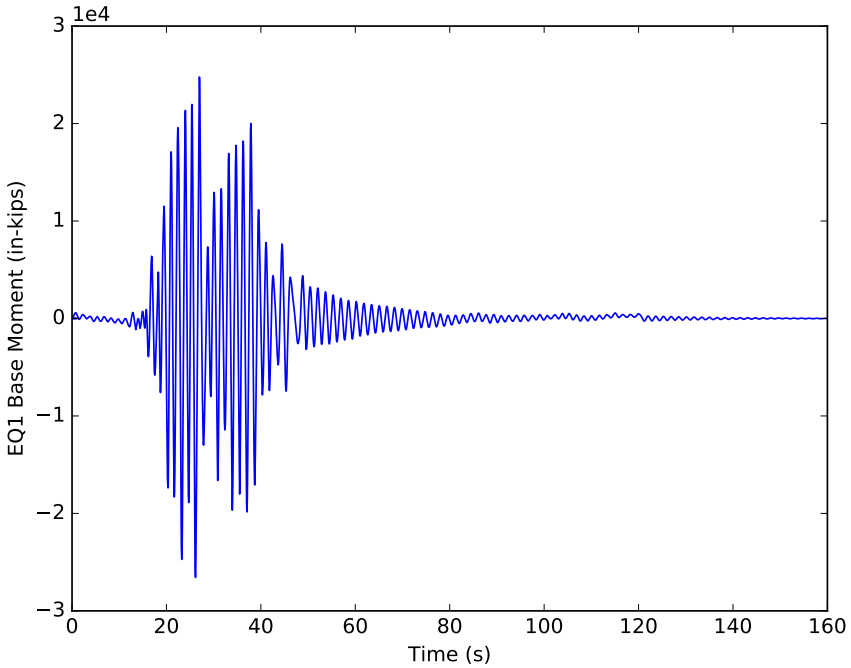

Figure G.19: Mz response of model 4c for EQ1

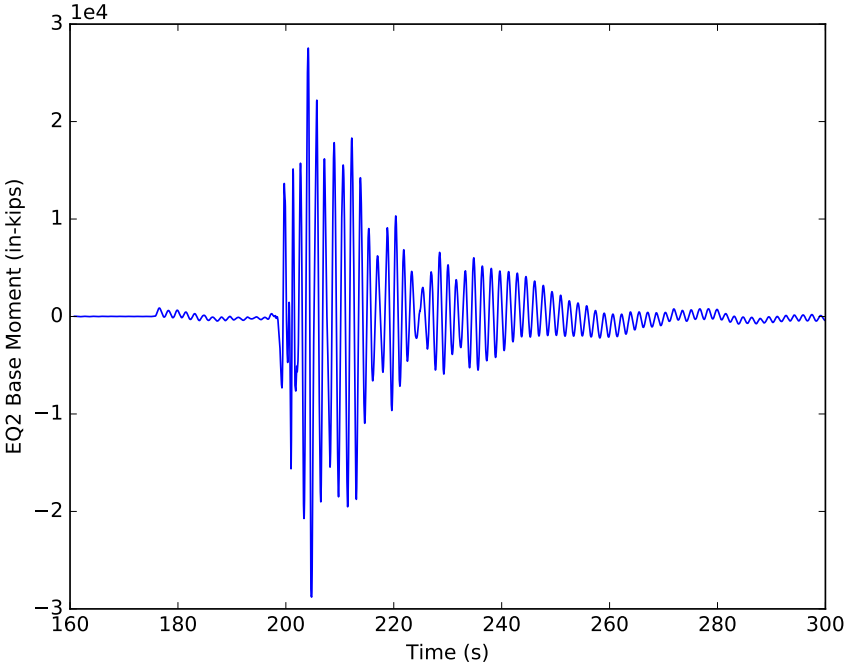

Figure G.20: Mz response of model 4c for EQ2

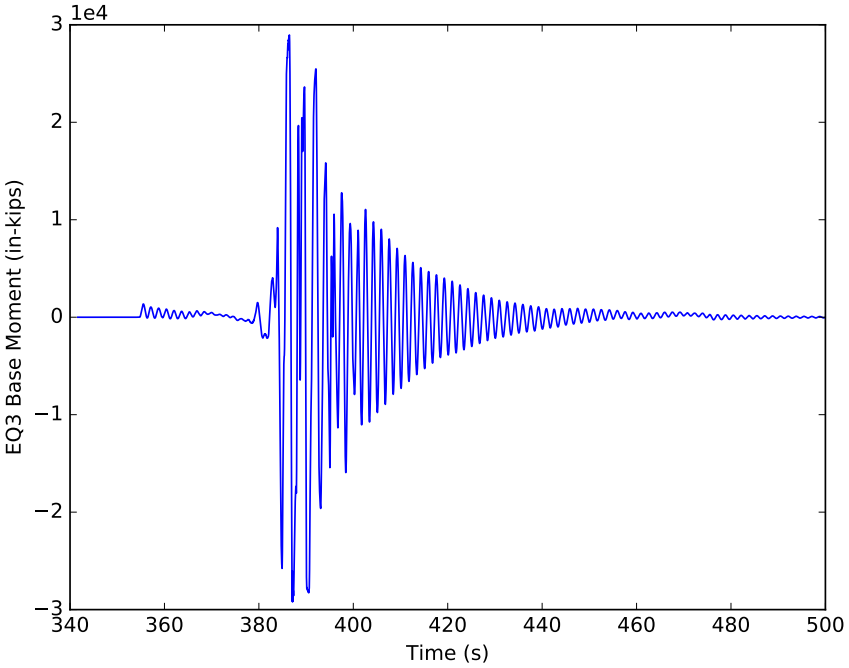

Figure G.21: Mz response of model 4c for EQ3

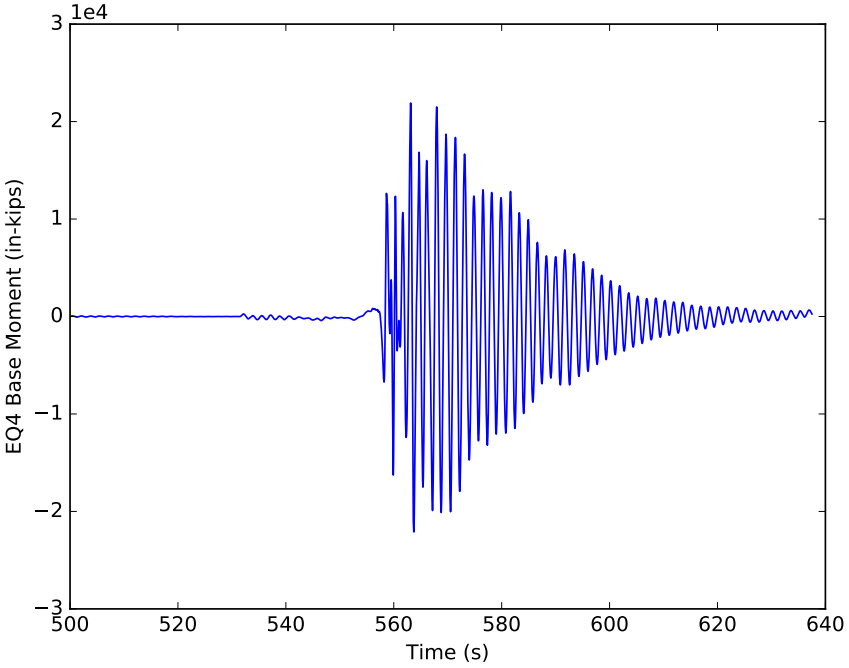

Figure G.22: Mz response of model 4c for EQ4

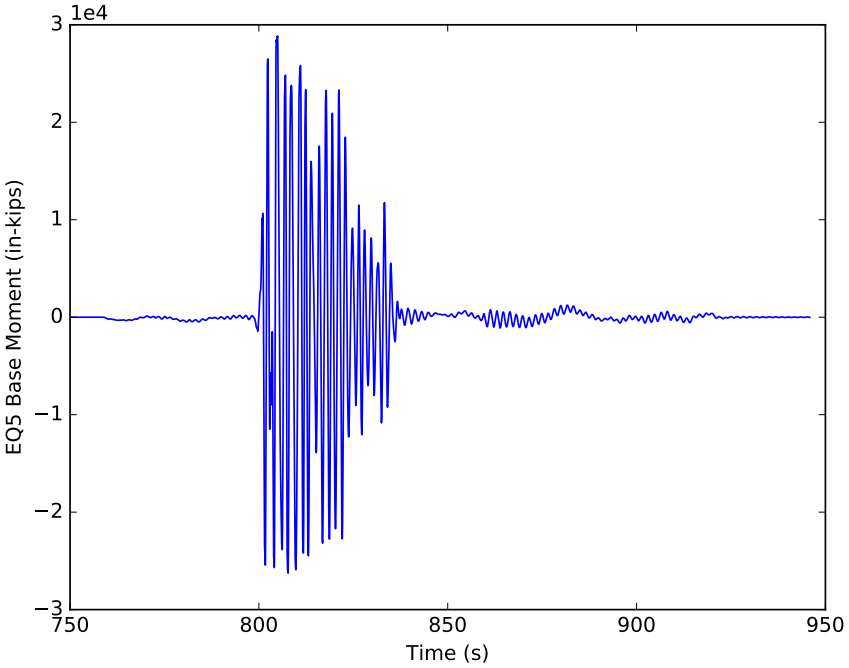

Figure G.23: Mz response of model 4c for EQ5

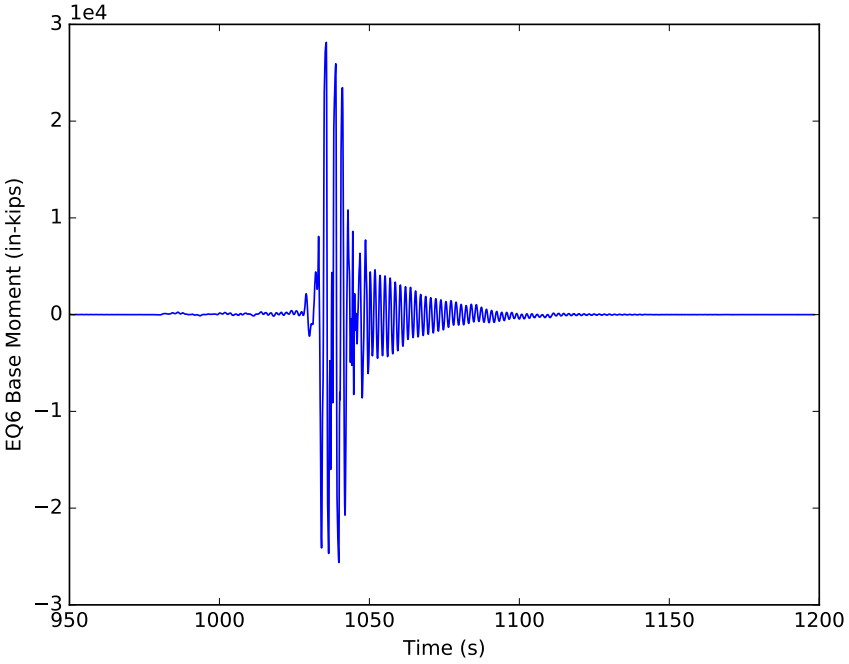

Figure G.24: Mz response of model 4c for EQ6

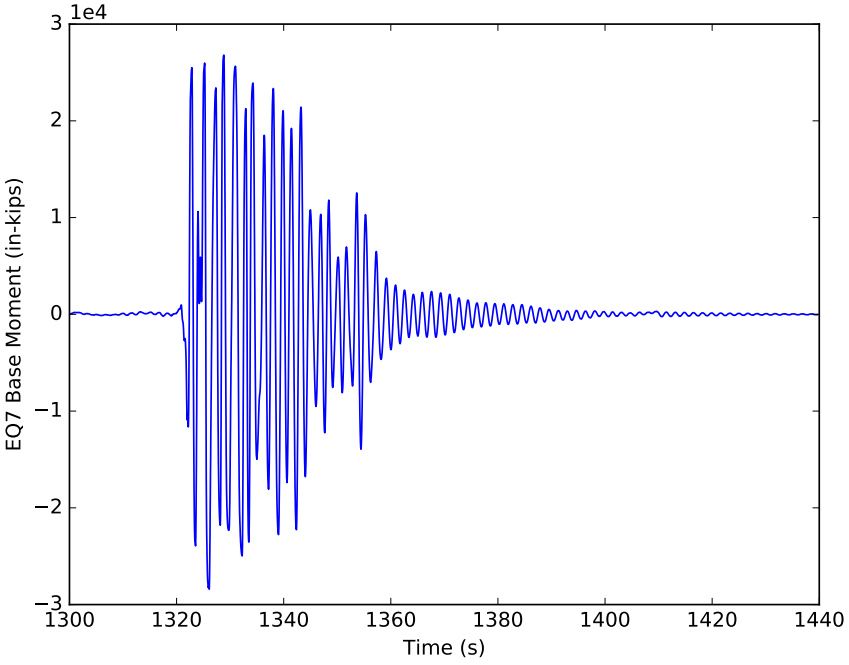

Figure G.25: Mz response of model 4c for EQ7

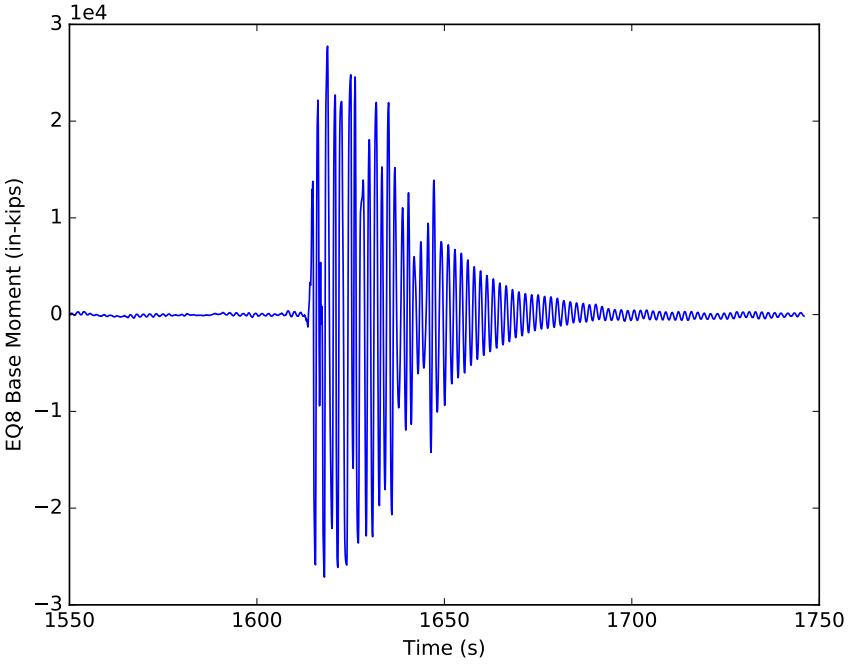

Figure G.26: Mz response of model 4c for EQ8

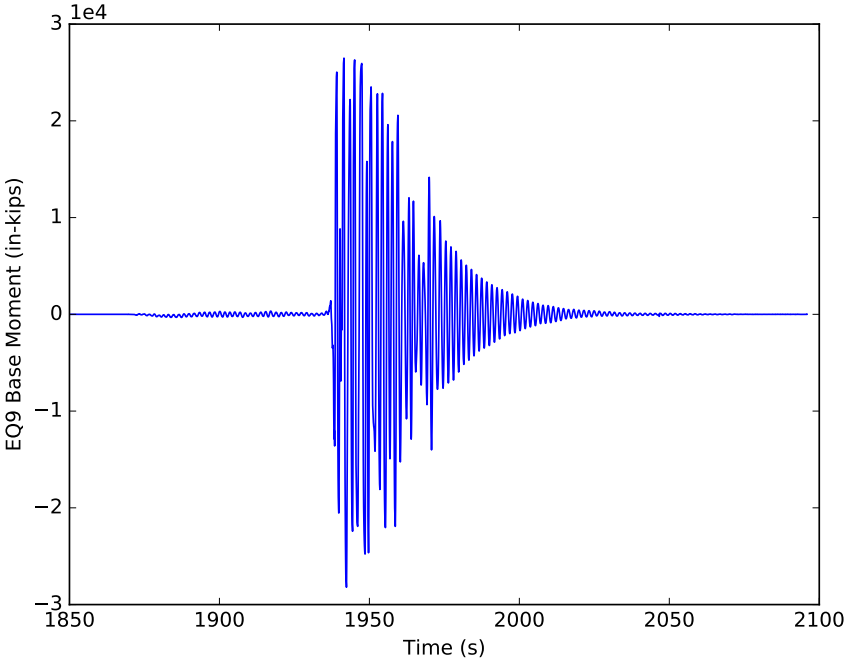

Figure G.27: Mz response of model 4c for EQ9

Appendix H

Model 4d Output

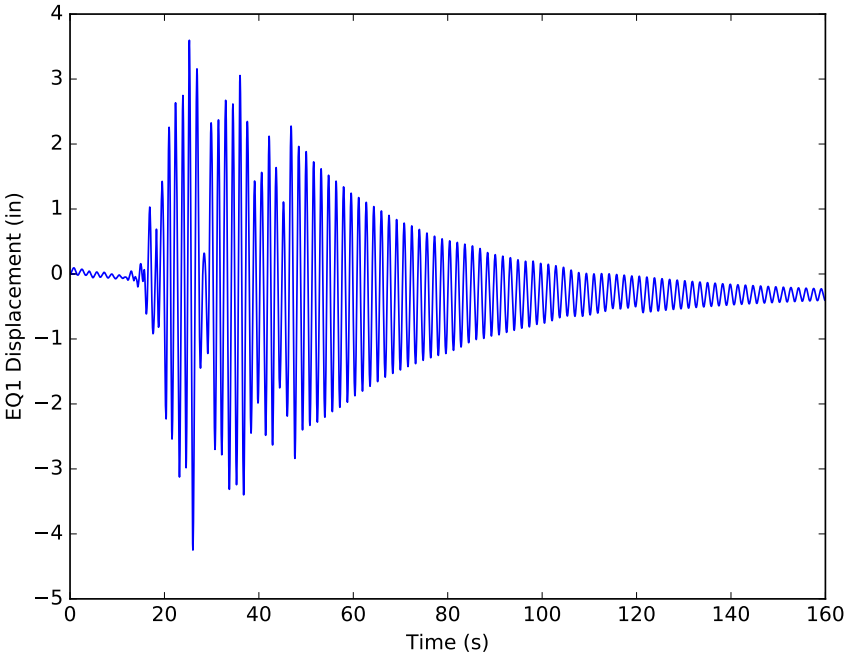

Figure H.1: Displacement response of model 4d for EQ1

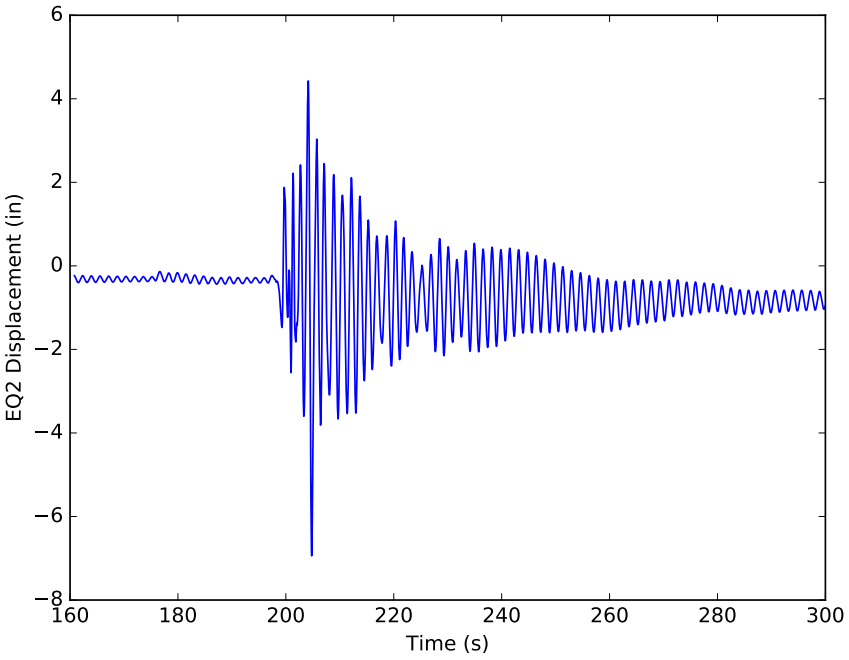

Figure H.2: Displacement response of model 4d for EQ2

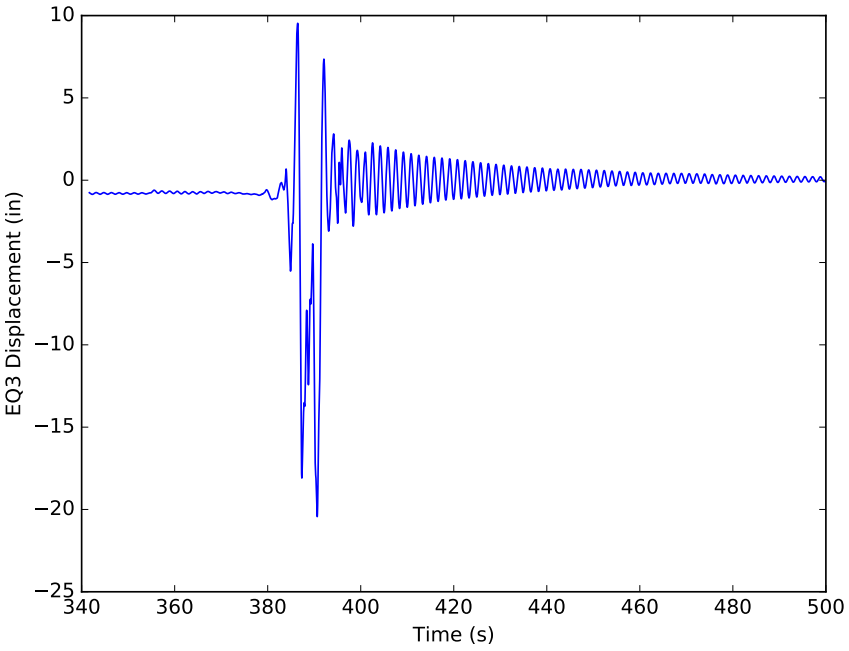

Figure H.3: Displacement response of model 4d for EQ3

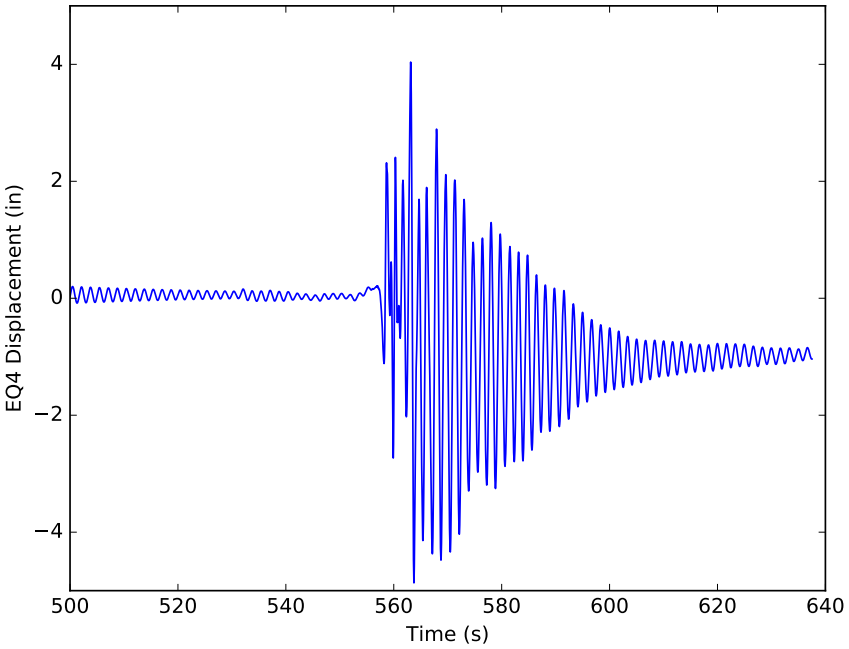

Figure H.4: Displacement response of model 4d for EQ4

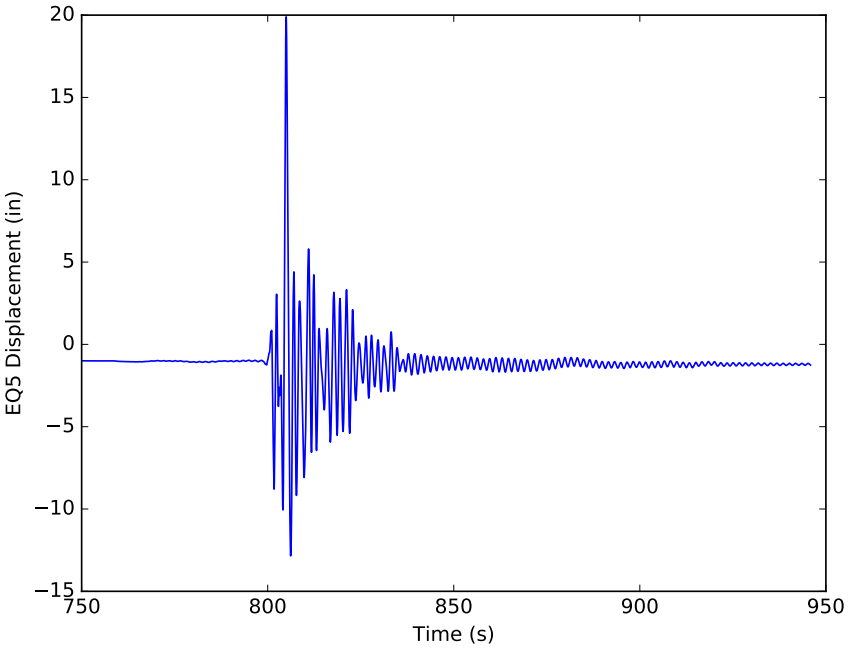

Figure H.5: Displacement response of model 4d for EQ5

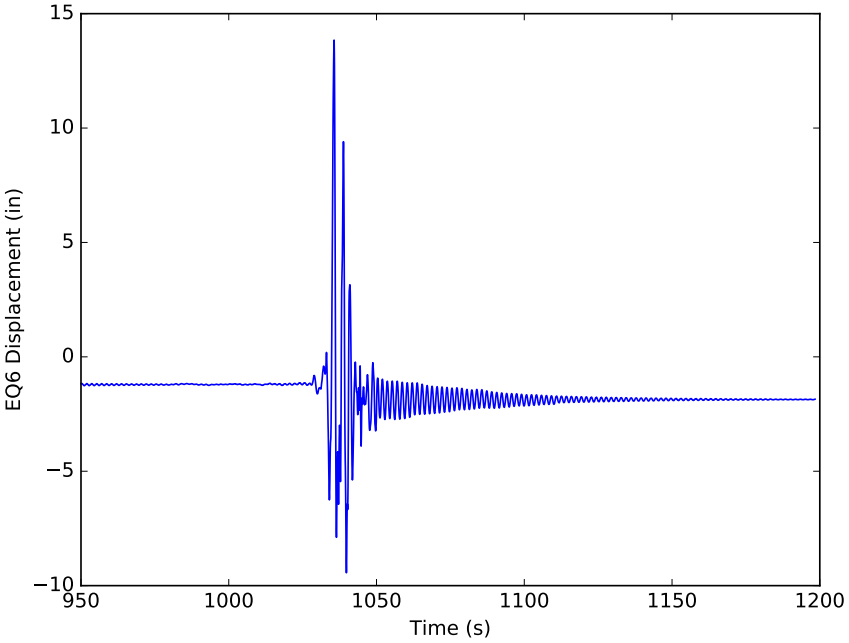

Figure H.6: Displacement response of model 4d for EQ6

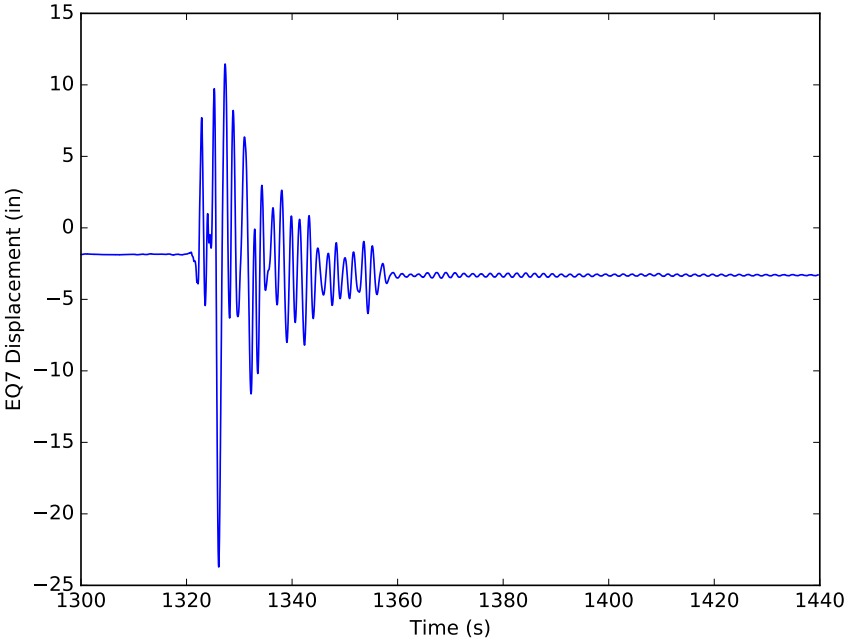

Figure H.7: Displacement response of model 4d for EQ7

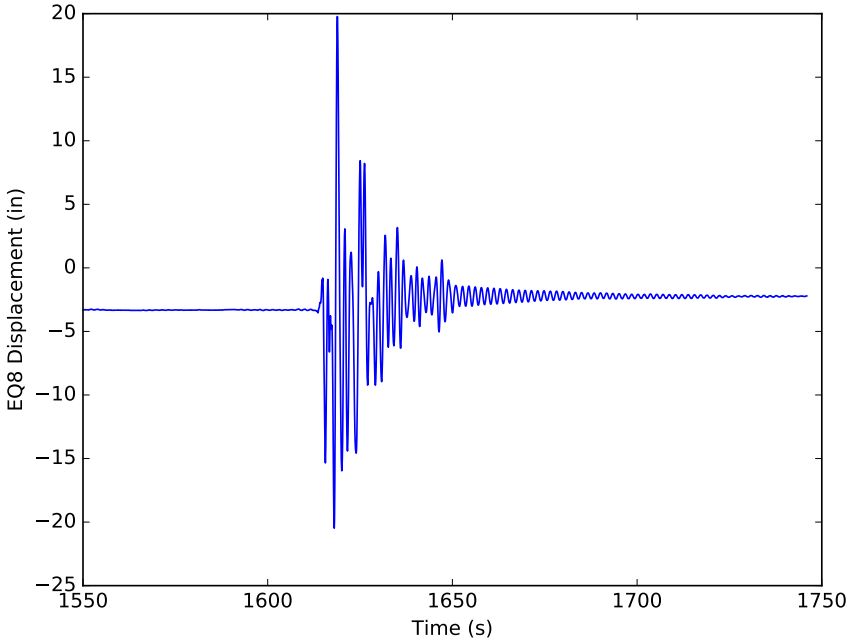

Figure H.8: Displacement response of model 4d for EQ8

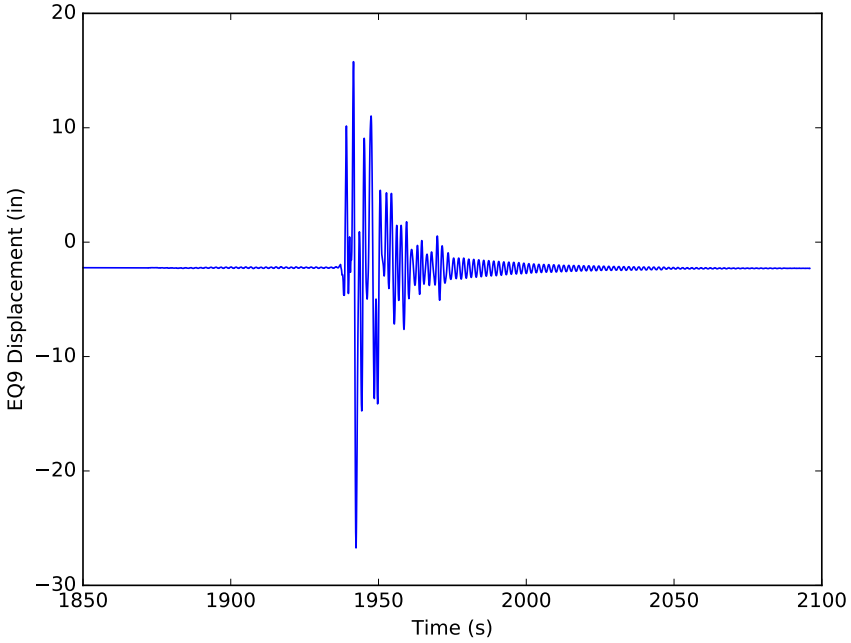

Figure H.9: Displacement response of model 4d for EQ9

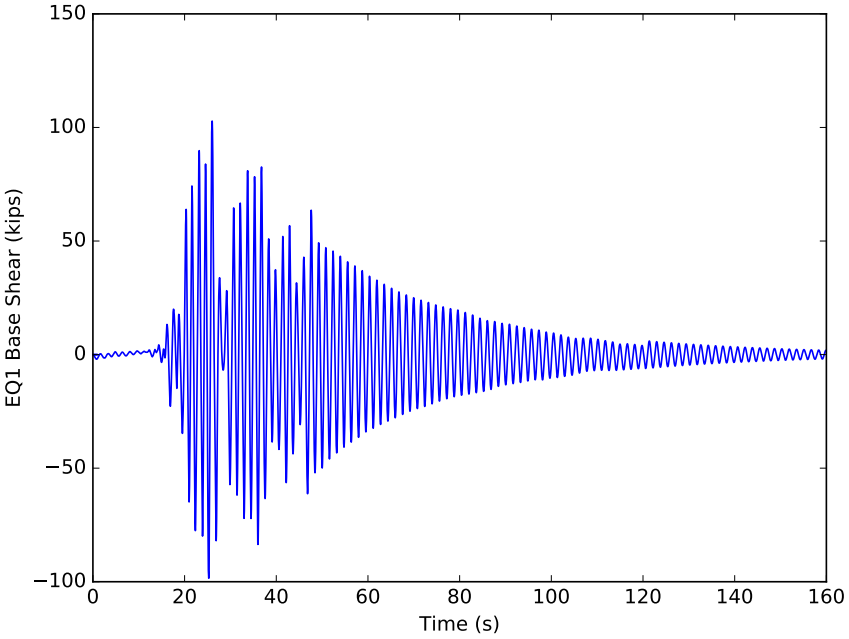

Figure H.10: Fx response of model 4d for EQ1

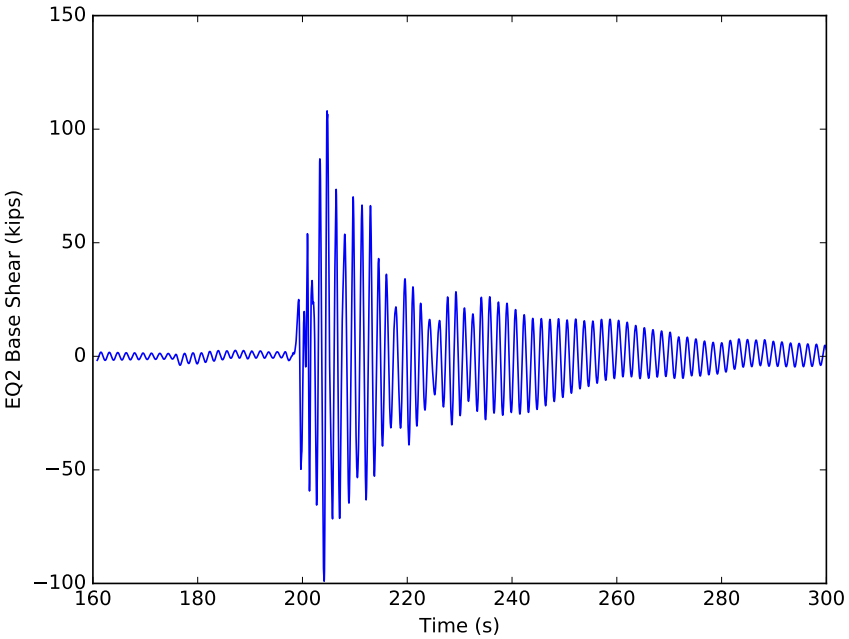

Figure H.11: Fx response of model 4d for EQ2

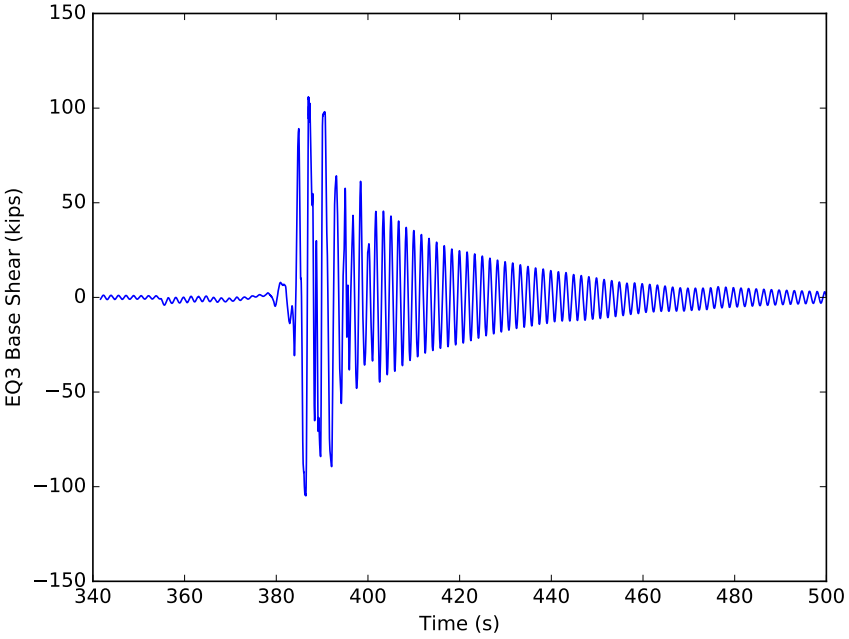

Figure H.12: Fx response of model 4d for EQ3

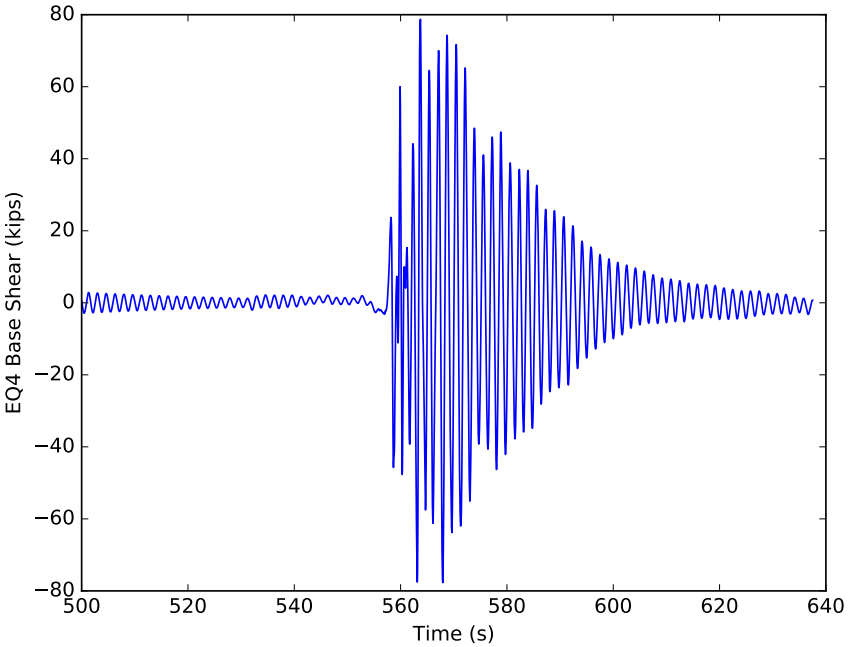

Figure H.13: Fx response of model 4d for EQ4

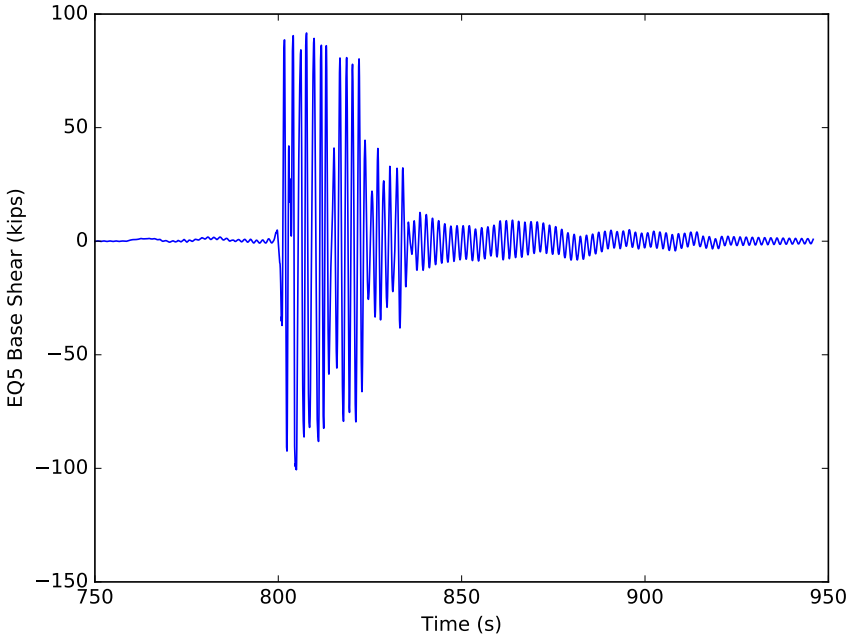

Figure H.14: Fx response of model 4d for EQ5

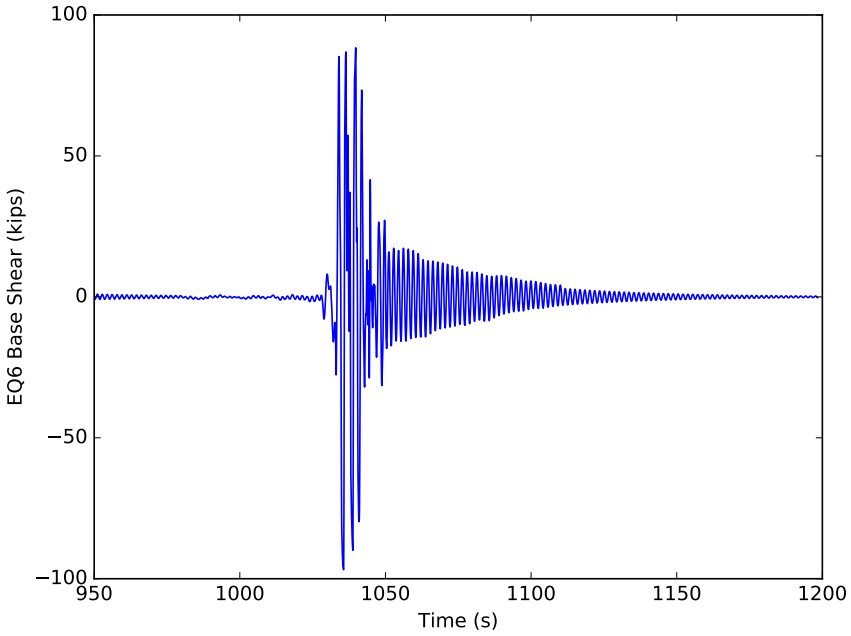

Figure H.15: Fx response of model 4d for EQ6

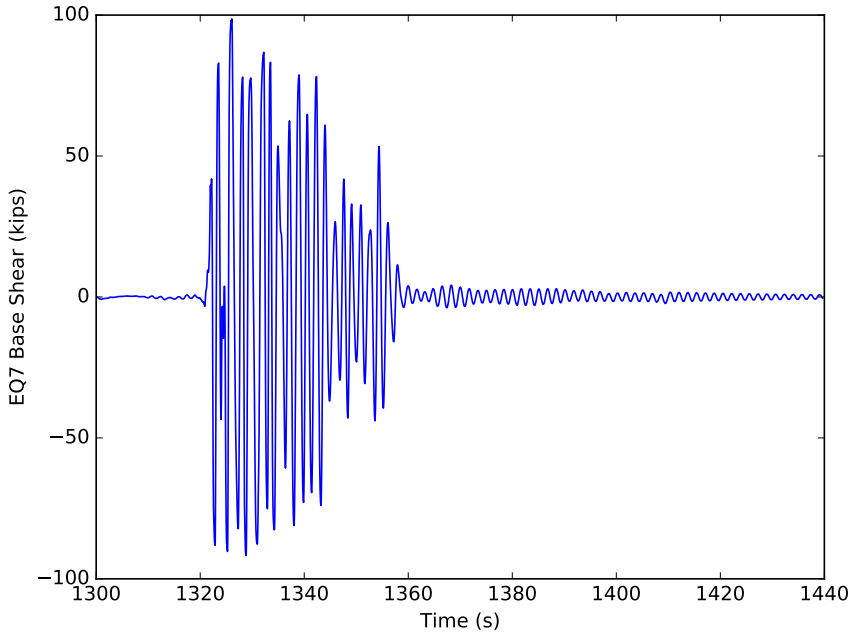

Figure H.16: Fx response of model 4d for EQ7

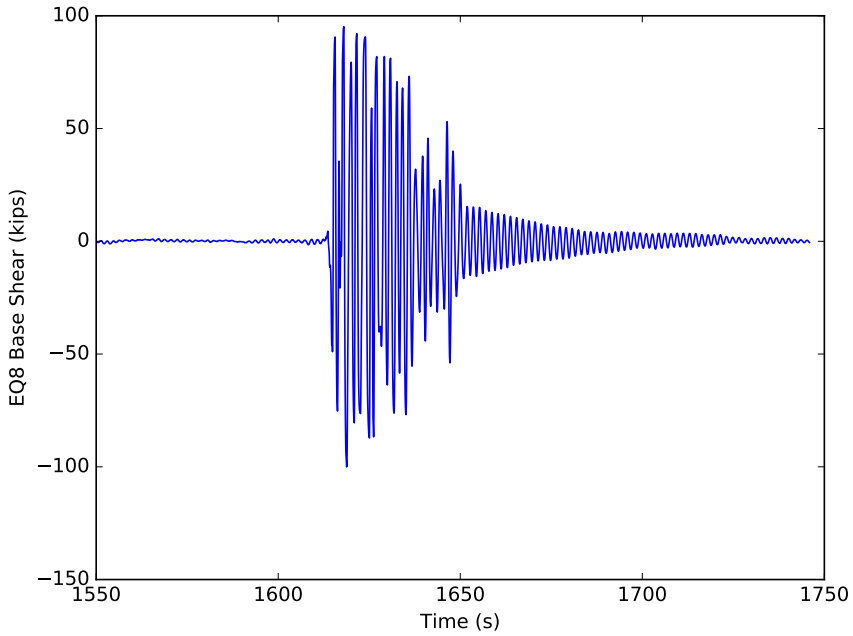

Figure H.17: Fx response of model 4d for EQ8

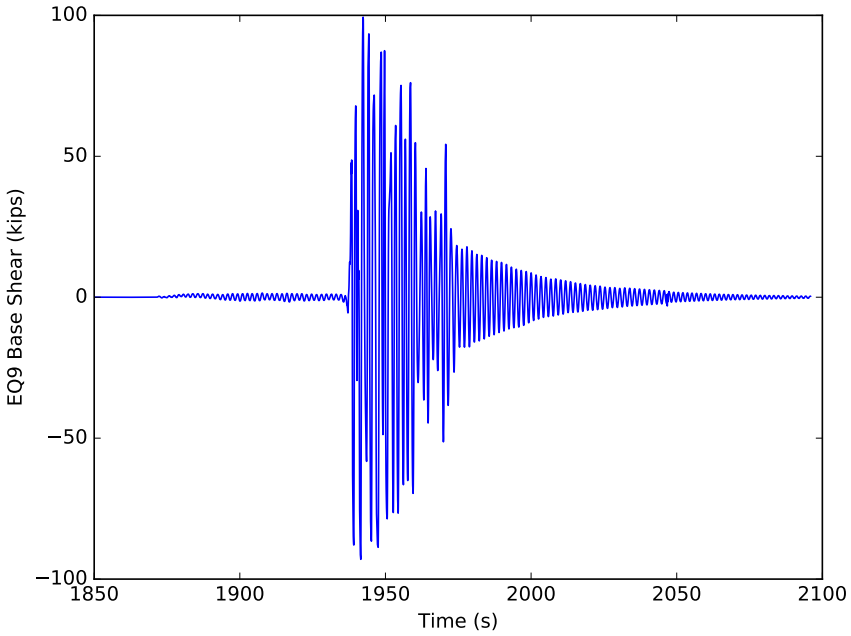

Figure H.18: Fx response of model 4d for EQ9

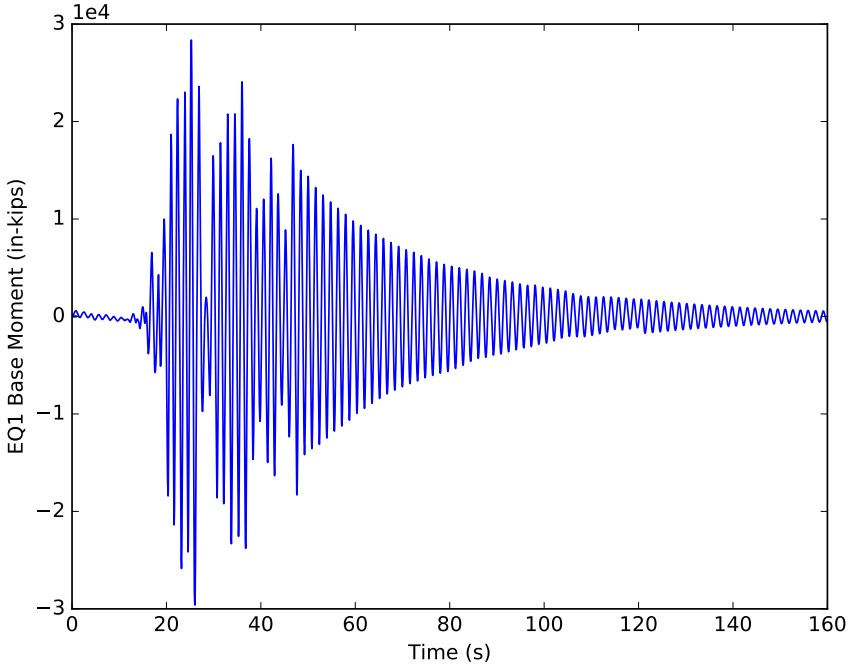

Figure H.19: Mz response of model 4d for EQ1

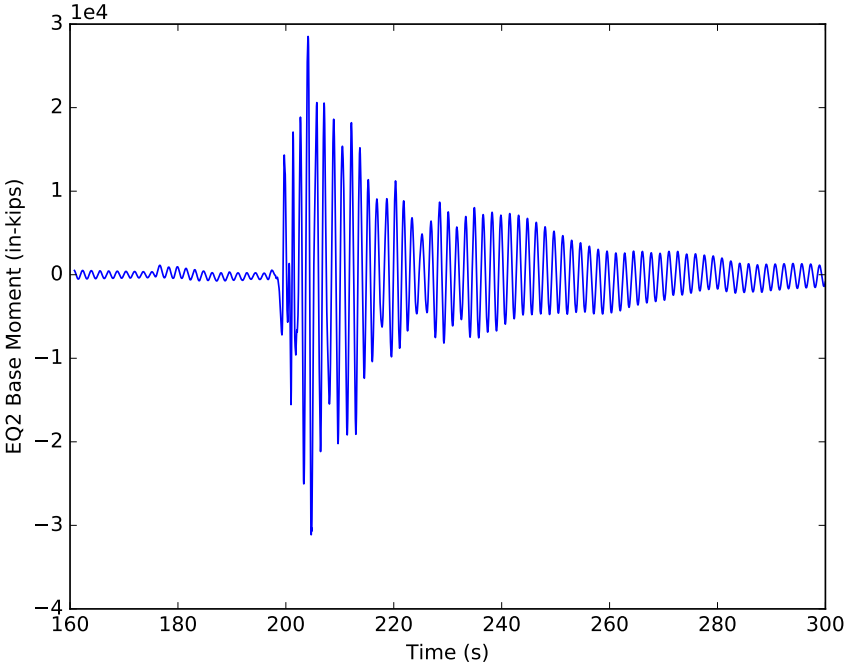

Figure H.20: Mz response of model 4d for EQ2

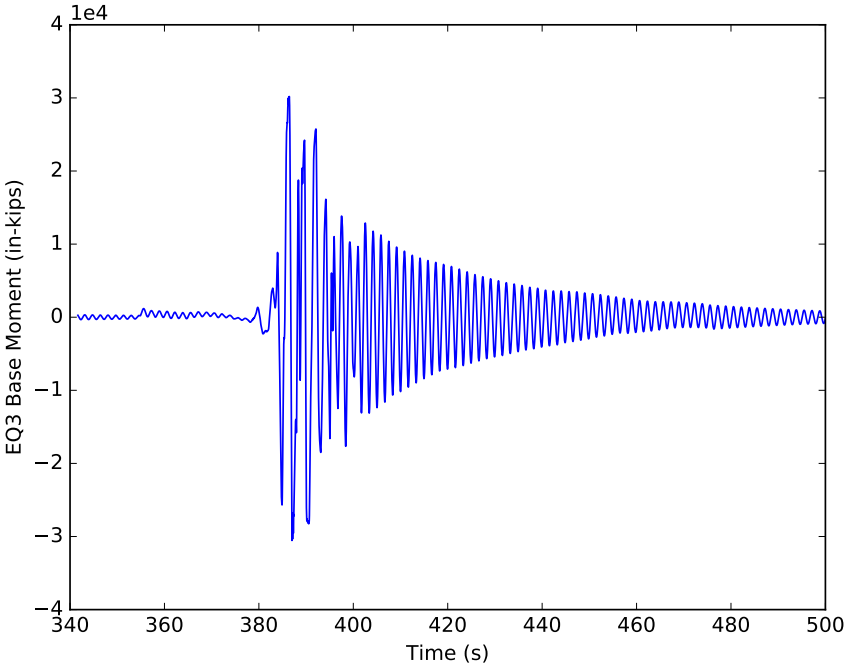

Figure H.21: Mz response of model 4d for EQ3

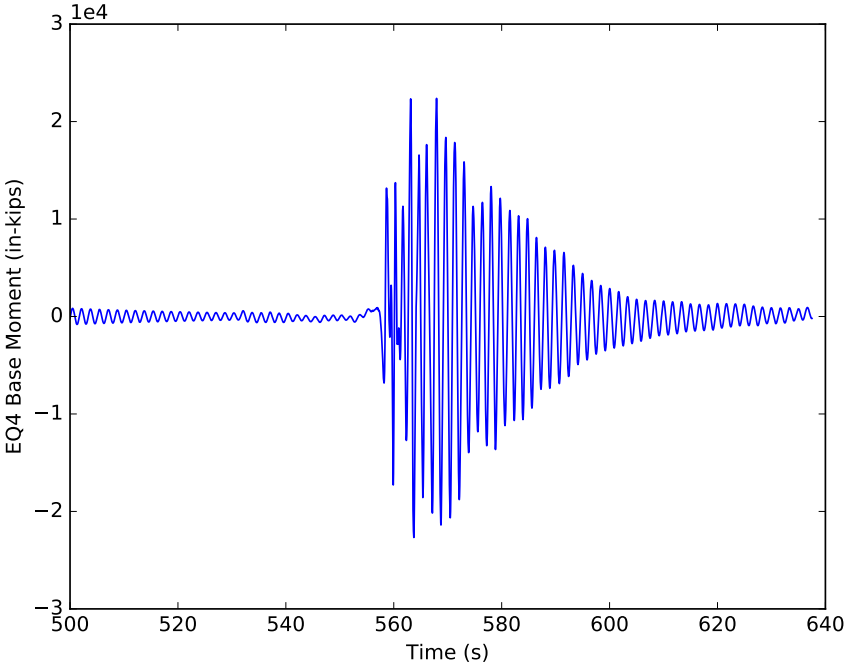

Figure H.22: Mz response of model 4d for EQ4

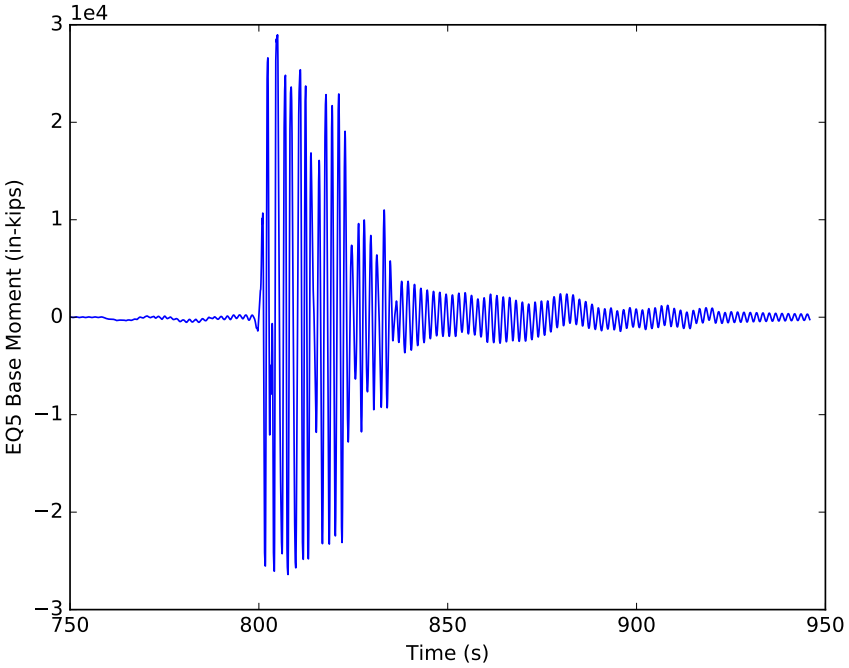

Figure H.23: Mz response of model 4d for EQ5

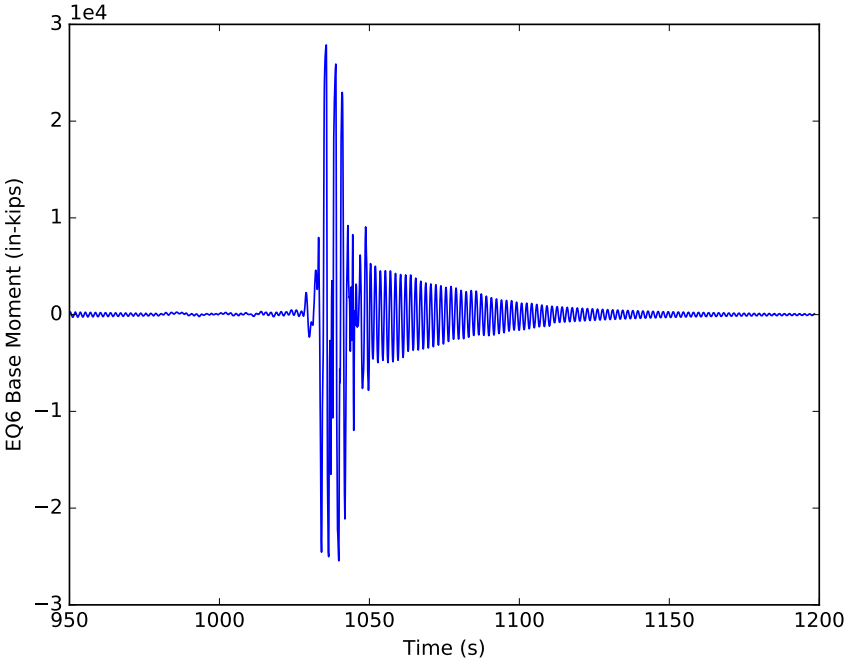

Figure H.24: Mz response of model 4d for EQ6

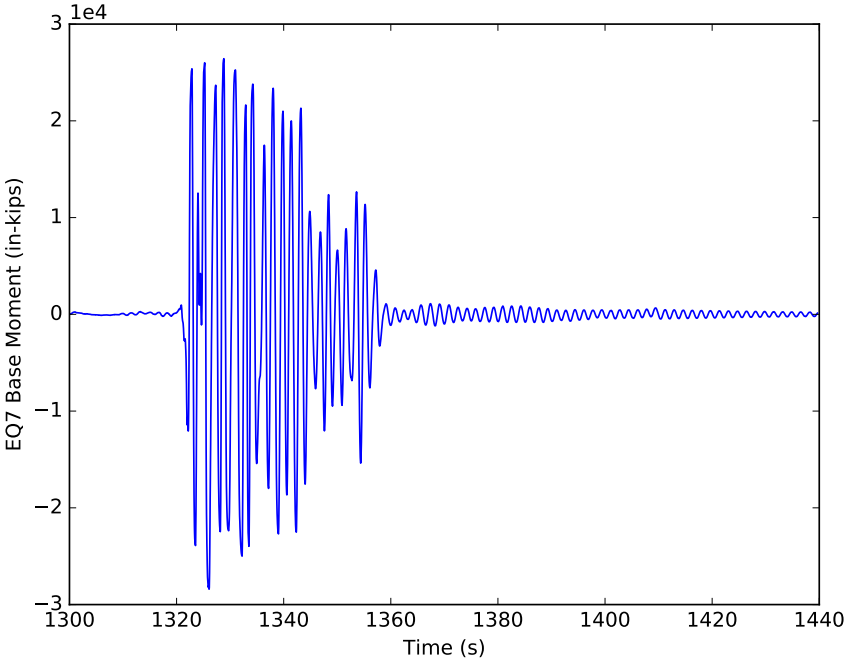

Figure H.25: Mz response of model 4d for EQ7

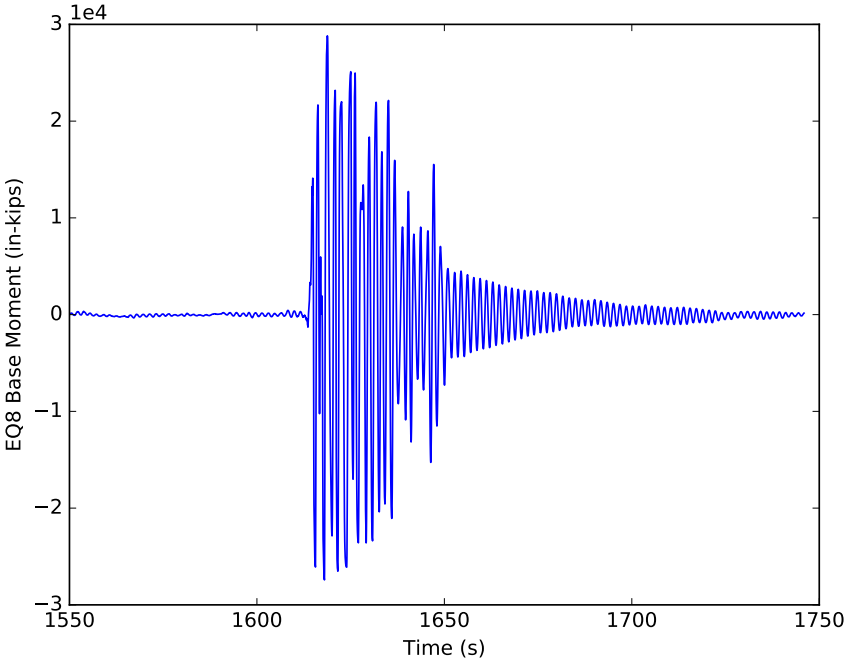

Figure H.26: Mz response of model 4d for EQ8

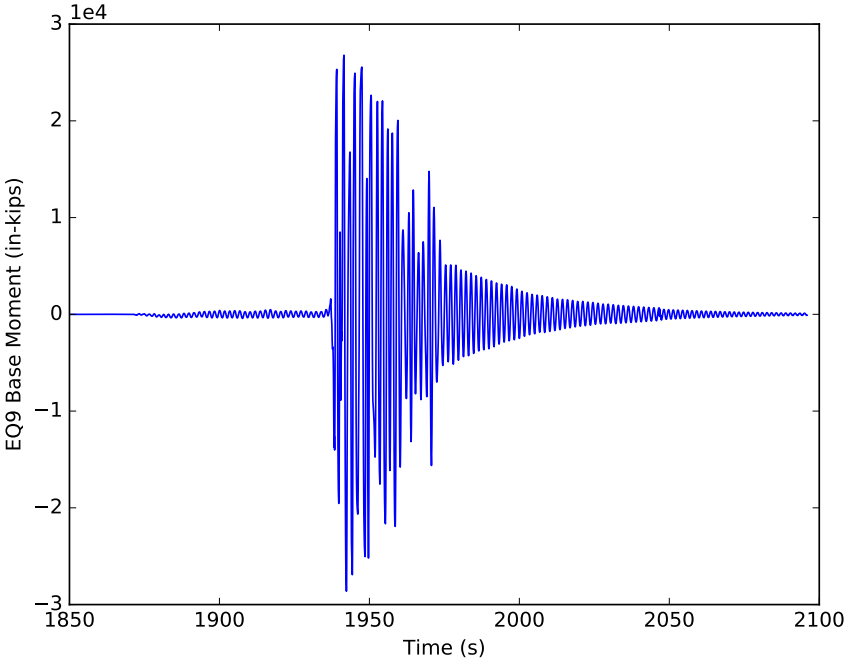

Figure H.27: Mz response of model 4d for EQ9

Appendix I

Model 5a Output

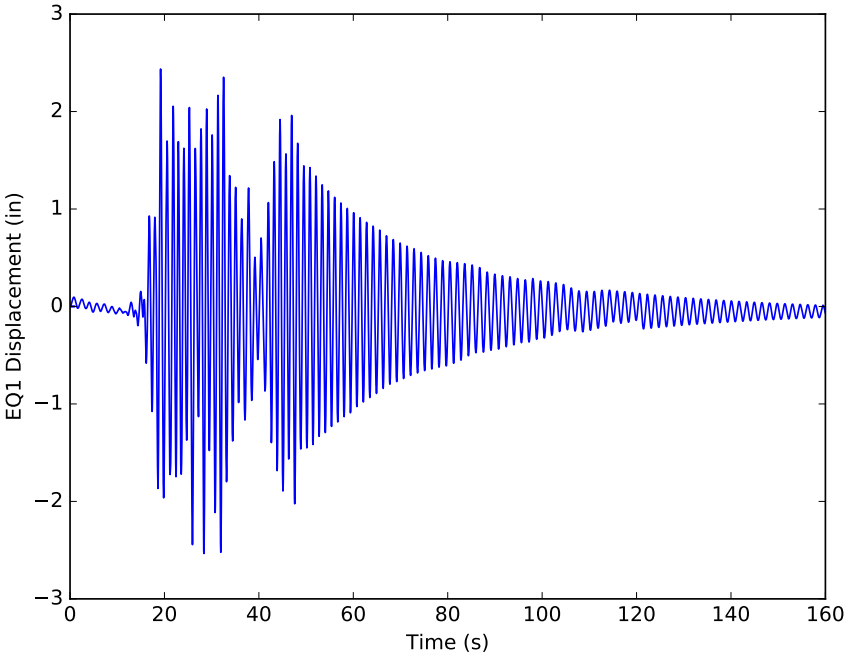

Figure I.1: Displacement response of model 5a for EQ1

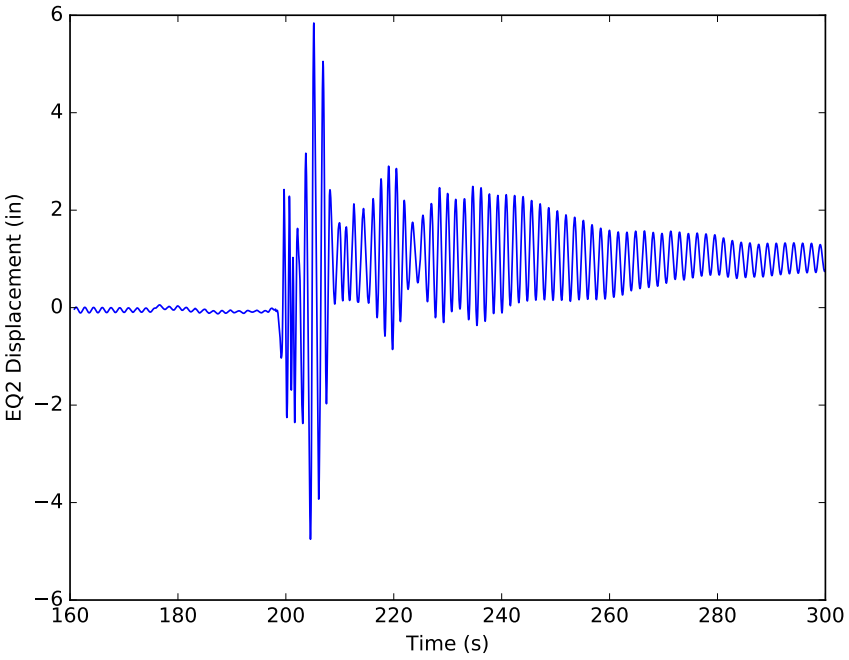

Figure I.2: Displacement response of model 5a for EQ2

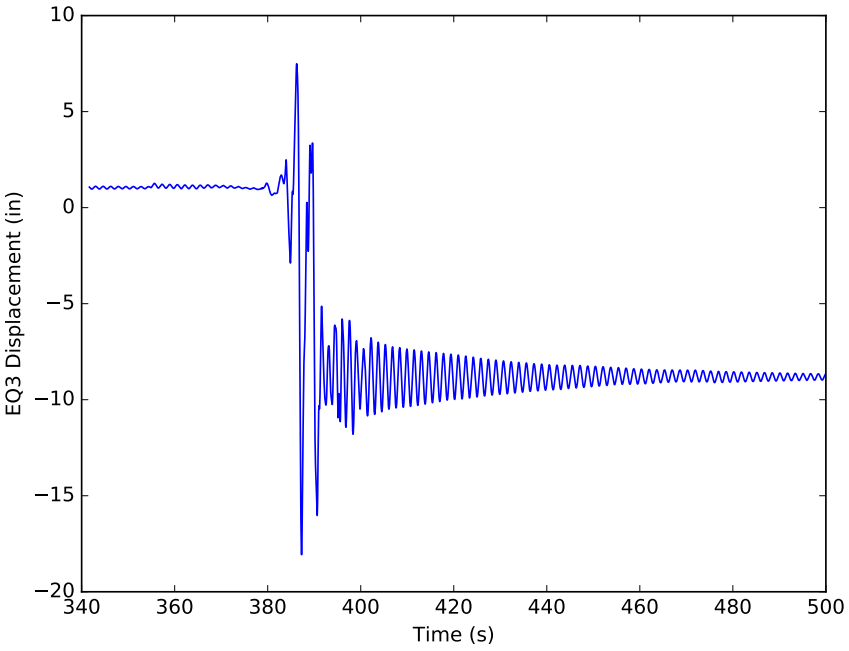

Figure I.3: Displacement response of model 5a for EQ3

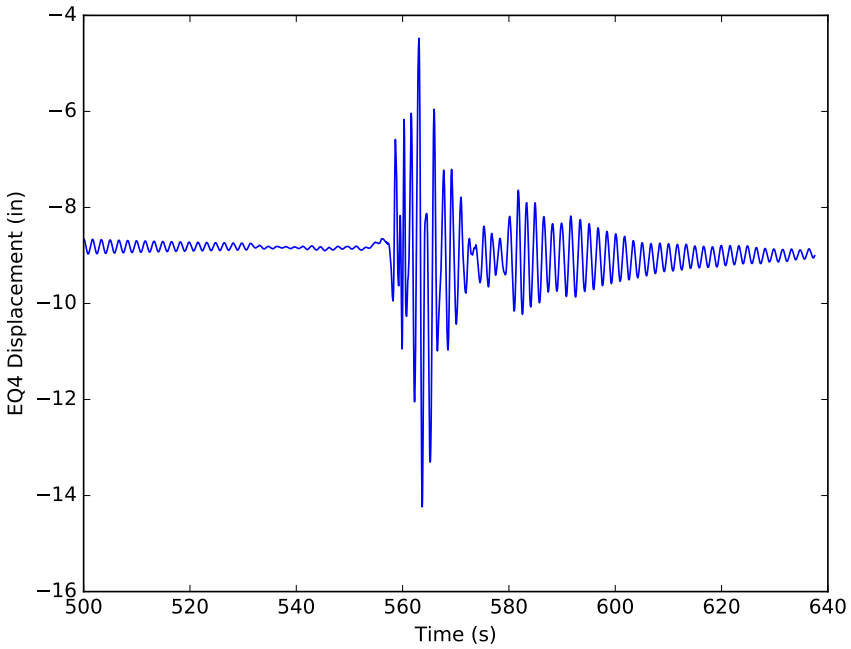

Figure I.4: Displacement response of model 5a for EQ4

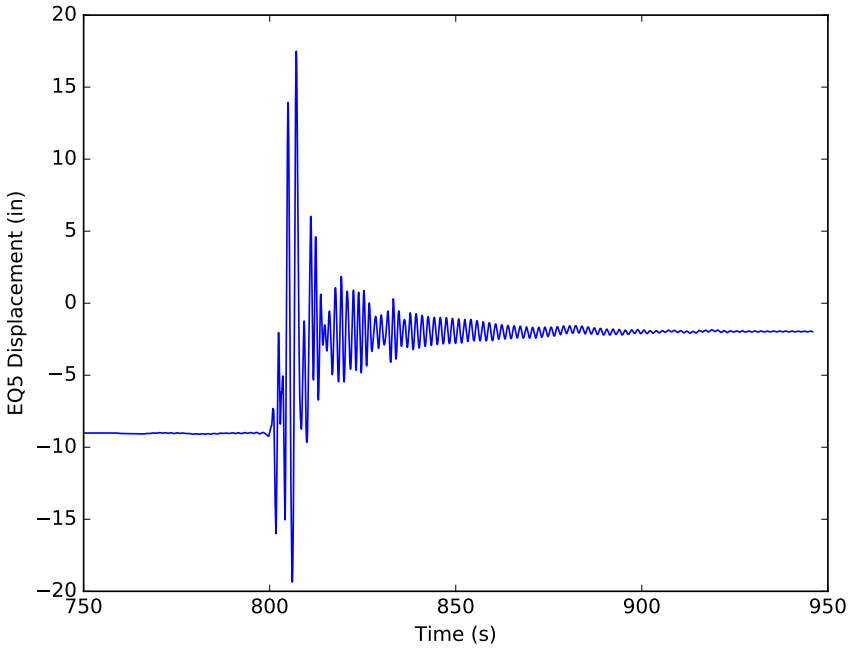

Figure I.5: Displacement response of model 5a for EQ5

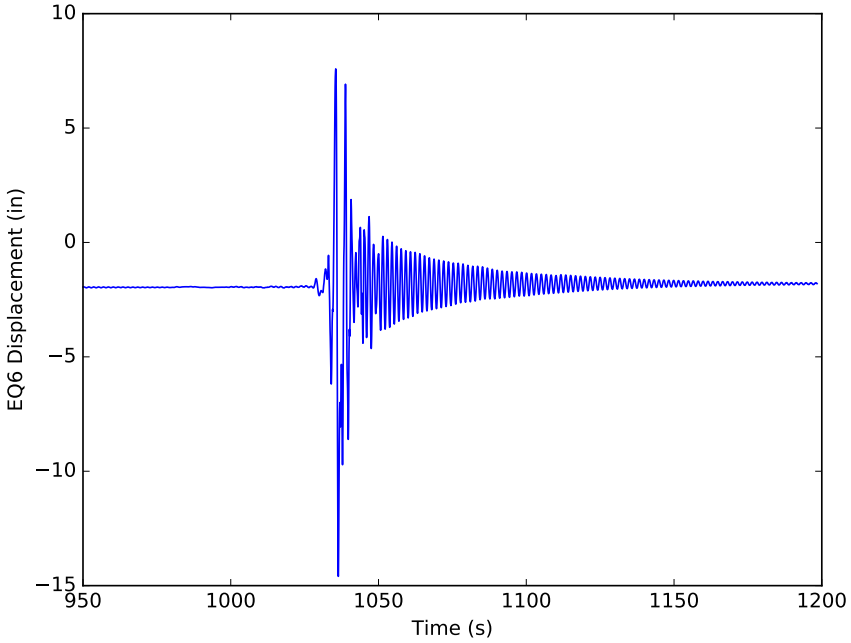

Figure I.6: Displacement response of model 5a for EQ6

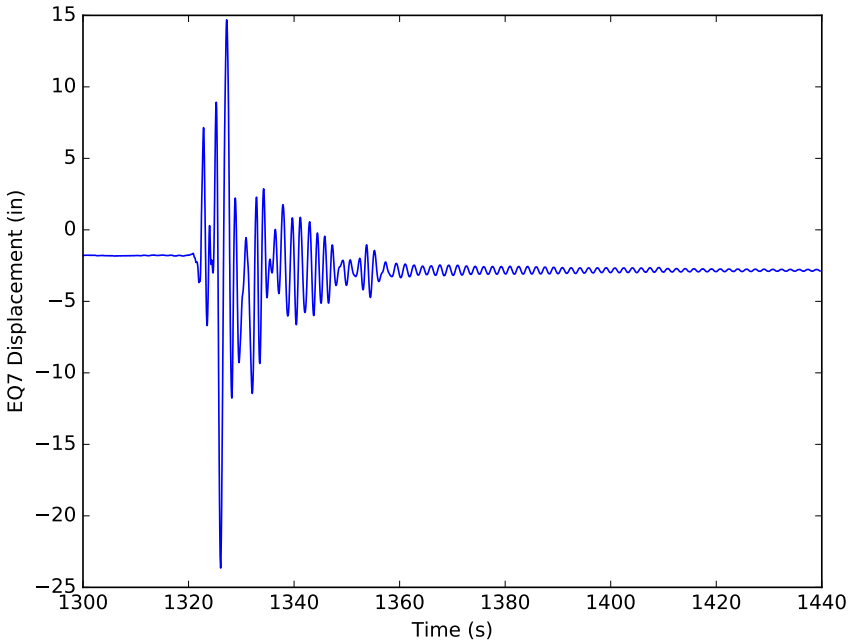

Figure I.7: Displacement response of model 5a for EQ7

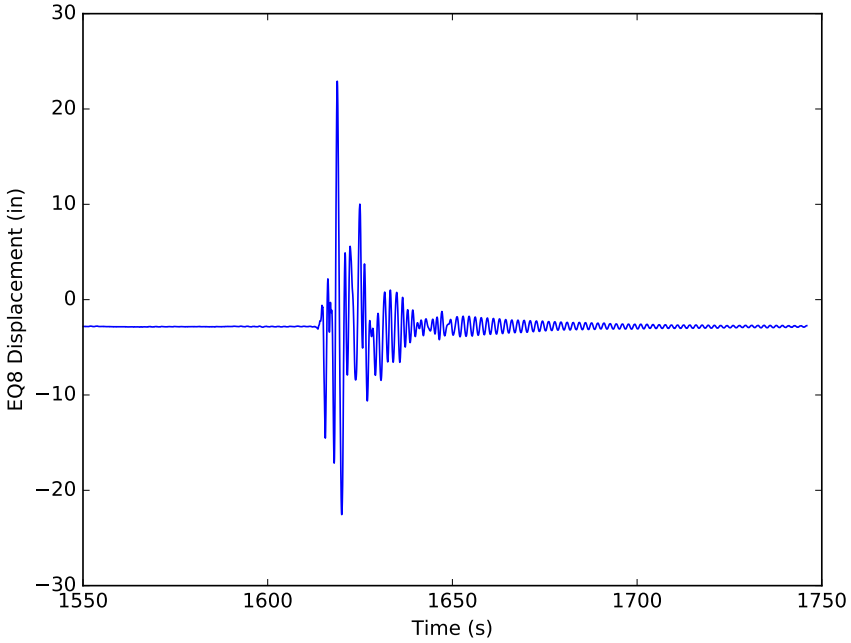

Figure I.8: Displacement response of model 5a for EQ8

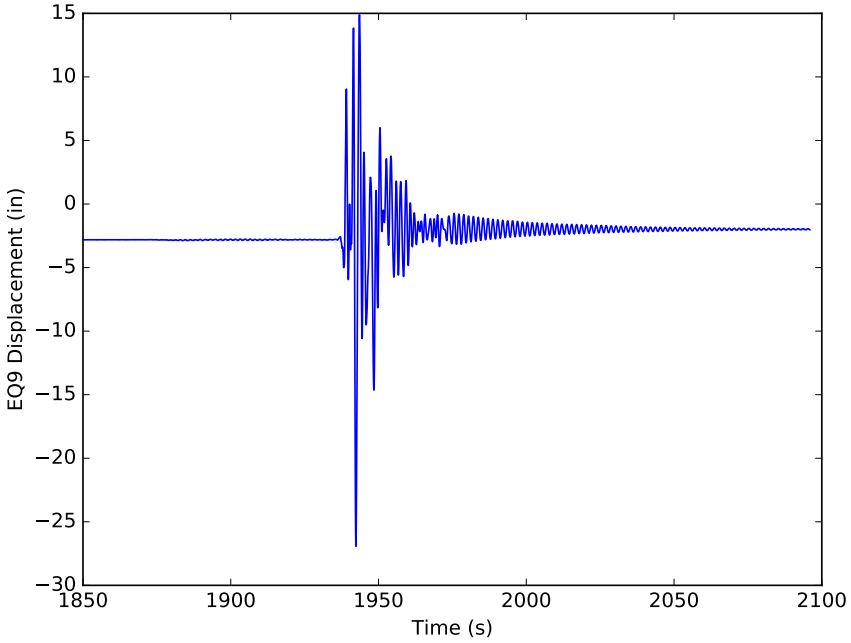

Figure I.9: Displacement response of model 5a for EQ9

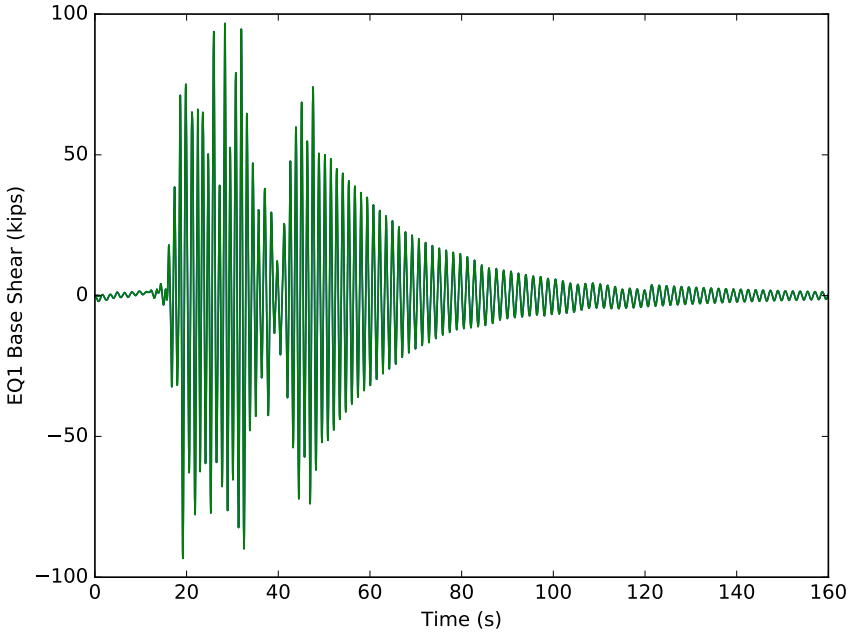

Figure I.10: Fx response of model 5a for EQ1

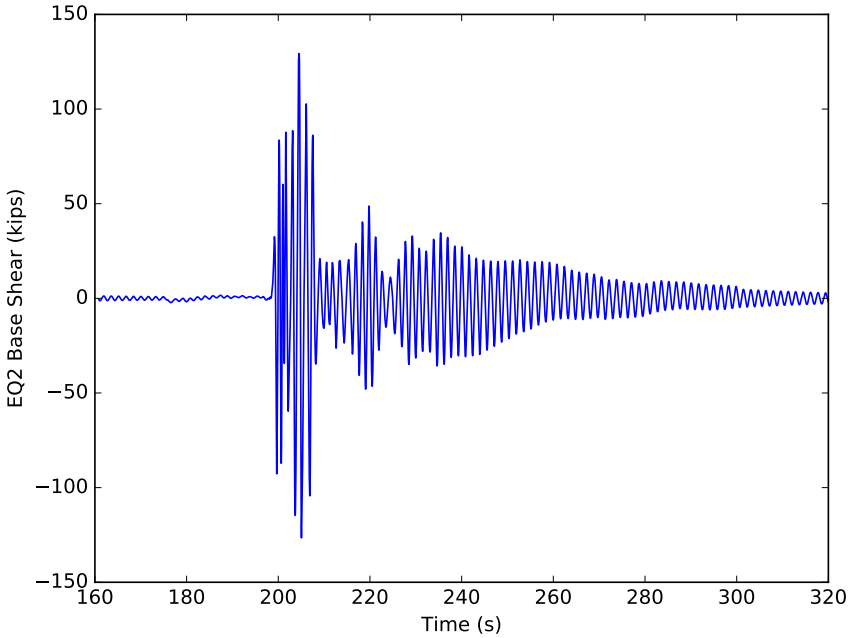

Figure I.11: Fx response of model 5a for EQ2

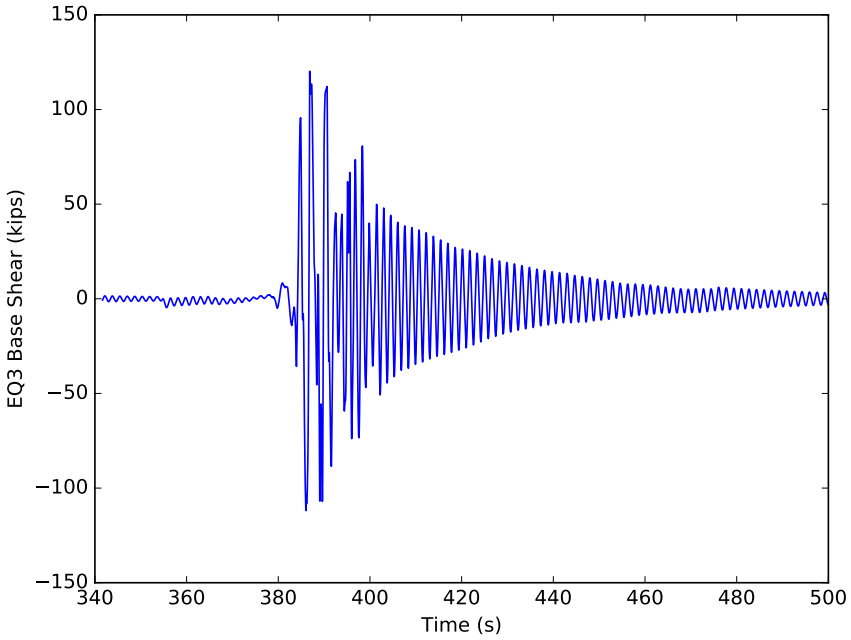

Figure I.12: Fx response of model 5a for EQ3

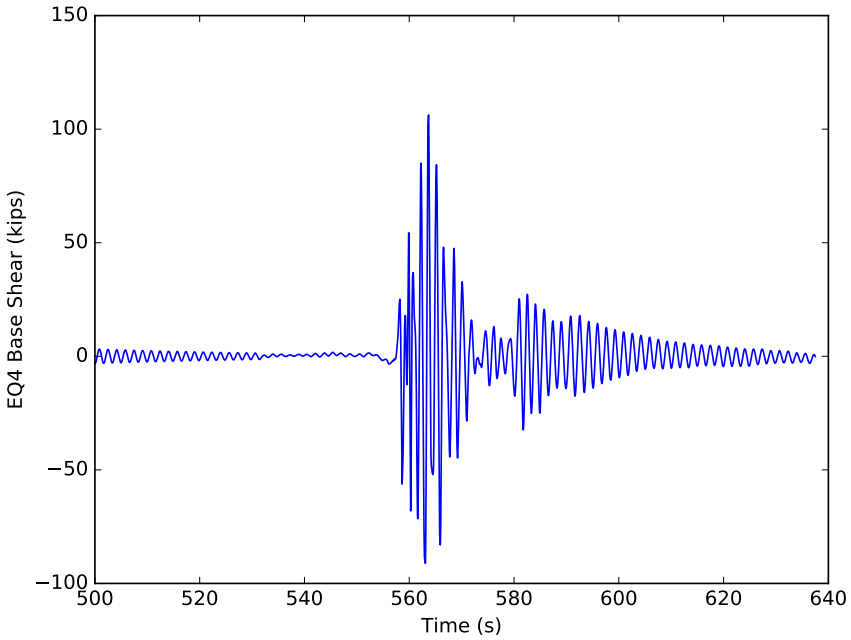

Figure I.13: Fx response of model 5a for EQ4

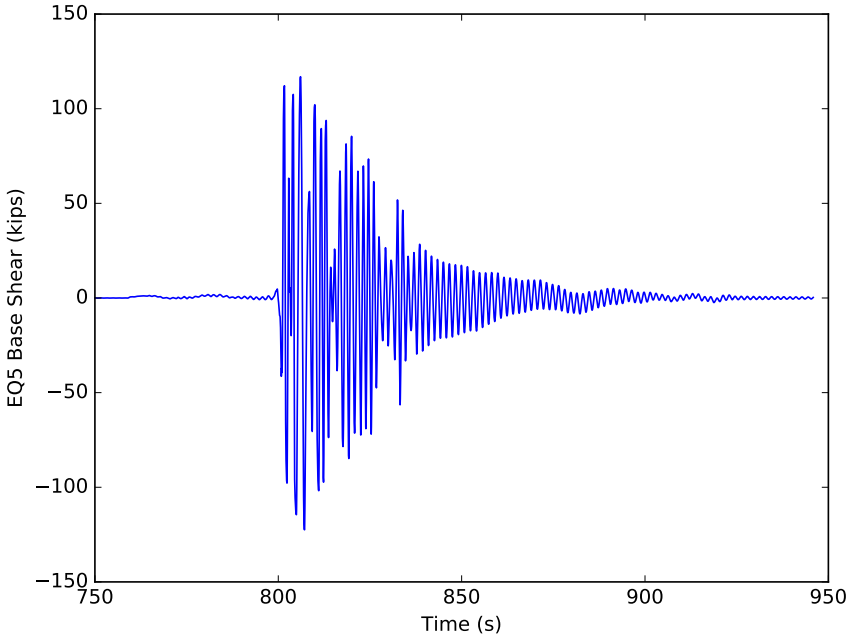

Figure I.14: Fx response of model 5a for EQ5

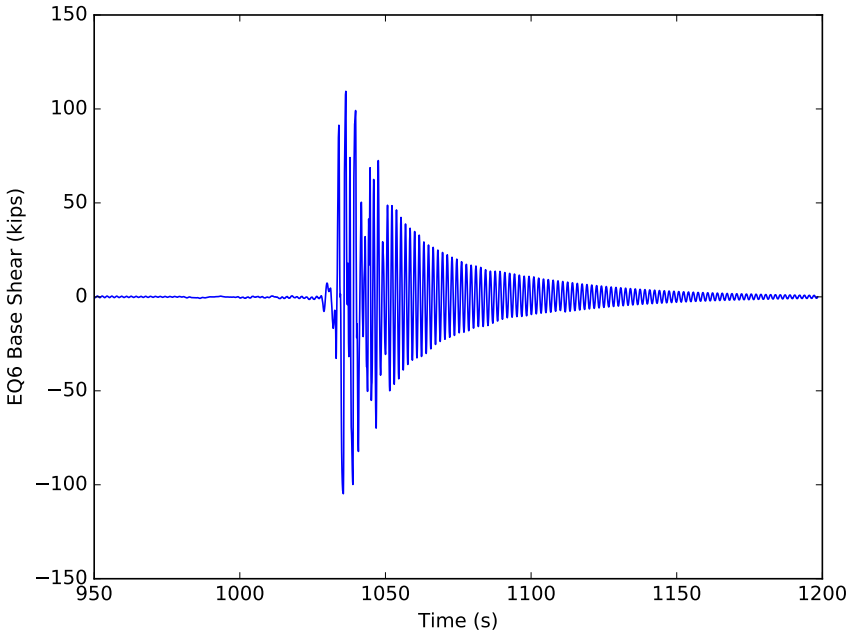

Figure I.15: Fx response of model 5a for EQ6

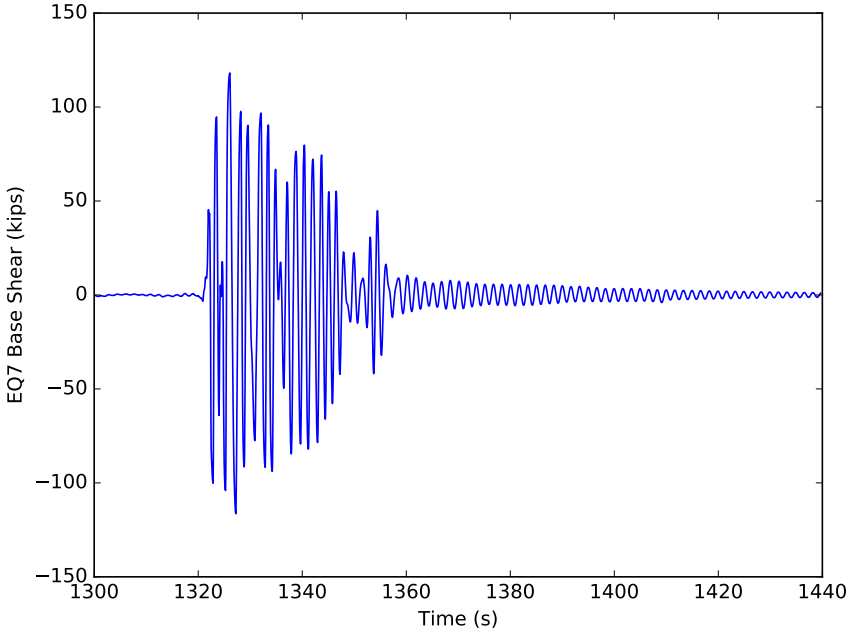

Figure I.16: Fx response of model 5a for EQ7

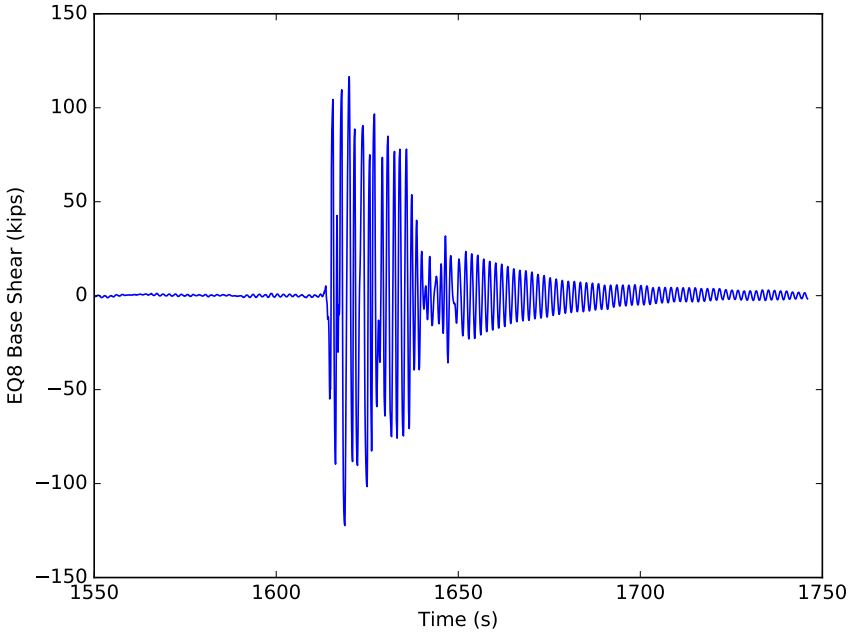

Figure I.17: Fx response of model 5a for EQ8

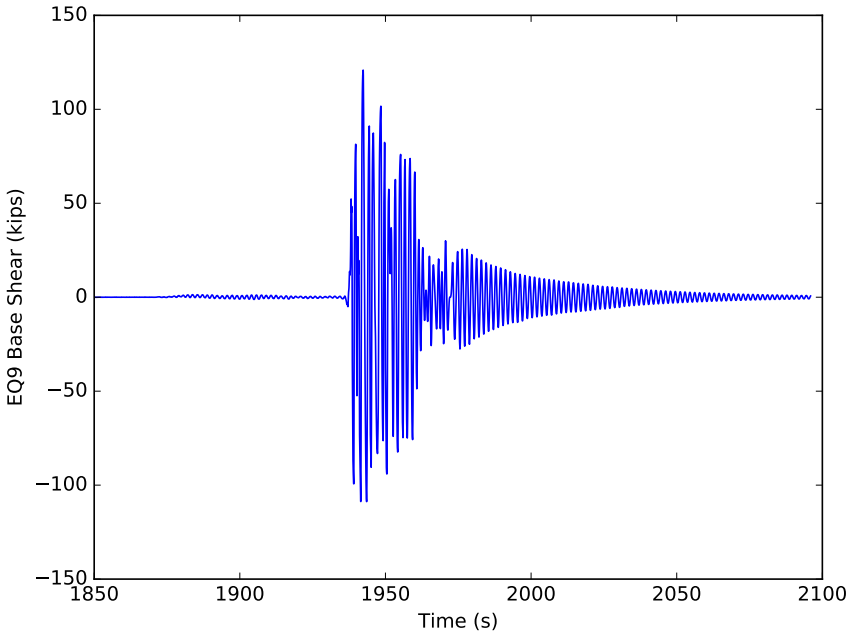

Figure I.18: Fx response of model 5a for EQ9

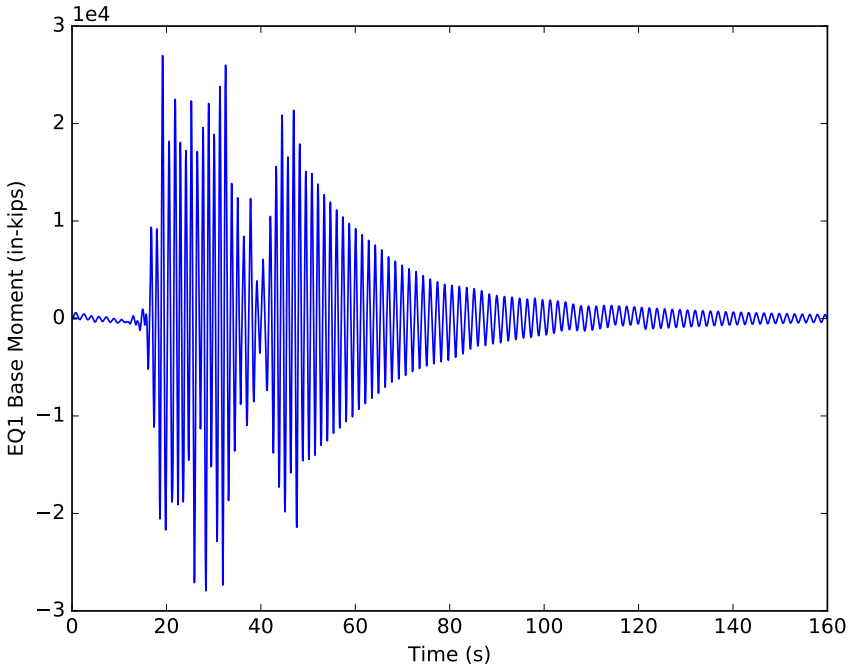

Figure I.19: Mz response of model 5a for EQ1

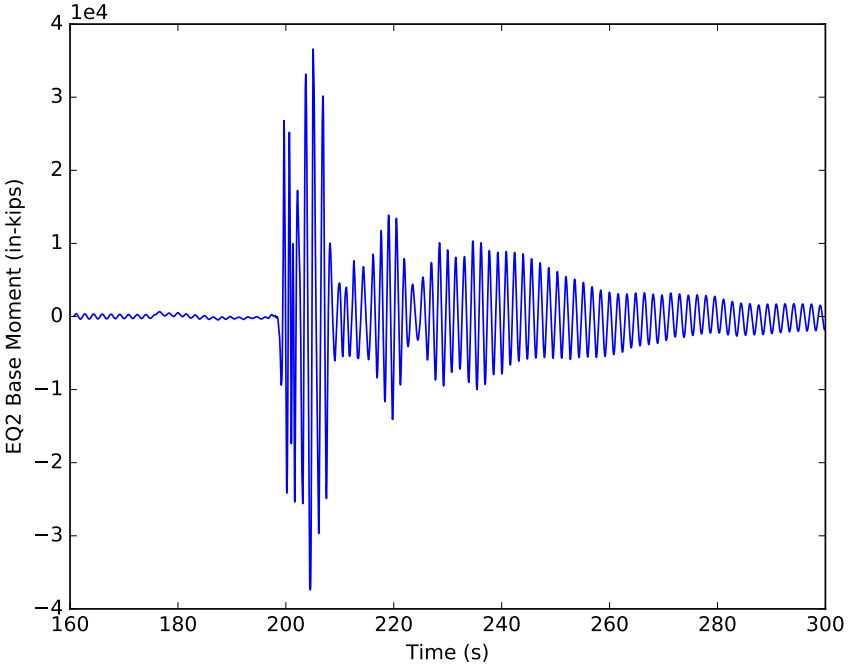

Figure I.20: Mz response of model 5a for EQ2

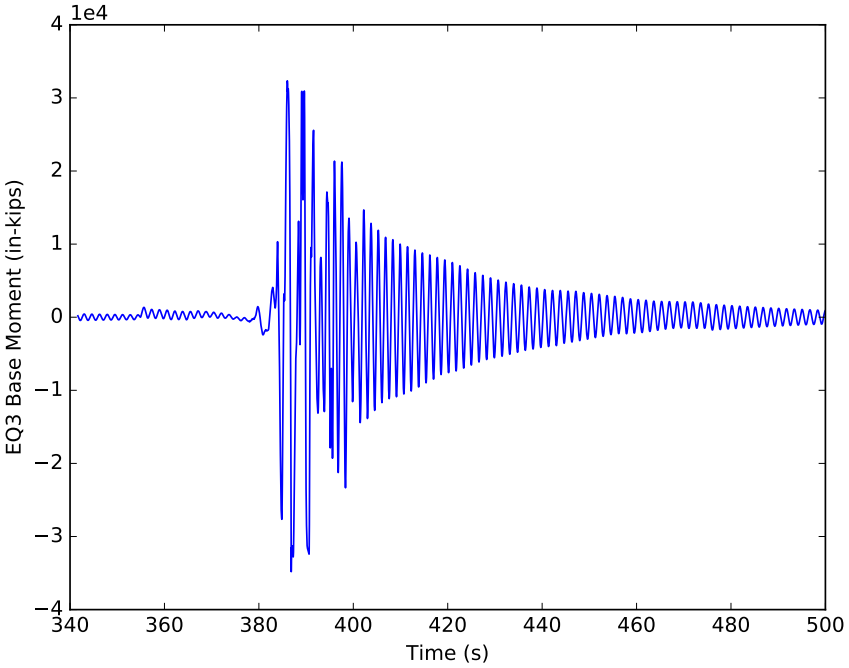

Figure I.21: Mz response of model 5a for EQ3

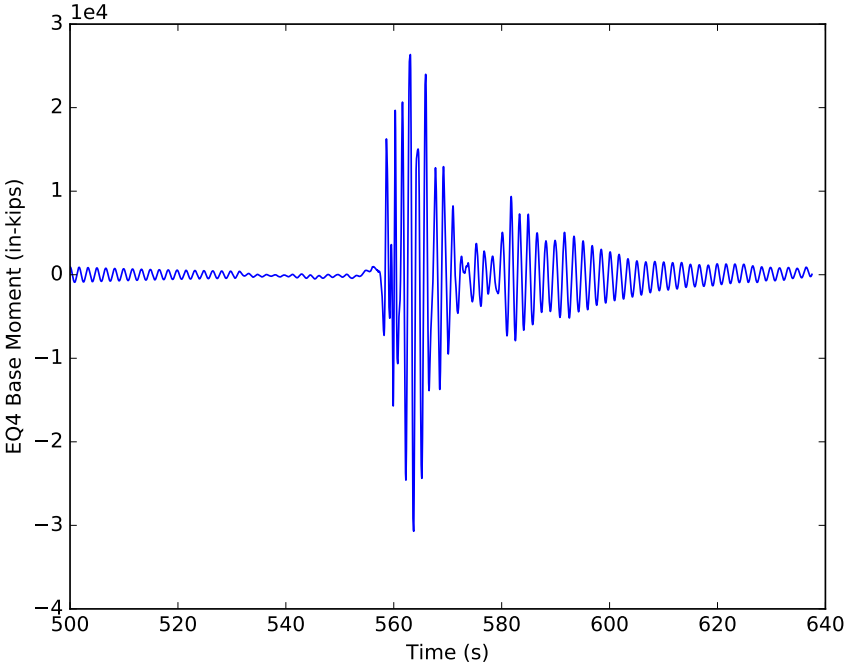

Figure I.22: Mz response of model 5a for EQ4

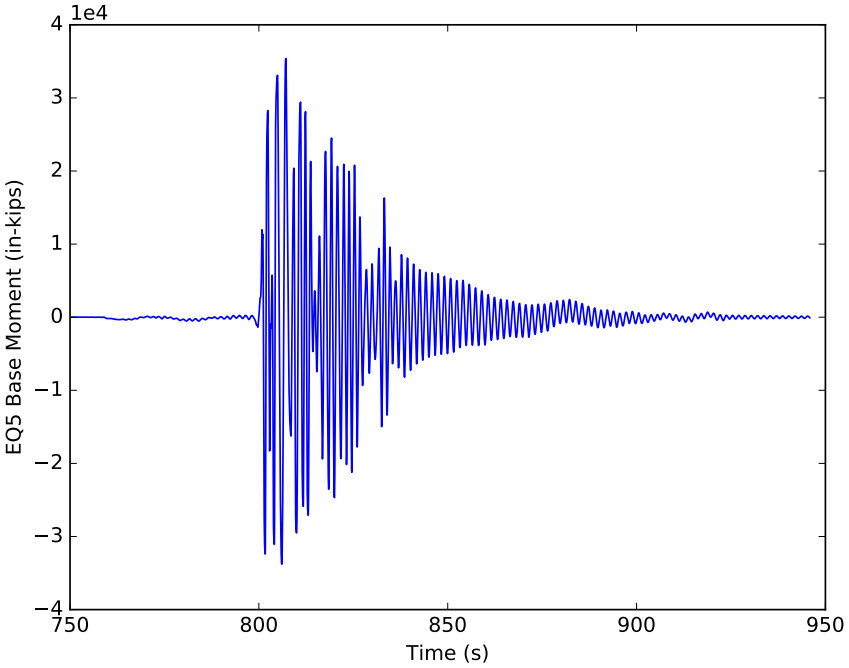

Figure I.23: Mz response of model 5a for EQ5

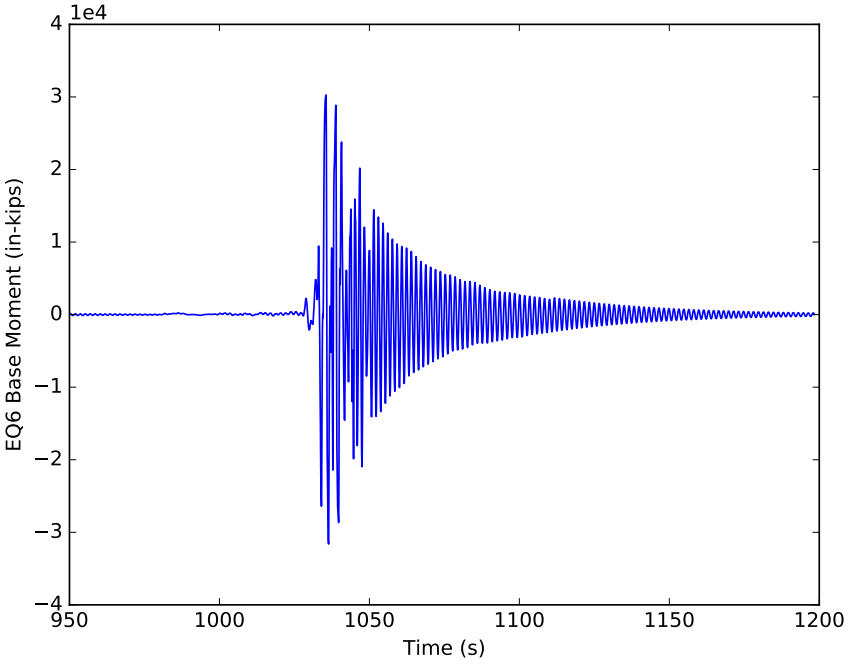

Figure I.24: Mz response of model 5a for EQ6

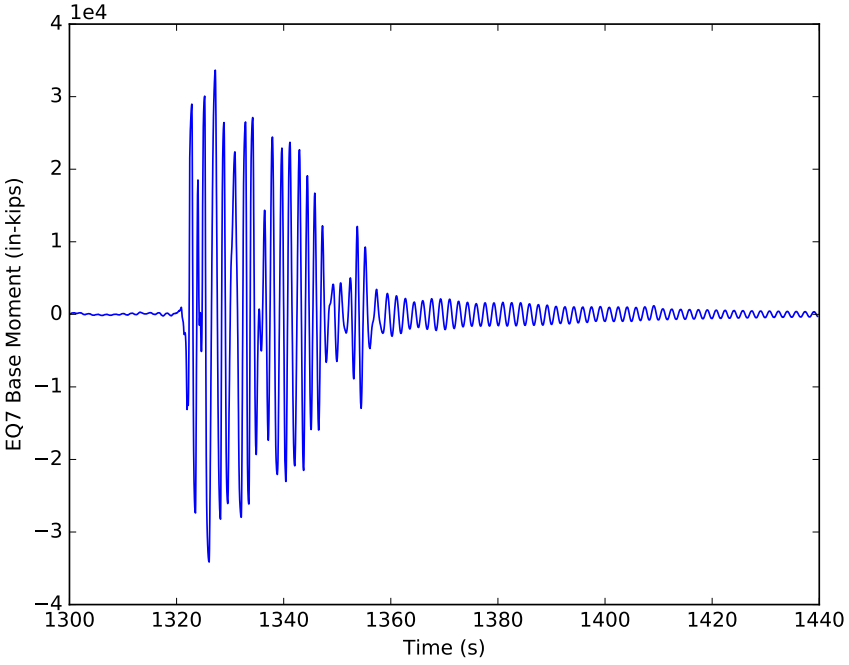

Figure I.25: Mz response of model 5a for EQ7

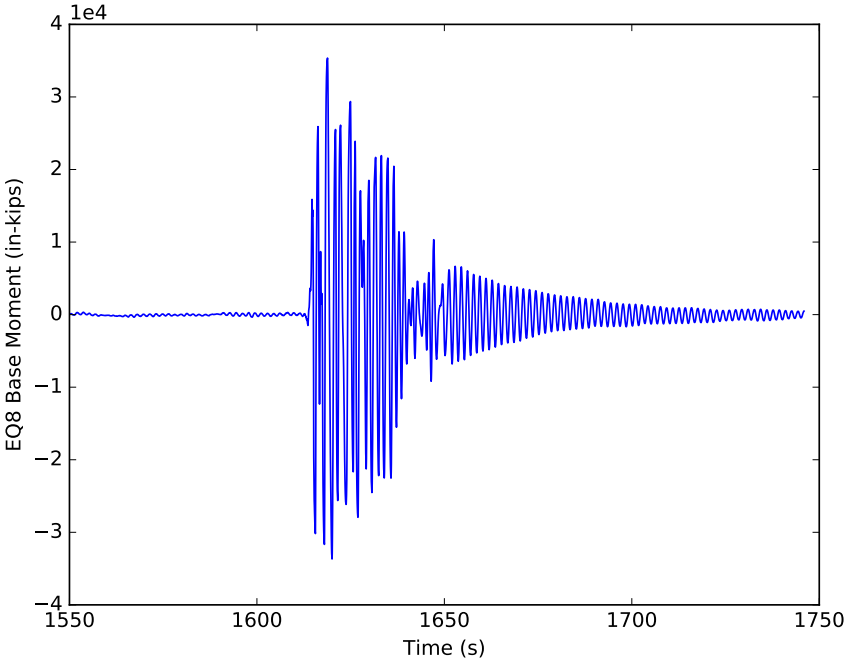

Figure I.26: Mz response of model 5a for EQ8

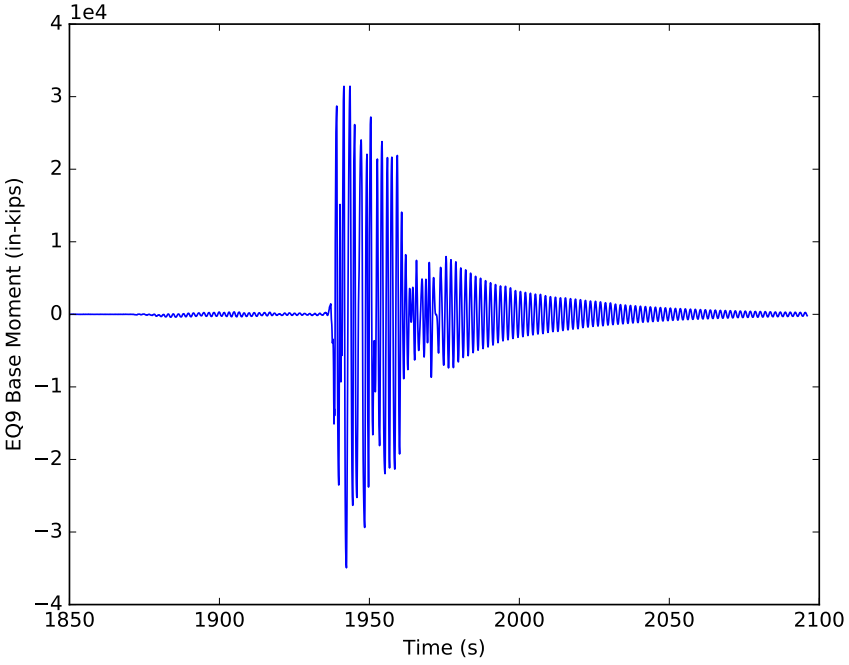

Figure I.27: Mz response of model 5a for EQ9

Appendix J

Model 5b Output

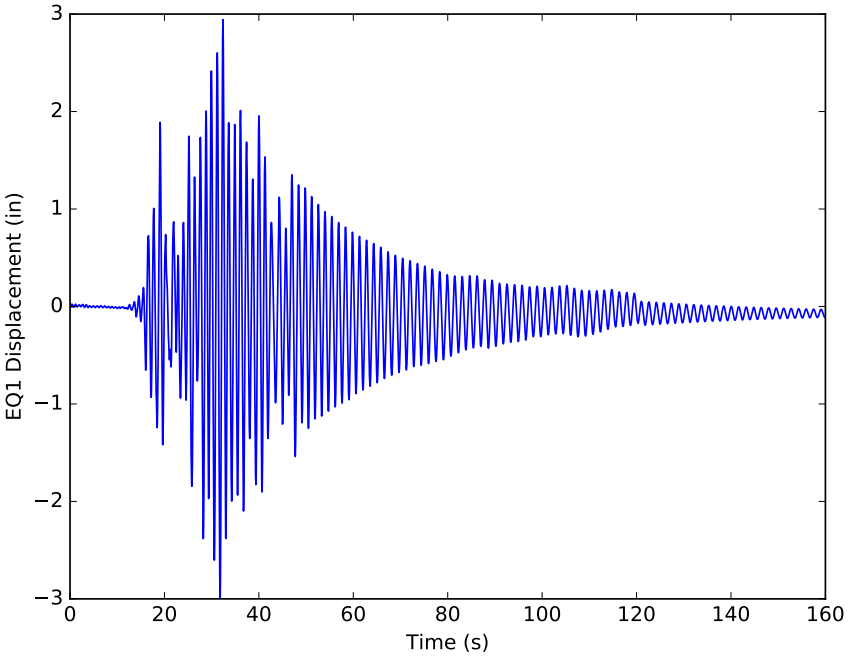

Figure J.1: Displacement response of model 5b for EQ1

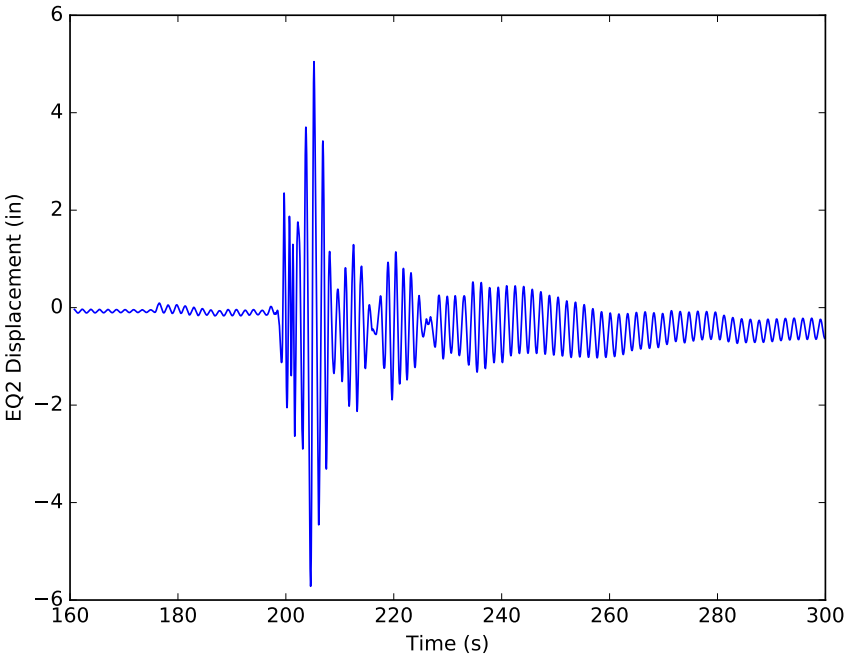

Figure J.2: Displacement response of model 5b for EQ2

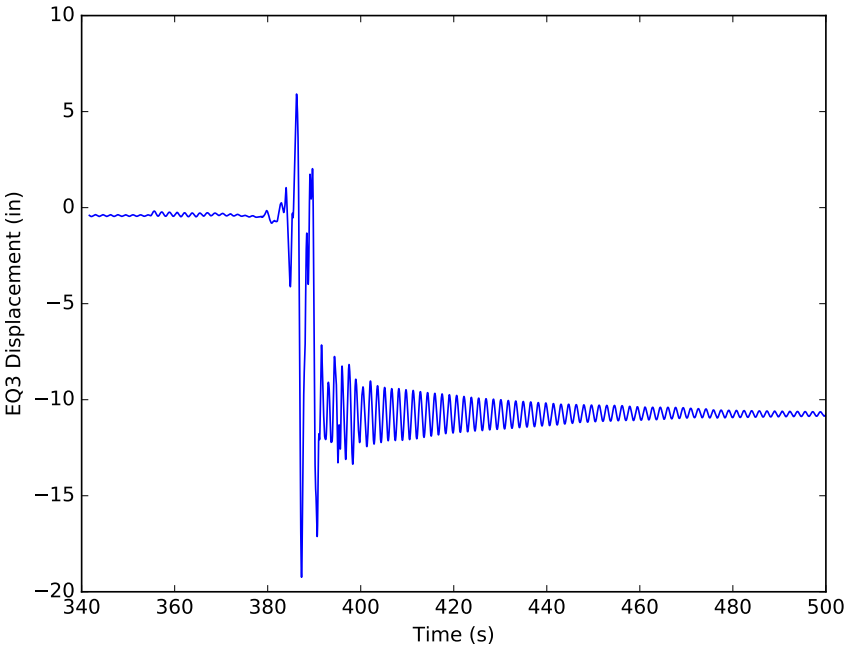

Figure J.3: Displacement response of model 5b for EQ3

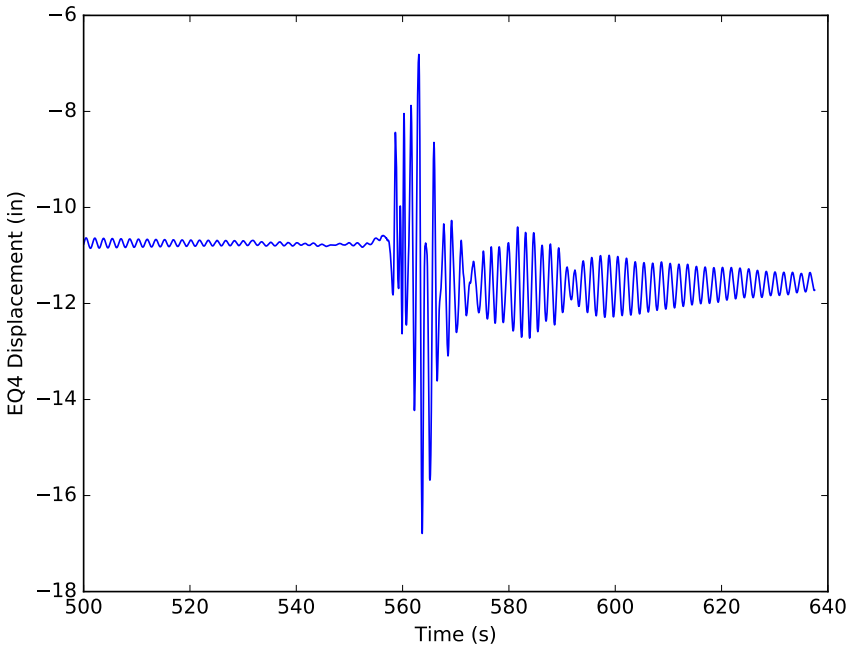

Figure J.4: Displacement response of model 5b for EQ4

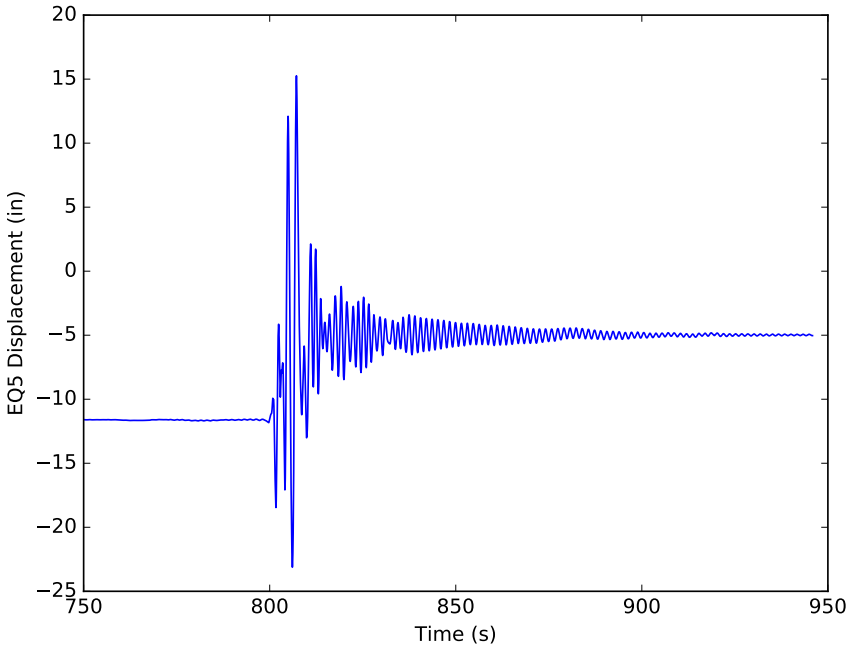

Figure J.5: Displacement response of model 5b for EQ5

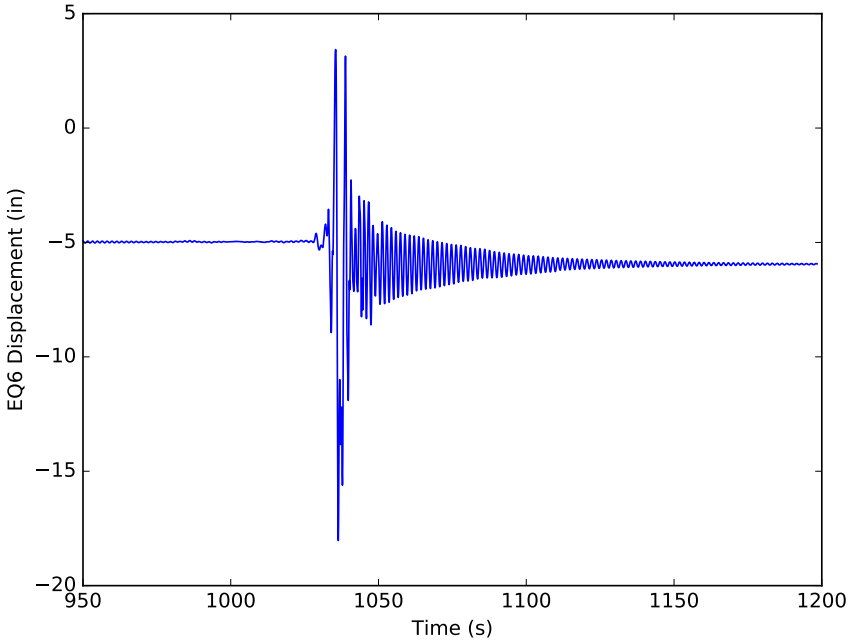

Figure J.6: Displacement response of model 5b for EQ6

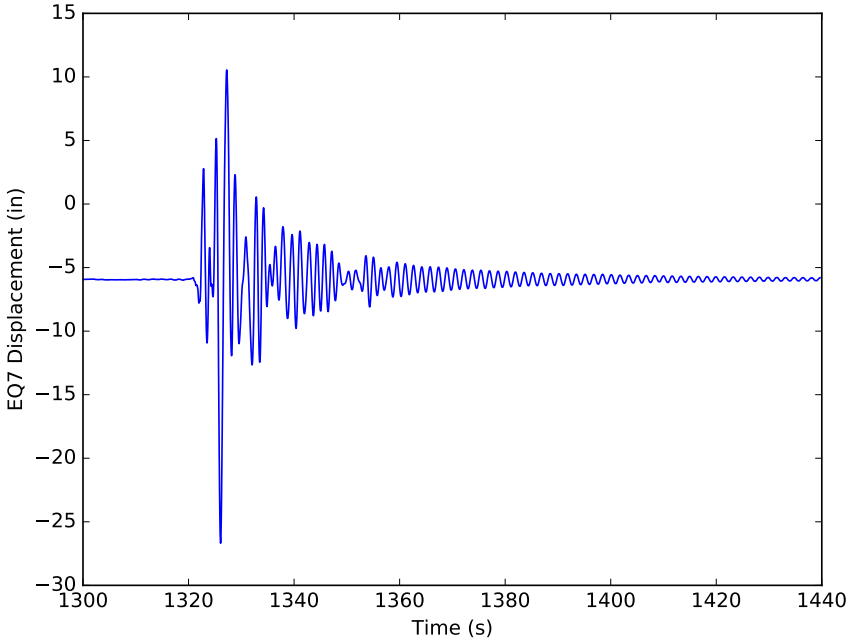

Figure J.7: Displacement response of model 5b for EQ7

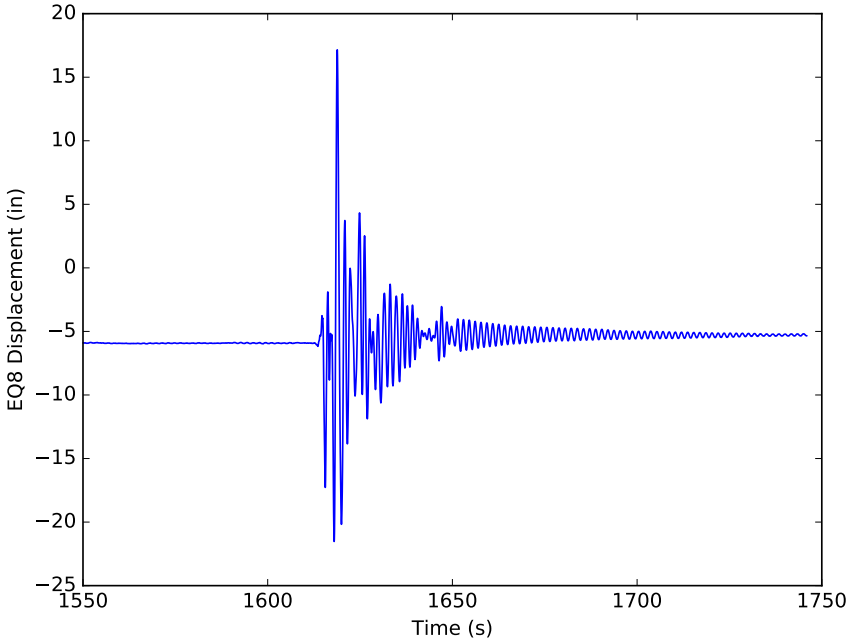

Figure J.8: Displacement response of model 5b for EQ8

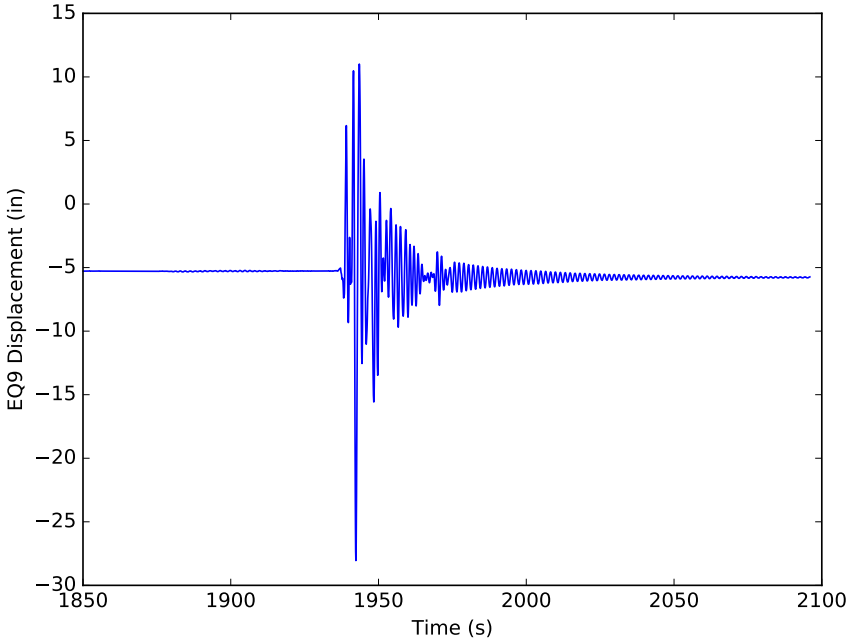

Figure J.9: Displacement response of model 5b for EQ9

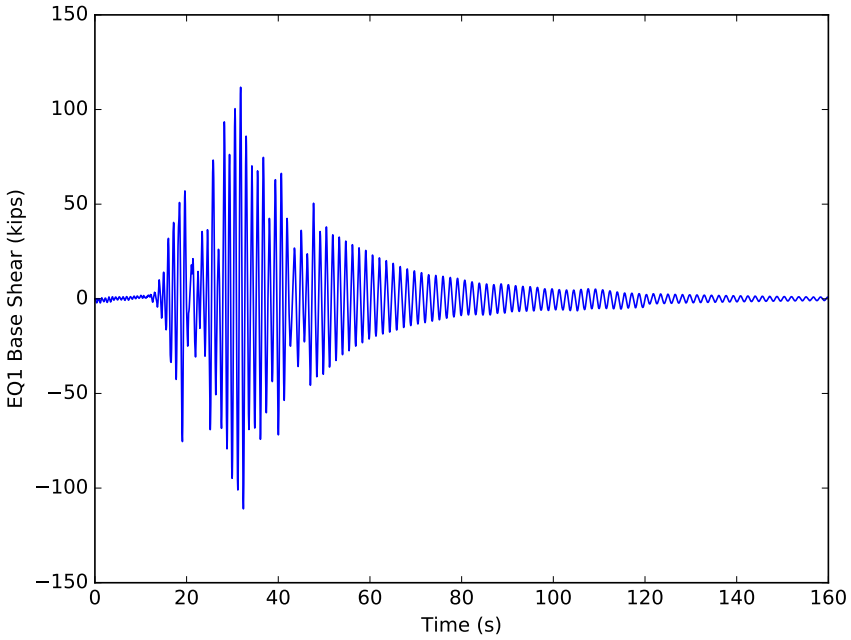

Figure J.10: Fx response of model 5b for EQ1

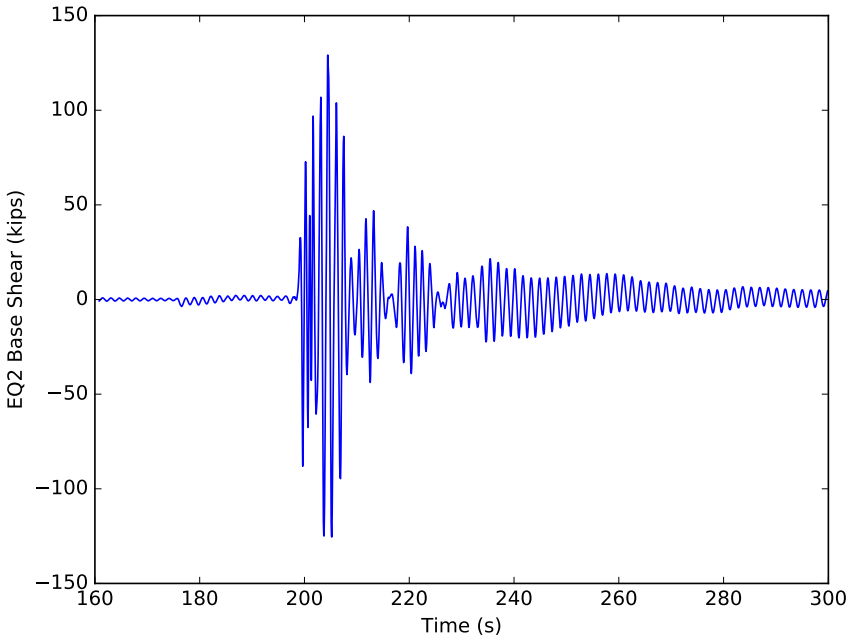

Figure J.11: Fx response of model 5b for EQ2

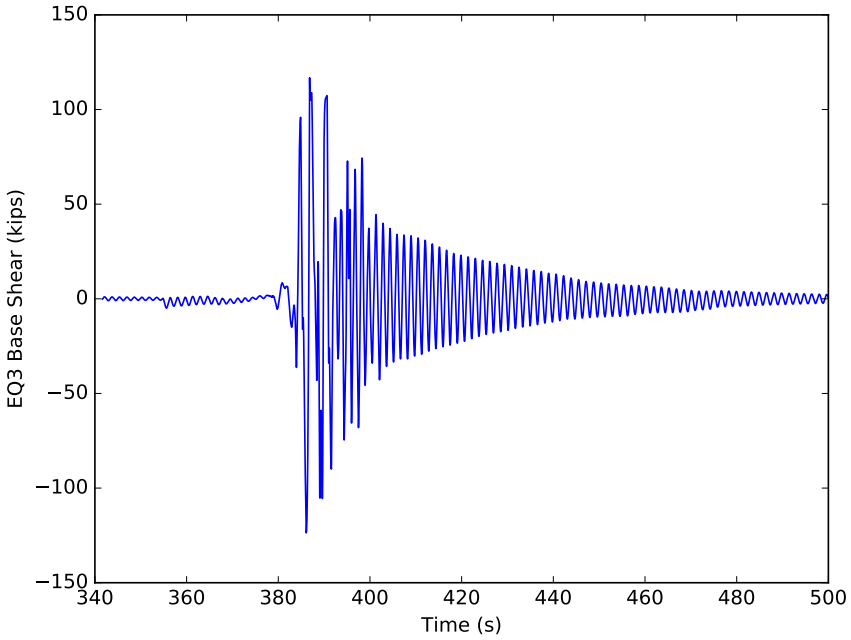

Figure J.12: Fx response of model 5b for EQ3

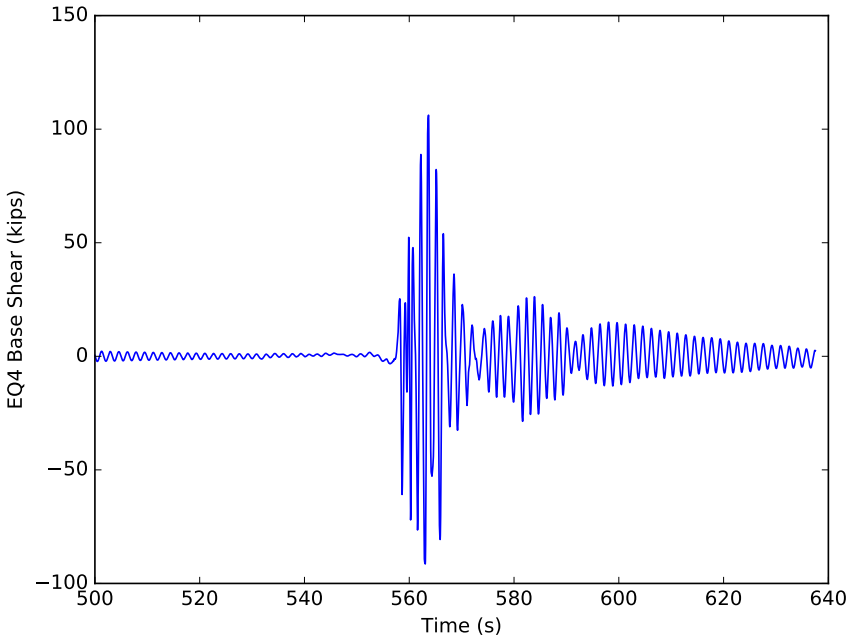

Figure J.13: Fx response of model 5b for EQ4

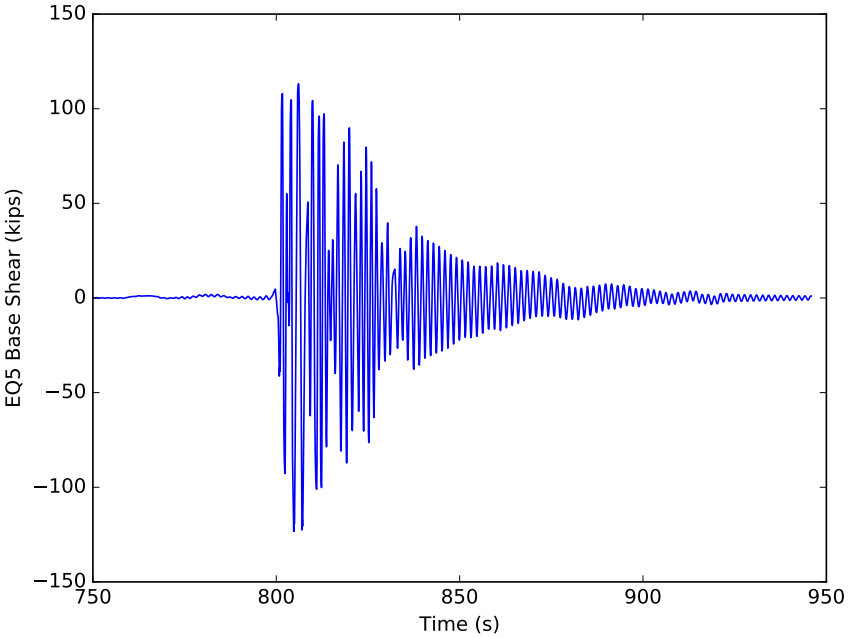

Figure J.14: Fx response of model 5b for EQ5

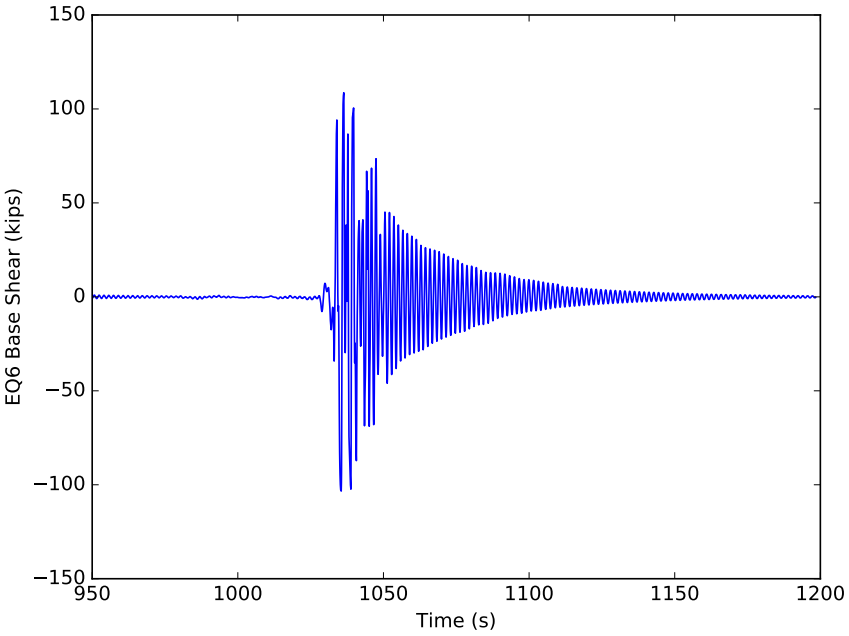

Figure J.15: Fx response of model 5b for EQ6

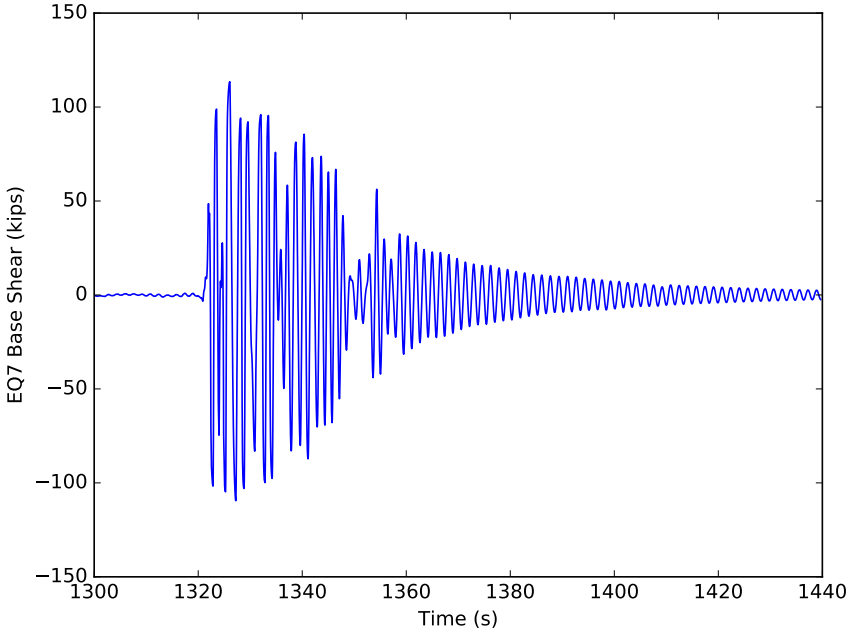

Figure J.16: Fx response of model 5b for EQ7

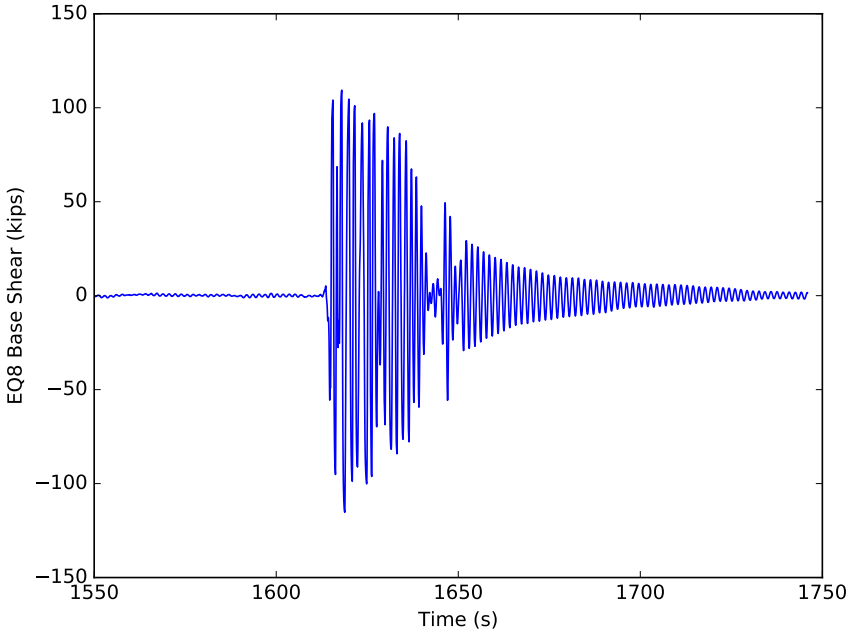

Figure J.17: Fx response of model 5b for EQ8

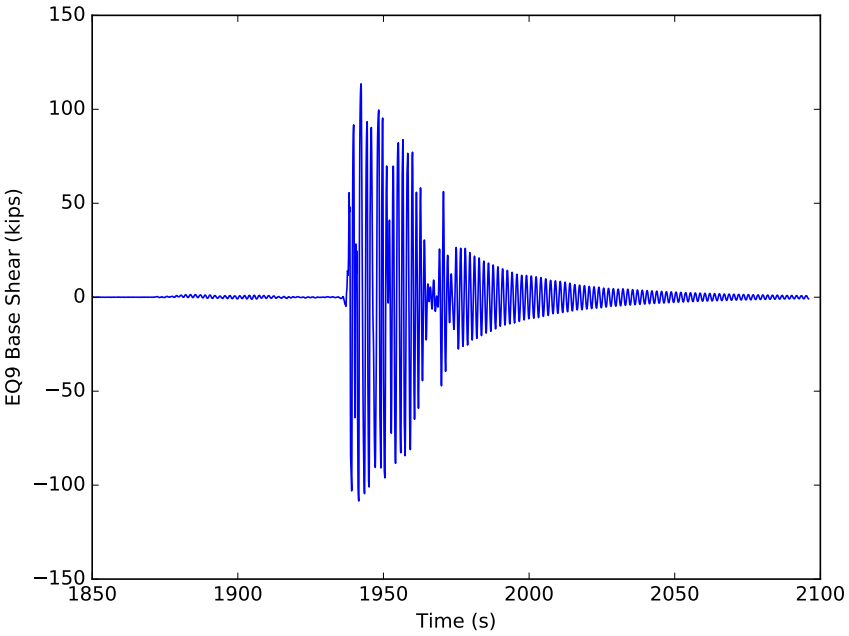

Figure J.18: Fx response of model 5b for EQ9

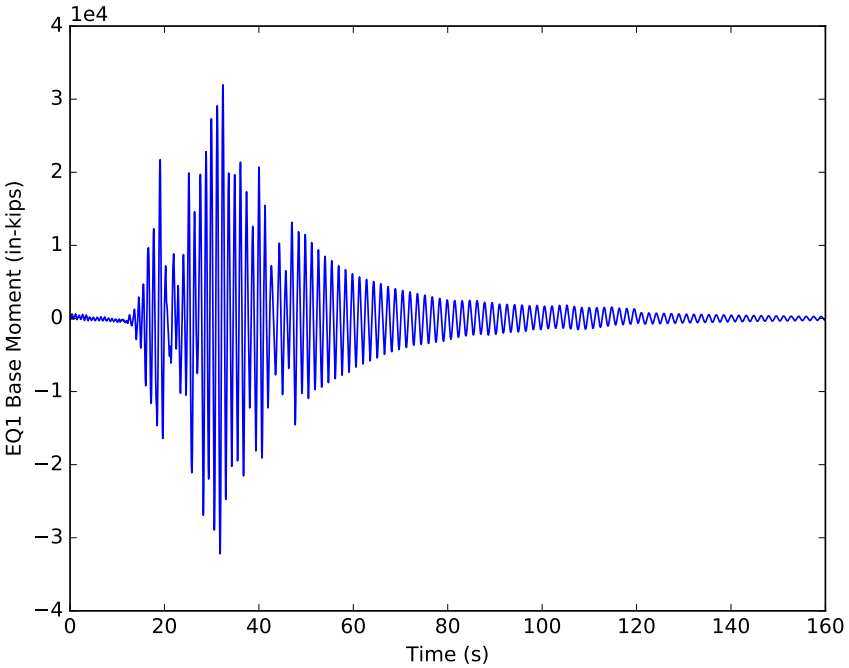

Figure J.19: Mz response of model 5b for EQ1

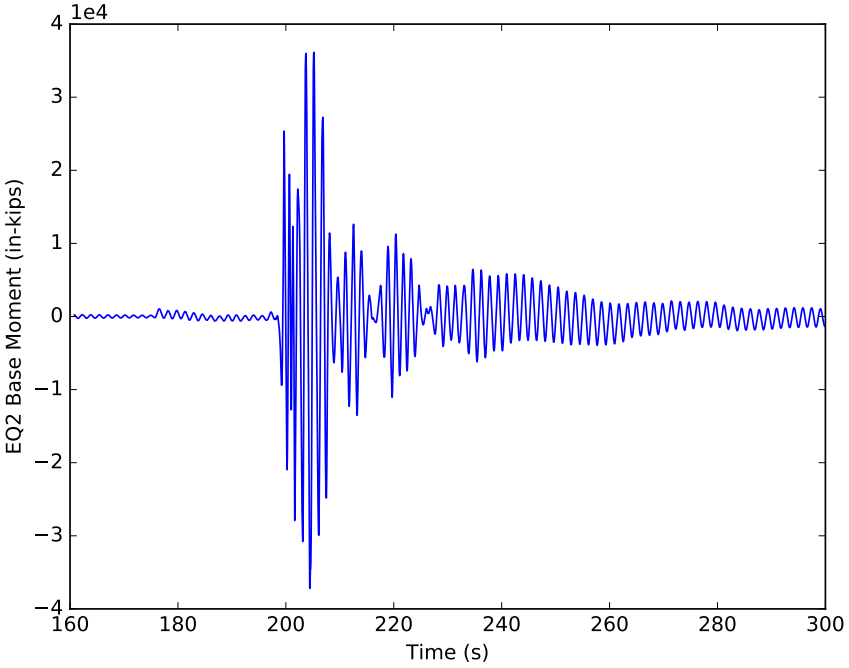

Figure J.20: Mz response of model 5b for EQ2

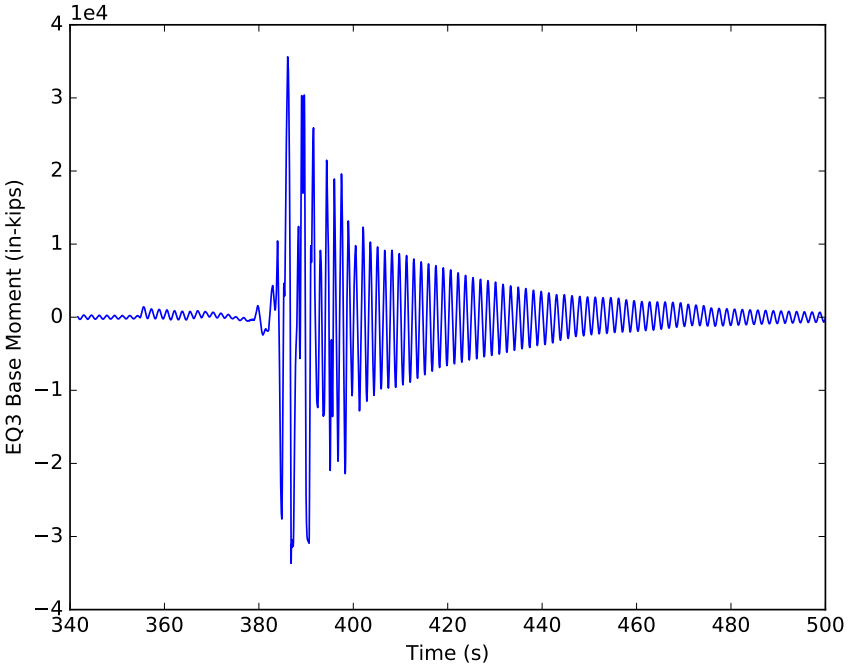

Figure J.21: Mz response of model 5b for EQ3

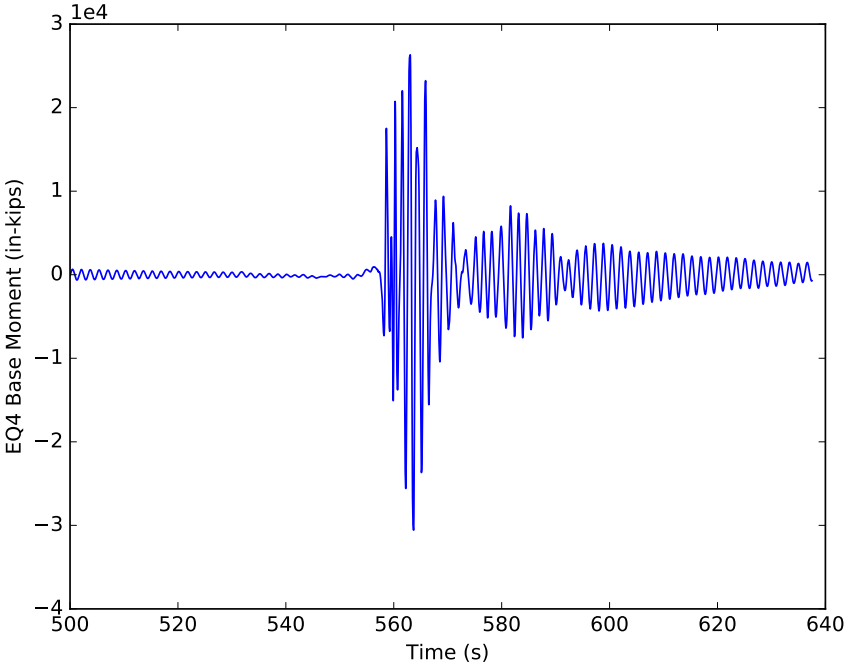

Figure J.22: Mz response of model 5b for EQ4

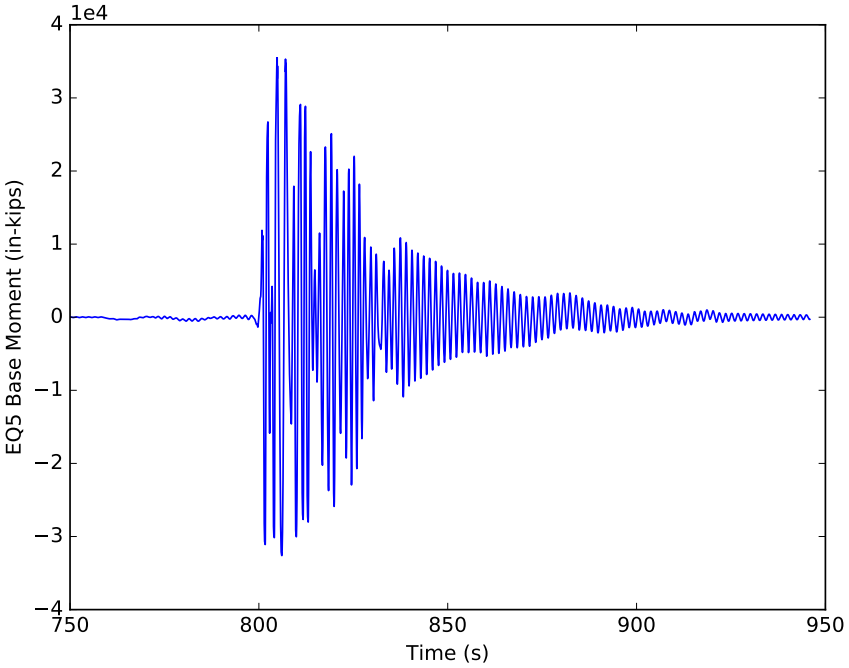

Figure J.23: Mz response of model 5b for EQ5

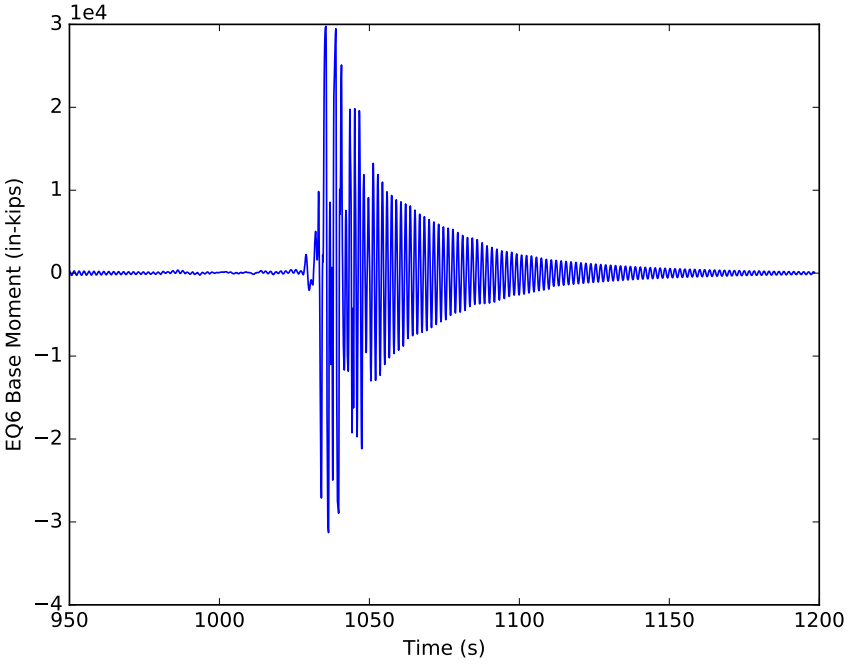

Figure J.24: Mz response of model 5b for EQ6

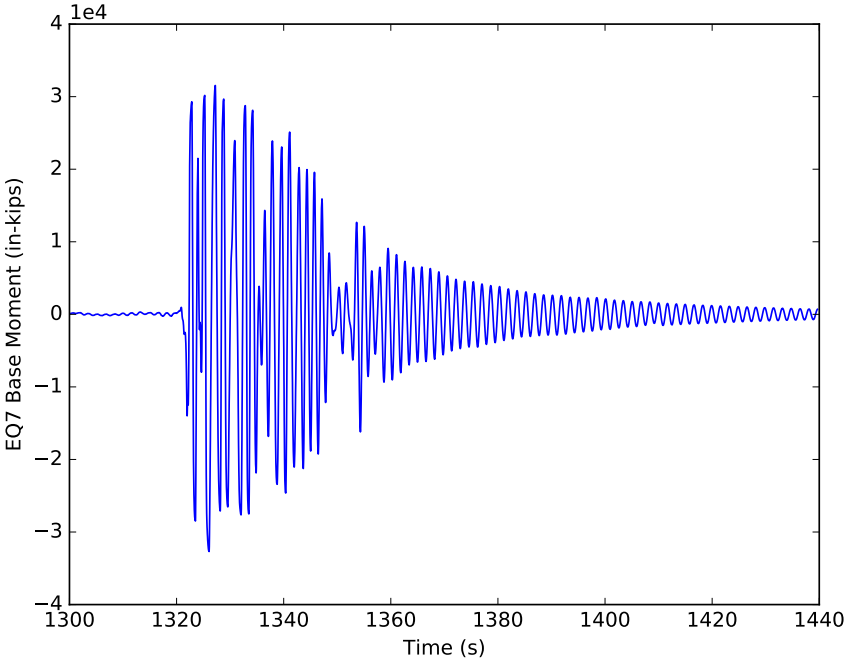

Figure J.25: Mz response of model 5b for EQ7

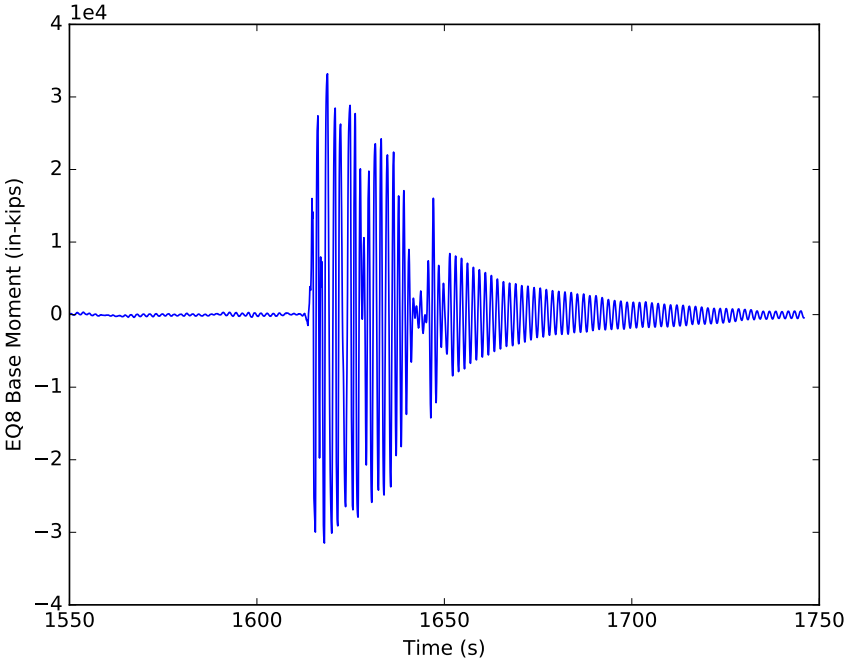

Figure J.26: Mz response of model 5b for EQ8

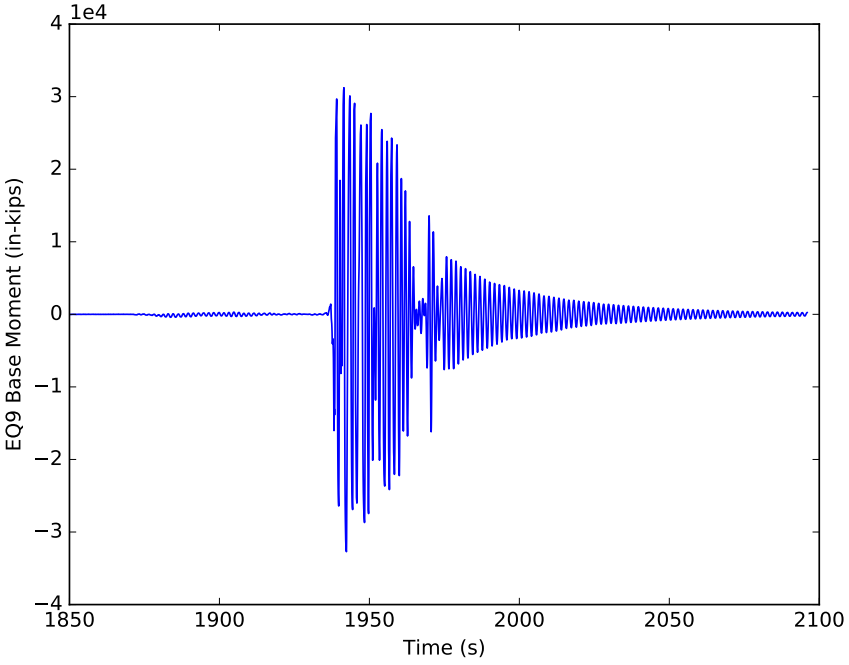

Figure J.27: Mz response of model 5b for EQ9

Appendix K

Model 5c Output

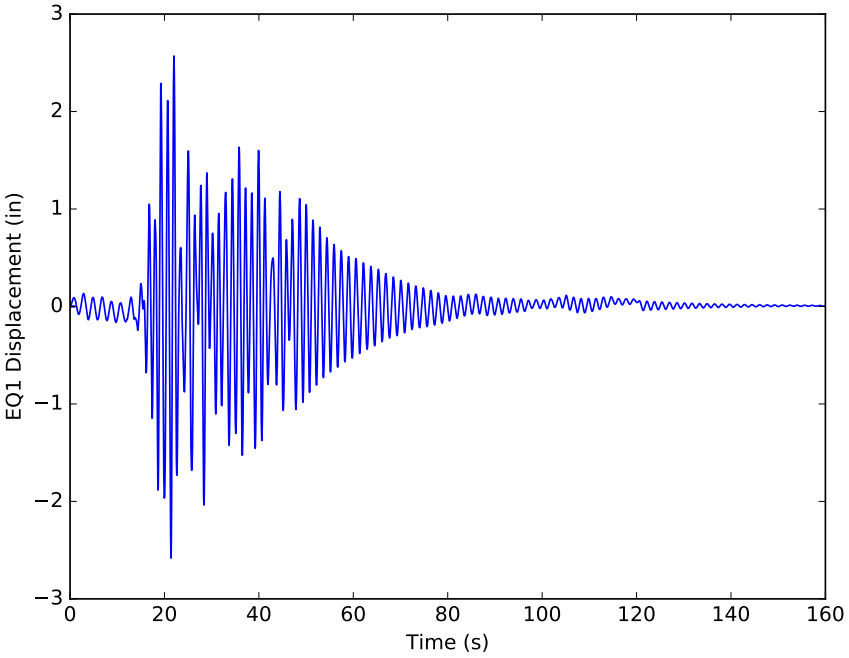

Figure K.1: Displacement response of model 5c for EQ1

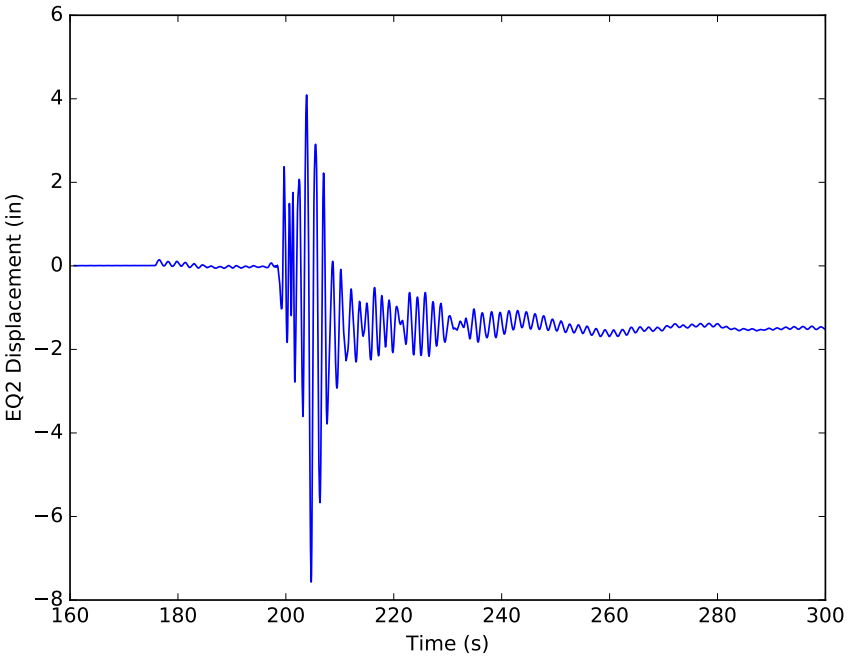

Figure K.2: Displacement response of model 5c for EQ2

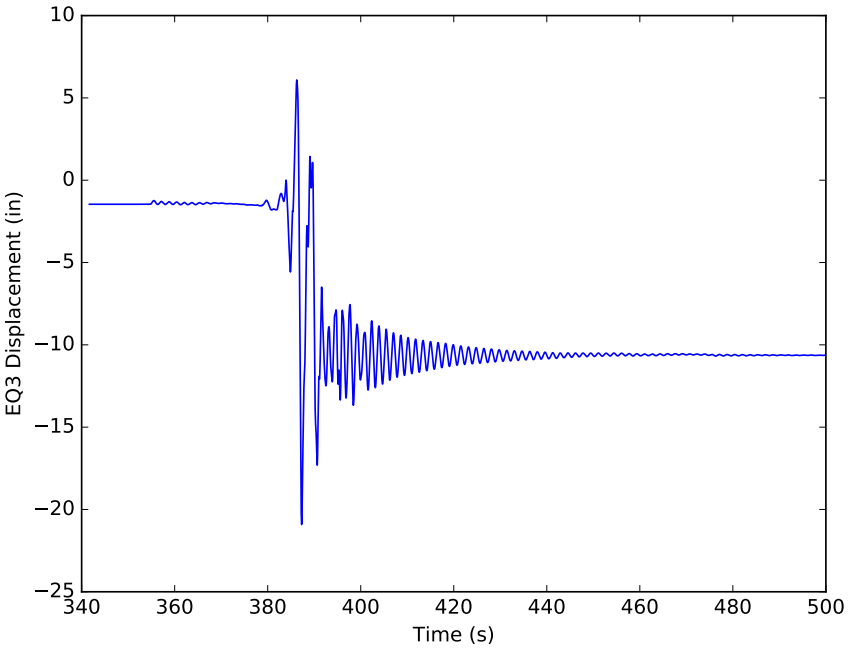

Figure K.3: Displacement response of model 5c for EQ3

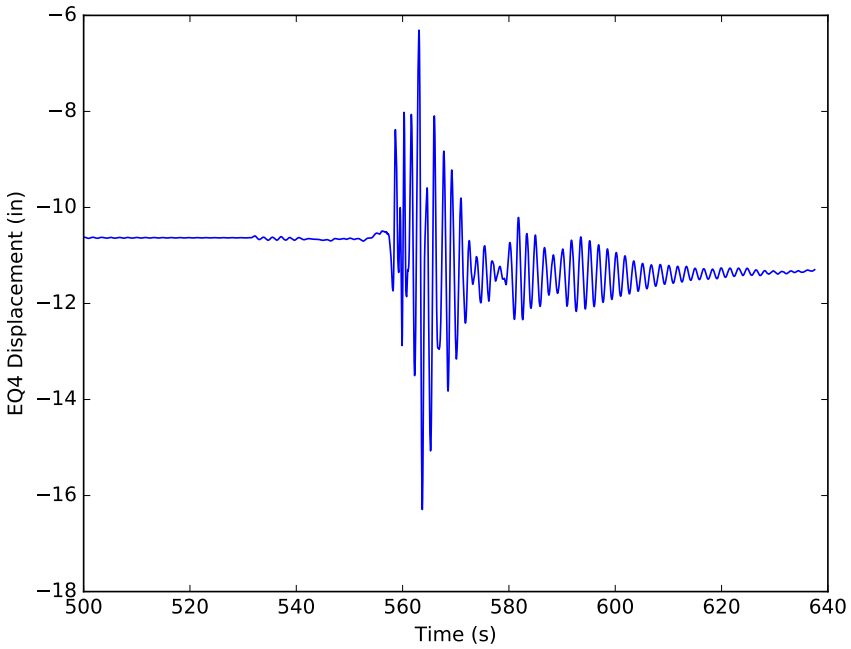

Figure K.4: Displacement response of model 5c for EQ4

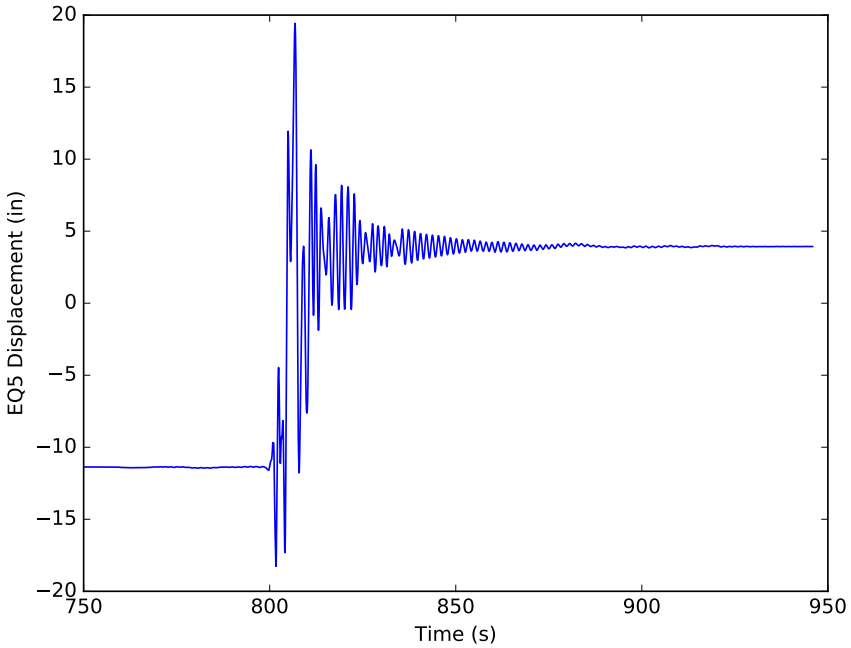

Figure K.5: Displacement response of model 5c for EQ5

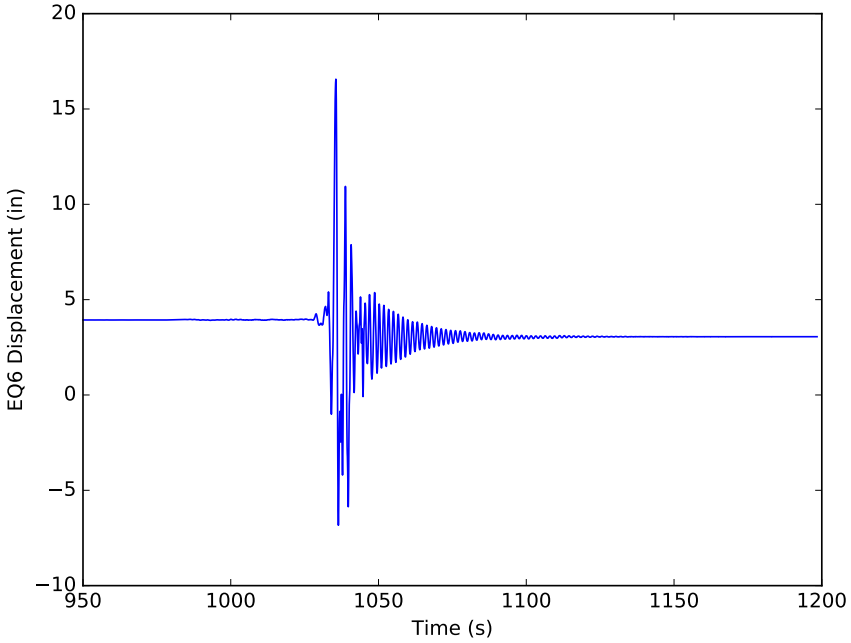

Figure K.6: Displacement response of model 5c for EQ6

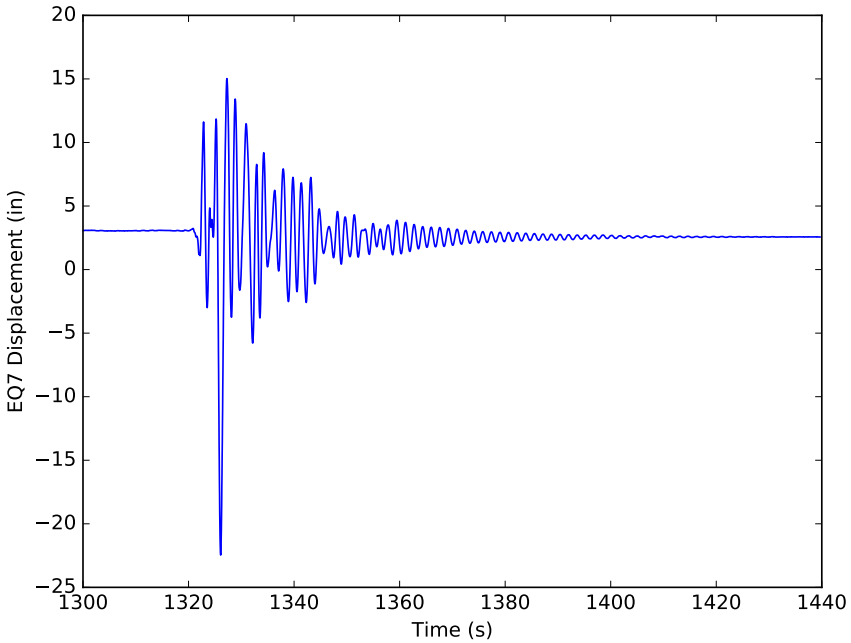

Figure K.7: Displacement response of model 5c for EQ7

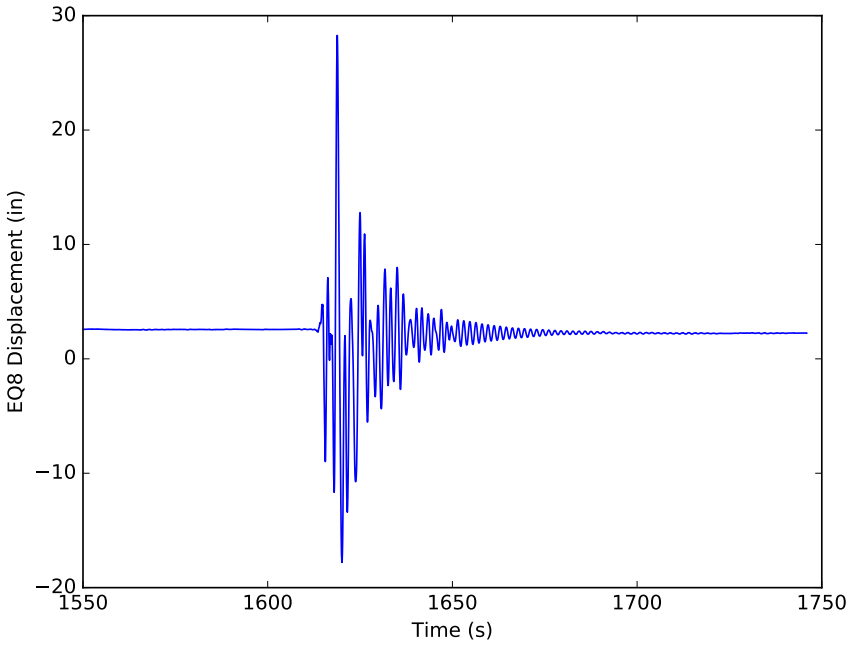

Figure K.8: Displacement response of model 5c for EQ8

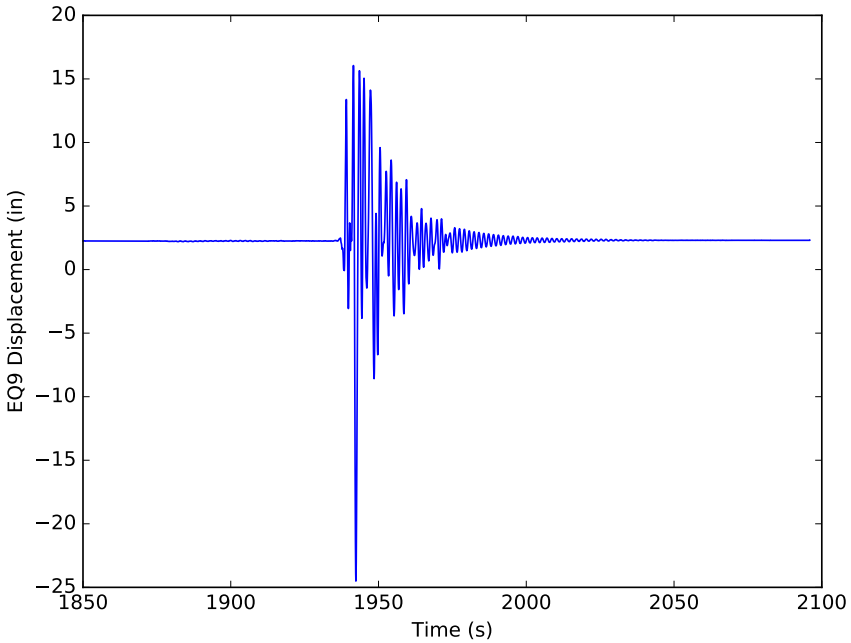

Figure K.9: Displacement response of model 5c for EQ9

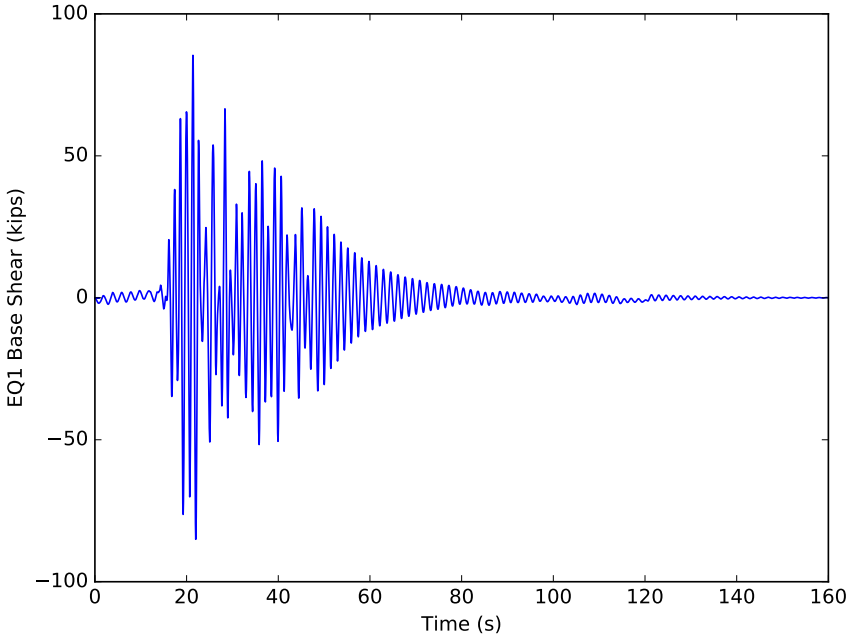

Figure K.10: Fx response of model 5c for EQ1

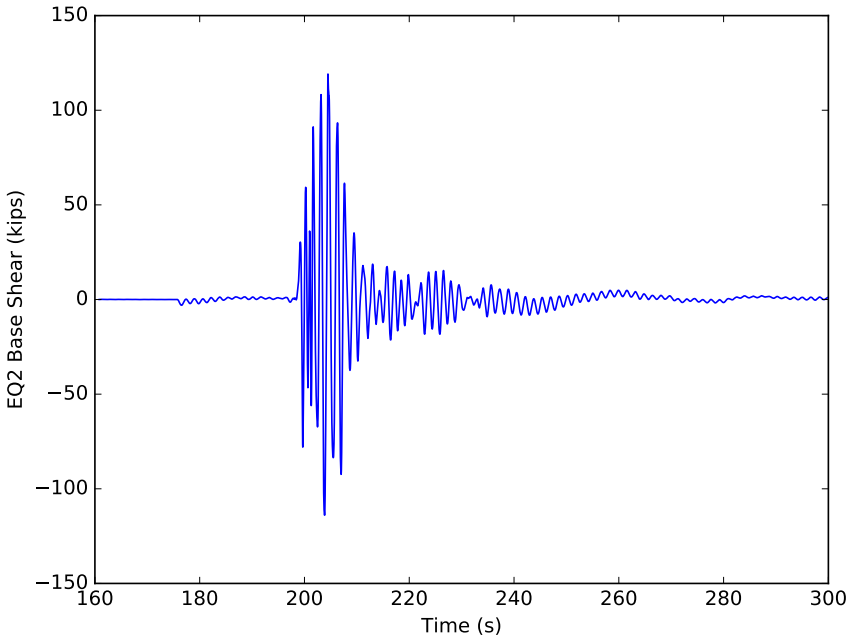

Figure K.11: Fx response of model 5c for EQ2

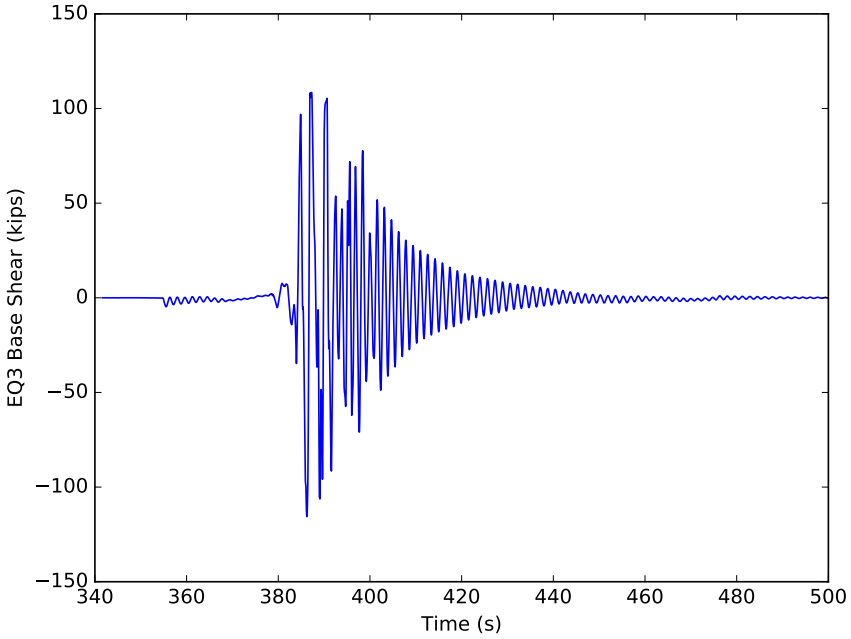

Figure K.12: Fx response of model 5c for EQ3

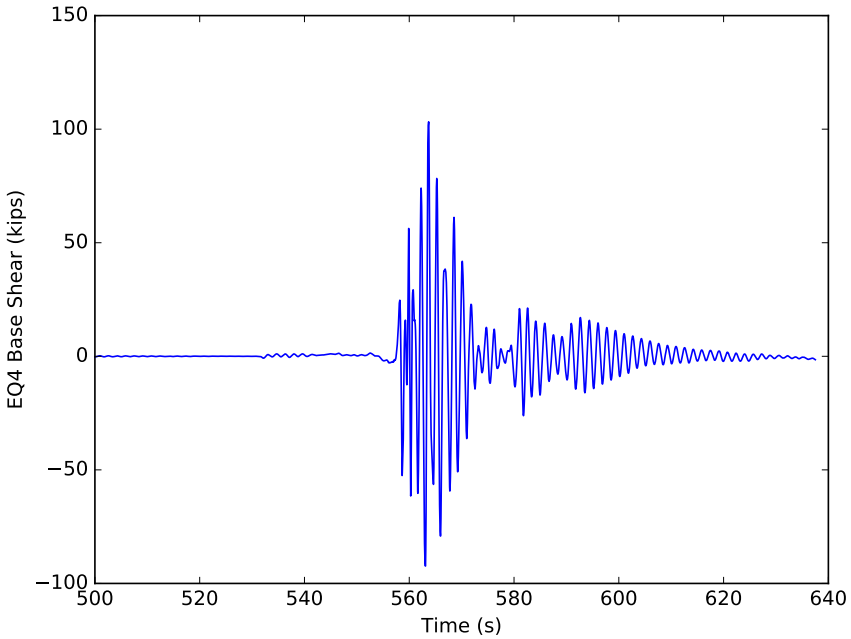

Figure K.13: Fx response of model 5c for EQ4

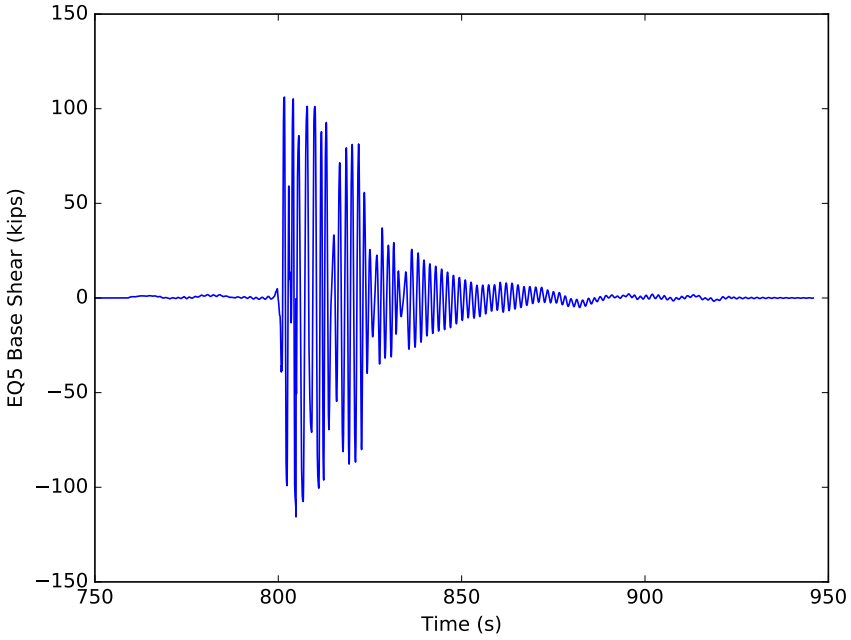

Figure K.14: Fx response of model 5c for EQ5

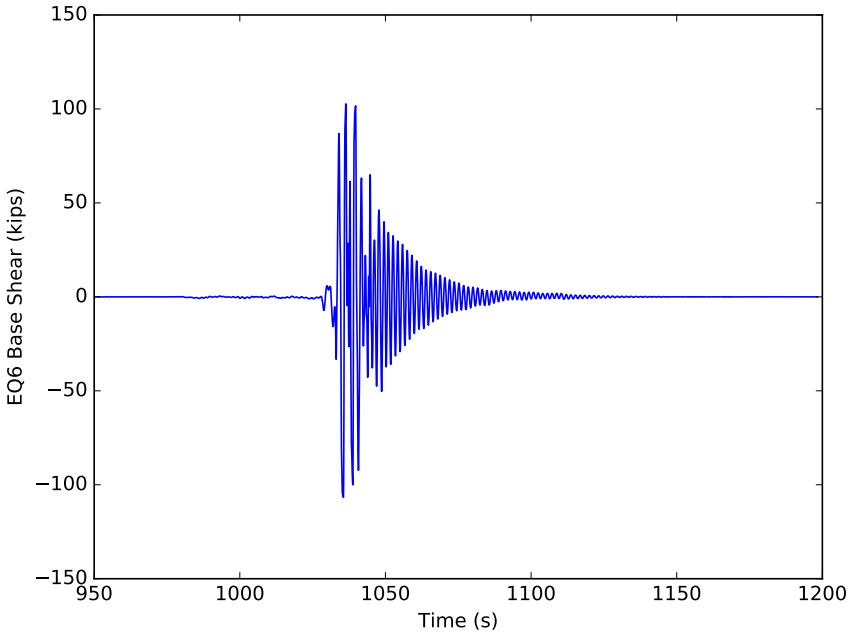

Figure K.15: Fx response of model 5c for EQ6

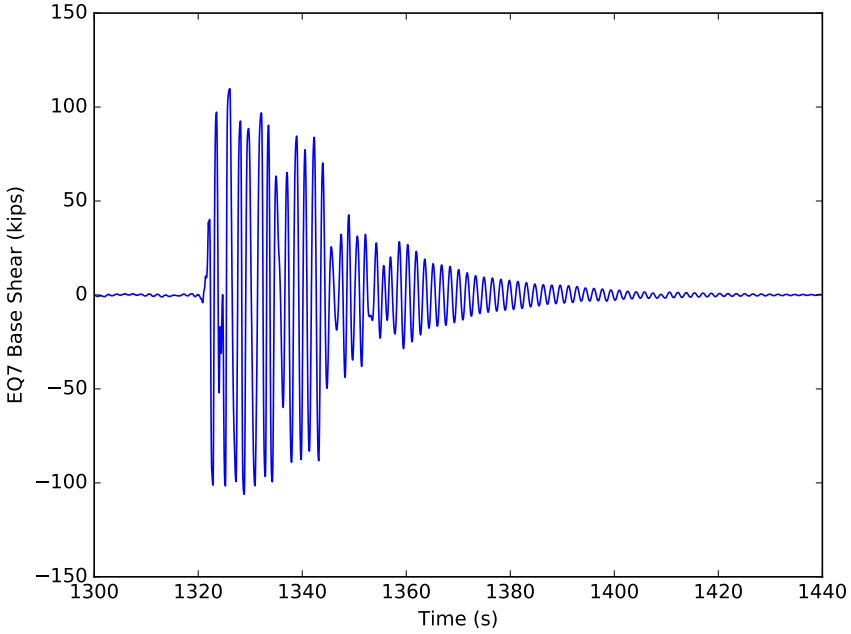

Figure K.16: Fx response of model 5c for EQ7

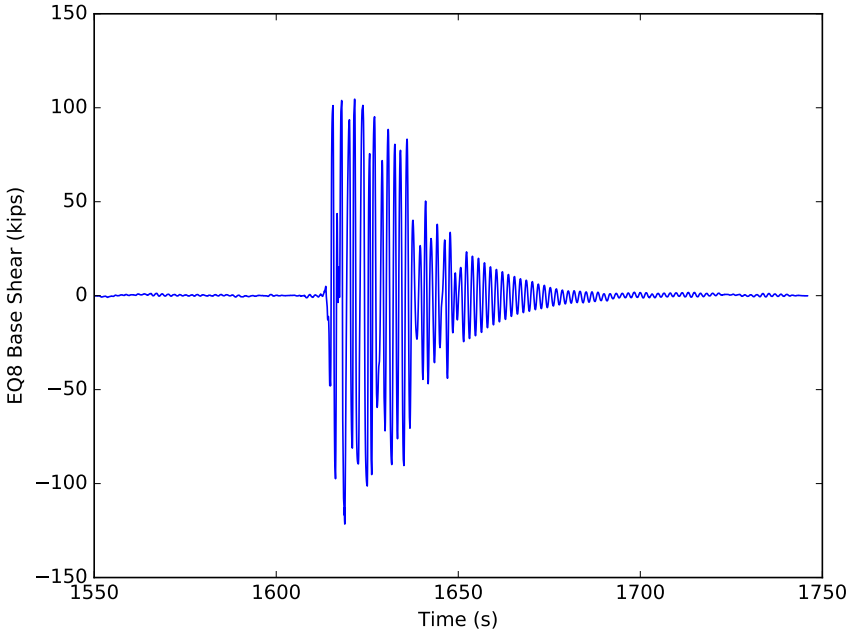

Figure K.17: Fx response of model 5c for EQ8

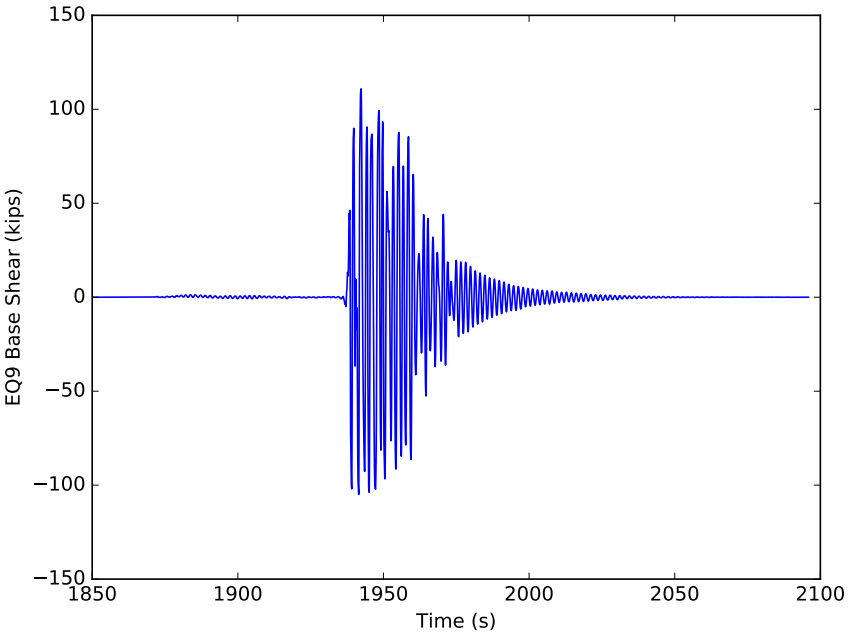

Figure K.18: Fx response of model 5c for EQ9

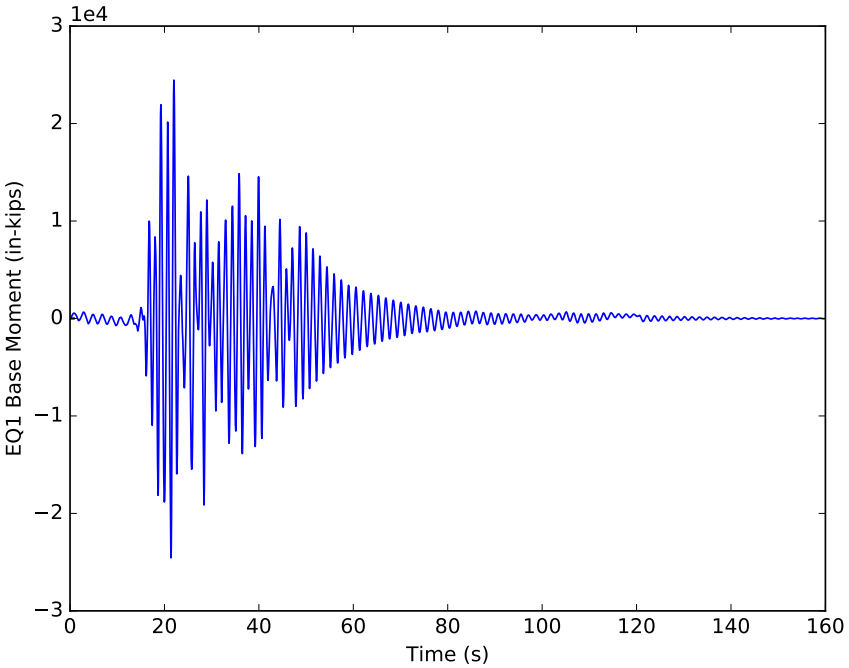

Figure K.19: Mz response of model 5c for EQ1

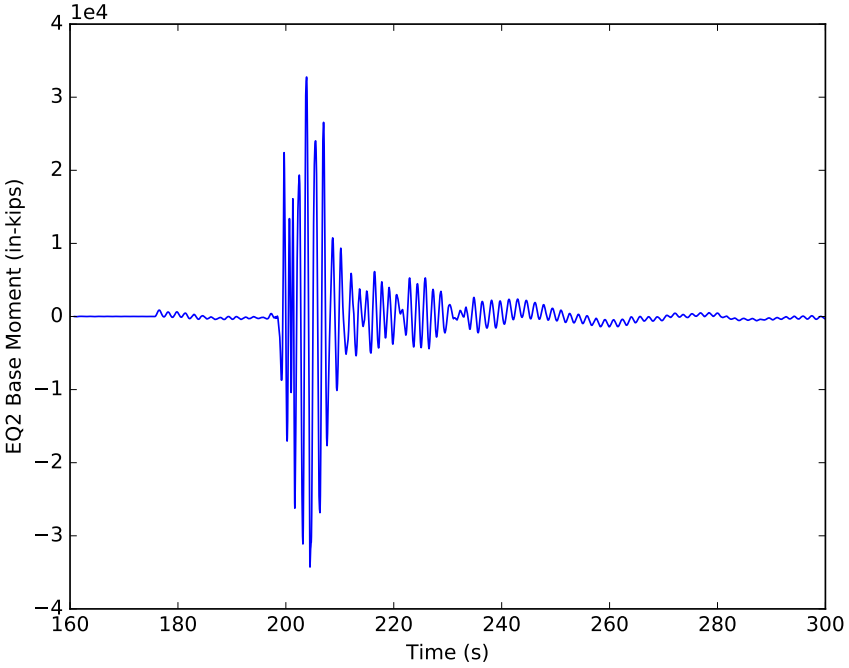

Figure K.20: Mz response of model 5c for EQ2

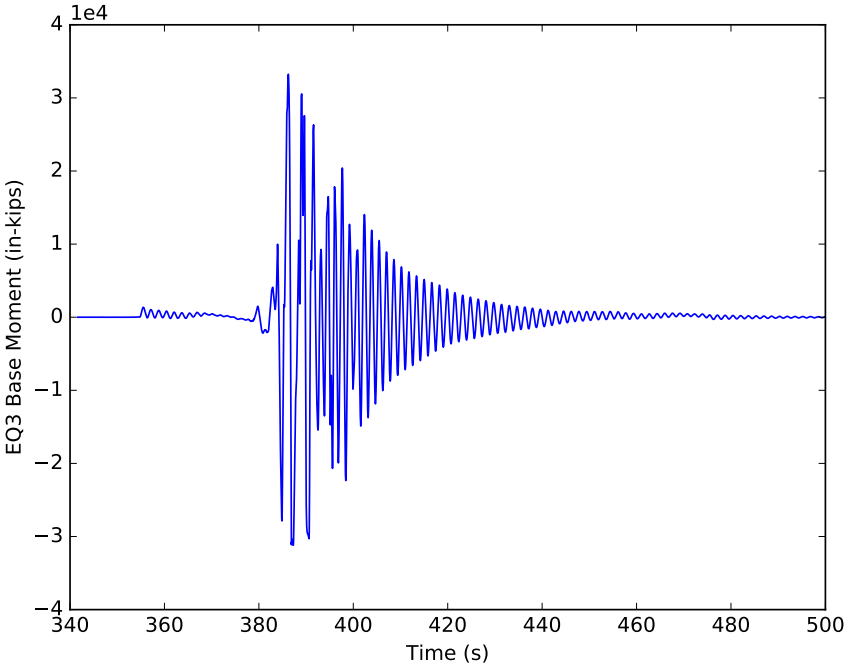

Figure K.21: Mz response of model 5c for EQ3

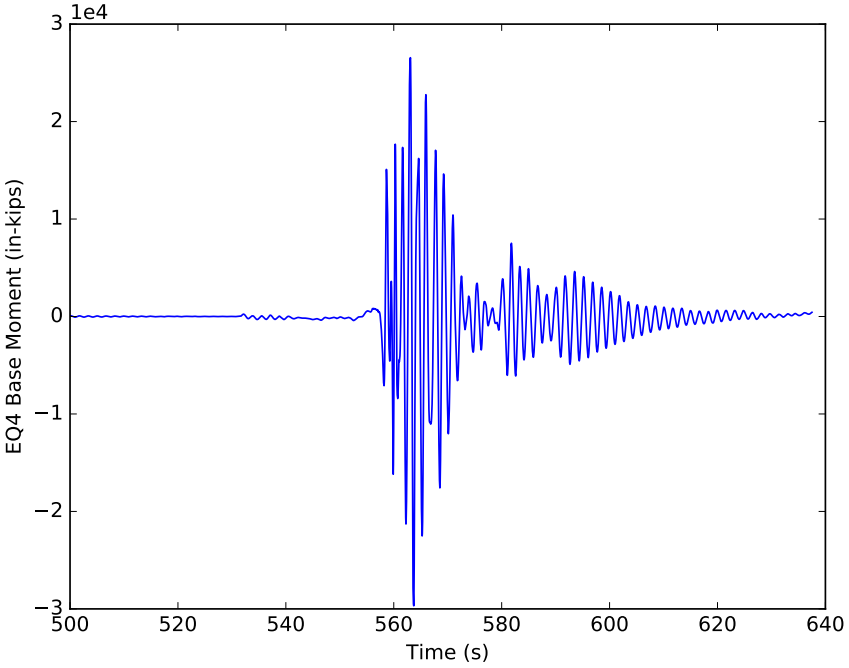

Figure K.22: Mz response of model 5c for EQ4

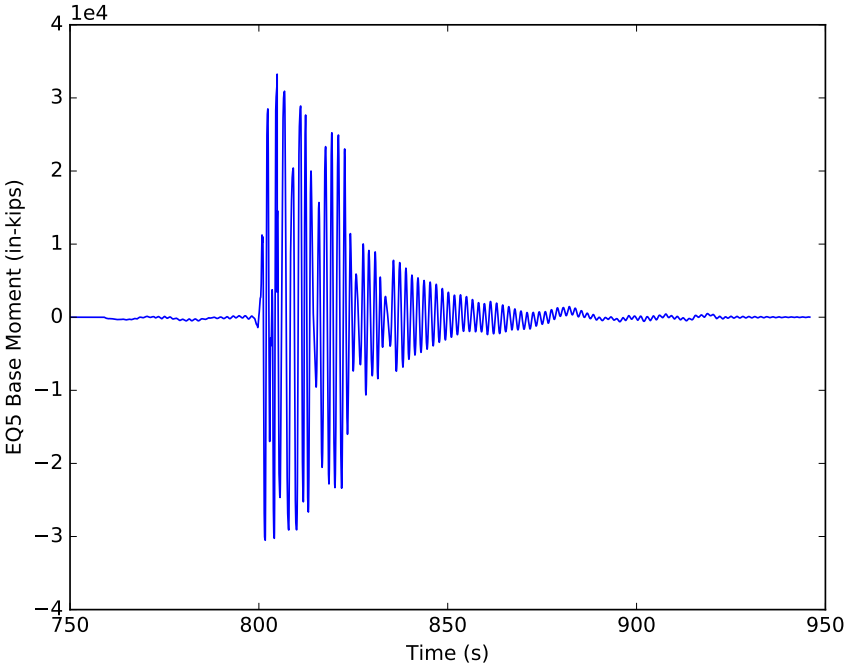

Figure K.23: Mz response of model 5c for EQ5

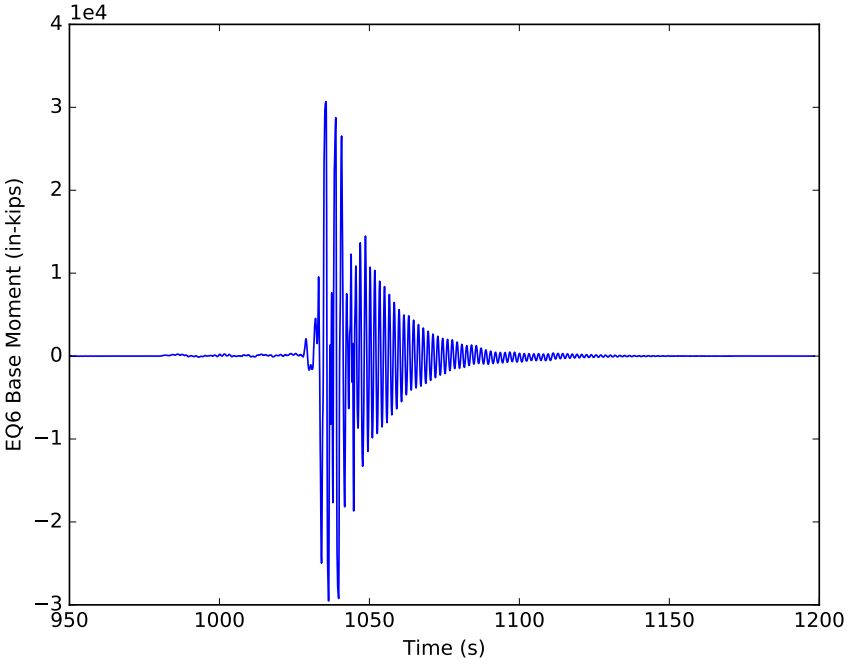

Figure K.24: Mz response of model 5c for EQ6

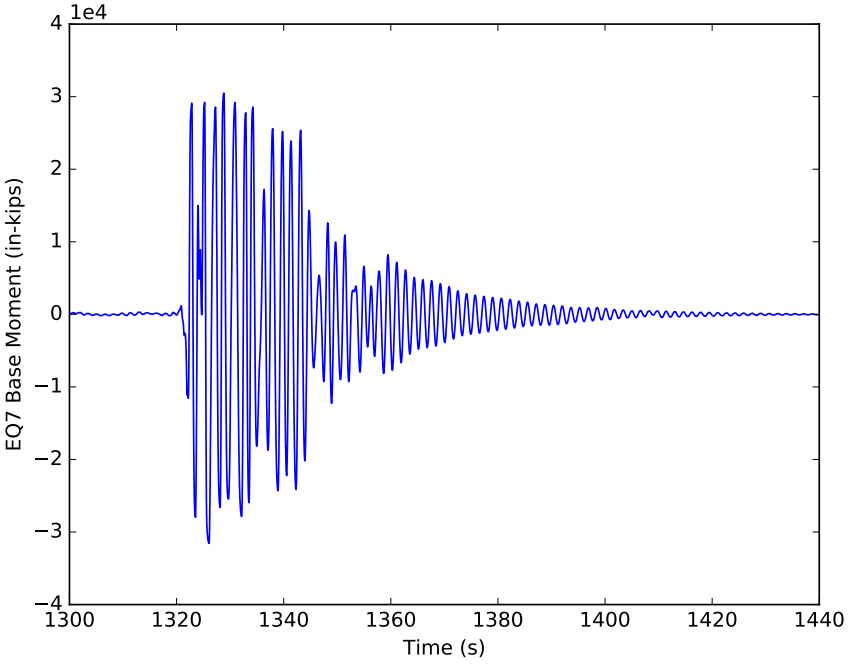

Figure K.25: Mz response of model 5c for EQ7

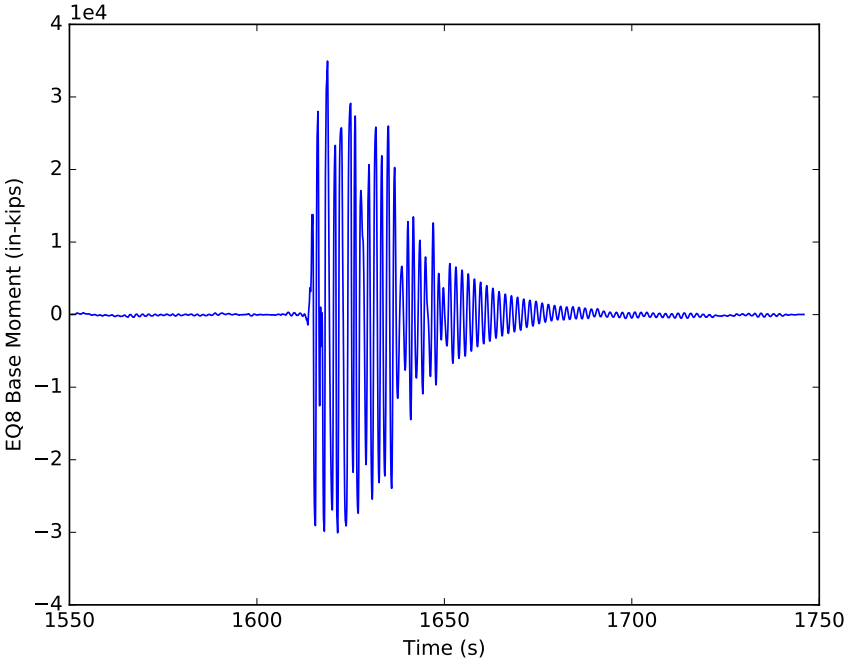

Figure K.26: Mz response of model 5c for EQ8

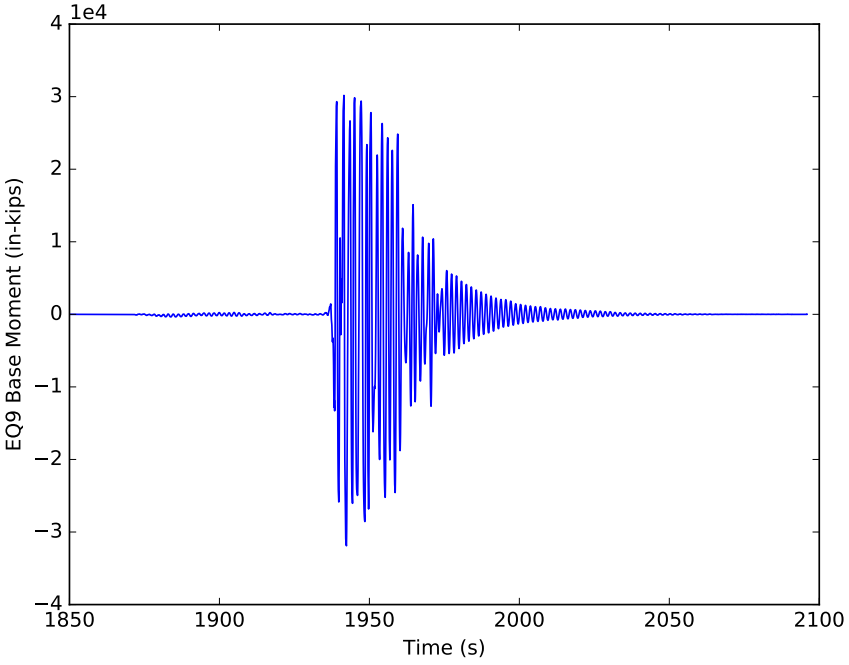

Figure K.27: Mz response of model 5c for EQ9

Appendix L

Model 5d Output

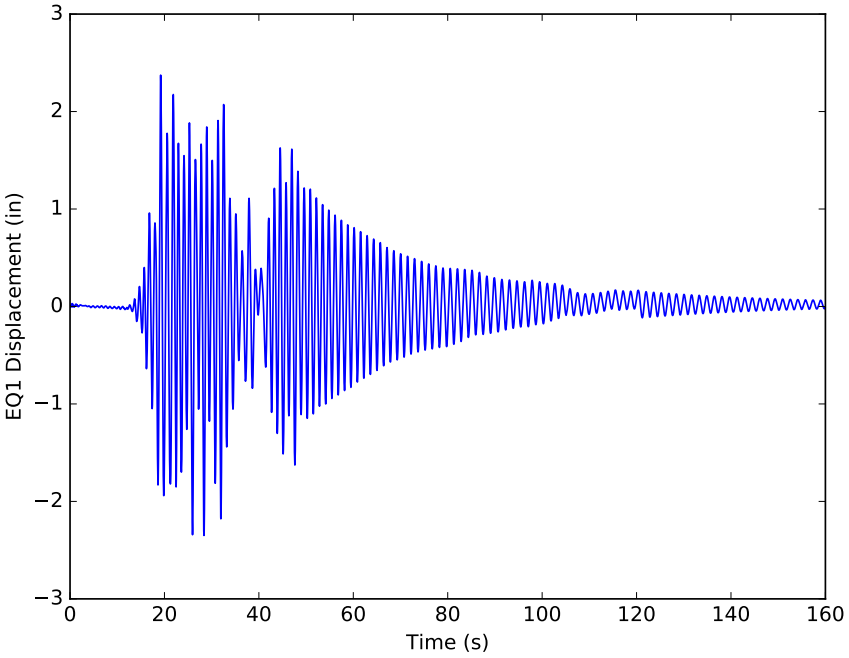

Figure L.1: Displacement response of model 5d for EQ1

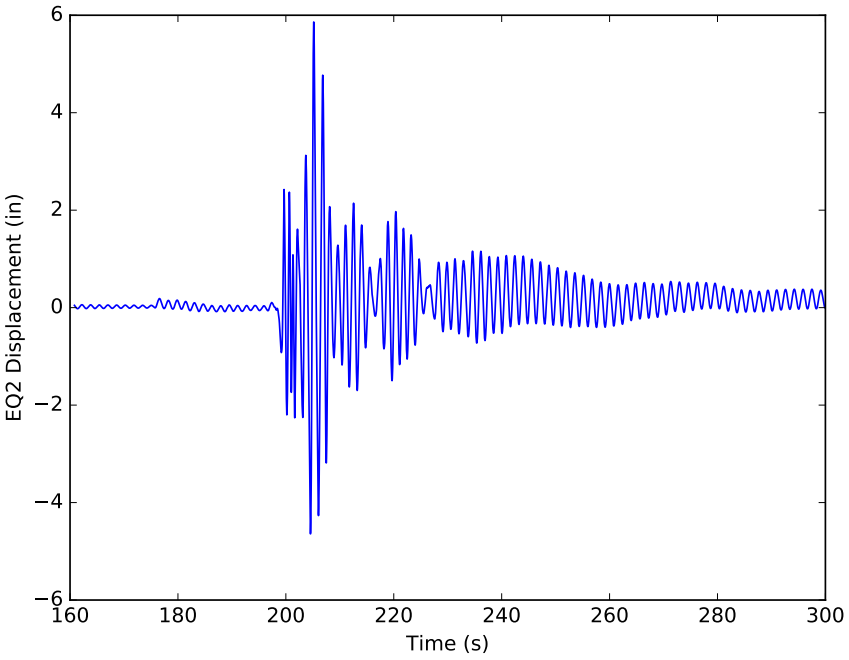

Figure L.2: Displacement response of model 5d for EQ2

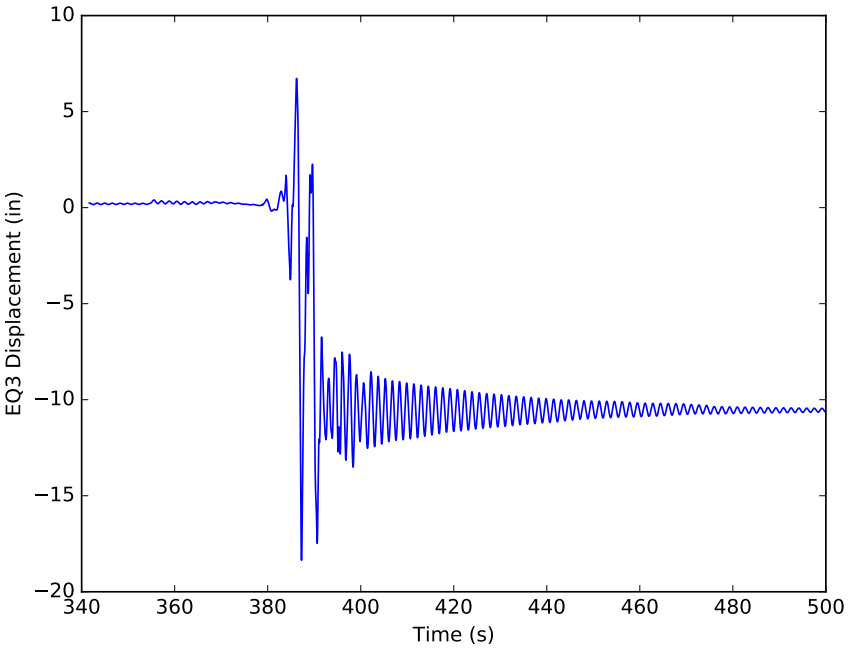

Figure L.3: Displacement response of model 5d for EQ3

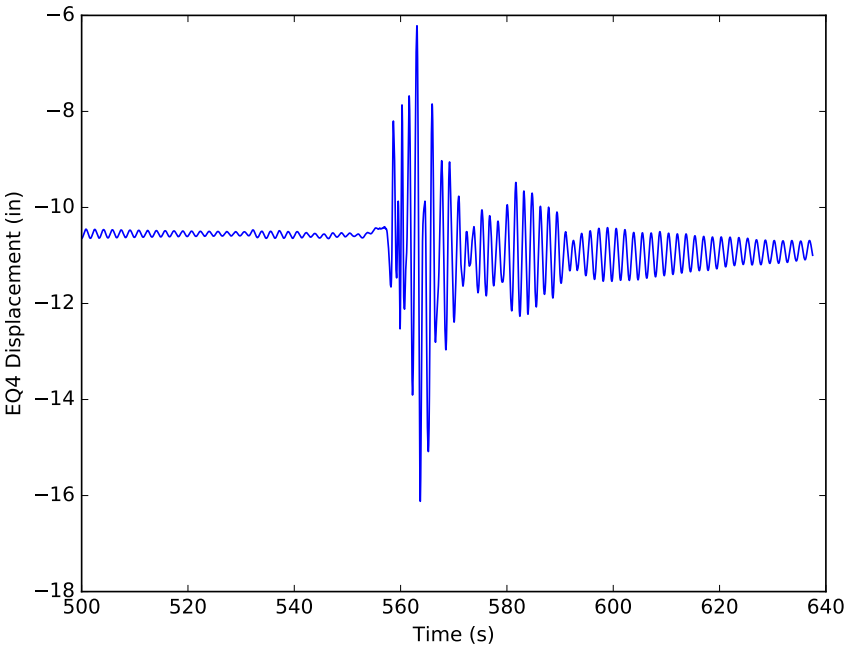

Figure L.4: Displacement response of model 5d for EQ4

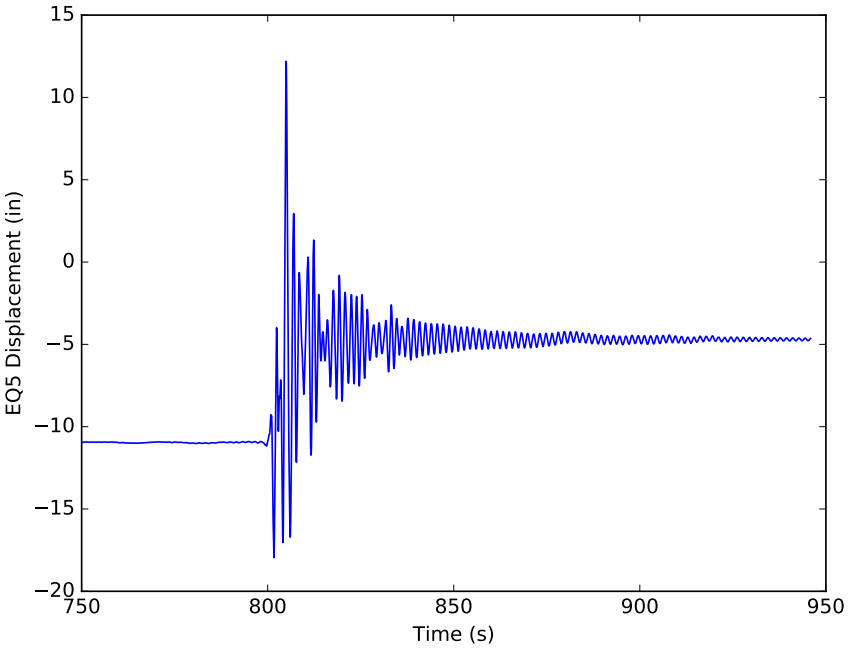

Figure L.5: Displacement response of model 5d for EQ5

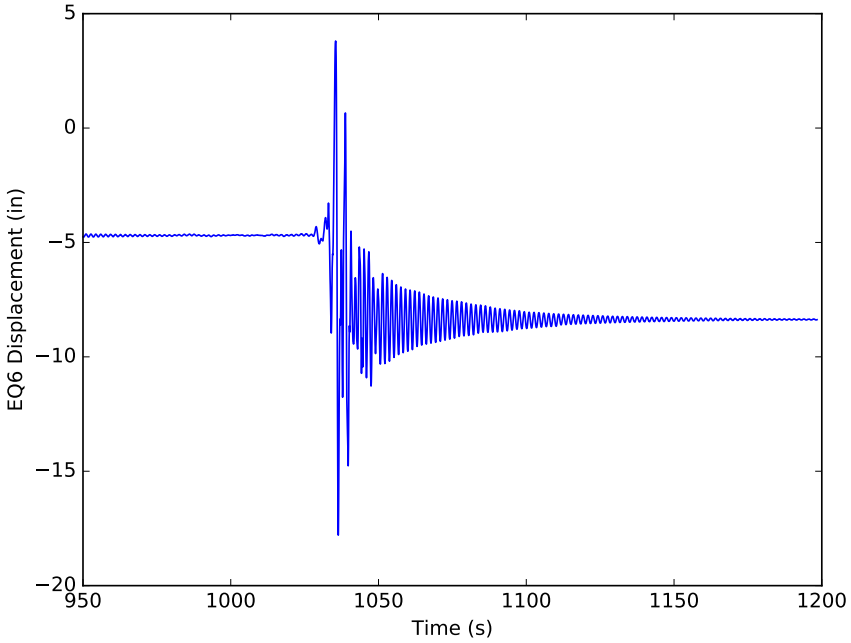

Figure L.6: Displacement response of model 5d for EQ6

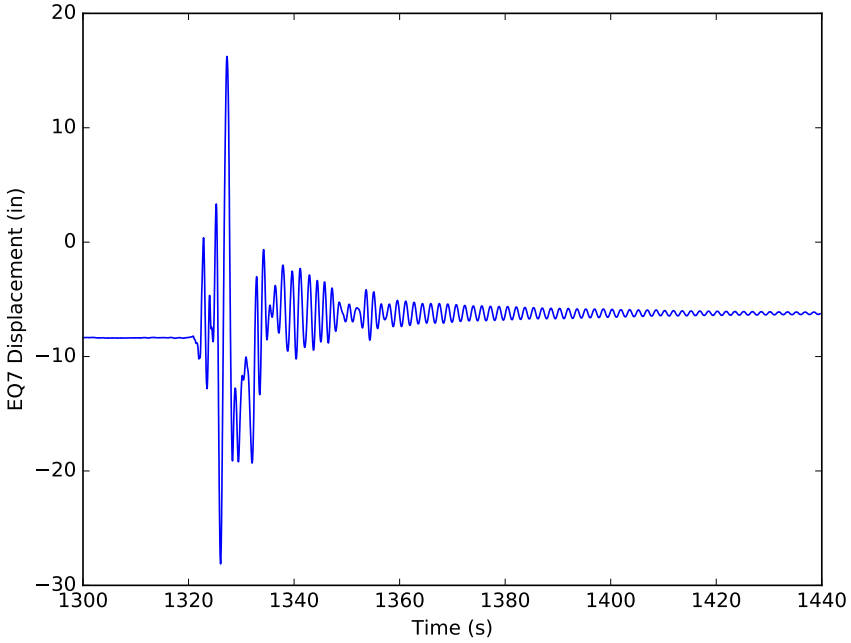

Figure L.7: Displacement response of model 5d for EQ7

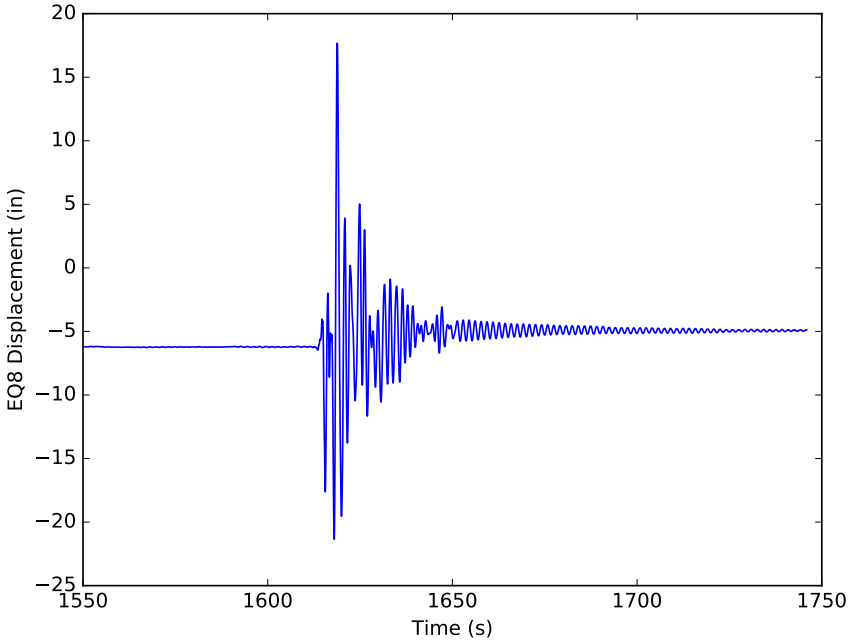

Figure L.8: Displacement response of model 5d for EQ8

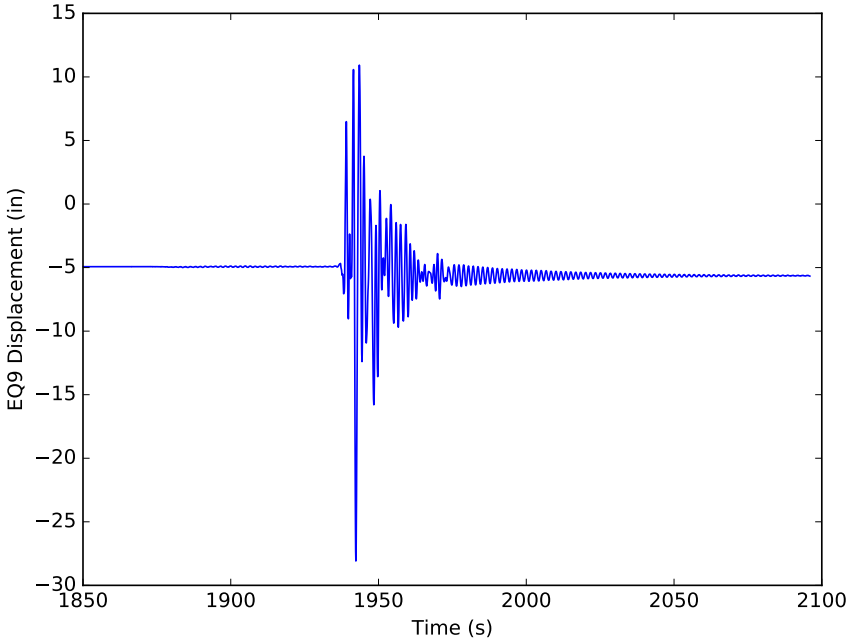

Figure L.9: Displacement response of model 5d for EQ9

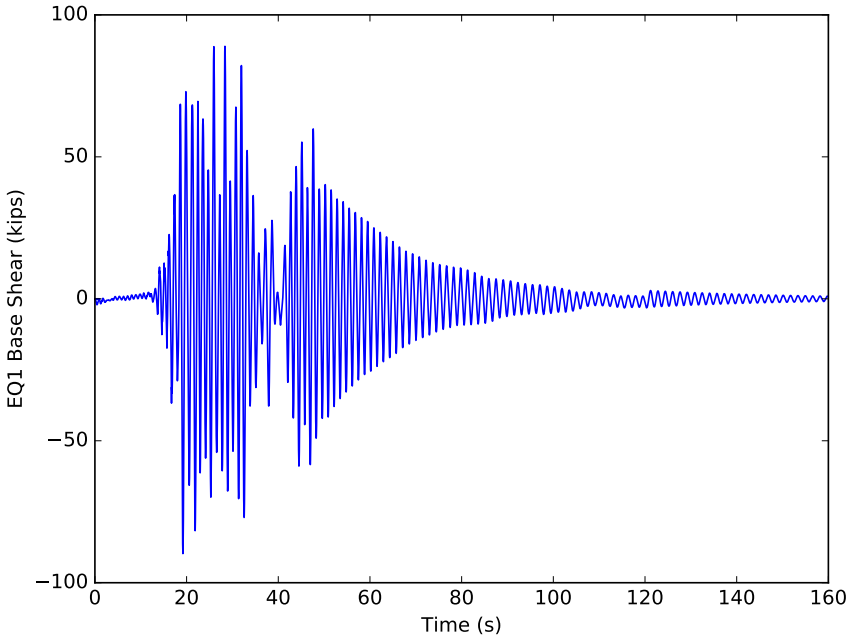

Figure L.10: Fx response of model 5d for EQ1

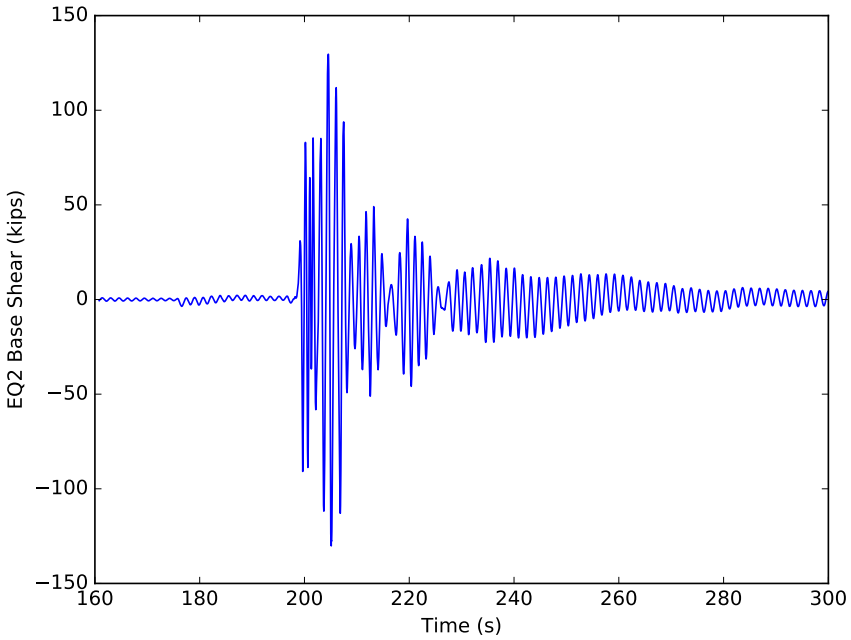

Figure L.11: Fx response of model 5d for EQ2

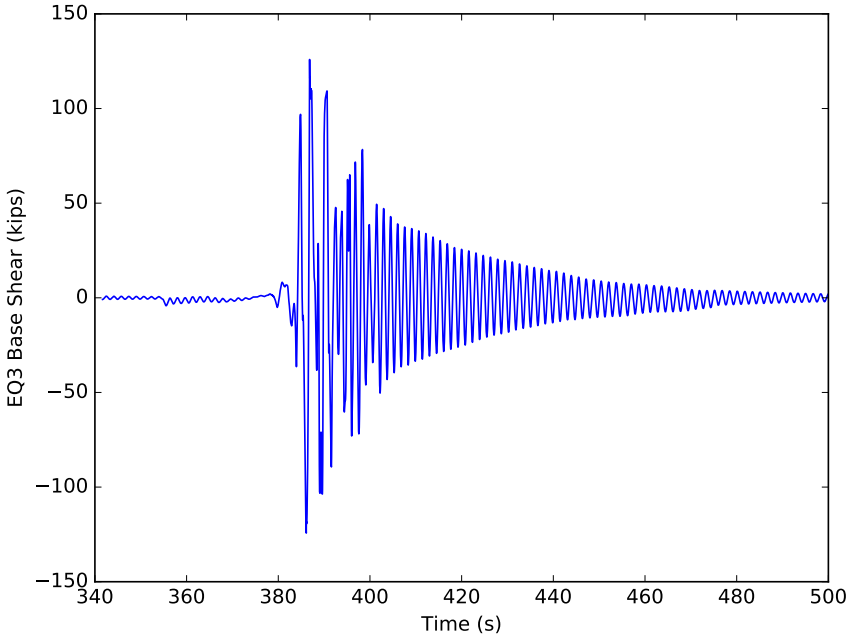

Figure L.12: Fx response of model 5d for EQ3

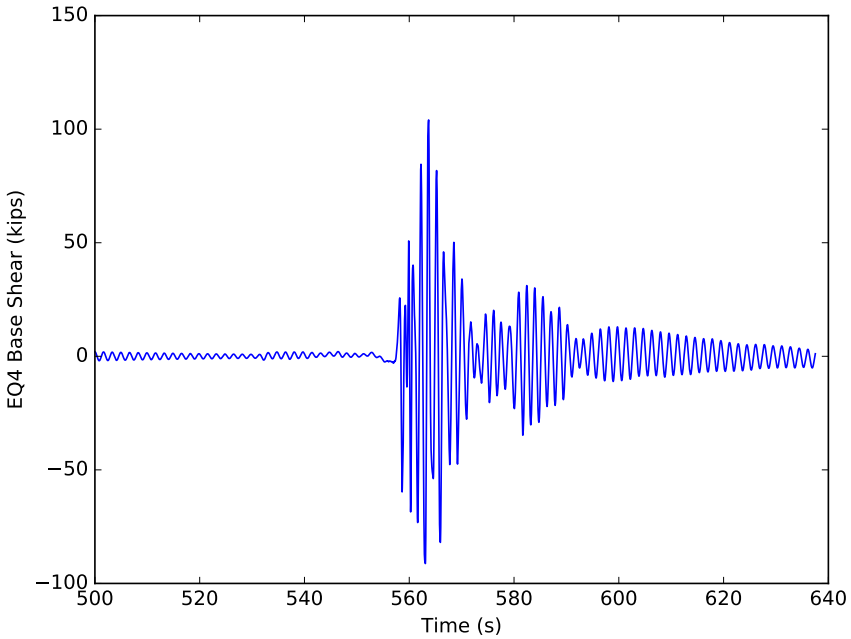

Figure L.13: Fx response of model 5d for EQ4

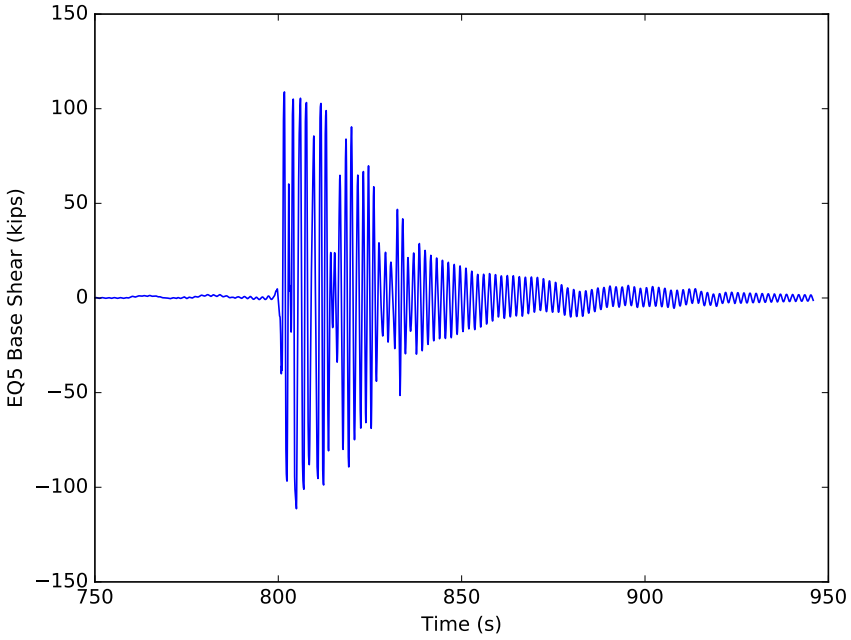

Figure L.14: Fx response of model 5d for EQ5

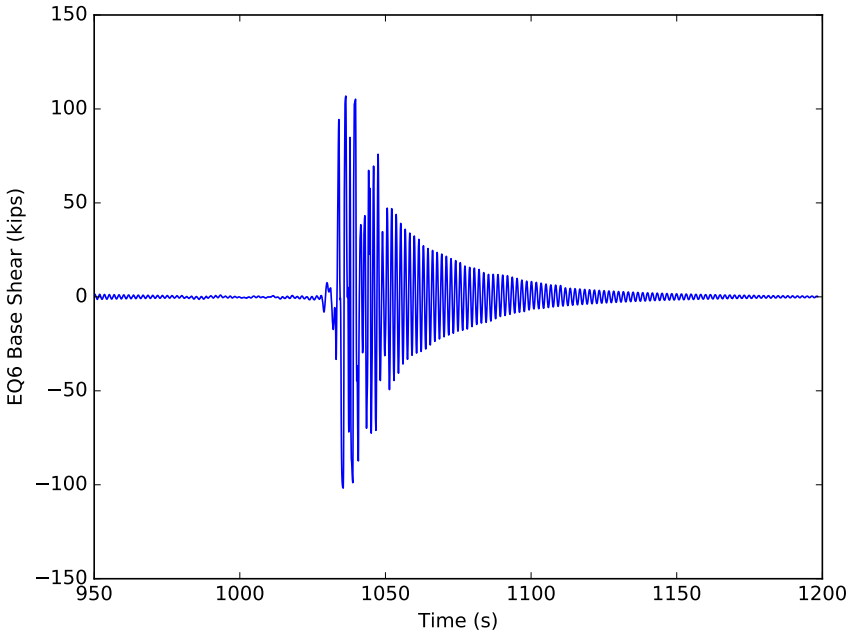

Figure L.15: Fx response of model 5d for EQ6

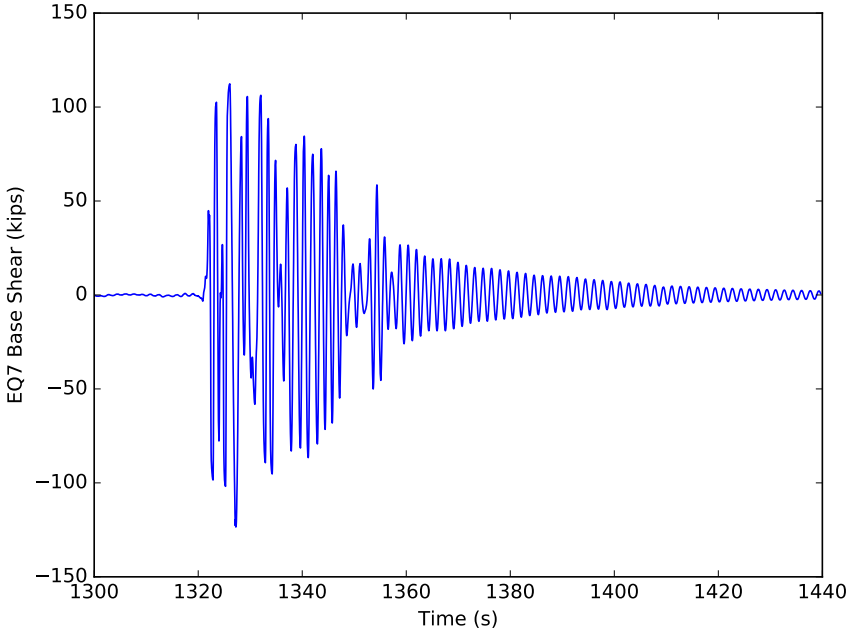

Figure L.16: Fx response of model 5d for EQ7

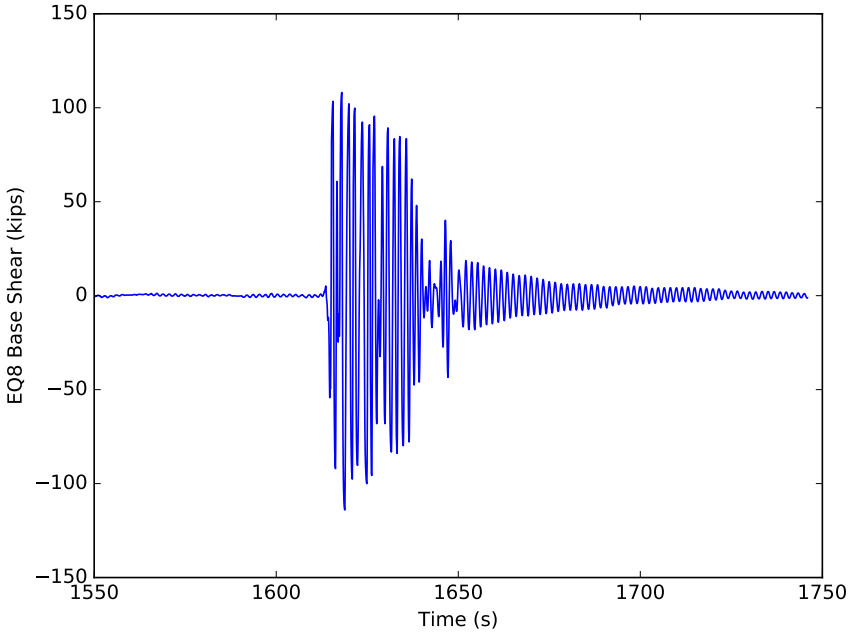

Figure L.17: Fx response of model 5d for EQ8

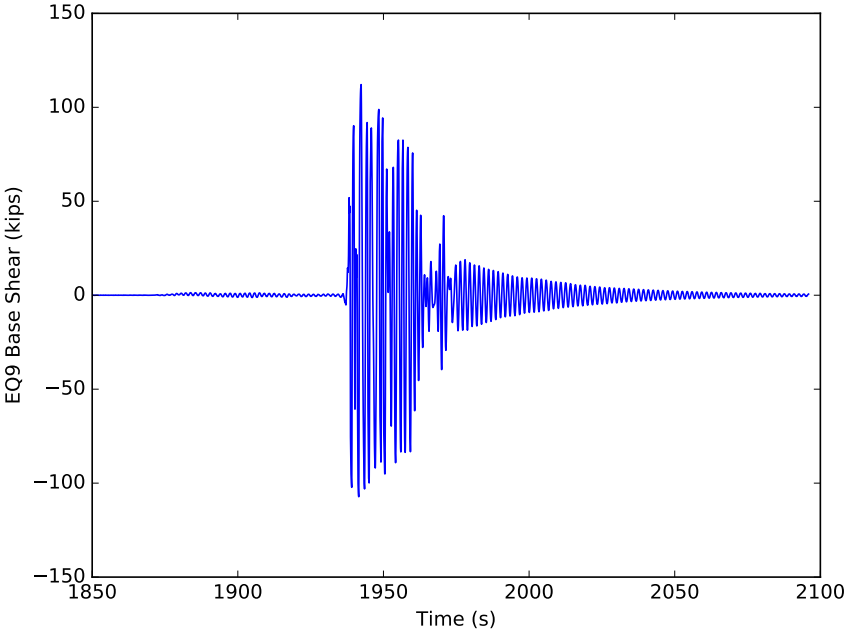

Figure L.18: Fx response of model 5d for EQ9

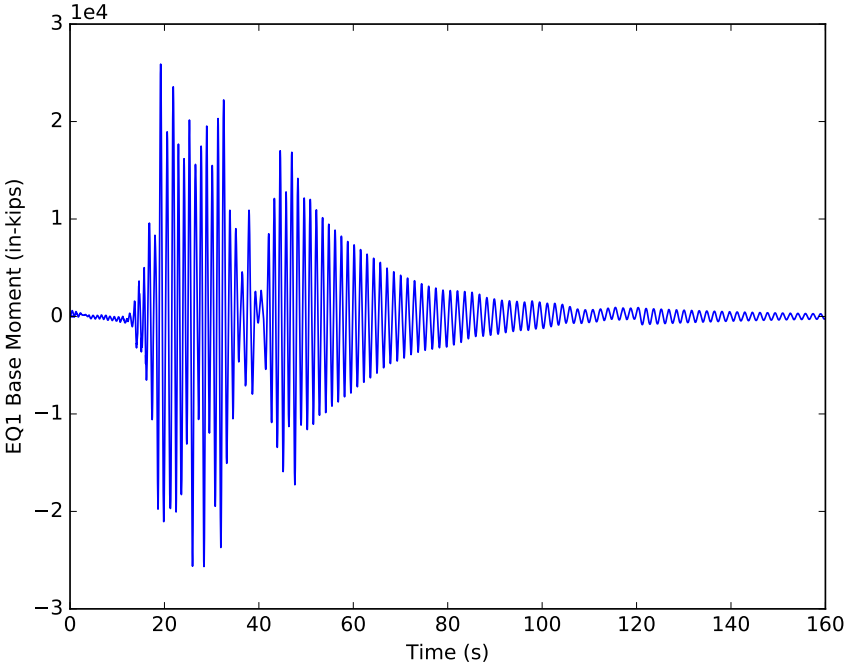

Figure L.19: Mz response of model 5d for EQ1

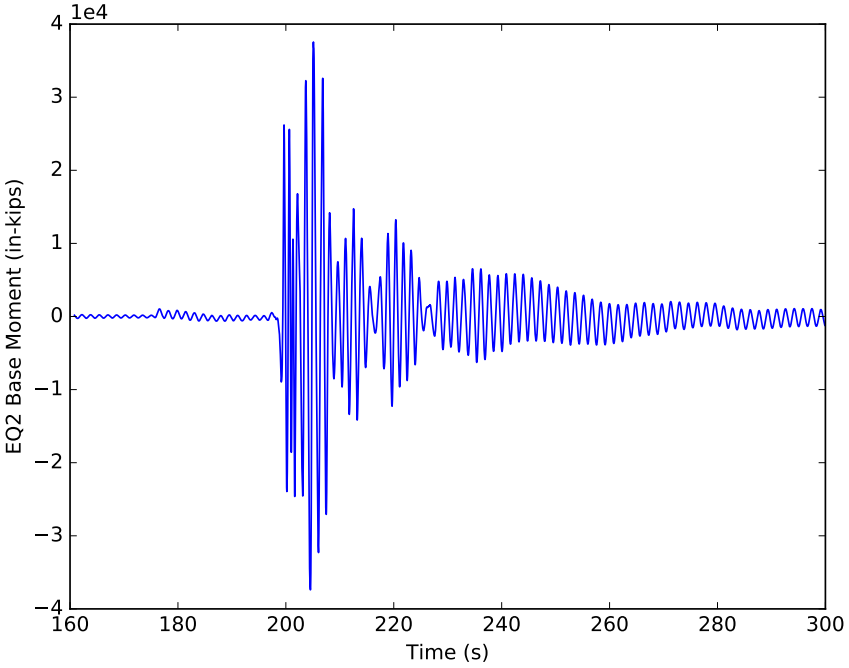

Figure L.20: Mz response of model 5d for EQ2

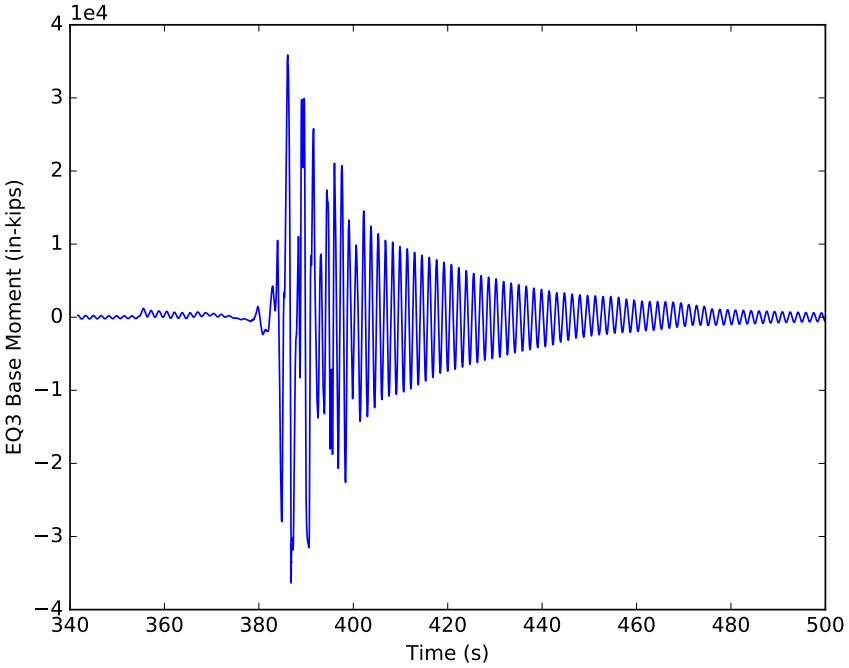

Figure L.21: Mz response of model 5d for EQ3

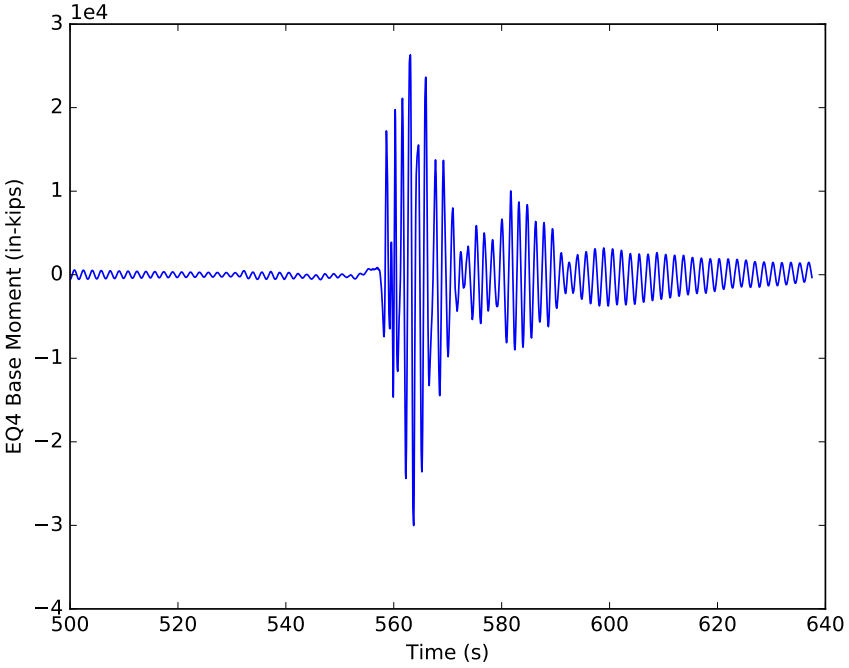

Figure L.22: Mz response of model 5d for EQ4

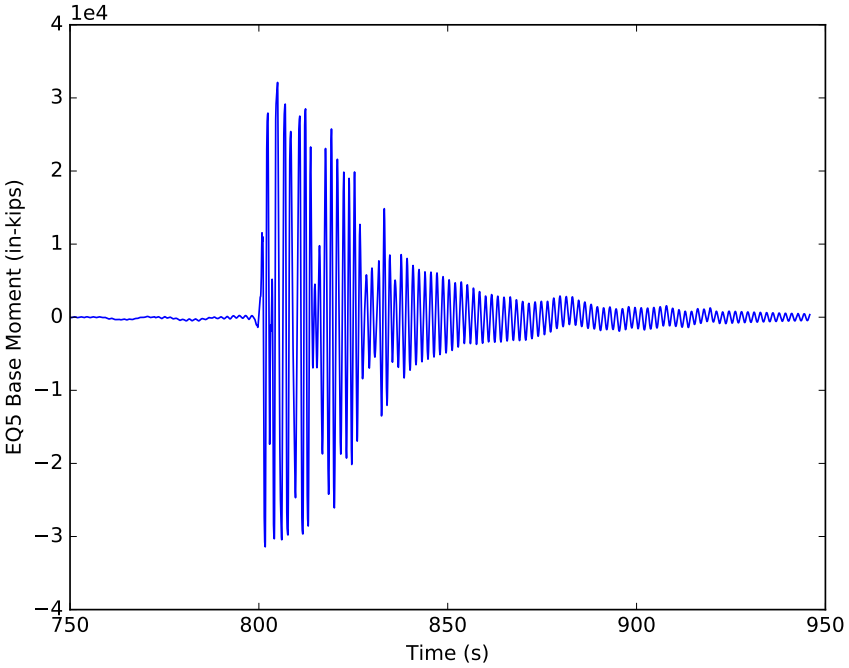

Figure L.23: Mz response of model 5d for EQ5

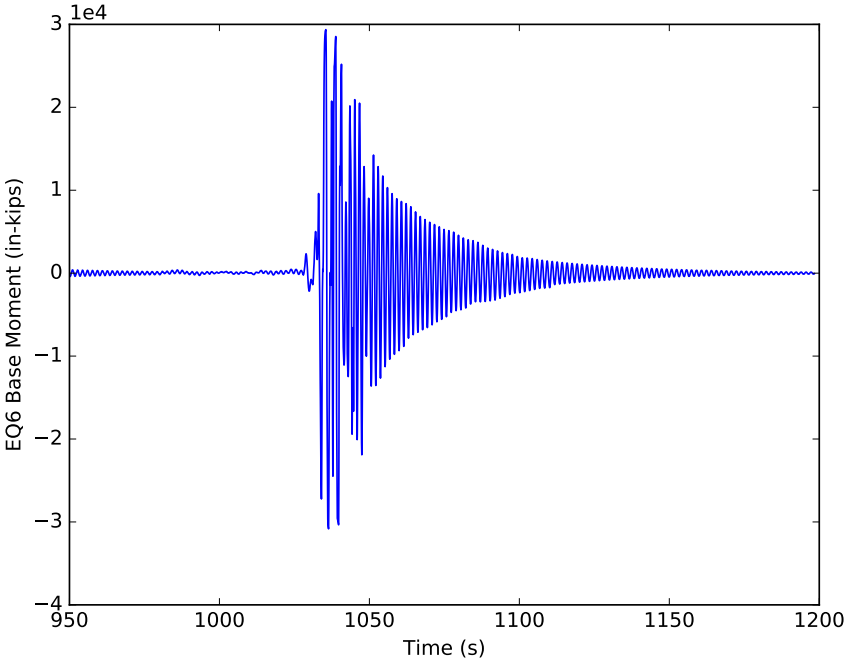

Figure L.24: Mz response of model 5d for EQ6

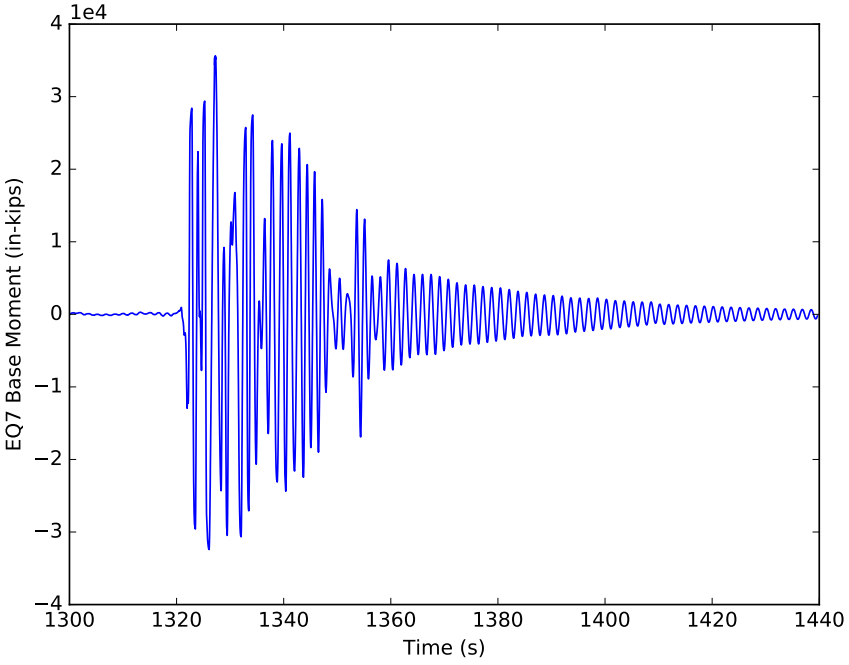

Figure L.25: Mz response of model 5d for EQ7

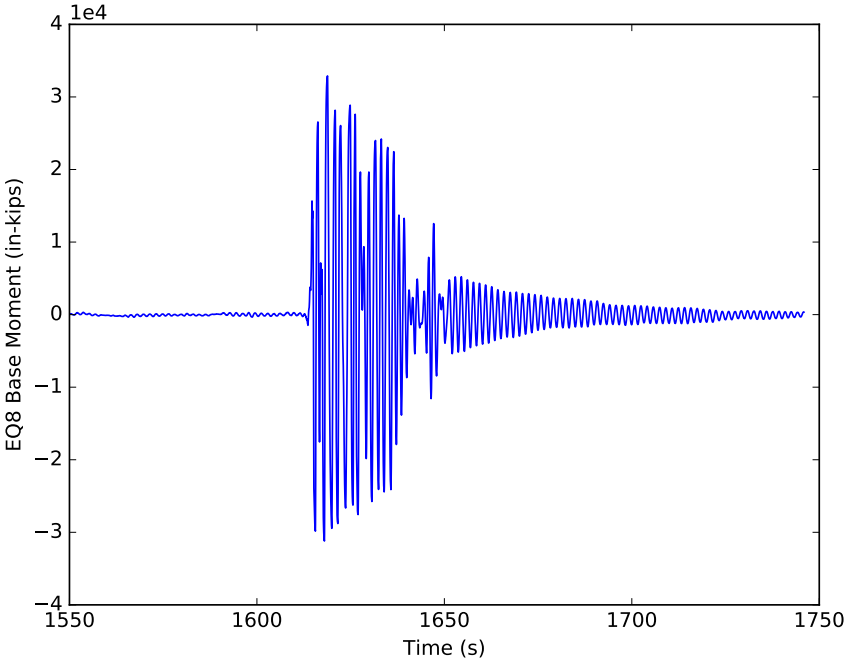

Figure L.26: Mz response of model 5d for EQ8

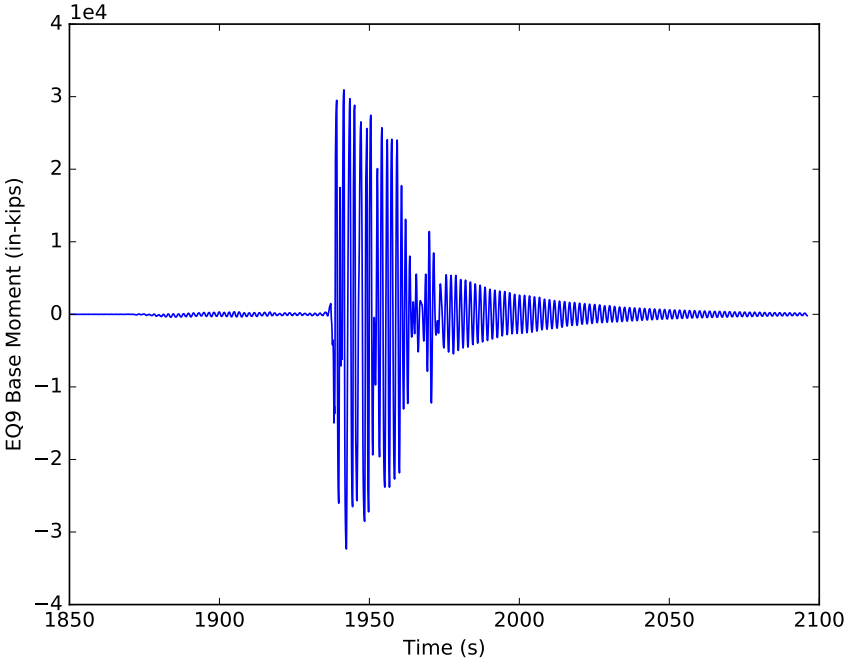

Figure L.27: Mz response of model 5d for EQ9

Appendix M

Model 3 Moment Curvature Plots

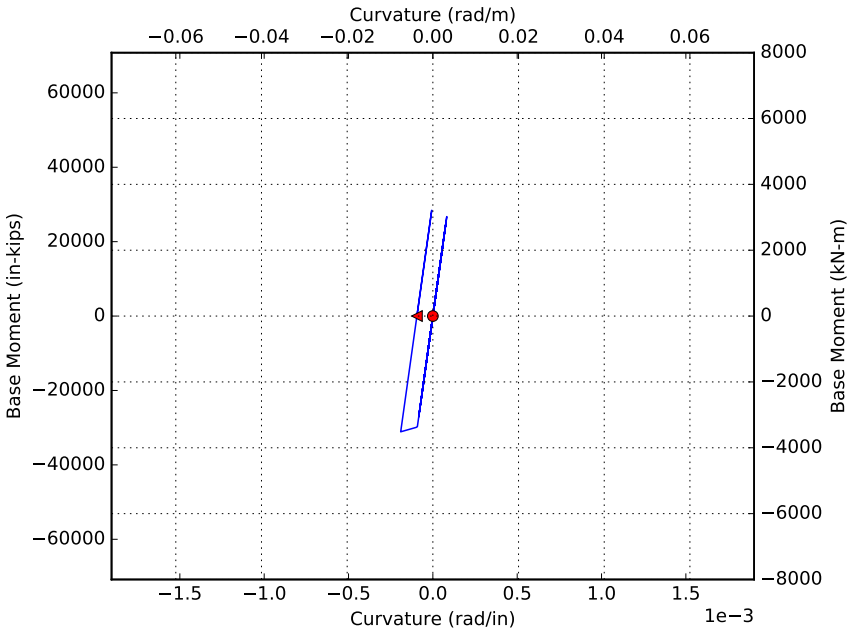

Figure M.1: Moment curvature response of model 3 for EQ1. Red circle indicates initial point

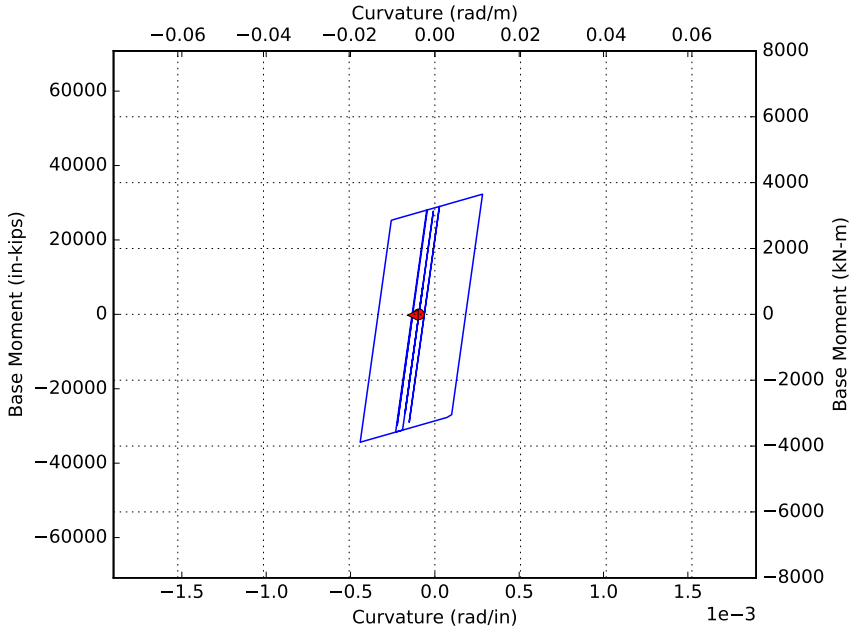

Figure M.2: Moment curvature response of model 3 for EQ2. Red circle indicates initial point

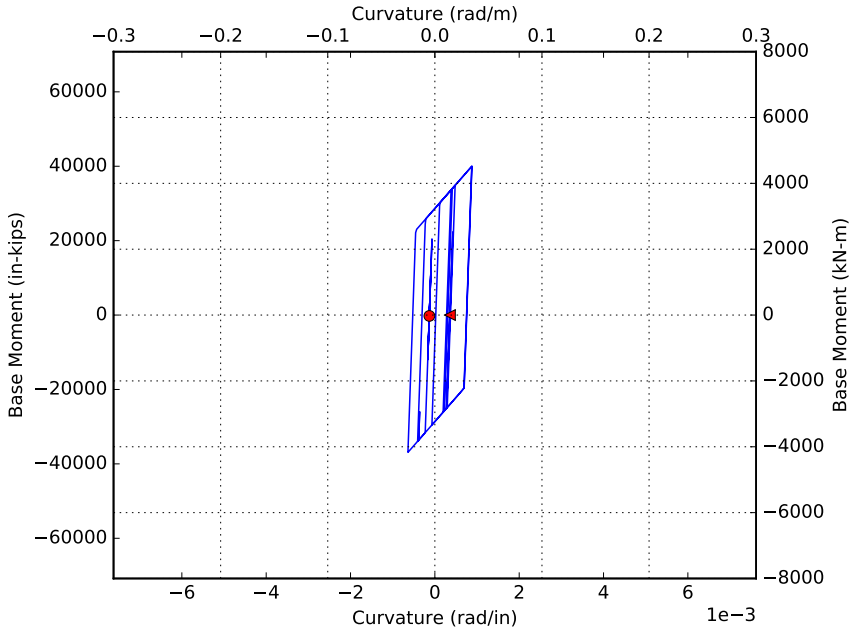

Figure M.3: Moment curvature response of model 3 for EQ3. Red circle indicates initial point

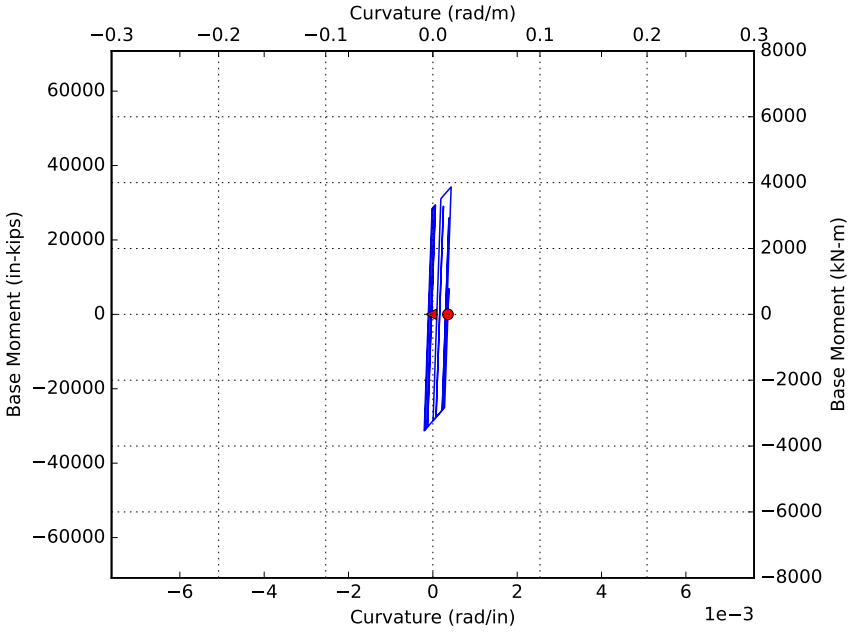

Figure M.4: Moment curvature response of model 3 for EQ4. Red circle indicates initial point

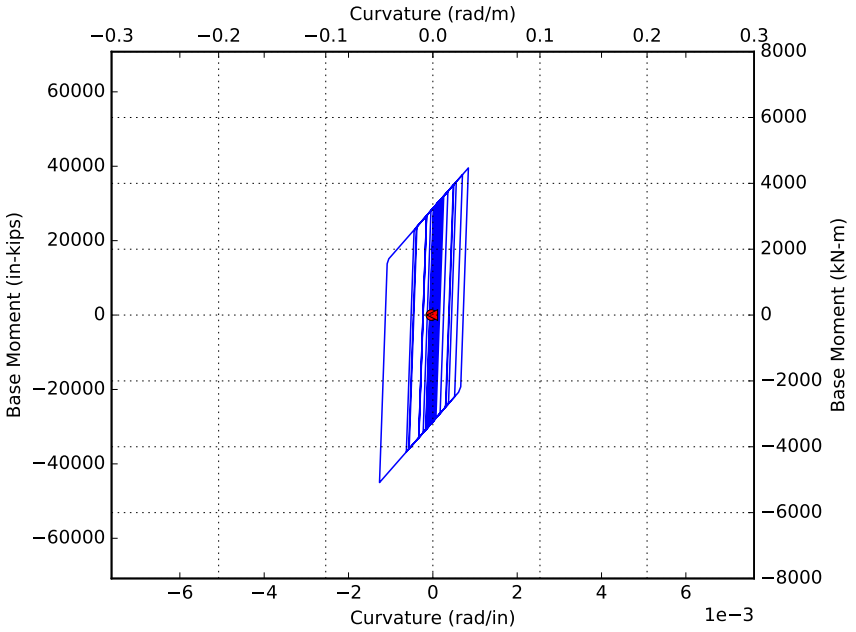

Figure M.5: Moment curvature response of model 3 for EQ5. Red circle indicates initial point

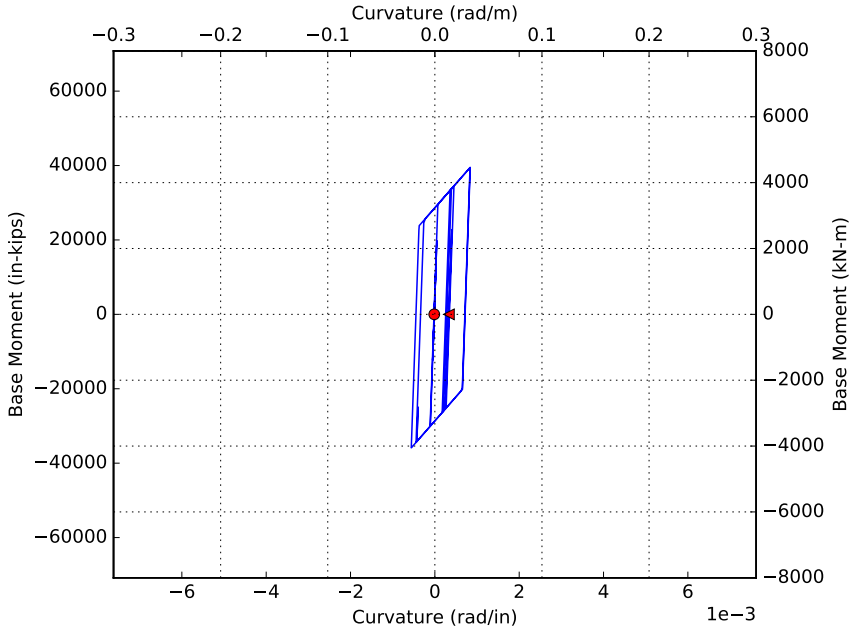

Figure M.6: Moment curvature response of model 3 for EQ6. Red circle indicates initial point

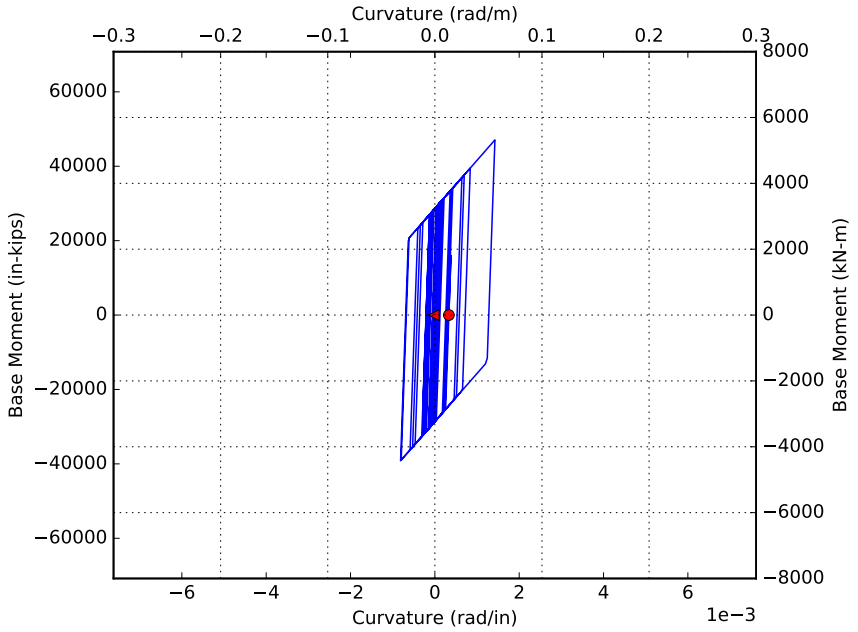

Figure M.7: Moment curvature response of model 3 for EQ7. Red circle indicates initial point

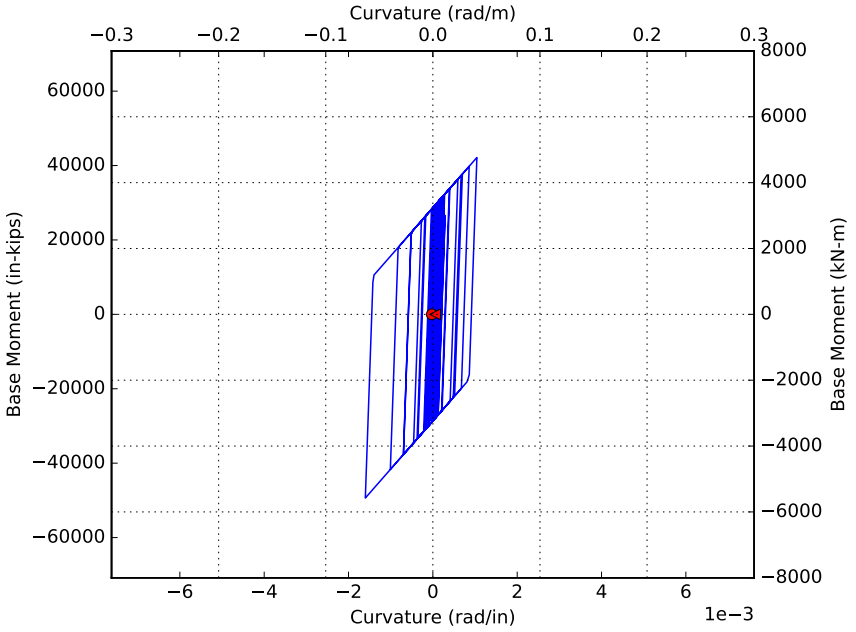

Figure M.8: Moment curvature response of model 3 for EQ8. Red circle indicates initial point

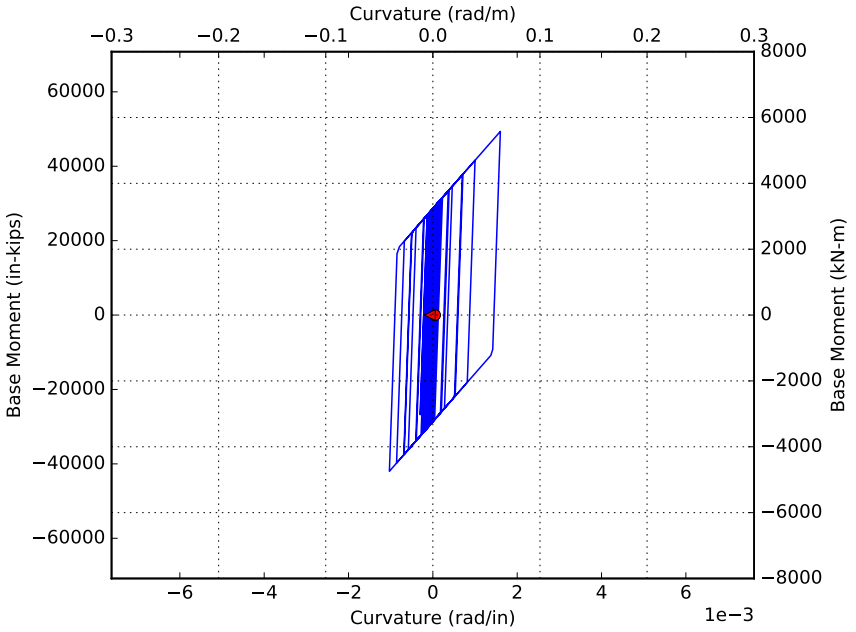

Figure M.9: Moment curvature response of model 3 for EQ9. Red circle indicates initial point

Appendix N

Model 4a Moment Curvature Plots

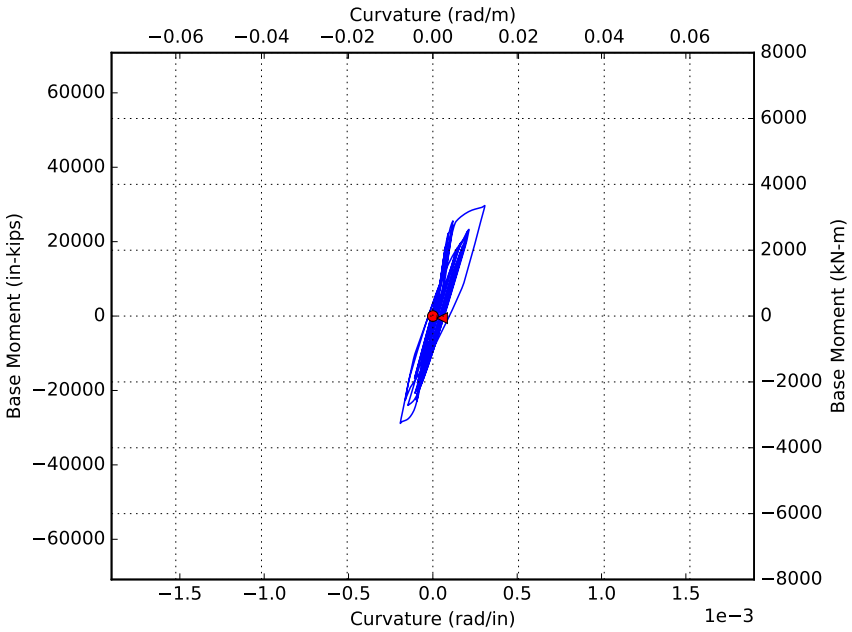

Figure N.1: Moment curvature response of model 4a for EQ1. Red circle indicates initial point

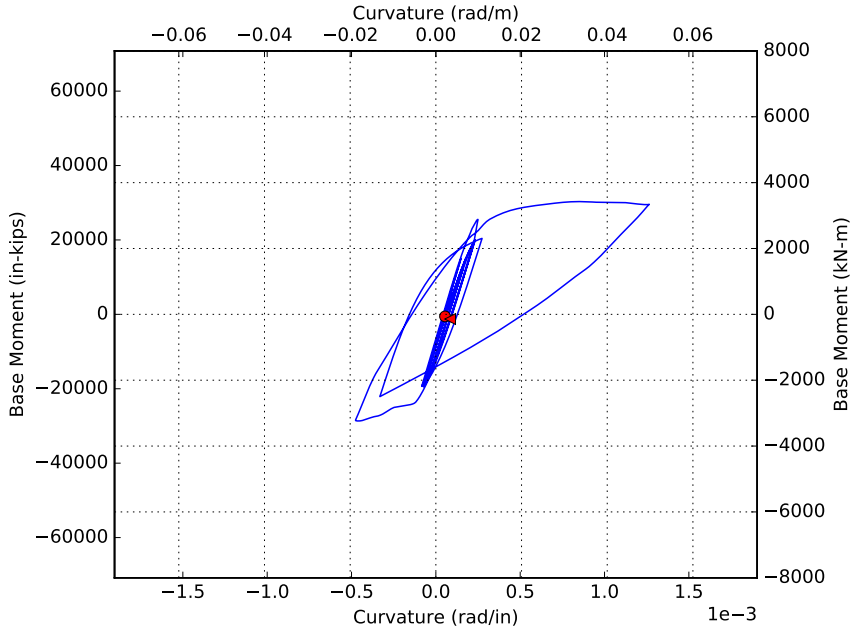

Figure N.2: Moment curvature response of model 4a for EQ2. Red circle indicates initial point

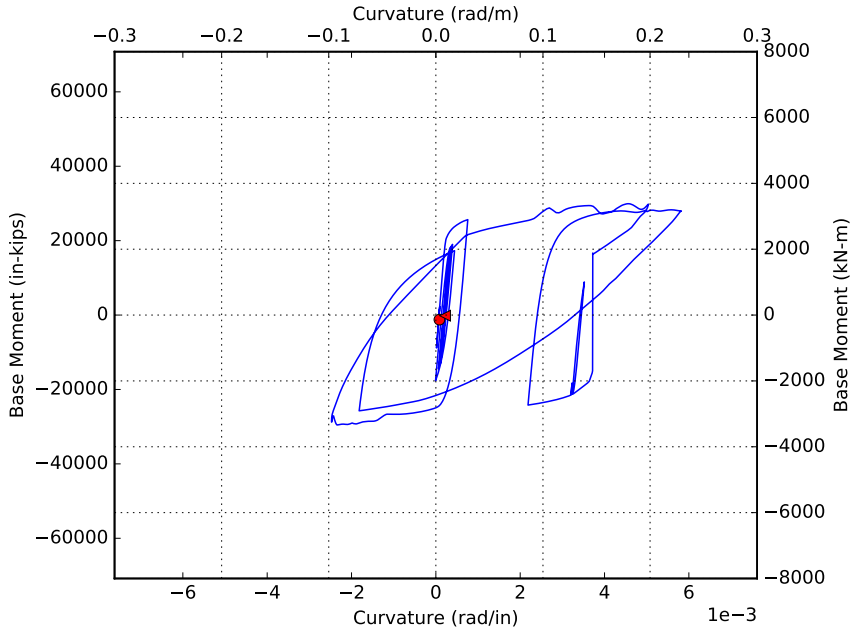

Figure N.3: Moment curvature response of model 4a for EQ3. Red circle indicates initial point

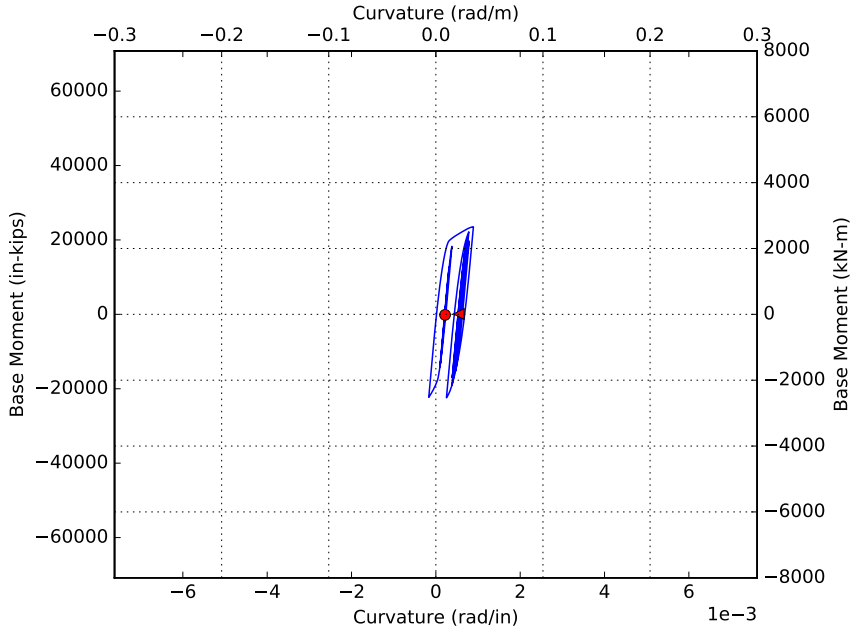

Figure N.4: Moment curvature response of model 4a for EQ4. Red circle indicates initial point

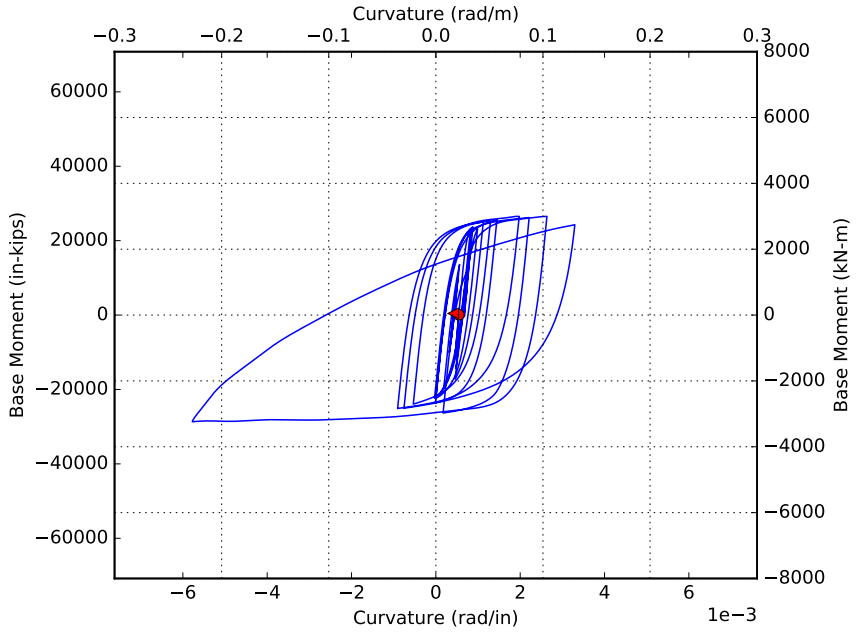

Figure N.5: Moment curvature response of model 4a for EQ5. Red circle indicates initial point

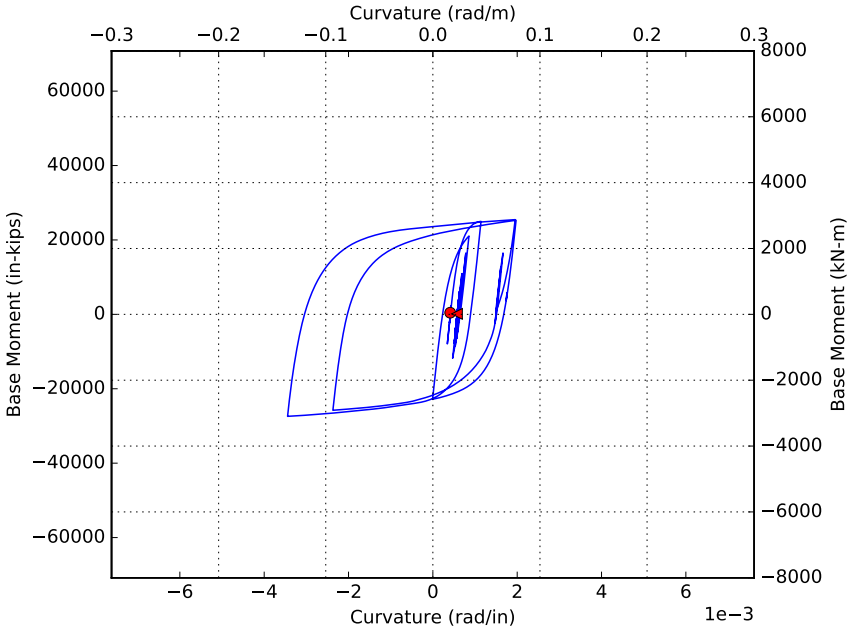

Figure N.6: Moment curvature response of model 4a for EQ6. Red circle indicates initial point

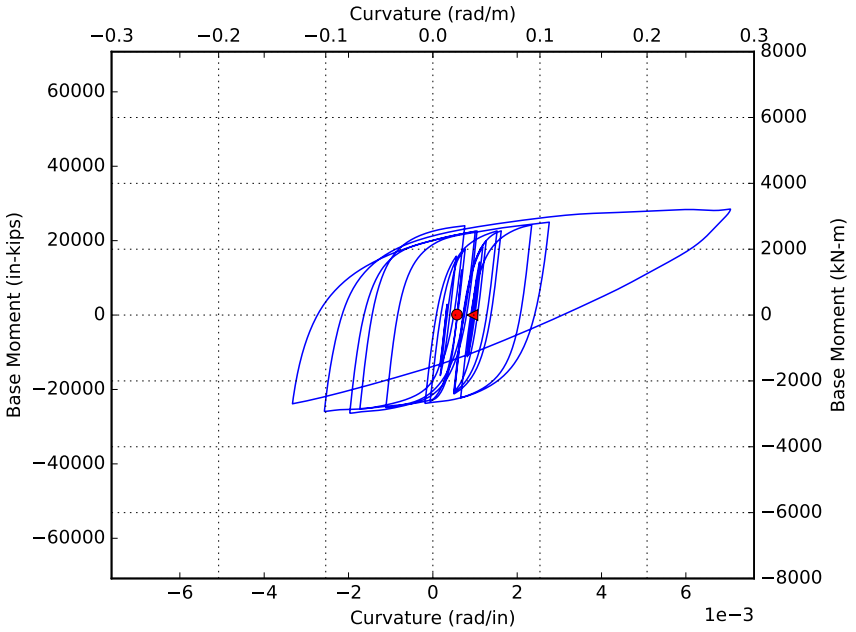

Figure N.7: Moment curvature response of model 4a for EQ7. Red circle indicates initial point

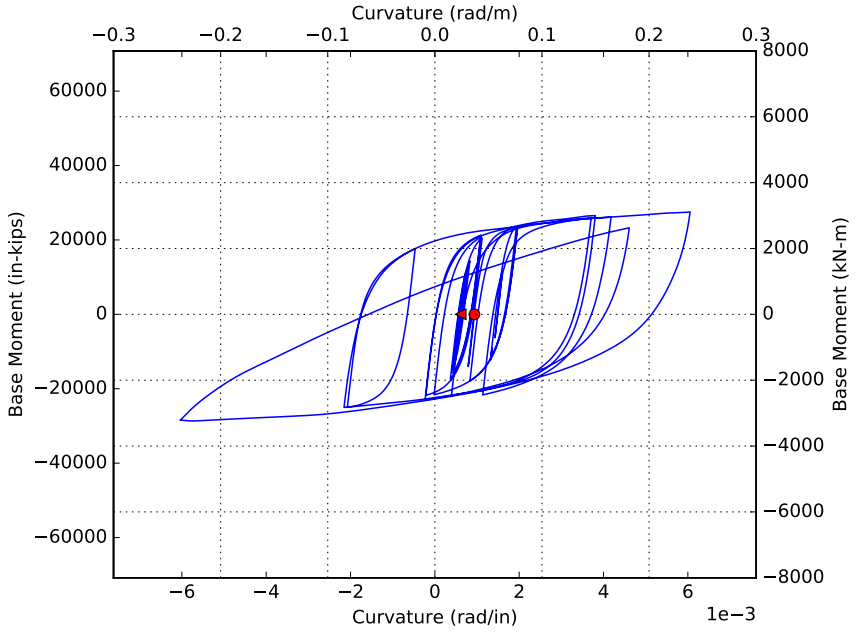

Figure N.8: Moment curvature response of model 4a for EQ8. Red circle indicates initial point

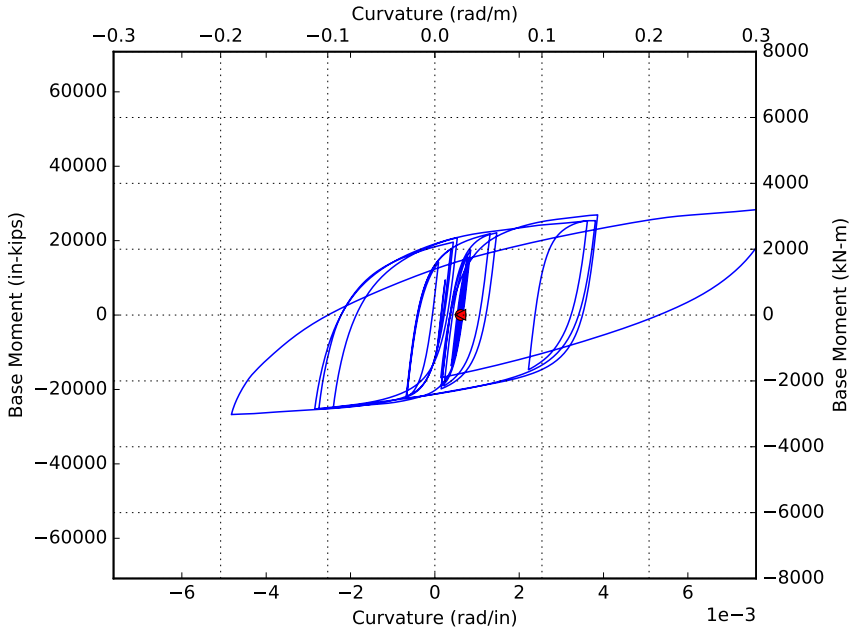

Figure N.9: Moment curvature response of model 4a for EQ9. Red circle indicates initial point

Appendix O

Model 4b Moment Curvature Plots

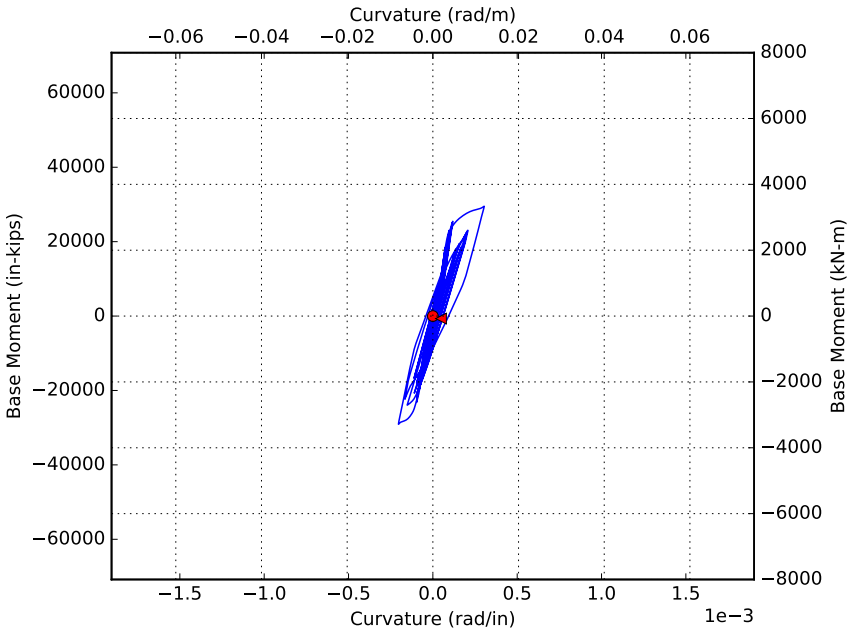

Figure O.1: Moment curvature response of model 4b for EQ1. Red circle indicates initial point

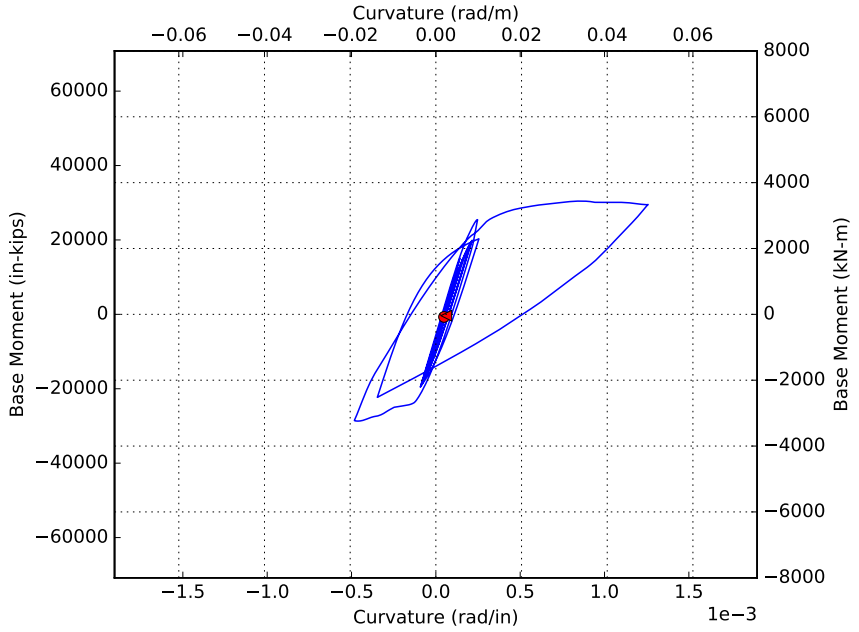

Figure O.2: Moment curvature response of model 4b for EQ2. Red circle indicates initial point

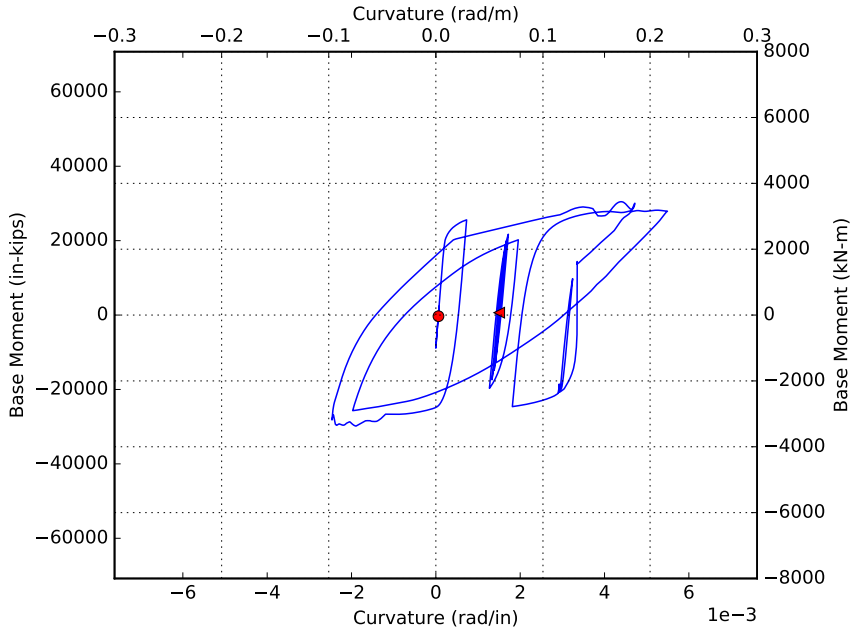

Figure O.3: Moment curvature response of model 4b for EQ3. Red circle indicates initial point

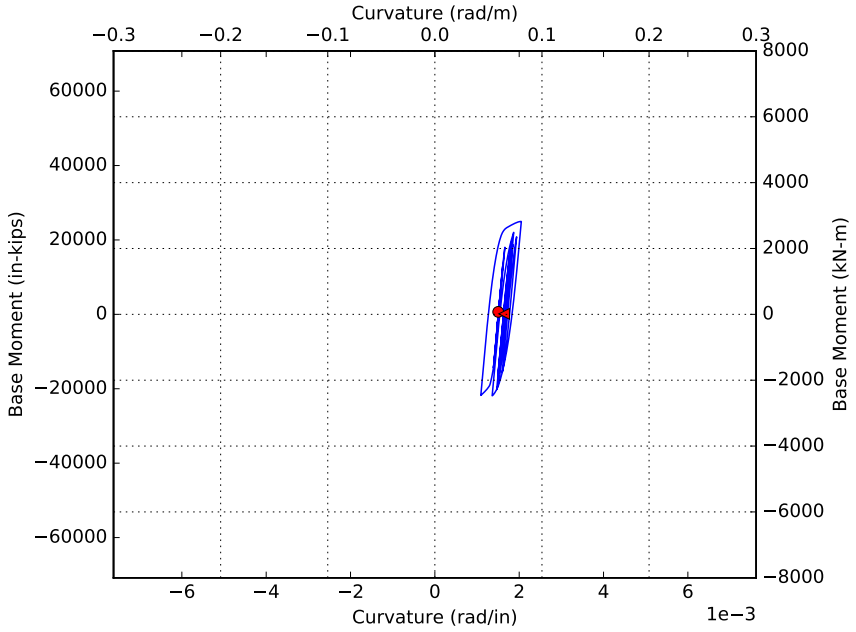

Figure O.4: Moment curvature response of model 4b for EQ4. Red circle indicates initial point

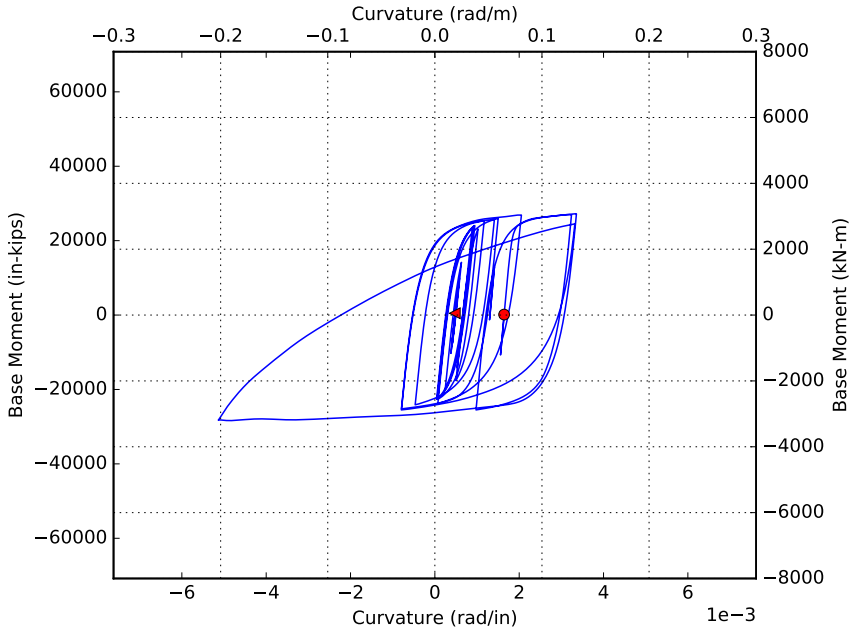

Figure O.5: Moment curvature response of model 4b for EQ5. Red circle indicates initial point

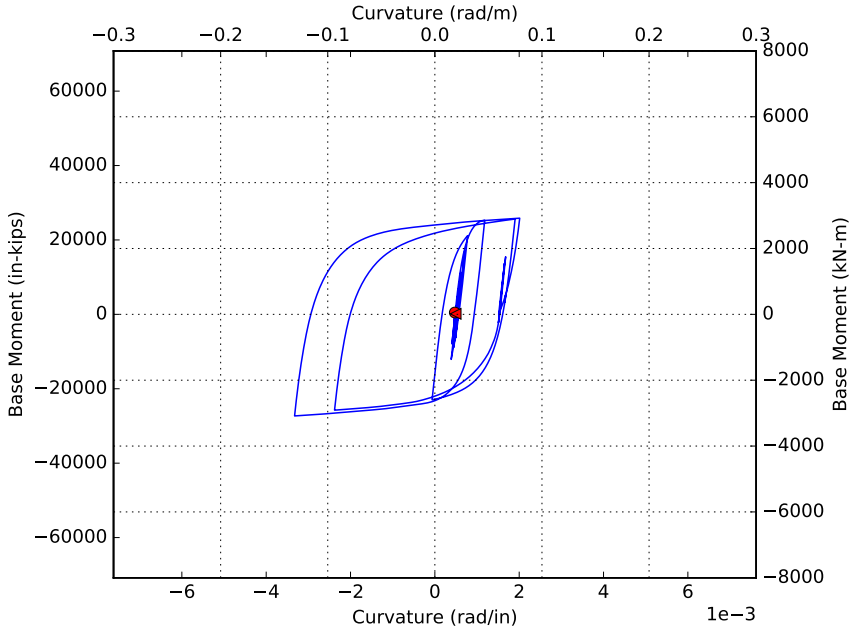

Figure O.6: Moment curvature response of model 4b for EQ6. Red circle indicates initial point

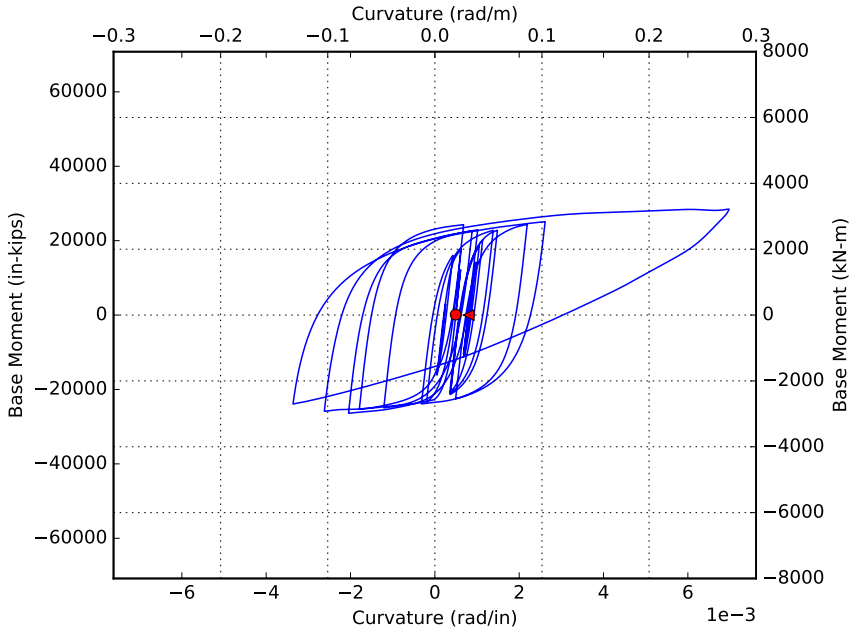

Figure O.7: Moment curvature response of model 4b for EQ7. Red circle indicates initial point

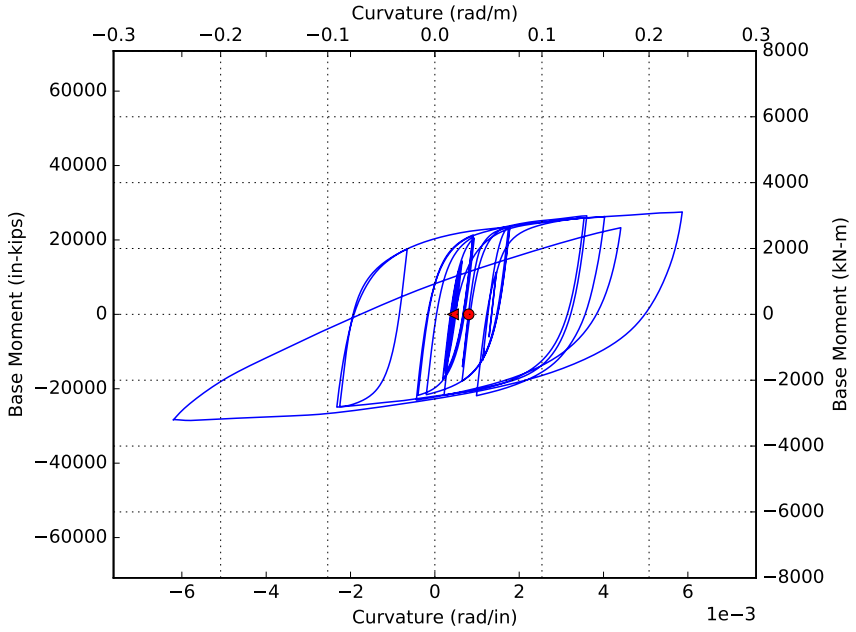

Figure O.8: Moment curvature response of model 4b for EQ8. Red circle indicates initial point

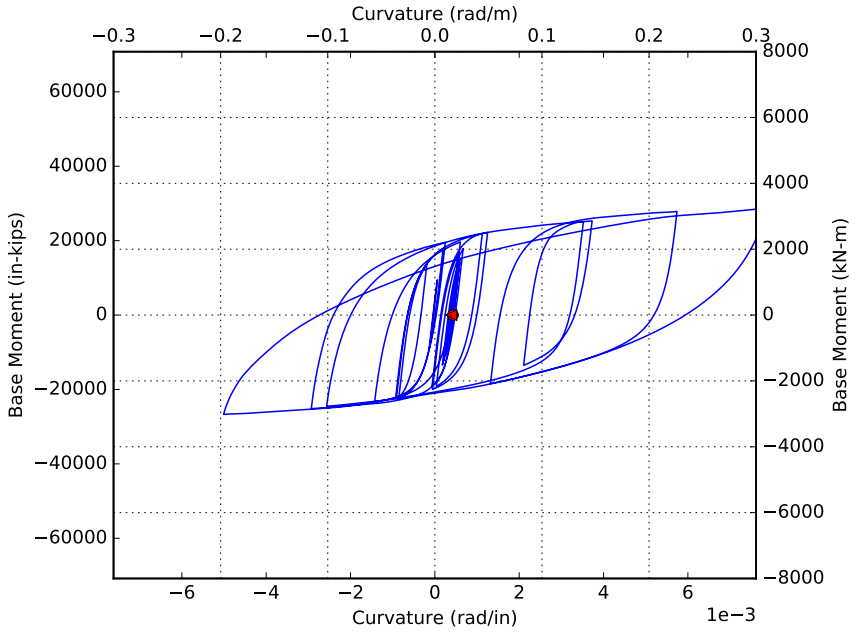

Figure O.9: Moment curvature response of model 4b for EQ9. Red circle indicates initial point

Appendix P

Model 4c Moment Curvature Plots

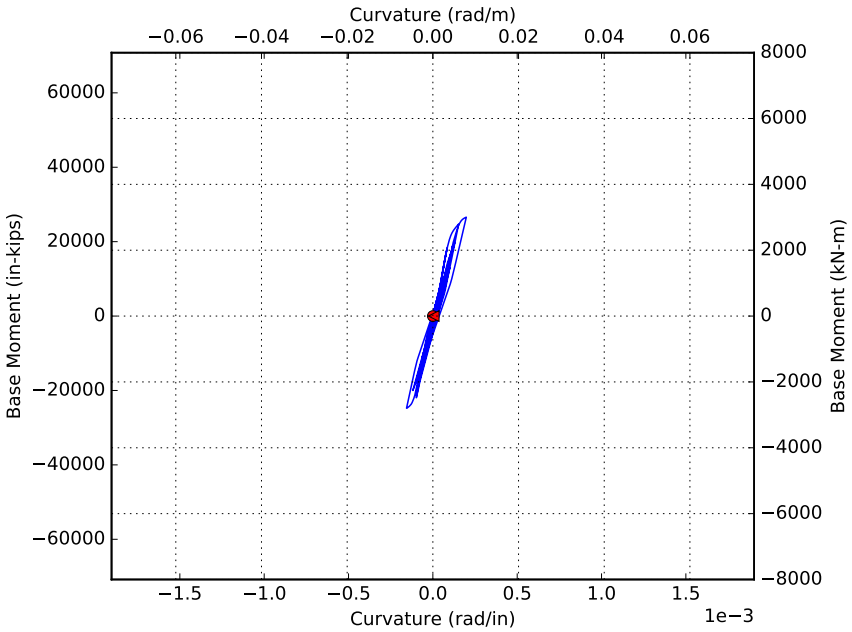

Figure P.1: Moment curvature response of model 4c for EQ1. Red circle indicates initial point

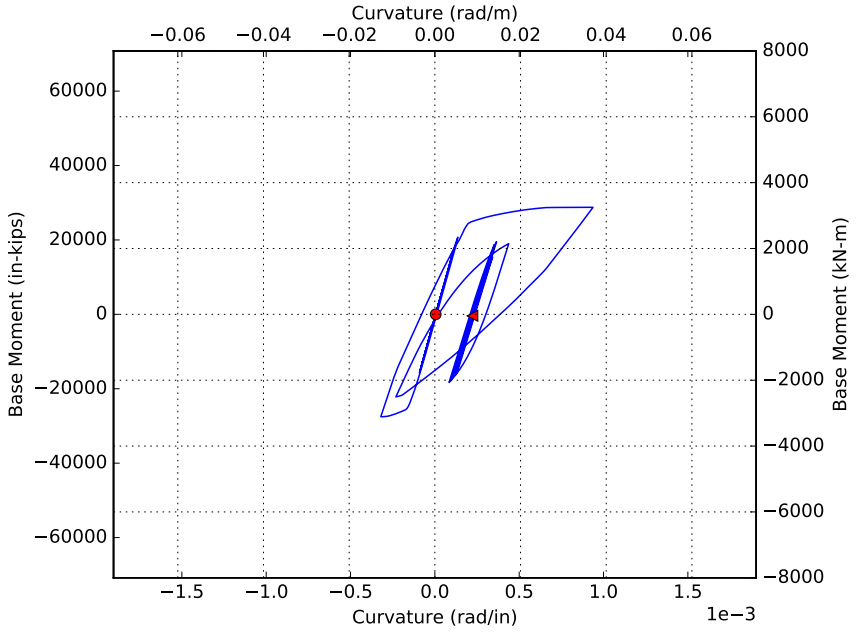

Figure P.2: Moment curvature response of model 4c for EQ2. Red circle indicates initial point

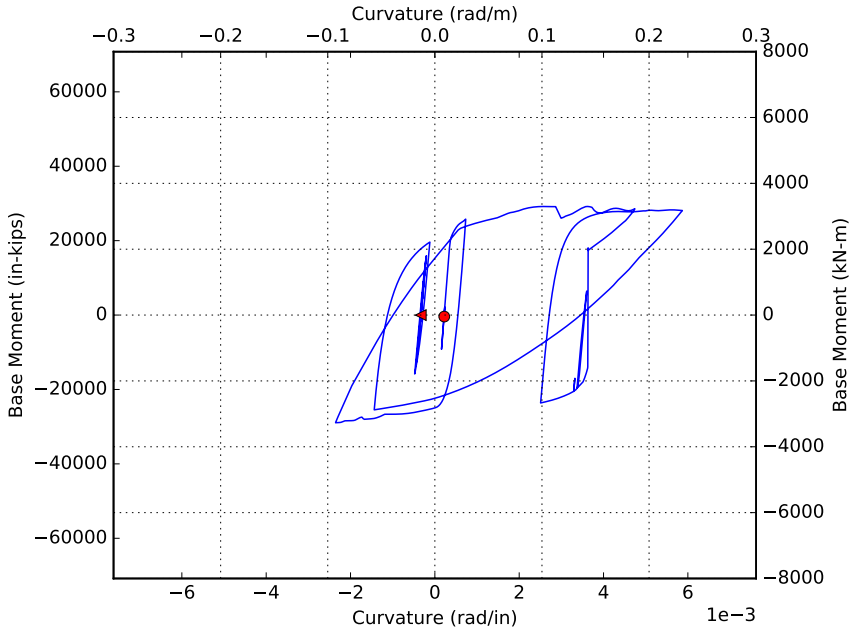

Figure P.3: Moment curvature response of model 4c for EQ3. Red circle indicates initial point

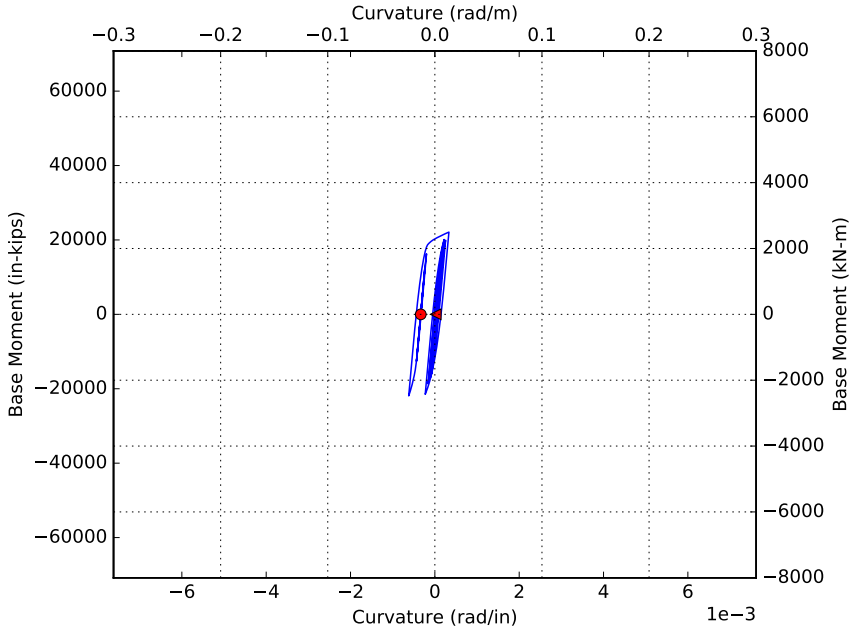

Figure P.4: Moment curvature response of model 4c for EQ4. Red circle indicates initial point

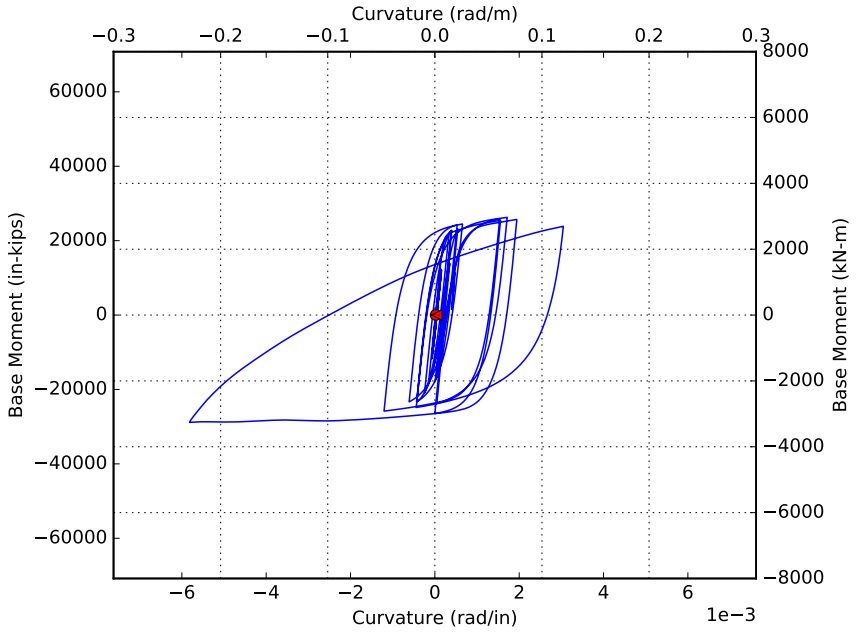

Figure P.5: Moment curvature response of model 4c for EQ5. Red circle indicates initial point

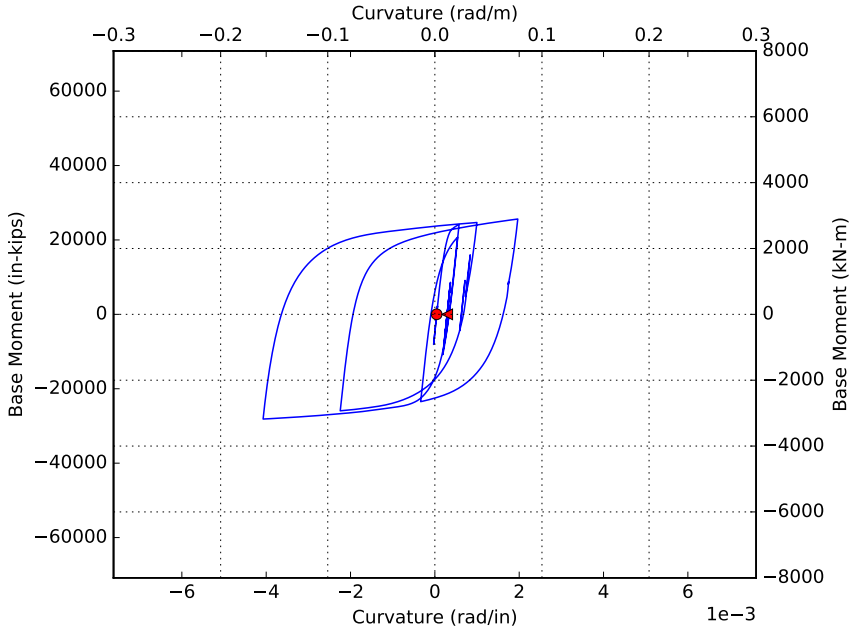

Figure P.6: Moment curvature response of model 4c for EQ6. Red circle indicates initial point

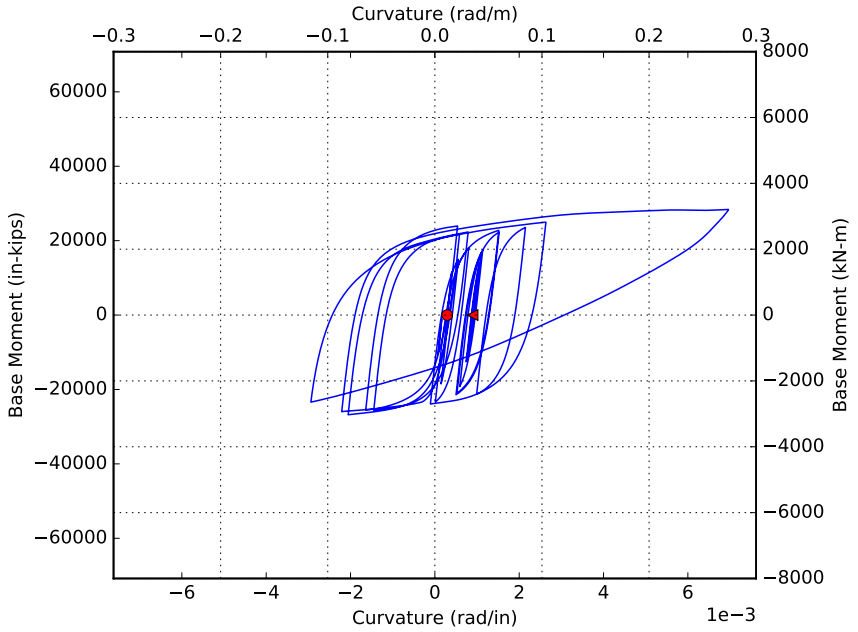

Figure P.7: Moment curvature response of model 4c for EQ7. Red circle indicates initial point

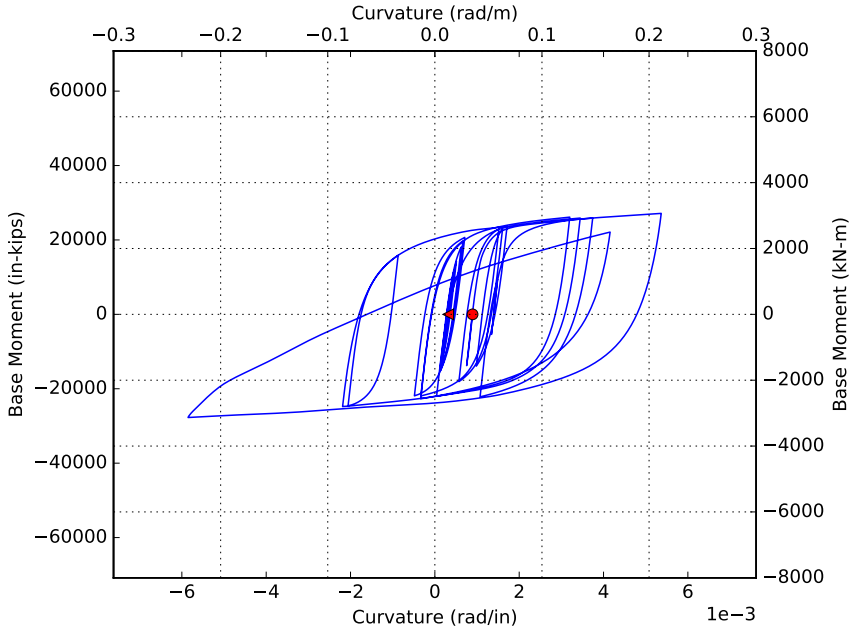

Figure P.8: Moment curvature response of model 4c for EQ8. Red circle indicates initial point

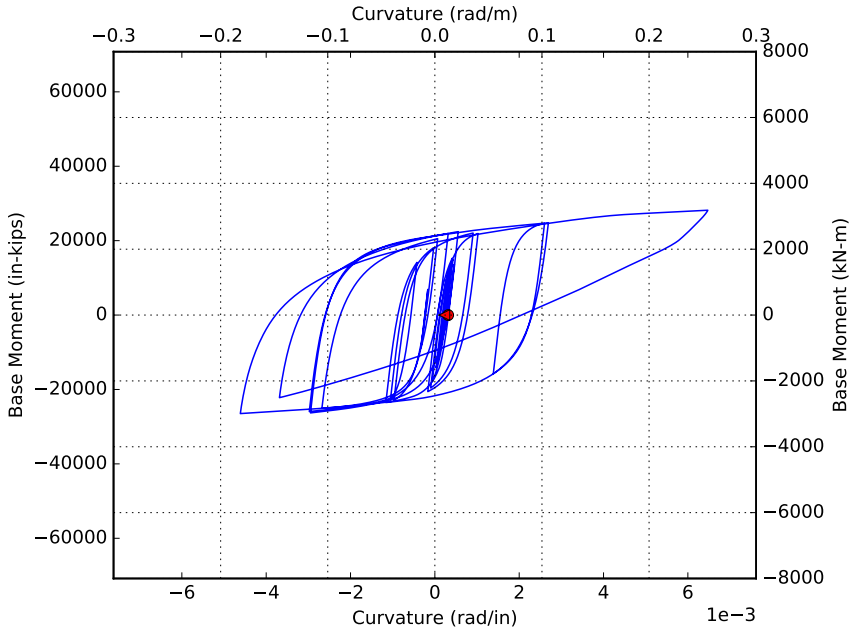

Figure P.9: Moment curvature response of model 4c for EQ9. Red circle indicates initial point

Appendix Q

Model 4d Moment Curvature Plots

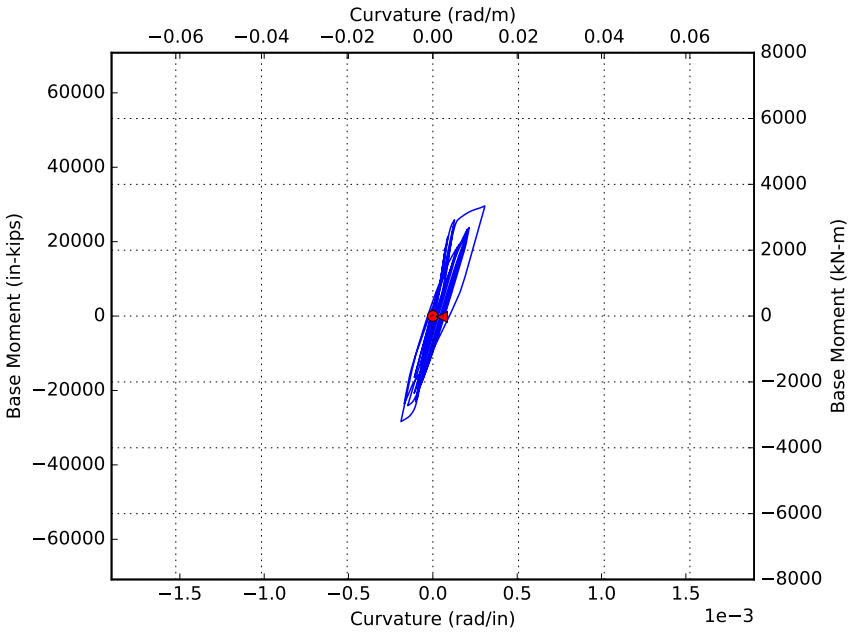

Figure Q.1: Moment curvature response of model 4d for EQ1. Red circle indicates initial point

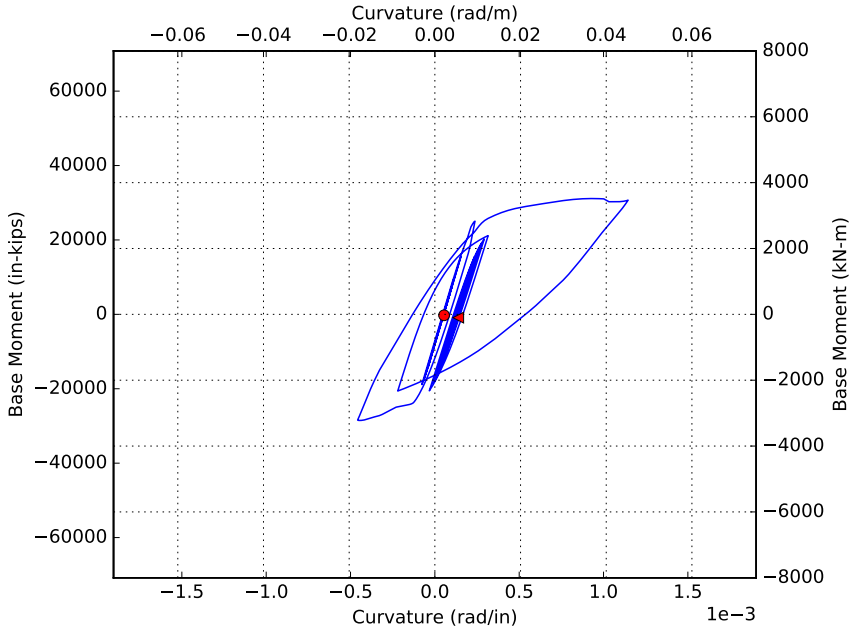

Figure Q.2: Moment curvature response of model 4d for EQ2. Red circle indicates initial point

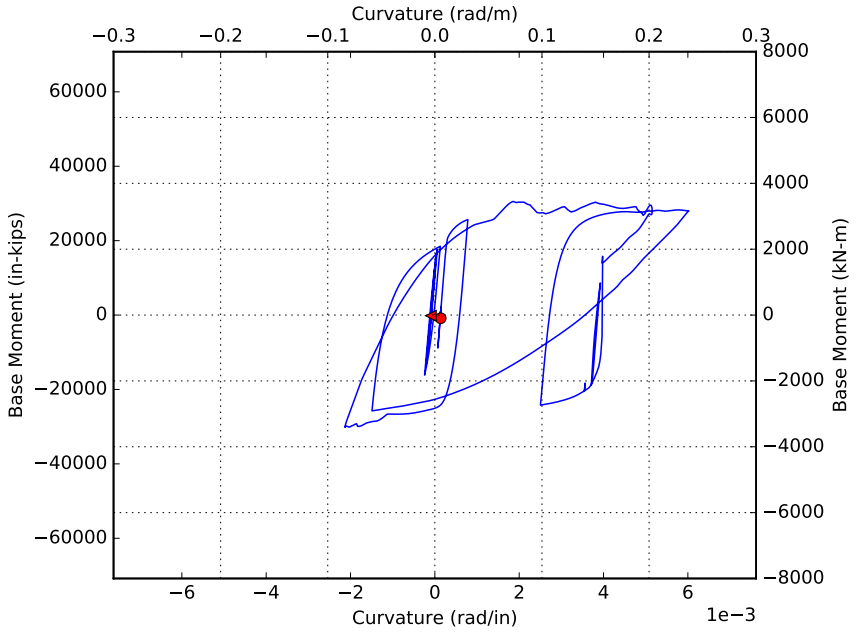

Figure Q.3: Moment curvature response of model 4d for EQ3. Red circle indicates initial point

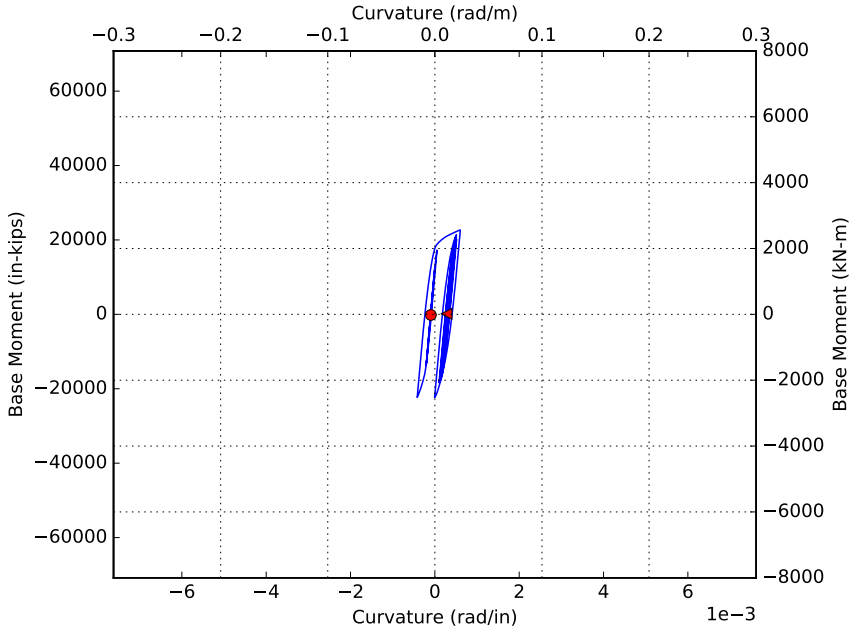

Figure Q.4: Moment curvature response of model 4d for EQ4. Red circle indicates initial point

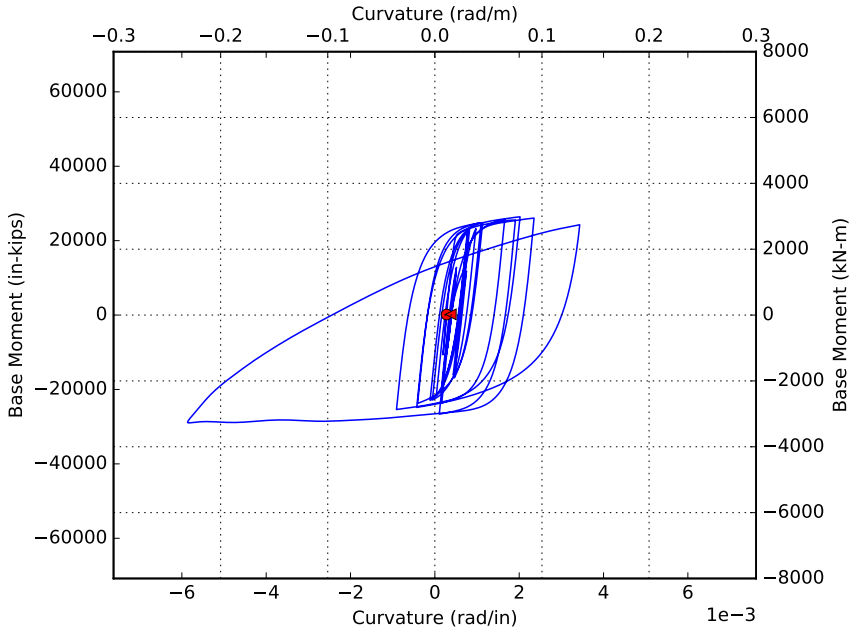

Figure Q.5: Moment curvature response of model 4d for EQ5. Red circle indicates initial point

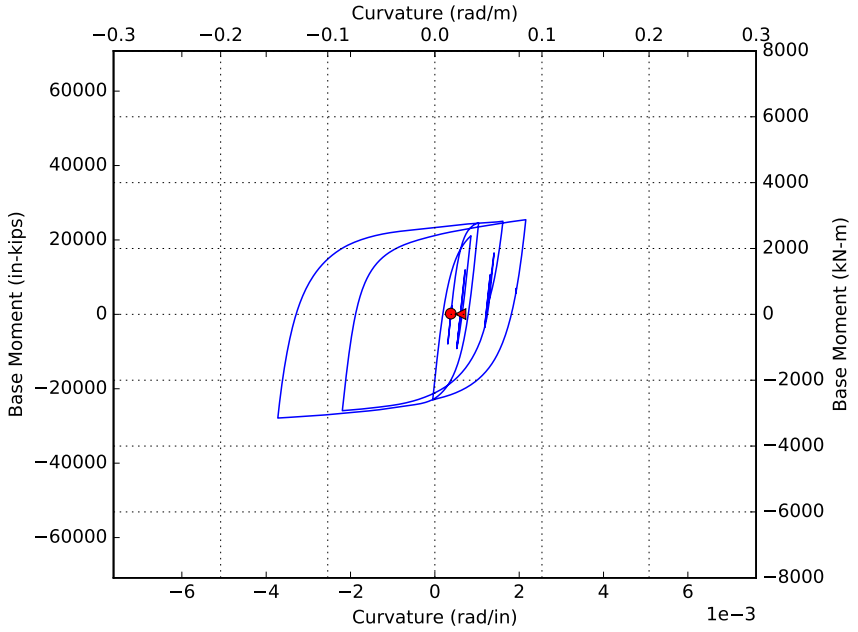

Figure Q.6: Moment curvature response of model 4d for EQ6. Red circle indicates initial point

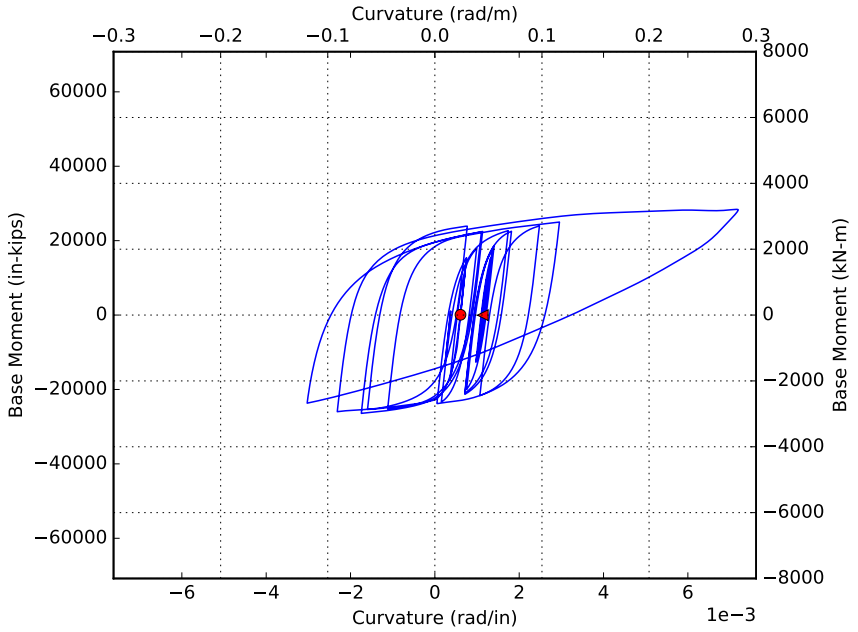

Figure Q.7: Moment curvature response of model 4d for EQ7. Red circle indicates initial point

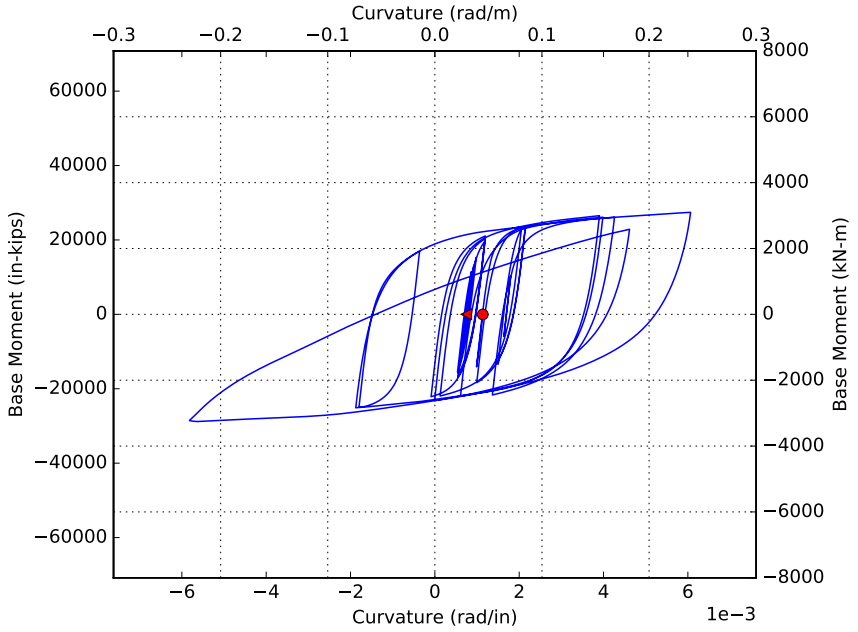

Figure Q.8: Moment curvature response of model 4d for EQ8. Red circle indicates initial point

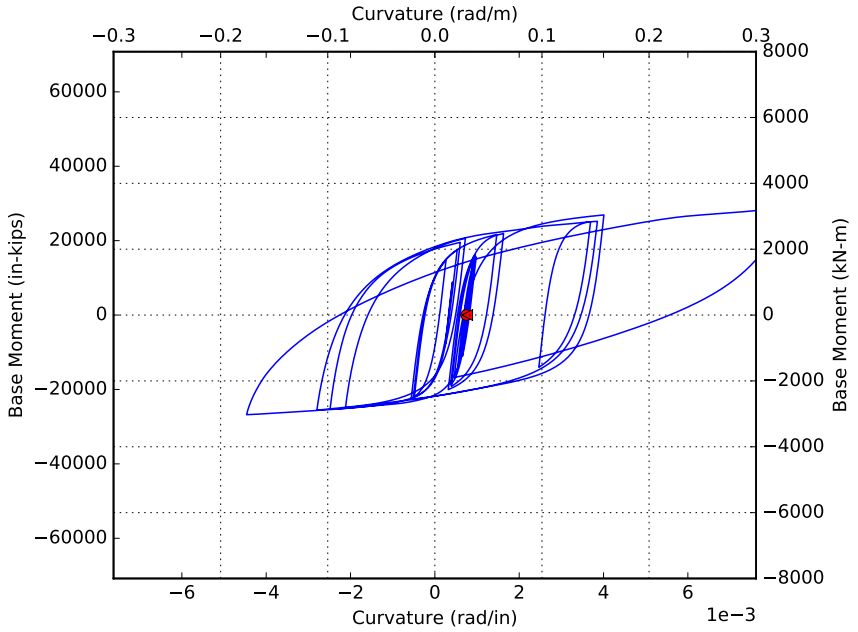

Figure Q.9: Moment curvature response of model 4d for EQ9. Red circle indicates initial point

Appendix R

Model 5a Moment Curvature Plots

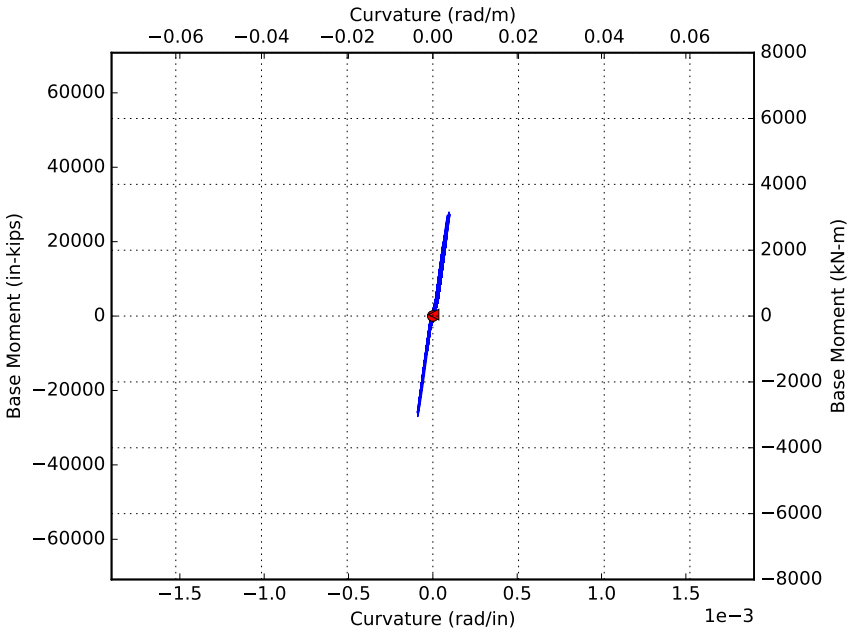

Figure R.1: Moment curvature response of model 5a for EQ1. Red circle indicates initial point

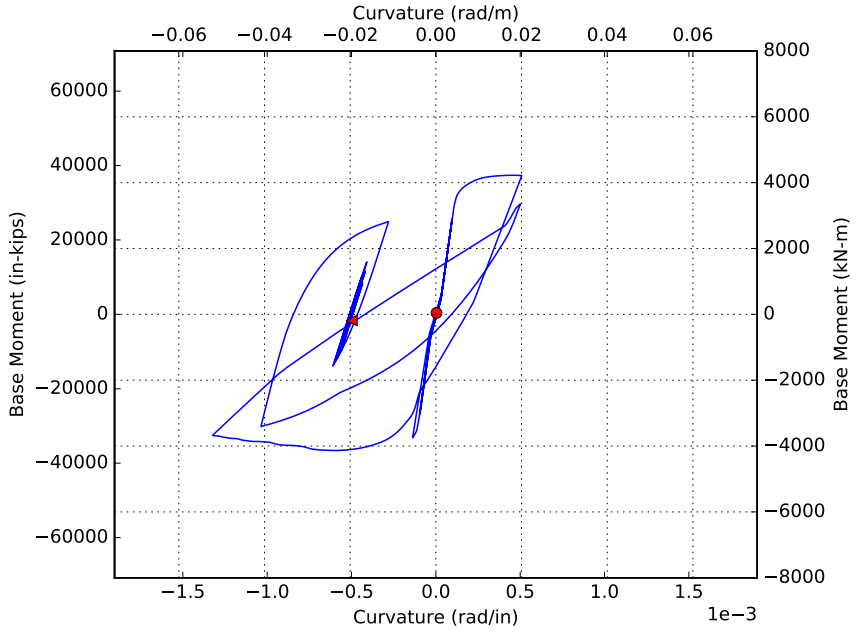

Figure R.2: Moment curvature response of model 5a for EQ2. Red circle indicates initial point

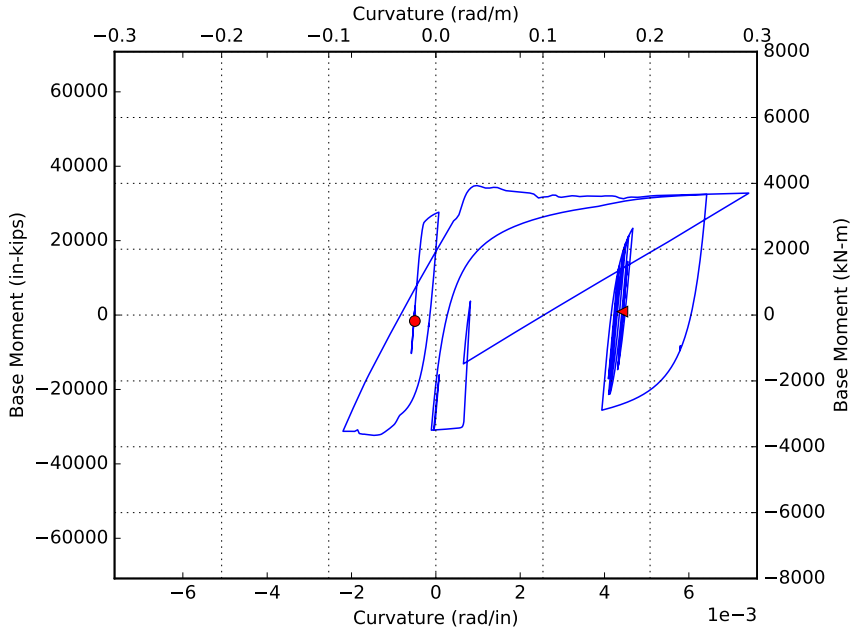

Figure R.3: Moment curvature response of model 5a for EQ3. Red circle indicates initial point

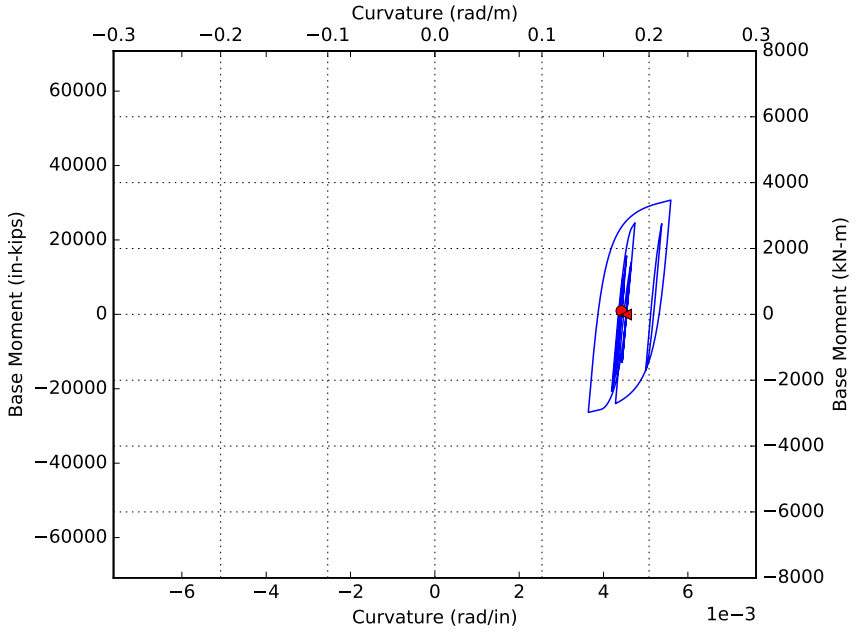

Figure R.4: Moment curvature response of model 5a for EQ4. Red circle indicates initial point

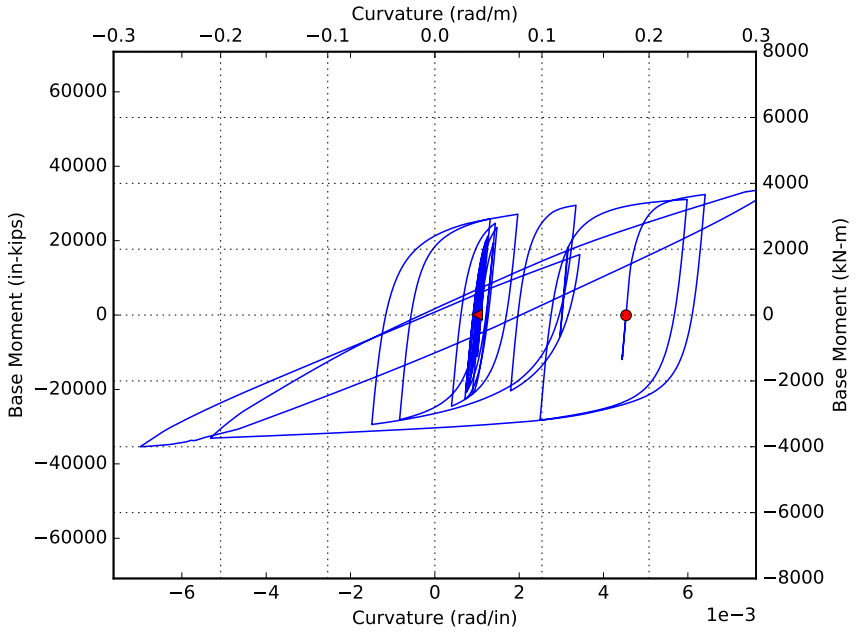

Figure R.5: Moment curvature response of model 5a for EQ5. Red circle indicates initial point

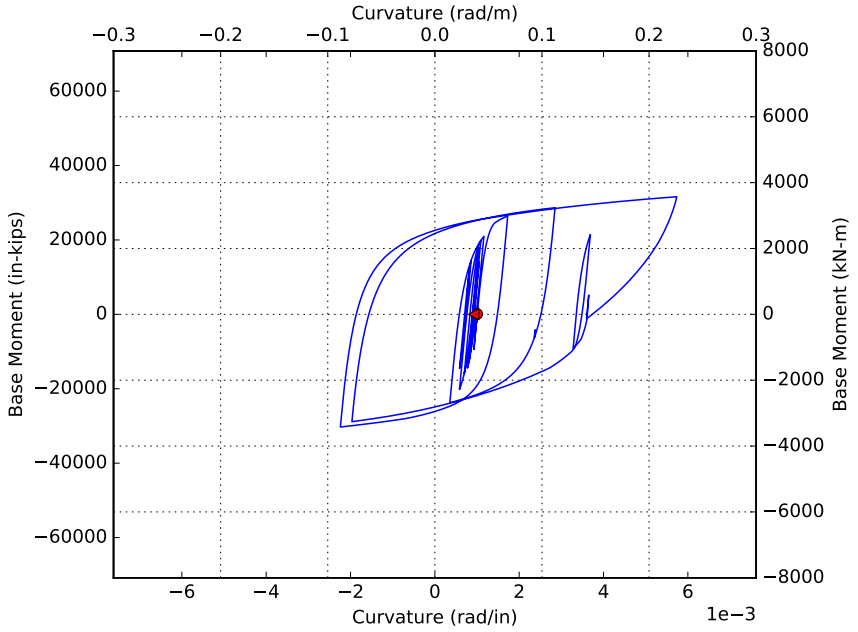

Figure R.6: Moment curvature response of model 5a for EQ6. Red circle indicates initial point

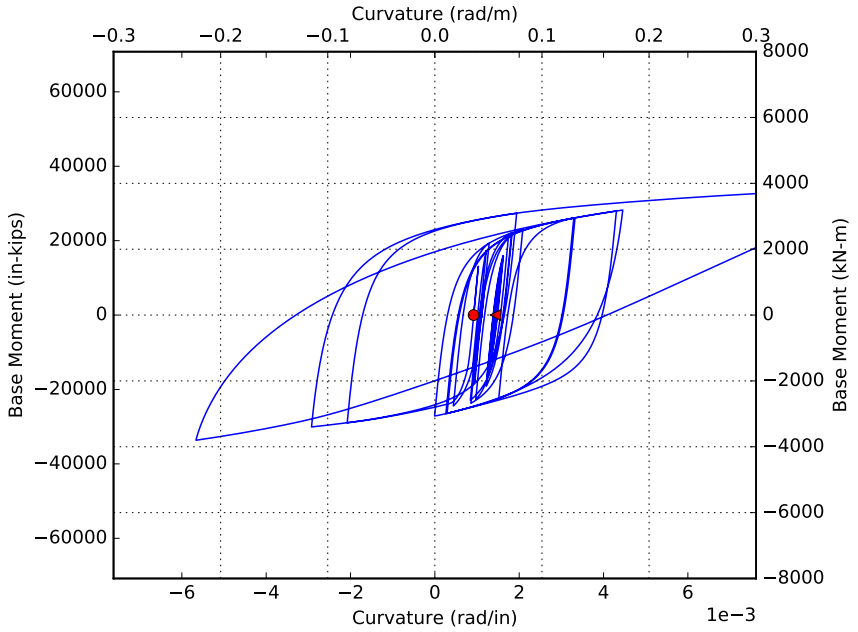

Figure R.7: Moment curvature response of model 5a for EQ7. Red circle indicates initial point

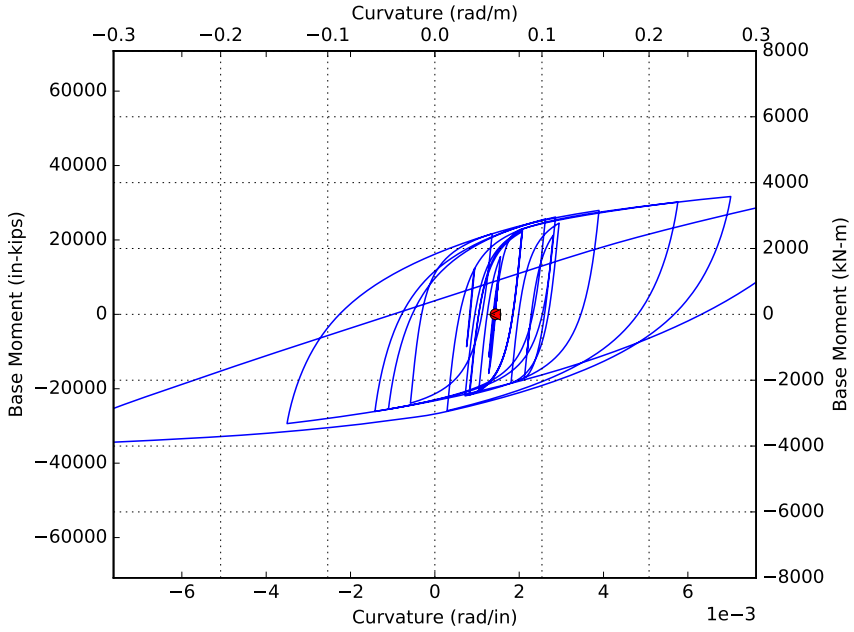

Figure R.8: Moment curvature response of model 5a for EQ8. Red circle indicates initial point

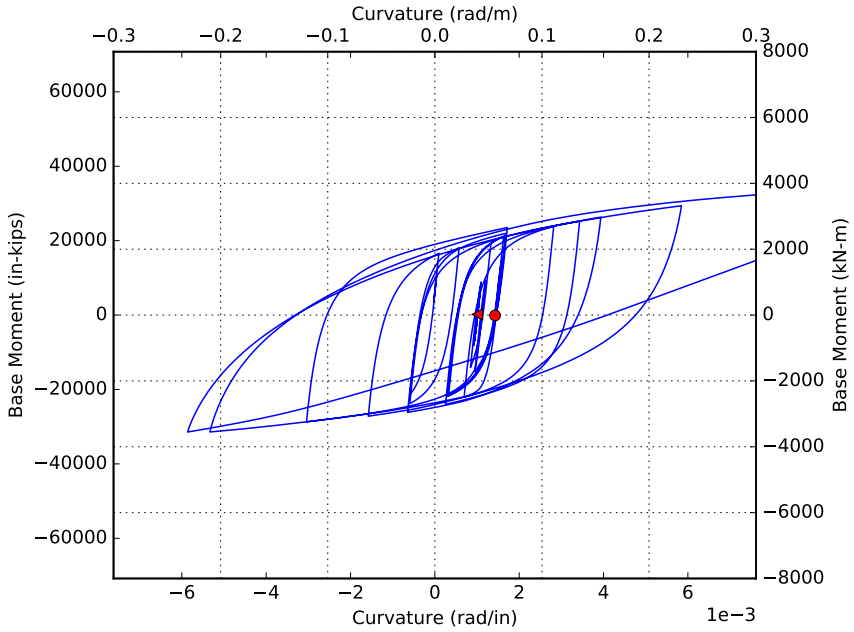

Figure R.9: Moment curvature response of model 5a for EQ9. Red circle indicates initial point

Appendix S

Model 5b Moment Curvature Plots

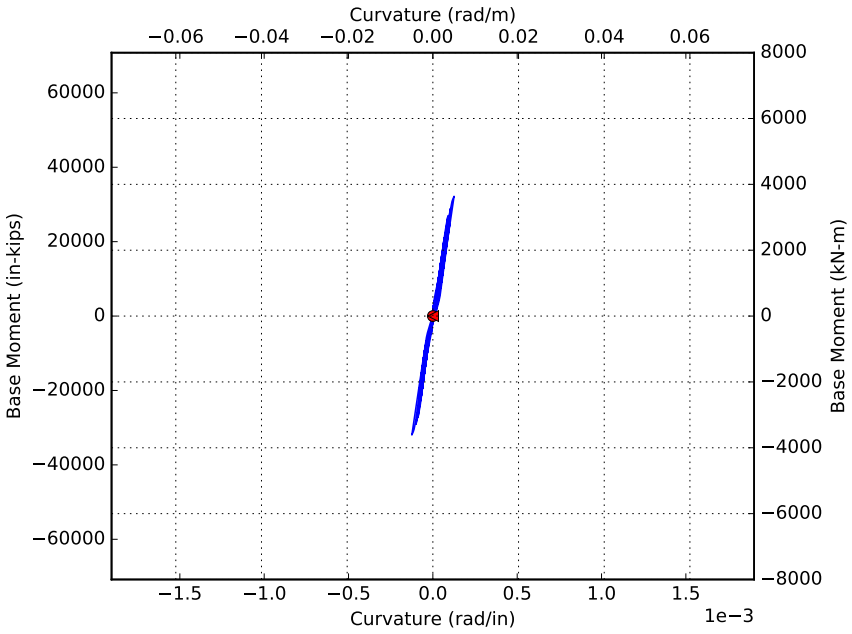

Figure S.1: Moment curvature response of model 5b for EQ1. Red circle indicates initial point

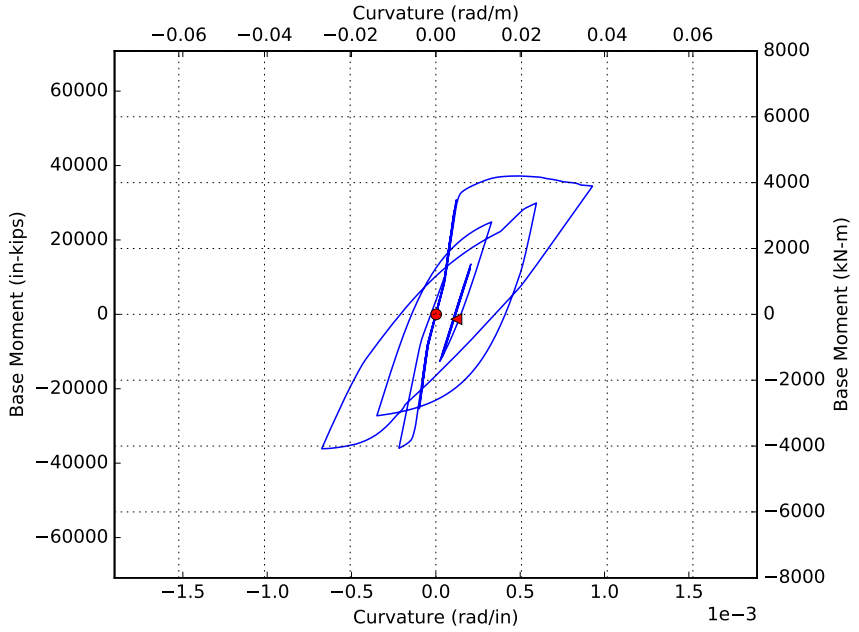

Figure S.2: Moment curvature response of model 5b for EQ2. Red circle indicates initial point

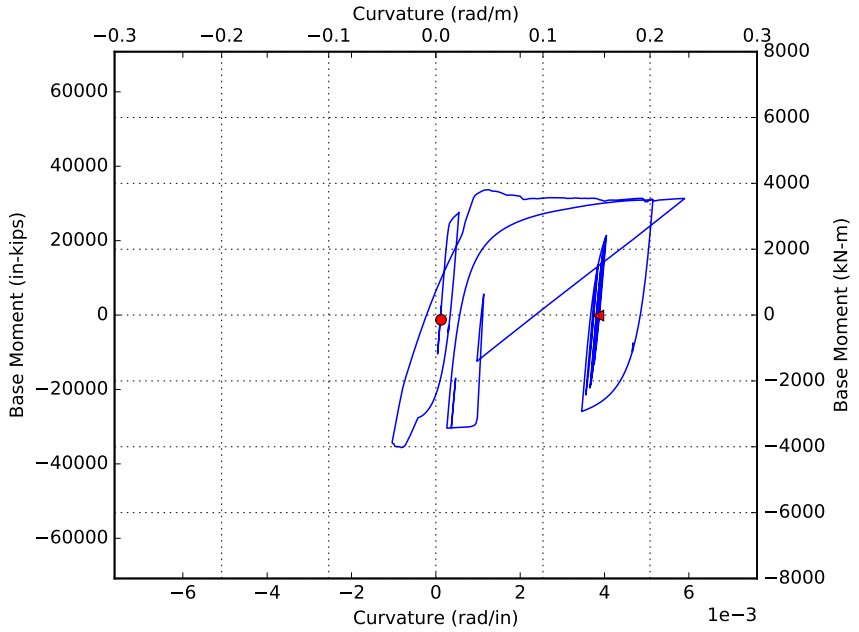

Figure S.3: Moment curvature response of model 5b for EQ3. Red circle indicates initial point

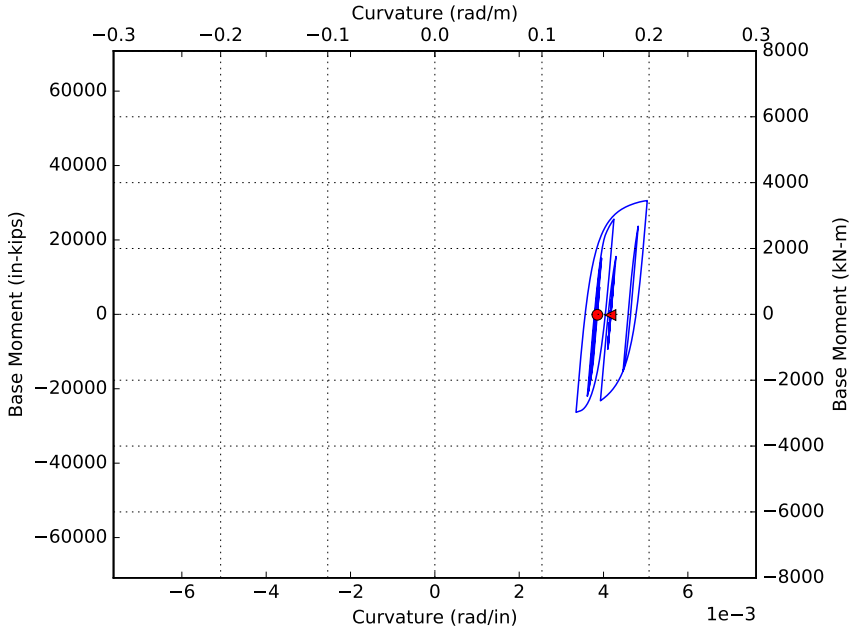

Figure S.4: Moment curvature response of model 5b for EQ4. Red circle indicates initial point

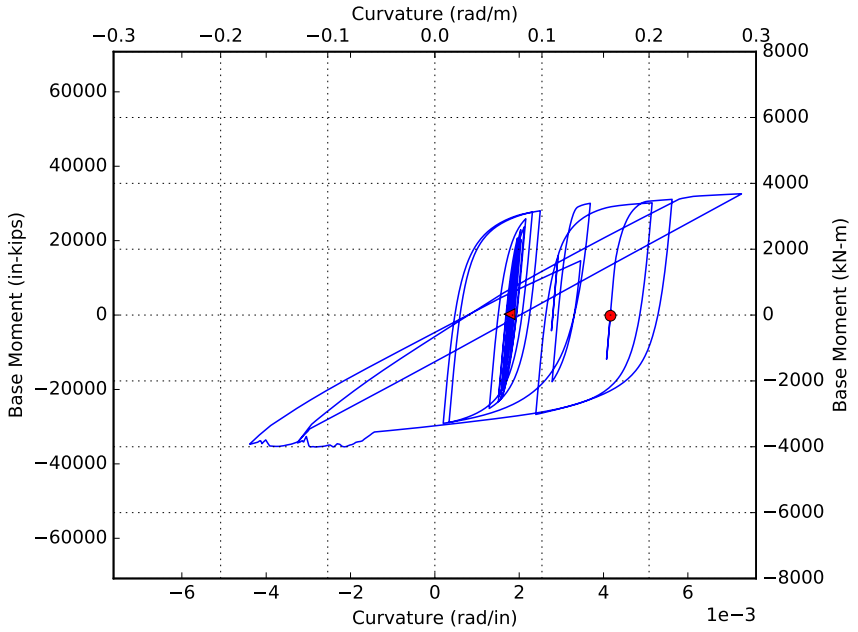

Figure S.5: Moment curvature response of model 5b for EQ5. Red circle indicates initial point

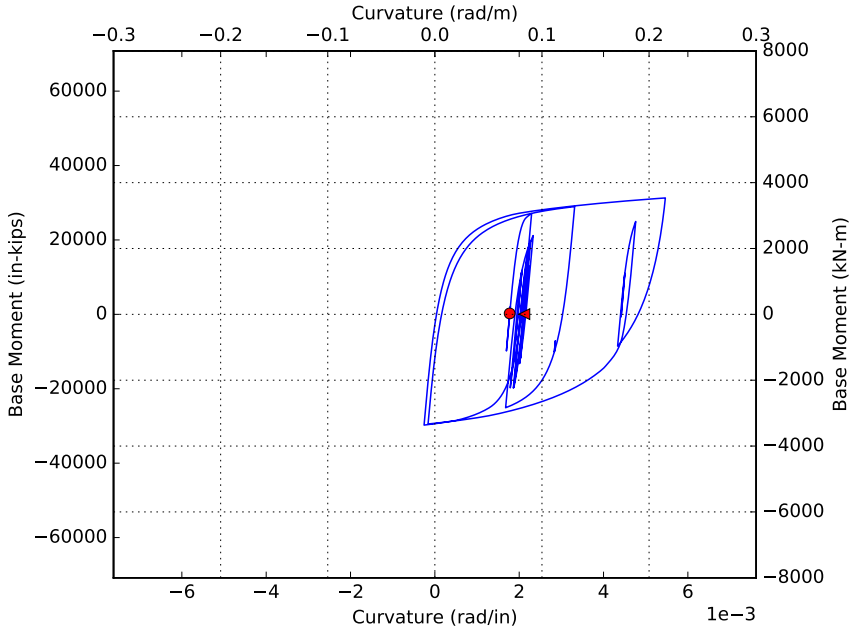

Figure S.6: Moment curvature response of model 5b for EQ6. Red circle indicates initial point

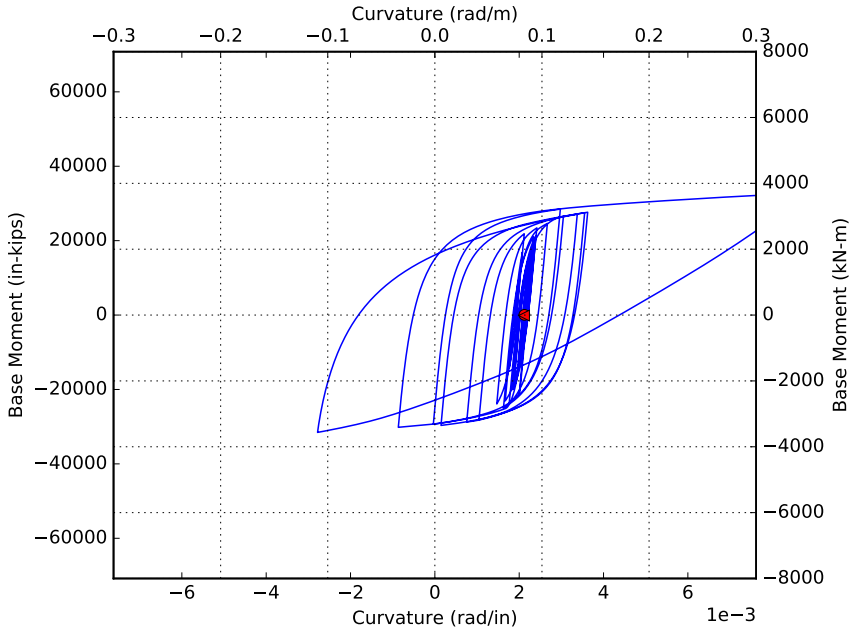

Figure S.7: Moment curvature response of model 5b for EQ7. Red circle indicates initial point

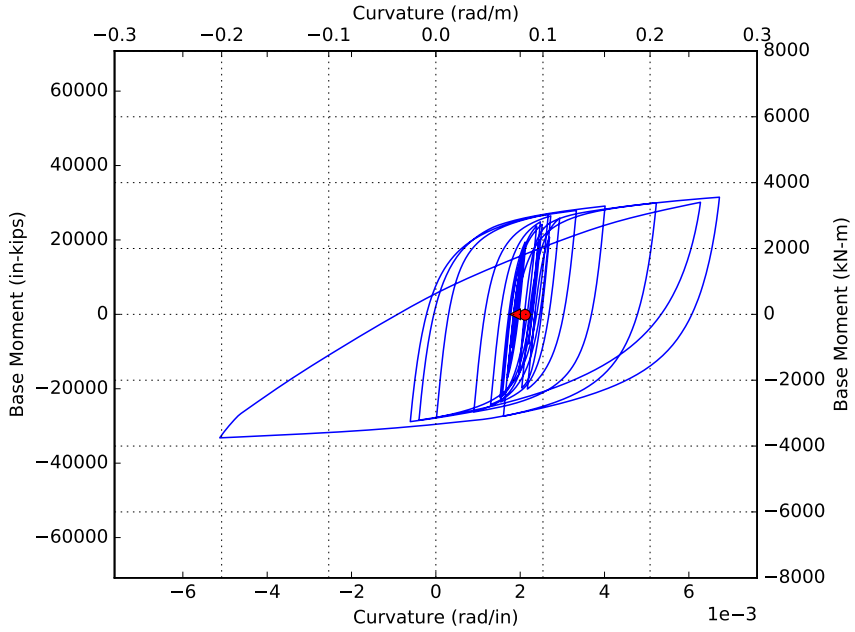

Figure S.8: Moment curvature response of model 5b for EQ8. Red circle indicates initial point

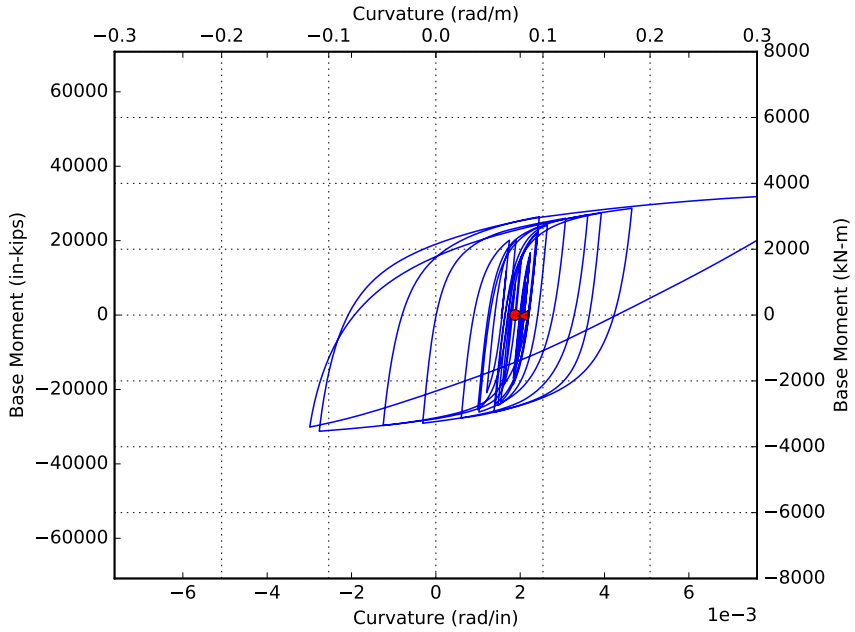

Figure S.9: Moment curvature response of model 5b for EQ9. Red circle indicates initial point

Appendix T

Model 5c Moment Curvature Plots

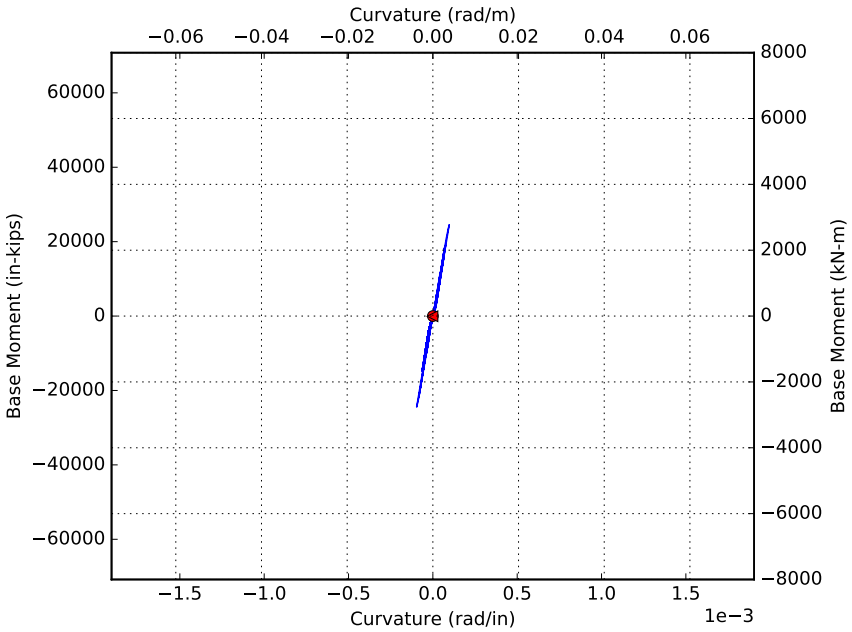

Figure T.1: Moment curvature response of model 5c for EQ1. Red circle indicates initial point

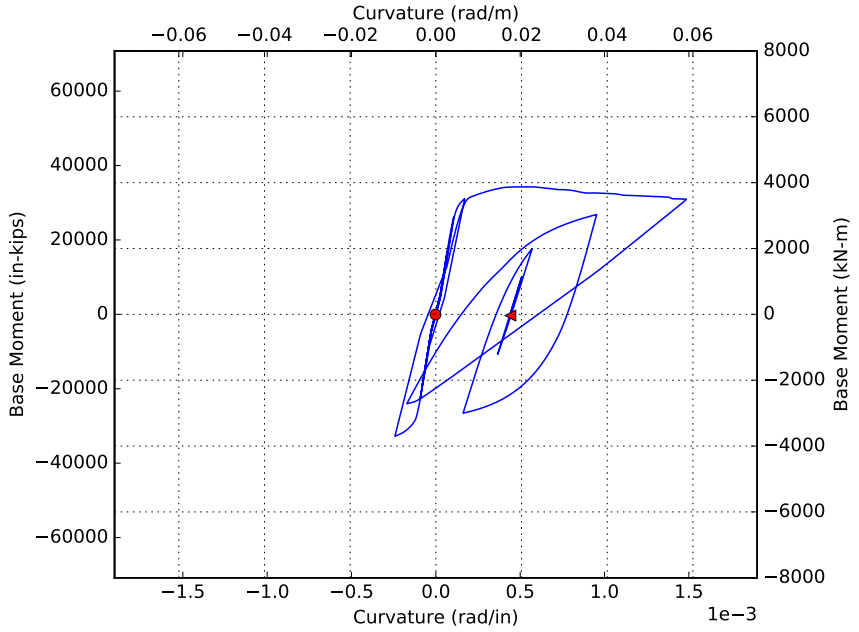

Figure T.2: Moment curvature response of model 5c for EQ2. Red circle indicates initial point

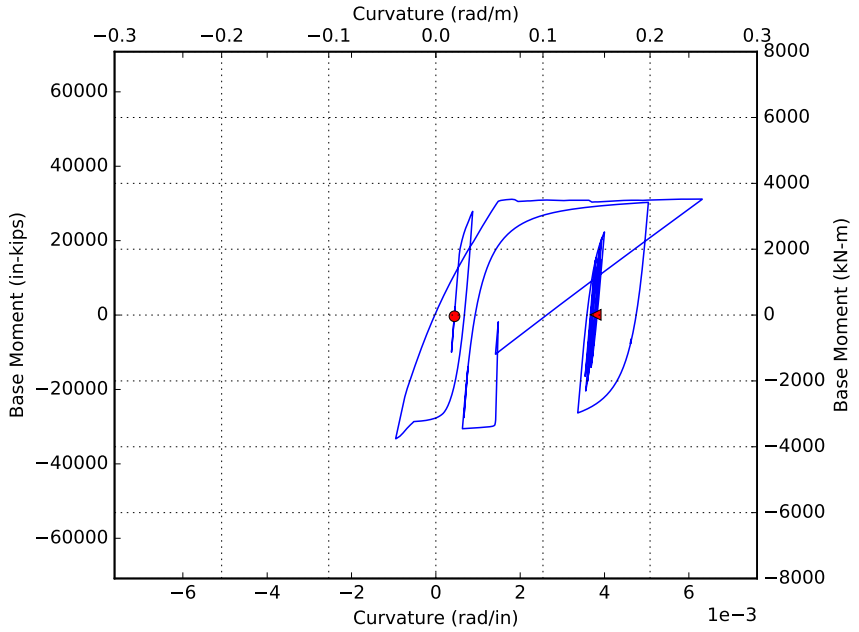

Figure T.3: Moment curvature response of model 5c for EQ3. Red circle indicates initial point

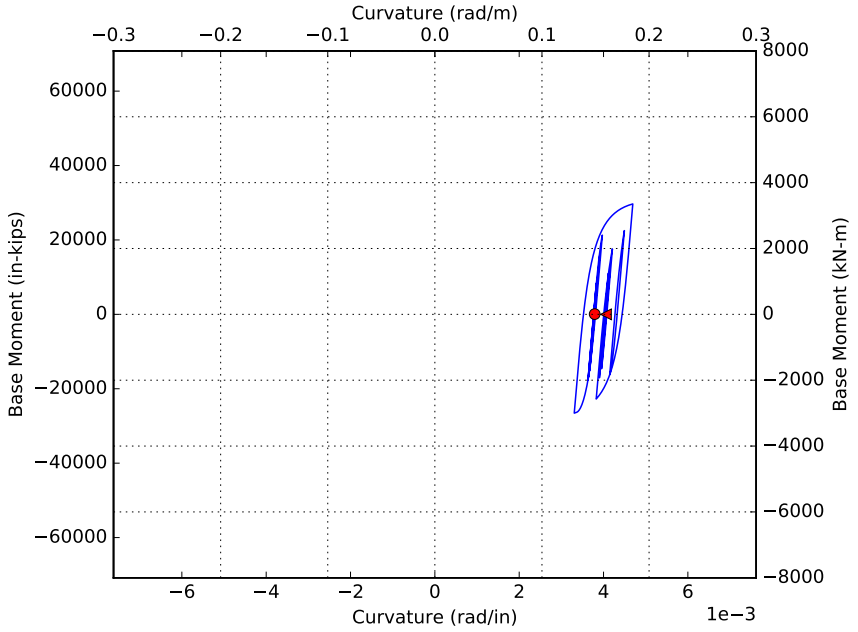

Figure T.4: Moment curvature response of model 5c for EQ4. Red circle indicates initial point

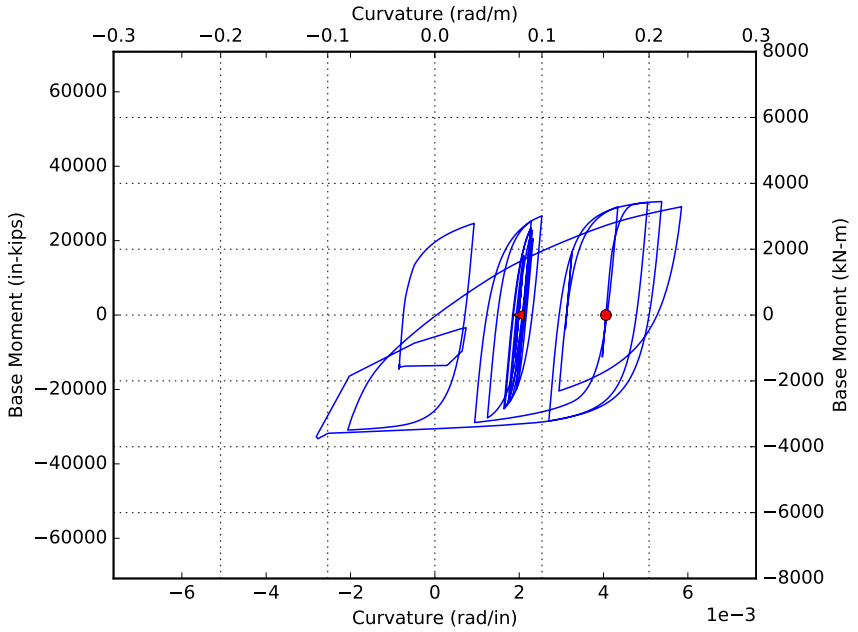

Figure T.5: Moment curvature response of model 5c for EQ5. Red circle indicates initial point

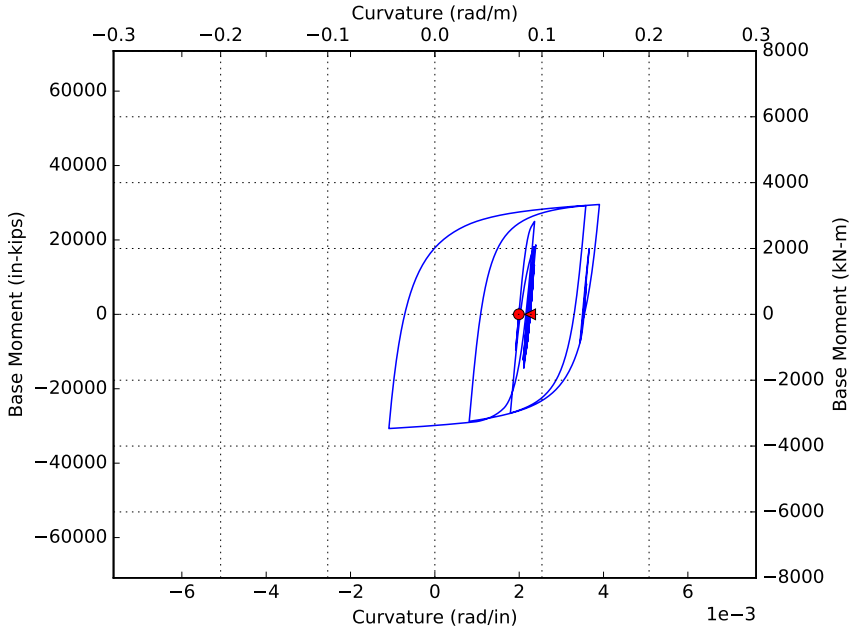

Figure T.6: Moment curvature response of model 5c for EQ6. Red circle indicates initial point

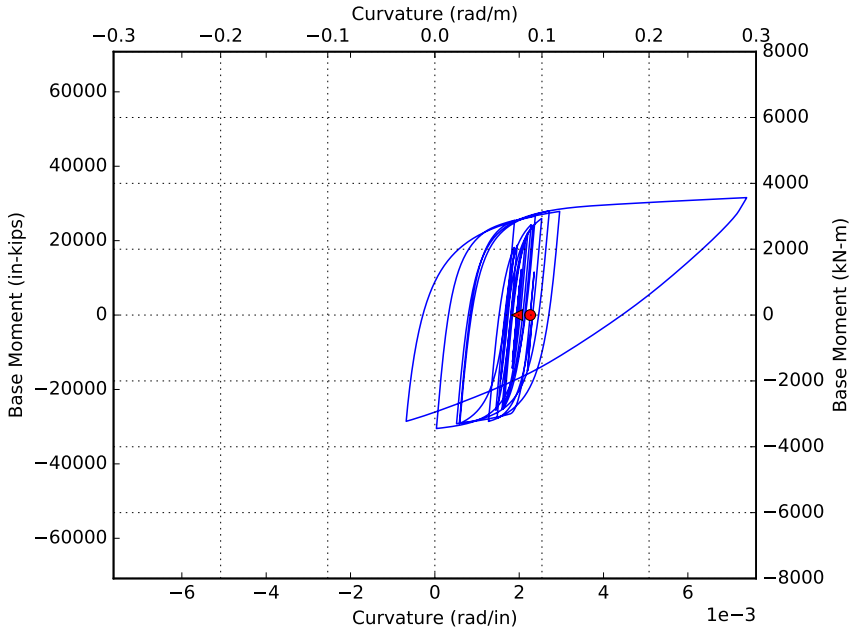

Figure T.7: Moment curvature response of model 5c for EQ7. Red circle indicates initial point

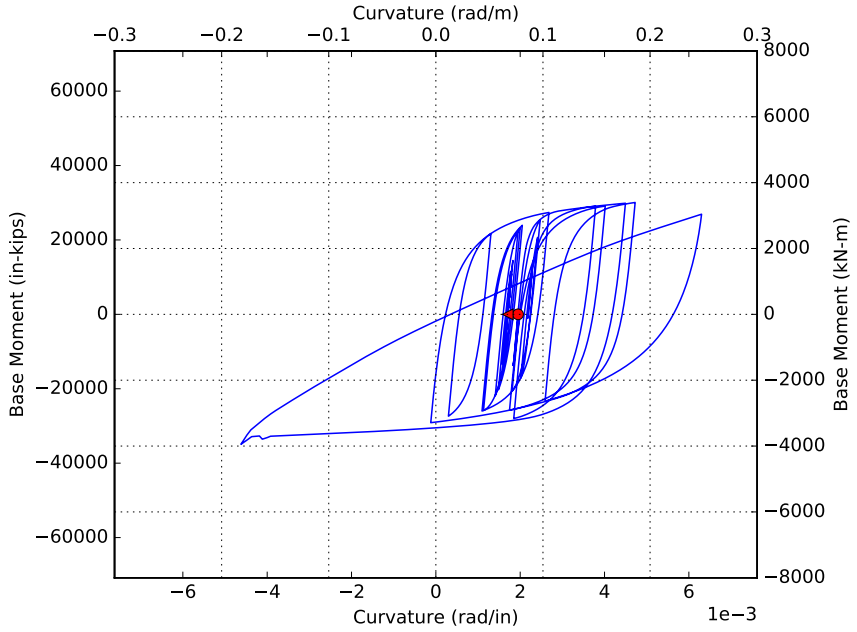

Figure T.8: Moment curvature response of model 5c for EQ8. Red circle indicates initial point

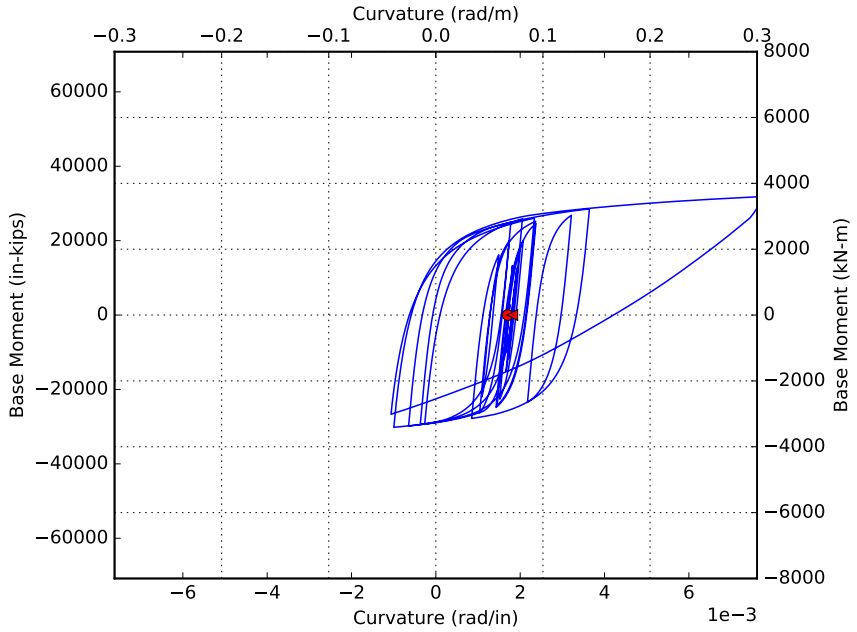

Figure T.9: Moment curvature response of model 5c for EQ9. Red circle indicates initial point

Appendix U

Model 5d Moment Curvature Plots

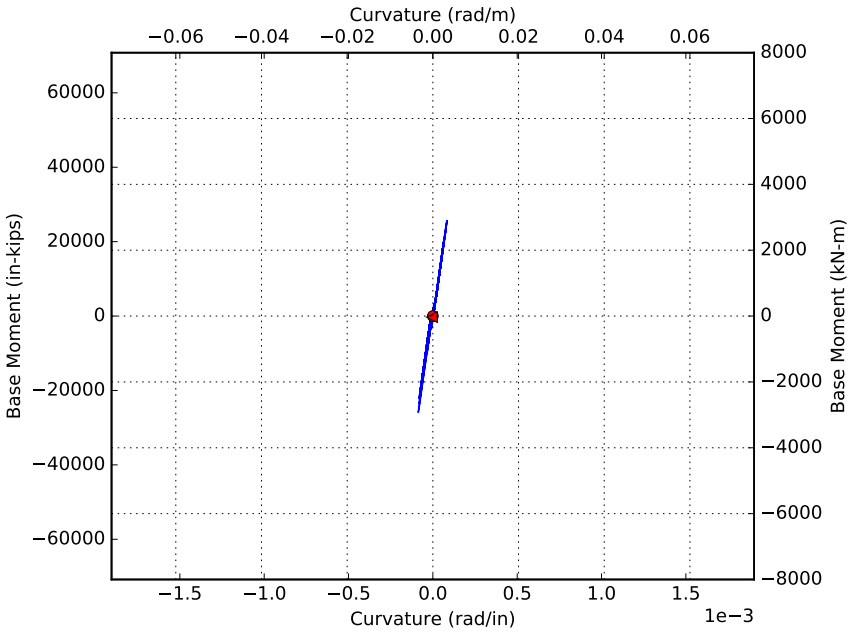

Figure U.1: Moment curvature response of model 5d for EQ1. Red circle indicates initial point

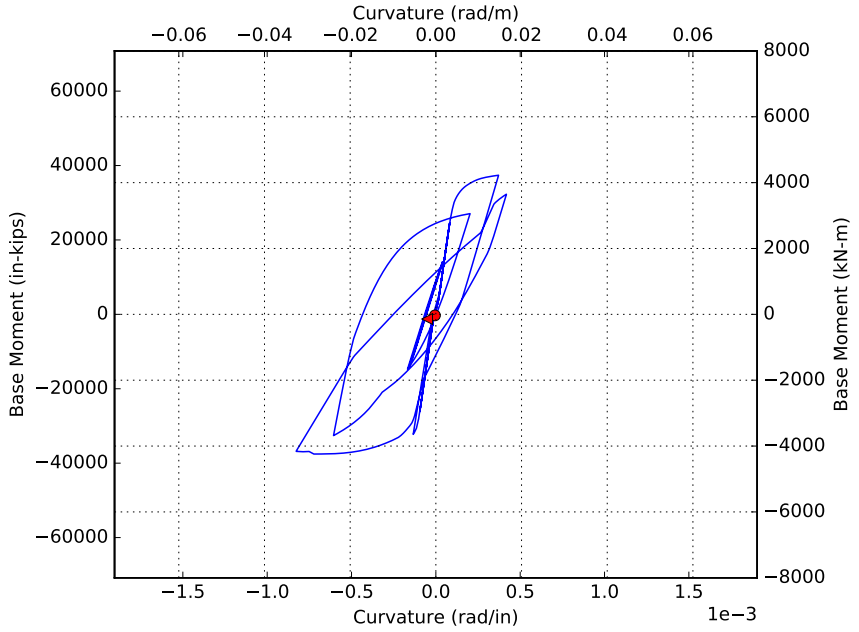

Figure U.2: Moment curvature response of model 5d for EQ2. Red circle indicates initial point

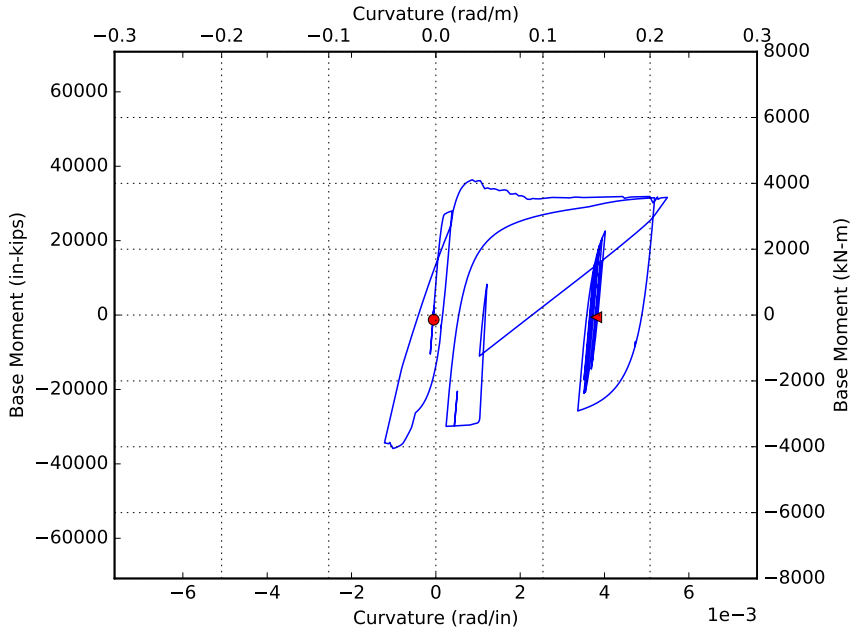

Figure U.3: Moment curvature response of model 5d for EQ3. Red circle indicates initial point

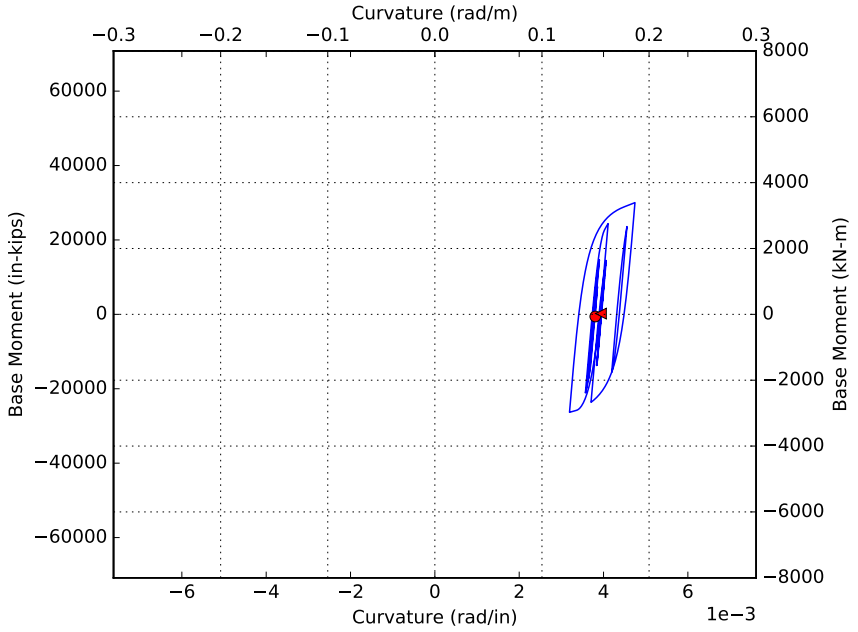

Figure U.4: Moment curvature response of model 5d for EQ4. Red circle indicates initial point

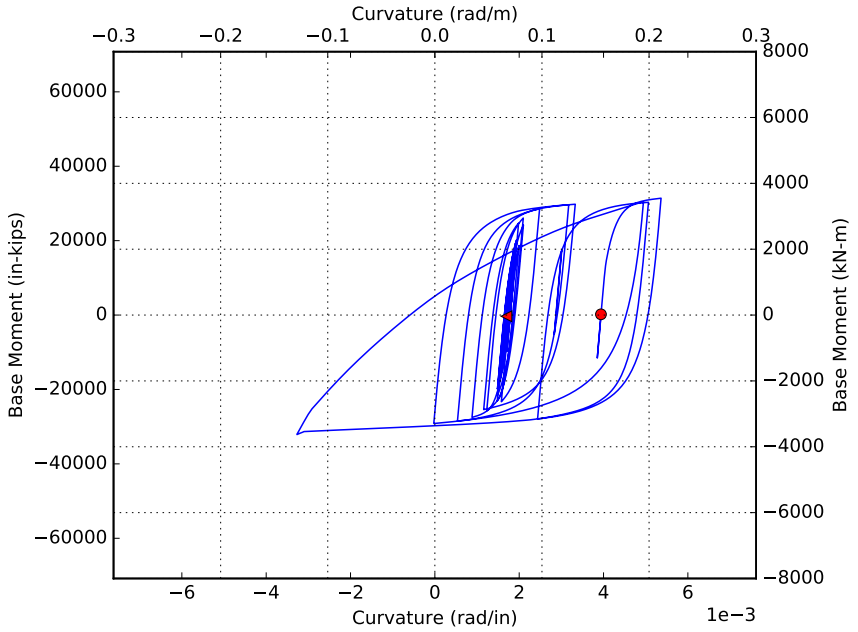

Figure U.5: Moment curvature response of model 5d for EQ5. Red circle indicates initial point

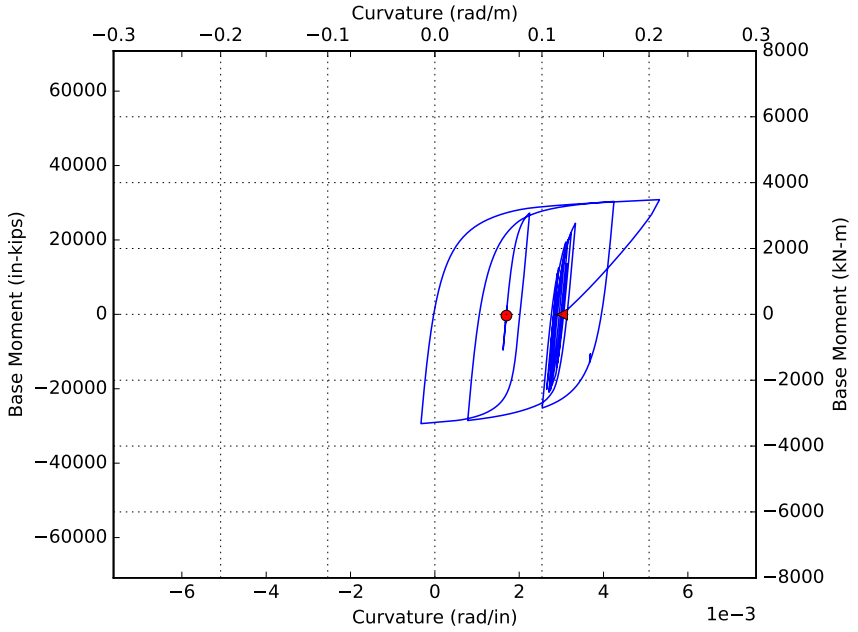

Figure U.6: Moment curvature response of model 5d for EQ6. Red circle indicates initial point

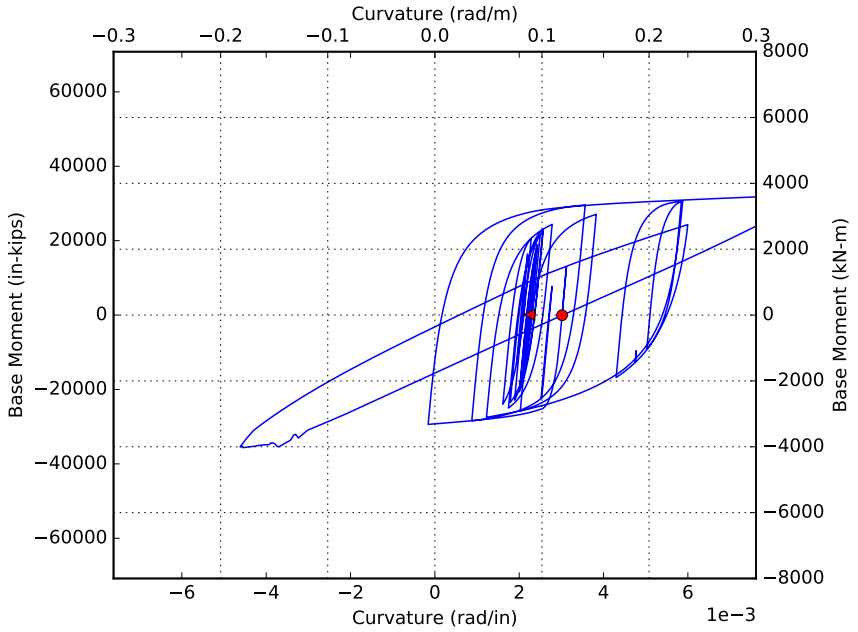

Figure U.7: Moment curvature response of model 5d for EQ7. Red circle indicates initial point

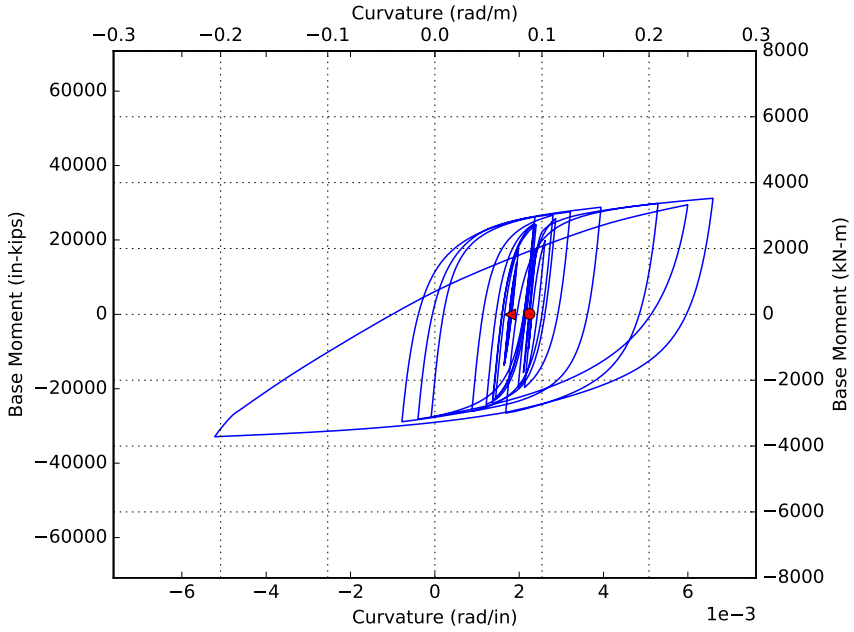

Figure U.8: Moment curvature response of model 5d for EQ8. Red circle indicates initial point

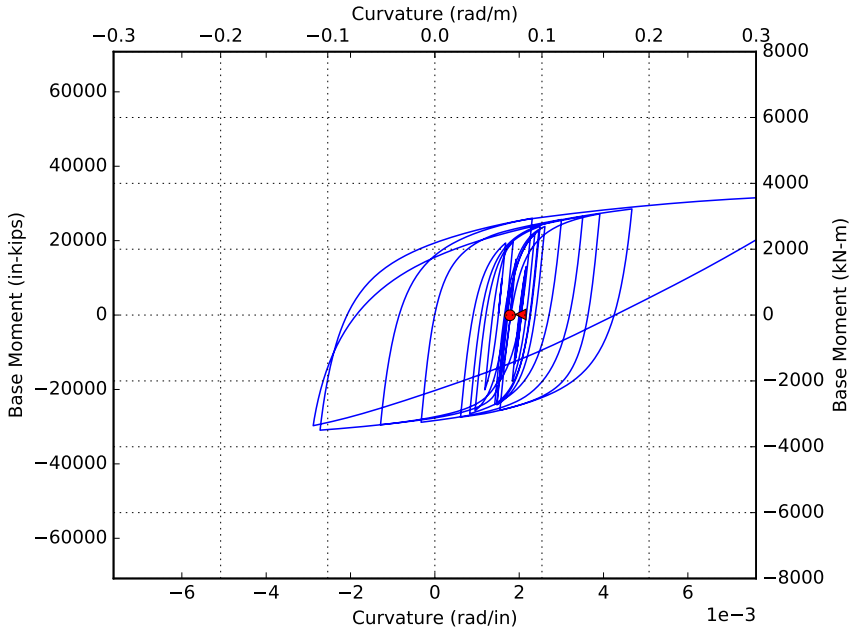

Figure U.9: Moment curvature response of model 5d for EQ9. Red circle indicates initial point

Appendix V

PEER Experiment Moment Curvature Plots

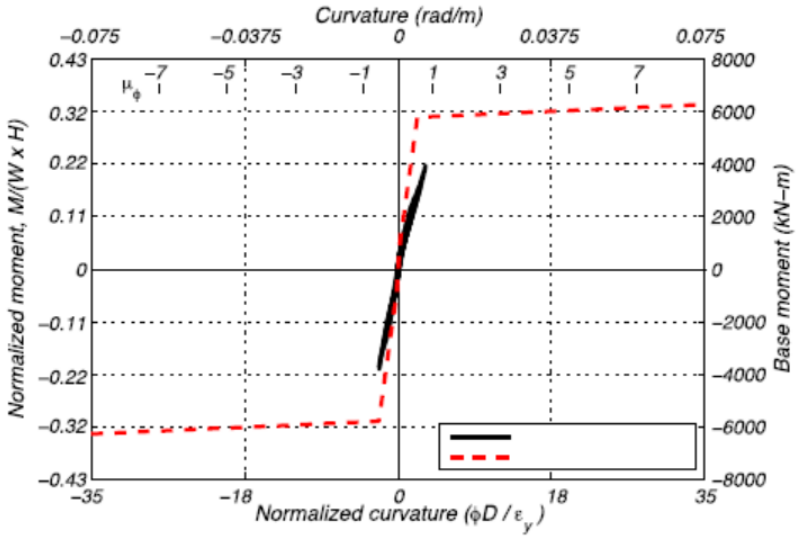

Figure V.1: Moment curvature response of column from PEER experiment (EQ1) [2]

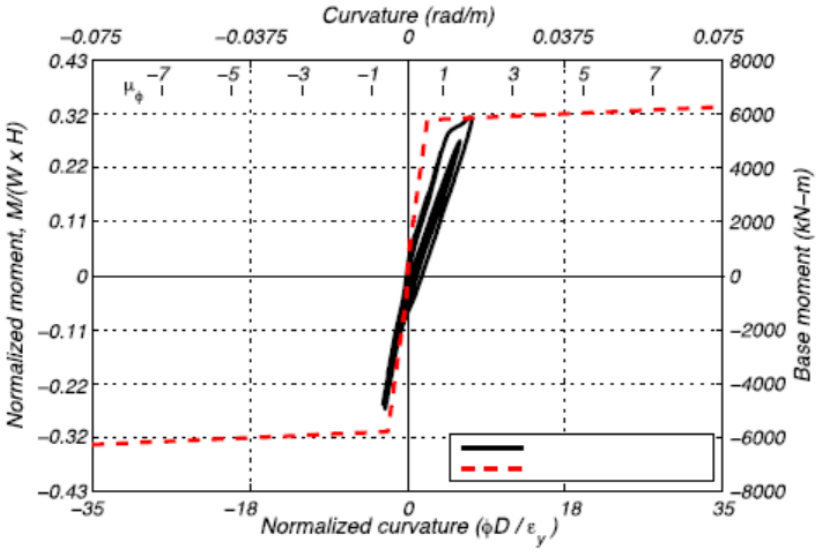

Figure V.2: Moment curvature response of column from PEER experiment (EQ2) [2]

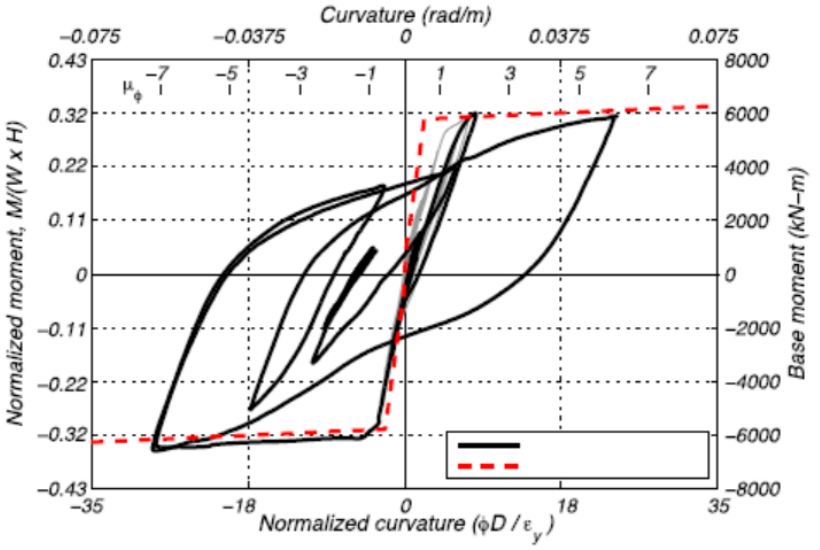

Figure V.3: Moment curvature response of column from PEER experiment (EQ3) [2]

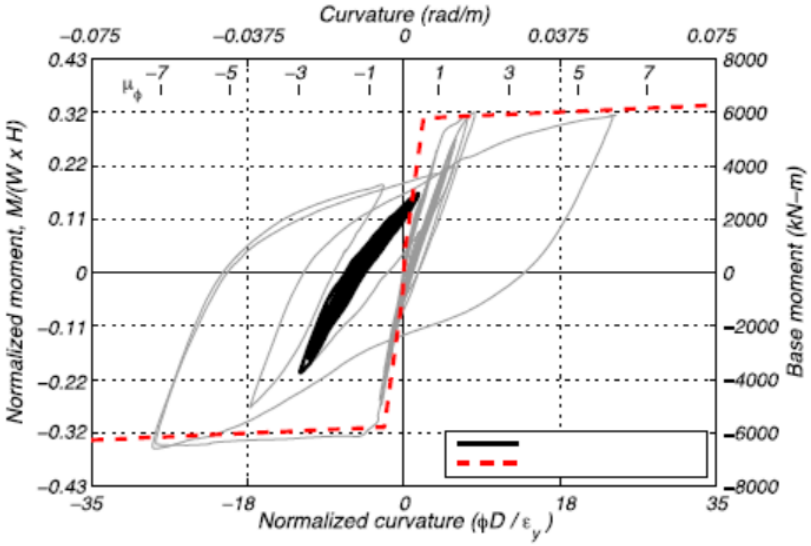

Figure V.4: Moment curvature response of column from PEER experiment (EQ4) [2]

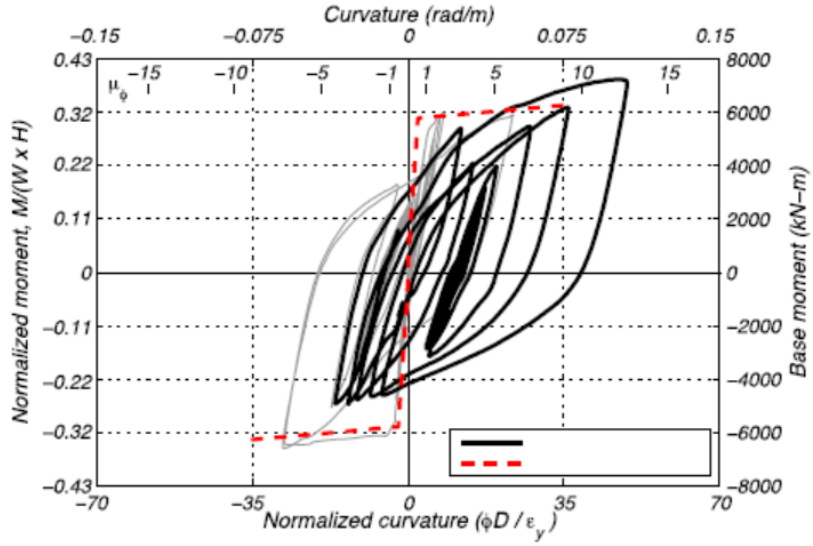

Figure V.5: Moment curvature response of column from PEER experiment (EQ5) [2]

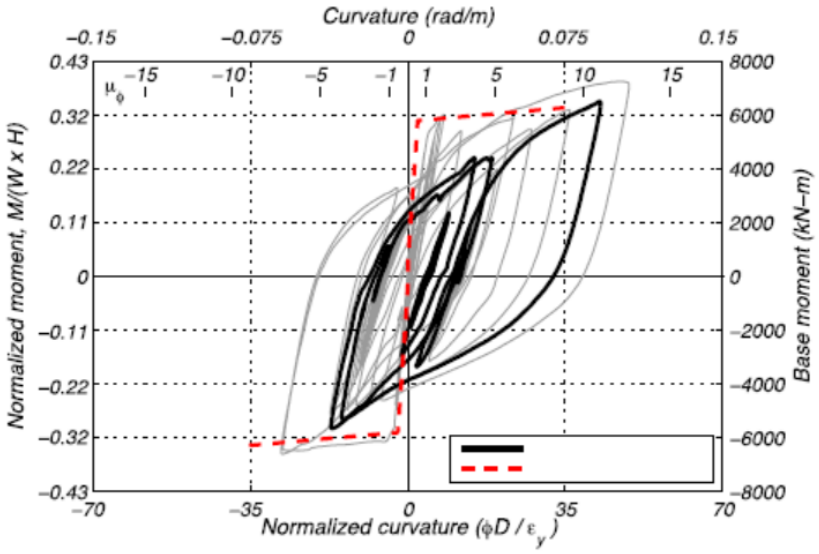

Figure V.6: Moment curvature response of column from PEER experiment (EQ6) [2]

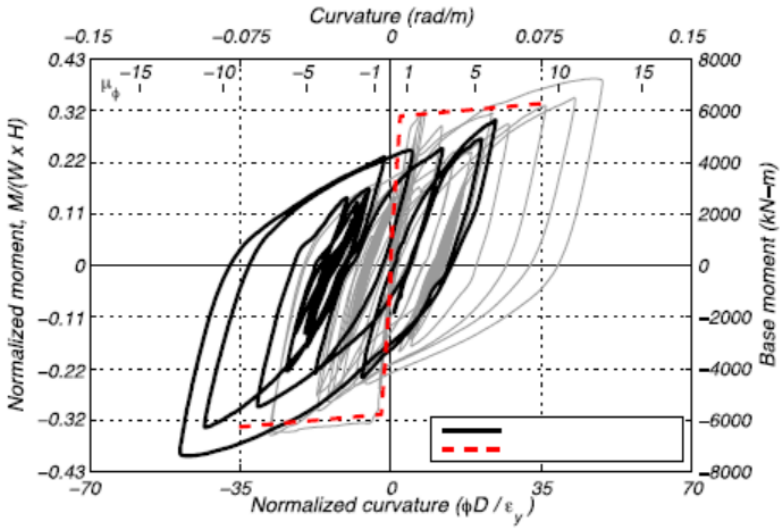

Figure V.7: Moment curvature response of column from PEER experiment (EQ7) [2]

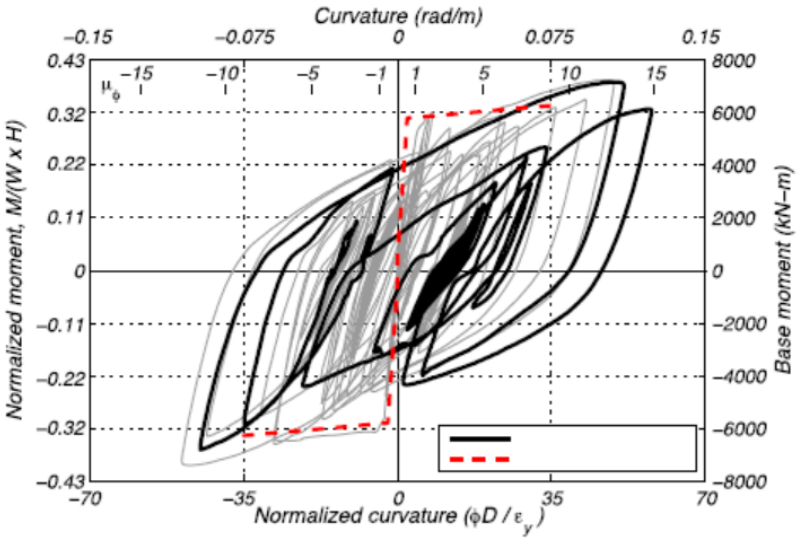

Figure V.8: Moment curvature response of column from PEER experiment (EQ8) [2]

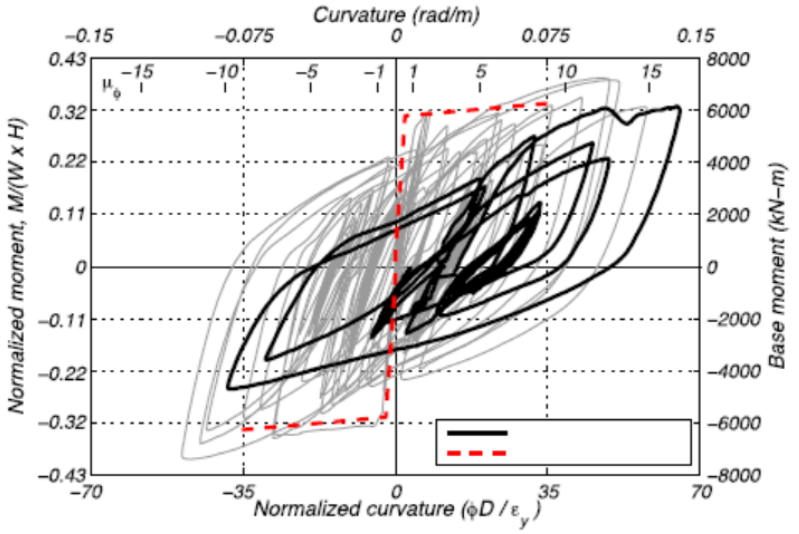

Figure V.9: Moment curvature response of column from PEER experiment (EQ9) [2]